

Cranfield University

School of Engineering

Department of Offshore, Process and Energy Engineering
Process Systems Engineering Group



**EXPERIMENTAL AND NUMERICAL
INVESTIGATION OF HIGH VISCOSITY
OIL-BASED MULTIPHASE FLOWS**

Solomon Oluyemi Alagbe

PhD Thesis

May, 2013

Cranfield University

SCHOOL OF ENGINEERING
Department of Offshore, Process and Energy Engineering
Process Systems Engineering Group

Ph.D. THESIS

Academic Year 2009 - 2012

SOLOMON OLUYEMI ALAGBE

EXPERIMENTAL AND NUMERICAL INVESTIGATION OF
HIGH VISCOSITY OIL-BASED MULTIPHASE FLOWS

Supervisor: Prof. Hoi Yeung

This thesis is submitted in partial fulfilment of the requirements for
the degree of Doctor of Philosophy

© Cranfield University 2012. All rights reserved. No part of this publication may be reproduced without the written permission of the copyright owner.

ABSTRACT

Multiphase flows are of great interest to a large variety of industries because flows of two or more immiscible liquids are encountered in a diverse range of processes and equipment. However, the advent of high viscosity oil requires more investigations to enhance good design of transportation system and forestall its inherent production difficulties.

Experimental and numerical studies were conducted on water-sand, oil-water and oil-water-sand respectively in 1-in ID 5m long horizontal pipe. The densities of CYL680 and CYL1000 oils employed are 917 and 916.2kg/m³ while their viscosities are 1.830 and 3.149Pa.s @ 25°C respectively. The solid-phase concentration ranged from 2.15e-04 to 10% v/v with mean diameter of 150micron and material density of 2650kg/m³.

Experimentally, the observed flow patterns are Water Assist Annular (WA-ANN), Dispersed Oil in Water (DOW/OF), Oil Plug in Water (OPW/OF) with oil film on the wall and Water Plug in Oil (WPO). These configurations were obtained through visualisation, trend and the probability density function (PDF) of pressure signals along with the statistical moments. Injection of water to assist high viscosity oil transport reduced the pressure gradient by an order of magnitude. No significant differences were found between the gradients of oil-water and oil-water-sand, however, increase in sand concentration led to increase in the pressure losses in oil-water-sand flow.

Numerically, Water Assist Annular (WA-ANN), Dispersed Oil in Water (DOW/OF), Oil Plug in Water (OPW/OF) with oil film on the wall, and Water Plug in Oil (WPO) flow pattern were successfully obtained by imposing a concentric inlet condition at the inlet of the horizontal pipe coupled with a newly developed turbulent kinetic energy budget equation coded as user defined function which was hooked up to the turbulence models. These modifications aided satisfactory predictions.

Keywords:

Minimum Transport Condition (MTC), Heavy oil, Water assisted flow, Core annular flow, Computational Fluid Dynamics (CFD), Probability Density Function (PDF)

ACKNOWLEDGEMENT

All thanks and glory to God, the Alpha and the Omega, who has been my source of strength to start and finish this programme.

Appreciation is due to my supervisor, Prof. Hoi Yeung who has been my guide throughout this research. In addition, a big thank you to all administrative staff, most especially Samantha Skears who is always ready to listen and help whenever there is a need, and the technical staff; David Whittington, Kelvin White, and Stan Collins who would not rest until the laboratory stays alive and conducive for me and my colleagues- You are all great men!!!

My special thanks go to my spiritual guide, Pastor and Pastor (Mrs) Biyi Ajala, the leaders and the entire family of Holding Forth the Word Ministry. Thank you for your spiritual, financial and emotional support that you have given to me and my family.

My thanks also go to my parents, in-laws and extended family. I cannot forget all my friends who would not be tired to join me in this struggle until it is achieved. Your prayers worked.

Special thanks to my wife, Temilade Oyeronke and my children, Moboluwarin and Enioluwanimi (Oyinloluwa) for their sacrifices. Without your support this would not have been a reality.

TABLE OF CONTENTS

ABSTRACT.....	i
ACKNOWLEDGEMENT	iii
TABLE OF CONTENTS.....	v
LIST OF FIGURES	ix
LIST OF TABLES	xiii
1 INTRODUCTION	1
1.1 Motivation for the Study.....	4
1.2 Research Aim and Objectives.....	7
1.3 Organisation of the Thesis	8
2 LITERATURE REVIEW	9
2.1 High Viscosity Oil	9
2.2 Production Methods.....	10
2.2.1 Thermal EOR.....	10
2.2.2 Non-thermal EOR.....	16
2.3 Multiphase Flow Studies	17
2.3.1 Experimental study of multiphase flows	17
2.3.2 Two-phase flows	18
2.3.3 Three-phase flows	40
2.3.4 Restart.....	43
2.3.5 Theoretical Approach	47
2.4 Chapter Summary	60
3 RESEARCH METHODOLOGY	63
3.1 Oil- Water- and Sand- Handling Facilities	63
3.1.1 Oil supply	63
3.1.2 Water supply.....	64
3.1.3 Slurry mixer.....	65
3.1.4 Oil/water/sand separator	66
3.1.5 Test section	68
3.2 Data collection method.....	73
3.2.1 Numeric data acquisition.....	73
3.2.2 Image data acquisition.....	74
3.3 Fluid and Solid Properties	74
3.3.1 Fluid.....	75
3.3.2 Particle size distribution	77
3.4 Experimental Procedures	78
3.4.1 Calibration of pressure transducer.....	79
3.4.2 Water-sand test procedure	81
3.4.3 Oil-water test procedure	81
3.4.4 Oil-water-sand test procedure.....	82
3.5 Data Analysis.....	82
3.5.1 Flow pattern identification	82
3.5.2 Pressure gradient	85
3.5.3 Reduction factor	85
3.6 Chapter Summary	86
4 COMPUTATIONAL FLUID DYNAMICS APPROACH.....	87

4.1 Model Development	87
4.2 Eulerian-Eulerian Model Approach.....	87
4.2.1 Volume of fluid model	87
4.2.2 Mixture model	88
4.2.3 Eulerian model.....	88
4.3 Eulerian-Langragian Model Approach	88
4.4 CFD Models Development.....	89
4.4.1 Model assumptions	89
4.4.2 Governing equations.....	89
4.4.3 Numerical scheme	105
4.4.4 Mesh	105
4.4.5 Y+ profile	109
4.4.6 Data analysis.....	110
4.4.7 Analysis of single phase flow	110
4.5 Chapter Summary	112
5 WATER-SAND FLOW IN 1” ID HORIZONTAL PIPE.....	113
5.1 Test Matrix	113
5.2 Flow Regime Identification	113
5.2.1 Flow regime identification using visual observation.....	113
5.3 Sand Minimum Transport Condition.....	116
5.4 Pressure Gradient.....	120
5.5 CFD of Water-Sand Multiphase Flow	124
5.5.1 Model geometry.....	124
5.5.2 Model formulation.....	124
5.5.3 Boundary and initial conditions.....	125
5.5.4 Solution method.....	125
5.5.5 Flow configuration	125
5.5.6 Pressure gradient	127
5.6 Chapter Summary	128
6 OIL-WATER FLOW IN 1” ID HORIZONTAL PIPE.....	131
6.1 Test matrix.....	131
6.2 Flow Regime Identification	131
6.2.1 Flow regime identification by visualisation	132
6.2.2 Flow regime identification by trend and PDF plot of pressure signals	137
6.2.3 Flow pattern map	150
6.2.4 PIP flow	155
6.3 Pressure gradient.....	159
6.3.1 Reduction Factor	167
6.3.2 Verification of SRC Model	168
6.4 CFD of Oil-Water Multiphase Flow	171
6.4.1 Description of model	171
6.4.2 Flow specification	172
6.4.3 Pipe inlet geometry design	173
6.4.4 Comparison of T-junction with concentric inlet pipe geometry	175
6.4.5 Choice of Turbulence Model for 2-Phase Oil-Water Flow	180
6.4.6 Identification of strategy for improvement of CFD model	181
6.4.7 Turbulence kinetic energy budget	186
6.4.8 Flow pattern identification	191

6.4.9 Pressure gradient	197
6.5 Restart	200
6.6 Chapter Summary	206
7 OIL-WATER-SAND FLOW IN 1” ID HORIZONTAL PIPE.....	209
7.1 Test Matrix	209
7.2 Flow Regime Identification	210
7.2.1 Flow regime identification using visual observation.....	210
7.2.2 Flow regime identification using PDF of pressure signals.....	214
7.3 Sand MTC in Oil-Water-Sand Flow	217
7.4 Pressure Gradient.....	218
7.4.1 Verification of SRC model	222
7.5 Comparison of Oil-Water and Oil-Water-Sand Flow Behaviour in Horizontal Pipe Flow	224
7.6 CFD of Oil-Water-Sand Multiphase Flow	229
7.6.1 Model geometry.....	229
7.6.2 Flow patterns	230
7.6.3 Pressure gradient	233
7.7 Chapter Summary	234
8 CONCLUSIONS AND FURTHER RESEARCH.....	237
8.1 Conclusions	237
8.1.1 Experiment	238
8.1.2 CFD	238
8.2 Contributions to Knowledge.....	239
8.2.1 Experiment	239
8.2.2 CFD	240
8.3 Limitations of Research.....	241
8.4 Recommendation and Further Research.....	241
REFERENCES	243
APPENDICES	255

LIST OF FIGURES

Figure 1-1: Relationship of oil viscosity with API gravity (Speight, 2009a).....	1
Figure 1-2: World Oil Classification	2
Figure 1-3: Geographical locations of world unconventional oil reserves.....	3
Figure 1-4: Geographical locations of world unconventional oil production	4
Figure 1-5: Flow behaviour of 1.15cP oil flow at 1.5m/s (Joseph et al., 1997)	6
Figure 2-1: Steam flooding (Veil and Quinn, 2009)	10
Figure 2-2: Production Technology of High viscosity oil.....	11
Figure 2-3: Traditional cyclic steam stimulation (Speight, 2009b).....	12
Figure 2-4: Horizontal cyclic steam stimulation (Veil and Quinn, 2009).....	13
Figure 2-5: Steam assisted gravity drainage (Veil and Quinn, 2009)	13
Figure 2-6: Inert gas injection (Veil and Quinn, 2009)	14
Figure 2-7: Toe-to-Heel Air Injection (Veil and Quinn, 2009).....	15
Figure 2-8: Vapour assisted petroleum extraction (Veil and Quinn, 2009)	15
Figure 2-9: Cold Heavy Oil Production with Sand (Veil and Quinn, 2009).....	17
Figure 2-10: Solid-liquid flow regimes in horizontal pipe (Multiphase design handbook, 2005).....	20
Figure 2-11: Liquid-Solid flow map (Doron and Barnea 1996).....	21
Figure 2-12: Comparison of Chakrabarti's results with existing flow regime data	29
Figure 2-13: Oil-water flow patterns by Trallero (1995)	31
Figure 2-14: Flow pattern map of oil-water for the 26mm horizontal Plexiglas pipe (Sotgia et al., 2008)	32
Figure 2-15: Schematic diagram and flow map of up-flows in vertical pipe (Joseph et al., 1997).....	33
Figure 2-16: Schematic diagram and flow map of down-flows in vertical pipe (Joseph et al., 1997).....	33
Figure 2-17: Schematic diagram and flow map of -flows types in horizontal pipe (Joseph et al., 1997).....	34
Figure 2-18: Schematic diagram and flow map of -flows types in horizontal pipe (Joseph et al., 1997).....	34
Figure 2-19: Experimental annular flow inlet geometry designs (Sotgia et al., 2008; Bensakhria et al., 2004a; Strazza et al., 2011; Prada and Bannwart, 2001c; Balakhrisna et al., 2010b)	35
Figure 2-20: Description of phase inversion (Arirachakaran et al., 1989b).....	37
Figure 3-1: Oil storage tank.....	64
Figure 3-2: Water storage tank	65
Figure 3-3: Slurry mixer and pumping system	66
Figure 3-4: Multiphase separator.....	67
Figure 3-5: Coriolis meter and pressure guage.....	67
Figure 3-6: Gas flowmeters, valve and pressure guages	68
Figure 3-7: Schematic of 1-inch four phase transport facility at Cranfield University PASE laboratory	69
Figure 3-8: Pictorial view of 1-inch four phase transport facility at Cranfield University PASE laboratory	70
Figure 3-9: Differential pressure transducer.....	73
Figure 3-10: Pressure transducer	74
Figure 3-11: Viscosity-Temperature data of CYL1000	76

Figure 3-12: Viscosity-Temperature data of CYL680	77
Figure 3-13: Sand distribution of HST 95	78
Figure 4-1: Pipe geometry	106
Figure 4-2: Pressure gradients of the mesh profiles	109
Figure 4-3: Y+ profile for water turbulent flows in 1-in ID pipe	110
Figure 4-4: Comparison of D-W, Experimental and CFD pressure gradients of a single phase water in 1-in ID 5m long pipe	111
Figure 4-5: Comparison of CFD, D-W and Experimental pressure gradients of a single phase oil in 1-in ID 5m long pipe.	112
Figure 5-1: Pressure gradients of low concentration slurry flow in 1-in ID horizontal pipe	121
Figure 5-2: Pressure gradients of high concentration slurry flow in 1-in ID horizontal pipe	122
Figure 6-1: Anemometer profile $r/R = 0.8, \theta = 0$ and pressure gradient result for mixture velocity =0.038m/s with 10% water cut (McKibben et al., 2000a)	143
Figure 6-2: Instantaneous pressure gradient data at 67% water cut	149
Figure 6-3: Flow regime map for oil-water flow in 1-in horizontal pipe	150
Figure 6-4: Flow regime map for oil-water flow in 1-in horizontal pipe	151
Figure 6-5: Flow regime map for oil-water flow in 1-in horizontal pipe	152
Figure 6-6: Comparing flow pattern of 3300cP oil and water with Sotgia etal (2008) literature data	153
Figure 6-7: Comparing flow pattern of 5000cP oil and water with Sotgia etal (2008) literature data	154
Figure 6-8: Comparing flow pattern of 7500cP oil and water with Sotgia (2008).....	154
Figure 6-9: Comparison of phase inversion models' prediction at different viscosities with the present research	157
Figure 6-10: Behaviour of water and oil velocity at PIP for 3300cP nominal viscosity	158
Figure 6-11: Behaviour of water and oil velocity at PIP for 5000cP nominal viscosity	158
Figure 6-12 Comparison of pressure gradient of oil-water flow for 3300cP nominal oil viscosity at different oil superficial velocities and water cut	160
Figure 6-13 Comparison of pressure gradient of oil-water flow for 3300cP nominal oil viscosity at different oil and and water superficial velocities	160
Figure 6-14 Comparison of pressure gradient of oil-water flow for 5000cP nominal oil viscosity at different oil superficial velocities and water cut	161
Figure 6-15 Comparison of pressure gradient of oil-water flow for 5000cP nominal oil viscosity at different oil and and water superficial velocities	161
Figure 6-16: Comparison of pressure gradient of oil-water flow for 7500cP nominal oil viscosity at different oil superficial velocities and water cut	162
Figure 6-17 Comparison of pressure gradient of oil-water flow for 7500cP nominal oil viscosity at different oil and and water superficial velocities	162
Figure 6-18: Effect of viscosity on pressure gradient @ $v_{so} = 0.06\text{m/s}$ and different water cut	163
Figure 6-19: Effect of viscosity on pressure gradient @ $v_{so} = 0.06\text{m/s}$ and different water superficial velocity.....	164
Figure 6-20: Effect of viscosity on pressure gradient @ $v_{so} = 0.2\text{m/s}$ and different water cut	165

Figure 6-21: Effect of viscosity on pressure gradient @ $v_{so} = 0.2\text{m/s}$ and different water superficial velocity	165
Figure 6-22: Effect of viscosity on pressure gradient @ $v_{so} = 0.4\text{m/s}$ and different water cut	166
Figure 6-23: Effect of viscosity on pressure gradient @ $v_{so} = 0.4\text{m/s}$ and different water superficial velocity	166
Figure 6-24: Pressure gradient reduction factor against water cut of oil-water flows at 3300cP oil viscosity (nominal).....	167
Figure 6-25: Pressure gradient reduction factor against water superficial velocity of oil-water flows at 3300cP oil viscosity	168
Figure 6-26: Validation of SRC model for 3300cP oil with water at $V_{so}=0.55\text{m/s}$	169
Figure 6-27: Validation of SRC model for 5500cP oil with water at $V_{so}=0.11\text{m/s}$	169
Figure 6-28: Validation of SRC model for 10000cP oil with water at $V_{so}=0.11\text{m/s}$...	170
Figure 6-29: CFD annular flow inlet geometry description	174
Figure 6-30: Pressure gradients of three different inner-inlet dimensions opening in oil-water transport for oil at 0.55m/s and water at 1.0m/s	175
Figure 6-31: T-junction pipe geometry	176
Figure 6-32: Performance analysis of turbulence flow for oil-water flow of $V_{so}=0.55\text{m/s}$ and $V_{sw}=0.2\text{m/s}$	180
Figure 6-33: Comparison of default turbulence models results with experimental data of oil-water flow at 0.55m/s oil superficial velocity.....	184
Figure 6-34: Comparison of fluctuation kinetic energy of experiment and CFD at 27% water cut	189
Figure 6-35: Pressure gradient against water cut @ $V_{so} = 0.55\text{m/s}$ for 3300cP oil using modified SKE CFD model	197
Figure 6-36: Pressure gradient against water cut @ $V_{so} = 0.55\text{m/s}$ for 3300cP oil using modified LRKE (L-S) CFD model.....	198
Figure 6-37: Pressure gradient against water cut @ $V_{so} = 0.20\text{m/s}$ for 5000cP oil using modified LRKE (L-S) CFD model.....	199
Figure 6-38: Pressure gradient against water cut @ $V_{so} = 0.10\text{m/s}$ for 7500cP oil using modified LRKE (L-S) CFD model.....	199
Figure 6-39: Plot of restart process for 3300cP oil at 0.55m/s oil superficial velocity and 0.20m/s water superficial velocity.....	202
Figure 6-40: Plot of restart process for 3300cP oil at 0.55m/s oil superficial velocity and 0.40m/s water superficial velocity.....	203
Figure 6-41: Plot of restart process for 3300cP oil at 0.55m/s oil superficial velocity and 0.90m/s water superficial velocity.....	204
Figure 6-42: Comparison of pressure surges at different flow conditions for 3300cP oil	204
Figure 6-43: Comparison of pressure surges at different flow conditions for 10000cP oil	205
Figure 6-44: Comparison of restart pressure surges at different oil viscosities	206
Figure 7-1: Pressure gradient of oil-water-sand flow with 1% v/v sand on different oil viscosities	219
Figure 7-2: Pressure gradient of oil-water-sand flow with 5% v/v sand on different oil viscosities	220
Figure 7-3: Pressure gradient of oil-water-sand flow with 10% v/v sand on different oil viscosities	220

Figure 7-4: Pressure gradients of varying sand concentration for relatively constant oil viscosity	221
Figure 7-5: Validation of SRC model using 3300cP oil with 1% sand.....	223
Figure 7-6: Validation of SRC model using 10000cP oil with 1% sand.....	223
Figure 7-7: Comparison of oil-water and oil-water-sand flow @ $V_{so}=0.1\text{m/s}$ and 1% v/v sand concentration for 3300cP nominal viscosity	224
Figure 7-8: Comparison of oil-water and oil-water-sand flow @ $V_{so}=0.1\text{m/s}$ and 1% v/v sand concentration for 7000cP nominal viscosity	225
Figure 7-9: Comparison of oil-water and oil-water-sand flow @ $V_{so}=0.1\text{m/s}$ and 1% v/v sand concentration for 1000cP nominal viscosity	225
Figure 7-10: Comparison of oil-water and oil-water-sand flow @ $V_{so}=0.11\text{m/s}$ and 5% v/v sand concentration for 3300cP nominal viscosity	226
Figure 7-11: Comparison of oil-water and oil-water-sand flow @ $V_{so}=0.1\text{m/s}$ and 5% v/v sand concentration	227
Figure 7-12: Comparison of oil-water and oil-water-sand flow @ $V_{so}=0.1\text{m/s}$ and 5% v/v sand concentration	227
Figure 7-13: Pressure gradient of oil-water-sand @ $V_{so}=0.1\text{m/s}$ with 1% v/v sand concentration (Oil viscosity=3300cP)	233

LIST OF TABLES

Table 2-1: Survey of experimental study on water-sand flow.....	22
Table 2-2 : Summary of 2-phase oil-water flow experiments in pipes	27
Table 2-3: Survey of oil-water flow regimes studies	30
Table 2-4: Comparison of different heavy oil transportation methods Guevara et al (1997)	46
Table 2-5: Survey of modelling and simulation study on water-sand flow in pipe.....	58
Table 3-1: Description of components of 1-in rig facility.....	71
Table 3-2: Phases properties description.....	76
Table 4-1: Geometry properties.....	106
Table 4-2: Mesh Dependence Profile	108
Table 5-1: Visual analysis of 8.10e-04% v/v (750lb/1000bbl) sand concentration water- sand flow	114
Table 5-2: Visual analysis of 1% (~90000lb/1000bbl) sand concentration water-sand flow.....	115
Table 5-3: Observed MTC of sand in 1in-ID pipe flow	117
Table 5-4: Comparison of sand MTC in pipes	118
Table 5-5: Comparison of some correlations at sand transport condition with the present research.....	119
Table 5-6: Comparison of the pressure gradient and correlations at sand transport condition	123
Table 5-7: Contours of water-sand (1% v/v sand concentration) flow.....	126
Table 5-8: Comparison of the experimental pressure gradient of 1% v/v water-sand with CFD	128
Table 6-1: Oil-water flow pattern at 0.06m/s oil superficial velocity	134
Table 6-2: Oil-water flow pattern at 0.2m/s oil superficial velocity	135
Table 6-3: Oil-water flow pattern at 0.55m/s oil superficial velocity	136
Table 6-4: Sample of additional oil-water flow pattern	137
Table 6-5: PDF description of oil-water flow at V_{so} 0.06m/s	140
Table 6-6: PDF description of oil-water flow at V_{so} 0.2m/s	145
Table 6-7: PDF description of oil-water flow at V_{so} 0.55m/s	147
Table 6-8: PIP identification by visualisation	156
Table 6-9: Fluid properties	172
Table 6-10: Geometry properties of T-junction pipe.....	175
Table 6-11: Inlet condition adaptability check using pressure gradient.....	176
Table 6-12: Inlet condition adaptability check using flow pattern.....	178
Table 6-13: Model constants of the low-Re k-epsilon models.....	182
Table 6-14: Source terms and boundary conditions	182
Table 6-15: Damping functions of the low-Re k-epsilon models	183
Table 6-16: Comparison of flow pattern of experimental and CFD turbulence models of oil-water flow at 27% water cut	185
Table 6-17: PDF-Contour analysis of oil-water flow of 10000cP at V_{so} =0.1m/s, and V_{sw} =0.02m/s.....	193
Table 6-18: PDF-Contour-Experiment analysis of oil-water flow of 7500cP at V_{so} =0.1m/s and V_{sw} =0.8m/s.....	194

Table 6-19: PDF-Contour-Experiment analysis of oil-water flow of 3300cP at $V_{so}=0.550\text{m/s}$ and $V_{sw}=1.0\text{m/s}$	195
Table 6-20: PDF-Contour-Experiment analysis of oil-water flow of 7500cP at $V_{so}=0.06\text{m/s}$ and $V_{sw}=0.80\text{m/s}$	196
Table 6-21: Restart pressure of 3300cP at different velocities.....	205
Table 6-22: Restart pressure of 10000cP at different velocities.....	206
Table 7-1: Oil-water-sand flows test matrix.....	210
Table 7-2: Oil-water-sand flow pattern for 3300cP nominal oil viscosity at 0.11m/s oil superficial velocity	211
Table 7-3: Oil-water-sand flow pattern (10000cP at $V_{so}=0.1\text{m/s}$ and 1% sand).....	213
Table 7-4: Trend and PDF plot of oil-water-sand flow for 3300cP nominal viscosity@ $V_{so}=0.1\text{m/s}$	215
Table 7-5: Trend and PDF plot of oil-water-sand flow for 10000cP nominal viscosity @ $V_{so}=0.1\text{m/s}$	216
Table 7-6: Summary of sand MTC in oil-water-sand flow in 1-in ID pipe for 3337cP nominal viscosity at different sand loading.....	217
Table 7-7: Summary of sand MTC in oil-water-sand flow in 1-in ID pipe for 10000cP nominal viscosity at different sand loading.....	218
Table 7-8: Pressure gradient @ MTC in oil-water-sand flow for 10000cP nominal viscosity at different sand loading	222
Table 7-9:Contour plots of oil-water-sand of 1%v/v sand with 3300cP oil.....	232

NOMENCLATURE

A	Area occupied by each phase	m^2
Ar	Archimedes	-
C	Concentration	-
d, D	Diameter	micron, m
E	Expected value of the quantity	-
$F(x)$	cumulative distribution function	-
f	Friction factor	-
g	Acceleration due to gravity	m/s^2
N	Number of elements	-
P	Pressure	Pa
	Pressure signal	-
ΔP	Pressure drop	Pa, kPa
R_F	Reduction factor	-
Re	Reynolds	-
s	skewness	-
s	Time	s
S	Perimeter	m
V	Velocity	m/s
x	Variable,	-
x	distance	-
μ	Viscosity	kg/m-s, Pa.s
$\bar{\mu}$	mean	-
ρ	Density	kg/m^3
τ	Shear stress	Pa
$\left(\frac{dP}{dZ}\right)_{sp}$	Frictional pressure gradient of a single-phase oil flow	Pa/m, kPa/m
$\left(\frac{dP}{dZ}\right)_{tp}$	Frictional pressure gradient of two-phase oil-water flow	Pa/m, kPa/m
Δt_{global}	Global time step	s

Subscripts

<i>CF</i>	Continuous fluid
<i>i</i>	Interface, count
<i>max</i>	Maximum
<i>min</i>	Minimum
<i>n</i>	Normalised
<i>o</i>	Oil
<i>p</i>	Particle
<i>so</i>	Superficial value of oil
<i>sw</i>	Superficial value of water
<i>w</i>	Water

ACRONYMS

API	America Petroleum Institute
CAF	Core Annular Flow
CFD	Computational Fluid Dynamics
CFL	Courant-Friedrich-Lewy; Courant number
CHOPS	Cold Heavy Oil Production with Sand
CSS	Cyclic Steam Stimulation
EOR	Enhanced Oil Recovery
HCSS	Horizontal Cyclic Steam Stimulation
ID	Internal Diameter
IEA	International Energy Agency
IGI	Inert Gas Injection
LHS	Left Hand Side
LRKE	Low Reynolds K-Epsilon
LRKW	Low Reynolds K-Omega
MRI	Magnetic Resonance Imaging
PAF	Perfect Core Annular Flow
PIP	Phase Inversion Point
PEPT	Positron Emission Particle Tracking
RANS	Reynolds-Average Navier-Stokes
RHS	Right Hand Side
SKE	Standard K-Epsilon
SRC	Saskatchewan Research Council
SST	Shear Stress Transport
SVX	Solvent Vapour Extraction
TCSS	Traditional Cyclic Steam Stimulation
THAI	Toe-to-Heel Air Injection
VAPEX	Vapour-Assisted Petroleum Extraction
VOF	Volume of Fluid
WAG	Water Alternate Gas
WCAF	Wavy Core Annular Flow

1 INTRODUCTION

Heavy oil, extra-heavy oil, and bitumen are naturally existing unconventional hydrocarbon/oil resources that are found below 20° API gravity (Figure 1-1). These oils are unconventional oil because of their very high viscosities and densities. These resources constitute about 70% of world oil reserve and found largely in unconsolidated sandstones (Veil and Quinn, 2009).

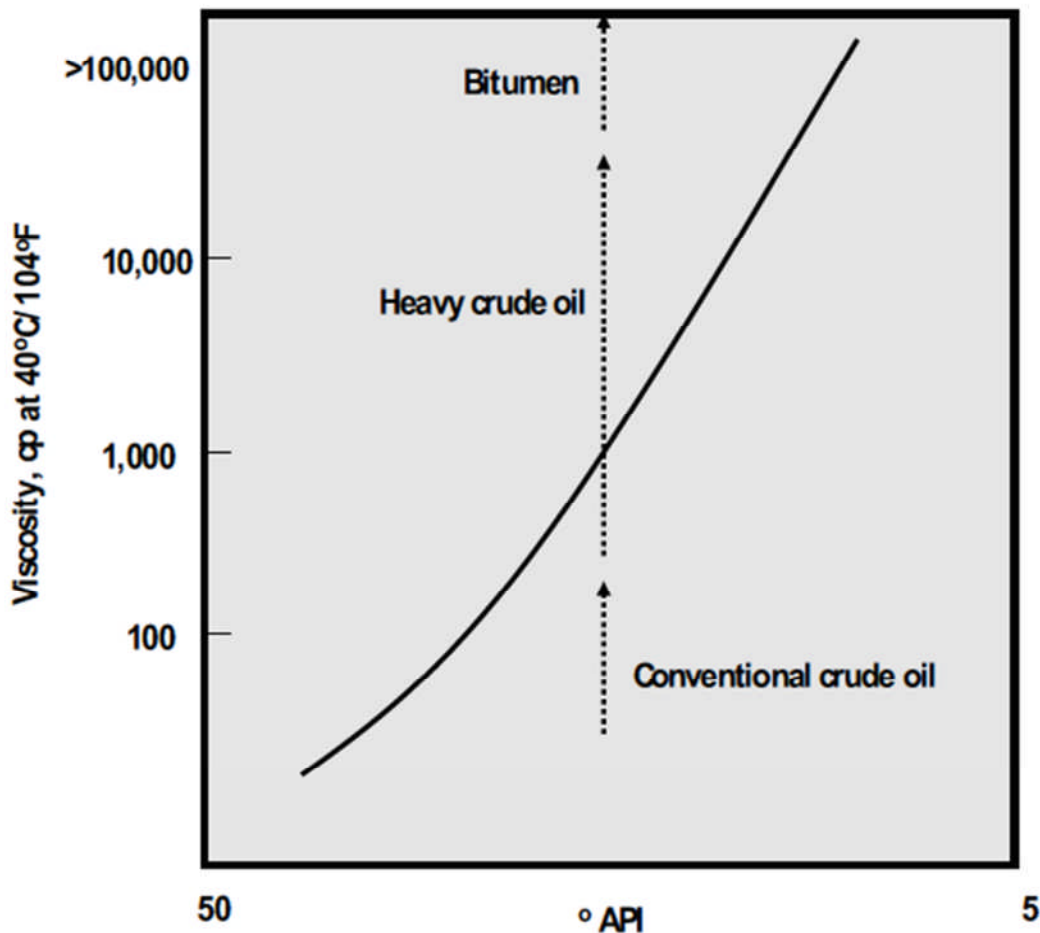


Figure 1-1: Relationship of oil viscosity with API gravity (Speight, 2009a)

The International Energy Agency (IEA, 2005) estimated that there are 6 trillion barrels of heavy oil in place worldwide. Despite the fact that heavy oil, extra heavy oil, and bitumen are found in abundance as shown in Figure 1-3, they do not sell at a lower price than conventional oil because production is more costly than for conventional oil, hence the profit margin is small. The production statistic captured in Figure 1-4 as reported by

IFP (Institut Francais de Petrol) and others in the IEA report shows that a few percentages of unconventional oils are being recovered, due to the difficulty in production and transportation.

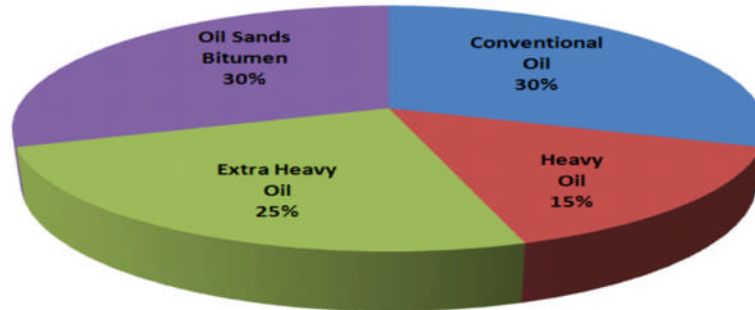


Figure 1-2: World Oil Classification

Frimpong et al. (2004) reported that Oil-sand production cost is about \$13/bbl compared with \$1.25/bbl for conventional crude oil as at 2004. The energy consumption to extract a barrel of bitumen and upgrade it to synthetic crude has been approximately valued as 1.0 – 1.25GJ while the energy content of a barrel of heavy oil is about 6.117 GJ (IEA, 2005); this translates to about 20% of the energy content for a barrel of high viscosity oil. Bulk of this energy cost is traceable to the transportation of the heavy oil from the reservoir to the well head and separator.

The transportation of the heavy type of crude has proven to be expensive because of the pumping cost involved due to the pressure loss which is higher than that of the conventional oils. In the same vein, the presence of other crude oil composition like gas, asphaltene, resin, hydrates, and wax which are unavoidable, compound the transportation problem of heavy oil in the pipeline. All of these have contributed to the concerns relating to sand in heavy oil transport.

The challenges enumerated above led to the usage of different recovery methods (which are discussed in the next chapter) for production/transportation of heavy crude through the pipe to encourage high productivity. Although all the proposed approaches are highly promising, they do not hold without problems to be solved if they will be economical. A very important recovery method pioneered in Alberta, Canada, is the

Cold Heavy oil Production with Sand (CHOPS); this is a technique proposed for extracting heavy oil where water and sand are used together as a means of enhancing the productivity of the oil well. This method employs the co-production of oil-sand with cold water; this is believed to help alleviate the problem of high energy demand as it exists in other methods. One of the major challenges of this method, from the previous research, is the issue of maintaining the water film on the pipe wall, in order to get the desired and optimum flow distribution throughout the pipe or for a good period of time. In addition, stabilizing this flow over a wide range of velocities for a long period of time, and determining the minimum/optimum water cut needed for the desired flow pattern are yet to be concluded. Although some researches have been done on liquid-liquid, gas-liquid and solid-liquid, a lot has not been said regarding the oil-based flow behaviour, but for low and medium viscosity oil. In addition, on-going research to address the issues of concern in the high viscosity oil-based flow is rather slow because experimental process takes time.

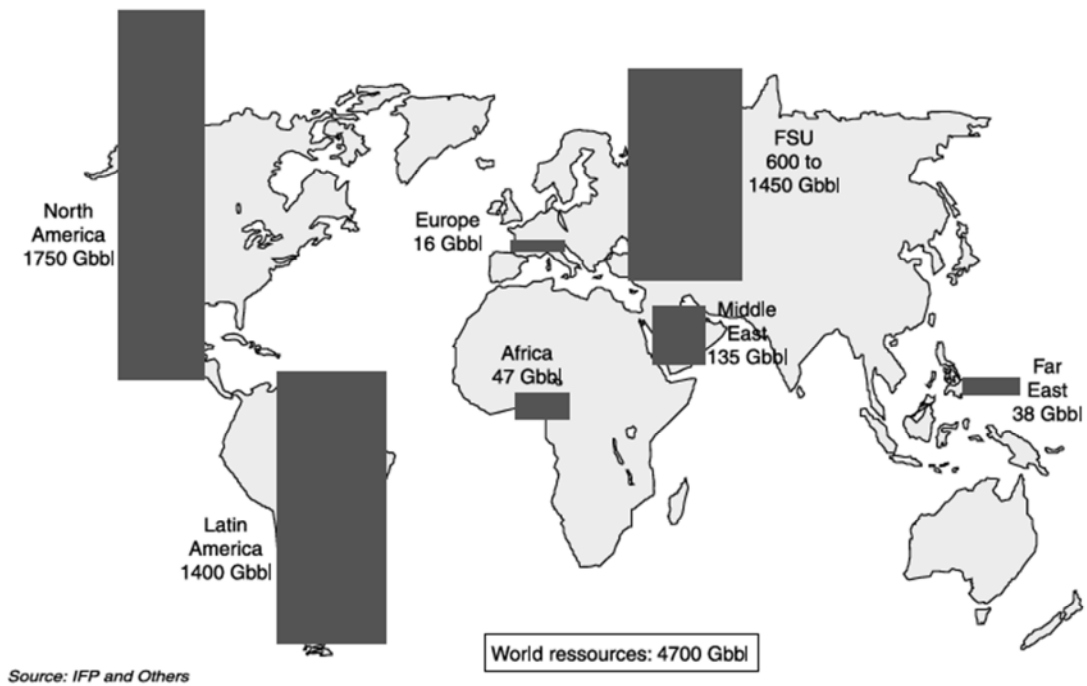


Figure 1-3: Geographical locations of world unconventional oil reserves

In the light of this, the focus of this research is to use Computational Fluid Dynamics (CFD) in addition to the experimental study, to investigate the behaviour of the heavy

oil in water with sand for cost effective multi-fluid transportation technology. This approach will help to provide quick and reliable predictions of multiphase flow behaviour under different conditions. In addition, attention shall be given to horizontal type of flow.

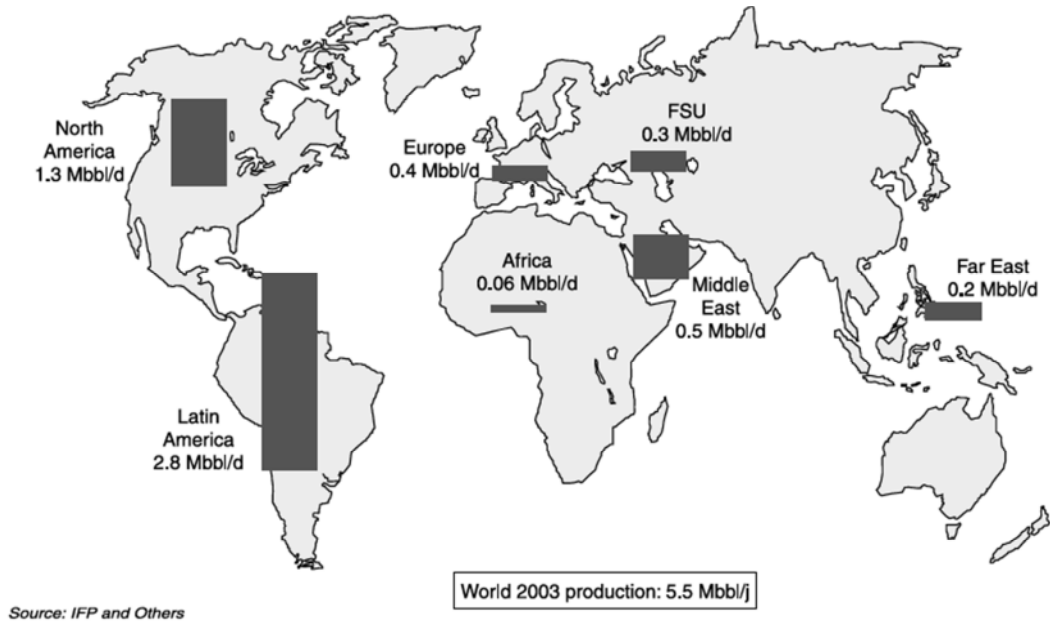


Figure 1-4: Geographical locations of world unconventional oil production

1.1 Motivation for the Study

CHOPS is proposed to be an effective production method for heavy (high viscosity) oils that are located in unconsolidated reservoirs (Dusseault, 1993; 1995). Although some research has been done on oil flows to describe their behaviour; the flow pattern, phase holdup, pressure drop along horizontal, vertical and inclined planes, however, the focus has been on low and medium viscosity oils (<1000cP), known as conventional oil (Barnea et al., 1980; Martinez et al., 1988; Brauner and Moalem Maron, 1992; Trallero et al., 1997; Angeli and Hewitt, 2000). These findings cannot be blindly relied upon because of the difference in the fluid properties, (most importantly, the viscosity). Most of the correlations developed to address the problems in the conventional oil are data specific, and they cannot be applied to other conditions other than the one under which they were developed. It has also been reported by several researchers e.g. Besson (2005) and Owen et al. (2010) that transportation of heavy oil is energy intensive and that the

technology of pipe wall lubrication with light oils or water would reduce the energy consumption in heavy oil production, but could become a nightmare if the phenomenon is not understood.

Transportation of oil-in-water (i.e. a situation in which water lubricates the pipe wall while the oil moves in the core) has attracted the attention of many researchers and industries, because the transport properties of such oil-in-water has been proposed to be independent of the oil viscosity. For instance, Joseph et al. (1997) reported that the pressure losses in the production of single phase oil with viscosity of 1.15cP increased monotonically as the pipeline fouled with oil adhesion on the wall (see Figure 1-5). If this behaviour continues, more energy would be consumed, oil deposition and adhesion will be aided because increase in pressure leads to increase in viscosity; consequently, the pipeline would be blocked. When the flow was lubricated with water, it yielded a varying pressure drop between 900psi (~6200kPa) and 1100psi (~7500kPa) at a flow rate of 24000 barrel per day which later led to oil fouling the pipe wall. The fresh water was replaced with the site well produced water (which was analysed to contain 0.6weight per cent sodium metasilicate) after which the pressure drop never varied much from 900psi, at flow velocity greater or equal to 1m/s.

Joseph et al. (1997) reported that pipeline lubrication could not be sustained for a very long period of time because oil gets attached to the pipe wall after a period of time, displaced the low viscosity fluid on the wall and caused the increase in the pressure gradient, but this assertion was not backed up with outcome of different viscosities and various percentages of water other than 4% that was presented. Hence the report could not be taken as a norm in this kind of multiphase flow. However, some research are on-going to investigate the characteristics of this energy saving technology but few are reported on the study of cold Enhanced Oil Recovery (EOR) for heavy oil where viscosity is higher than 1000cP (Gillies et al., 1995; McKibben et al., 2000b; 2009). Hence there is need for further research on high viscosity related multiphase flow to fill the gap that has been identified.

The issue of oil fouling the pipe wall has created a huge setback for the application of the annular flow phenomenon in the transport of high viscosity oil. In the light of the belief that core annular flow must have water or the lighter fluid wetting the wall, many researchers like Arney (1996) researched on the strategies to prevent fouling and came up with cement-lined pipe as a better option to ensure a preferential selection of the fluid that wet the pipe wall, while Angeli and Hewitt (1999) reported the effect of pipe wettability on the pressure gradients. In the theoretical approach, Ooms and Poesio (2003) developed a model based on lubrication theory to predict the stability of core annular flow. Rodriguez and Bannwatt (2008) proposed a stability model using an Inviscid Kelvin-Helmholtz (IKH) which provides a stability criterion that depends on Eotvos number. Kaushik (2012) carried out simulations on sudden contraction and expansion pipe and concluded that fouling can be minimised through such configuration. All these attempts are being suggested as means to get rid of fouling so as to encourage core-annular flow pattern but none has succeeded.

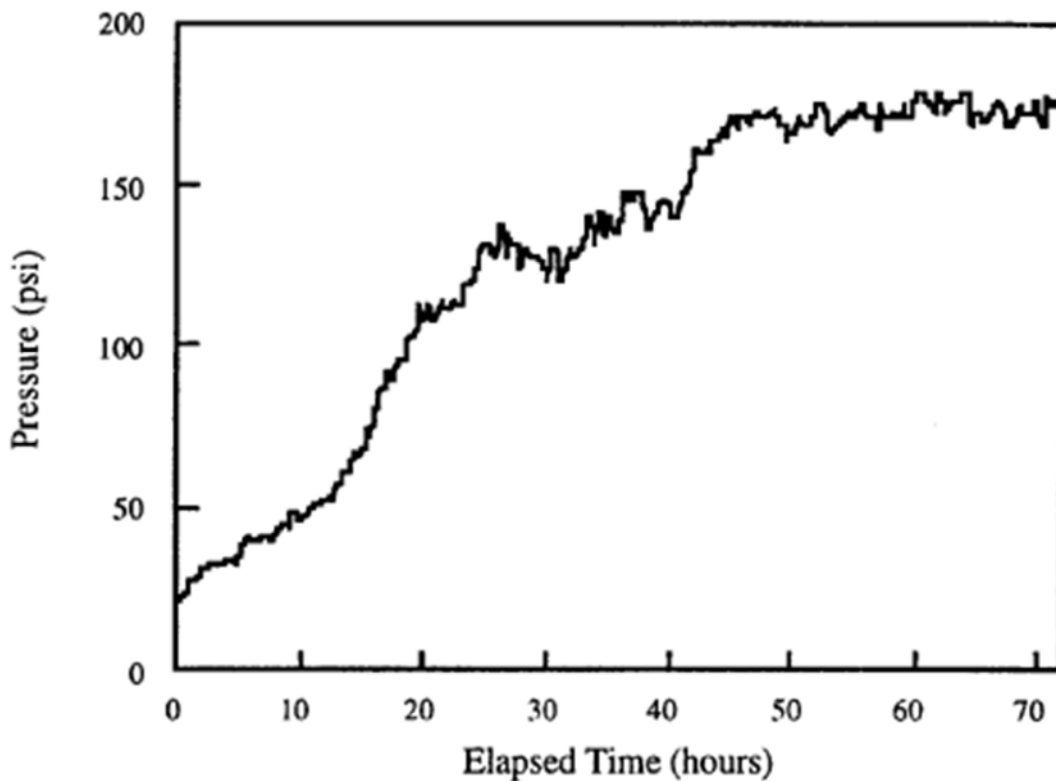


Figure 1-5: Flow behaviour of 1.15cP oil flow at 1.5m/s (Joseph et al., 1997)

Another important challenge that the Oil & Gas industries are facing is that of sand management. Sand management was reported to be a proven and workable method adopted in the improvement of conventional oil production from unconsolidated or poorly consolidated reservoirs (Tronvoll et al., 2001). However, there is no significant evidence to support this assertion in the co-production of heavy oil with water-sand in the horizontal pipe. Sand production, especially sand accumulation in horizontal wells was reported by Gillies et al. (1995) to be a major problem plaguing heavy oil operators. From the report, the petroleum industry spends millions of dollars each year to remove sand deposit in pipelines. This problem couples with the transport difficulty of heavy oil motivated this research to investigate the flow behaviour of high-viscous oil with water and sand in horizontal pipe using both experiments and CFD to explore the functionality and reliability of this technology.

1.2 Research Aim and Objectives

The aim of this research is to investigate the effect of water and water-sand on heavy oil based multiphase flow in 1-in internal diameter (ID) horizontal pipe.

In order to achieve the above aim, the objectives employed to understand this behaviour are to;

1. Investigate the sand minimum transport condition (MTC) in single phase water flow
2. Examine the effect of water injection on the behaviour of high viscosity oil flow at different flow conditions
3. Identify the flow patterns involve in this kind of multiphase flow using the trend plot and probability density function (PDF) of the pressure signals
4. Investigate the effect of oil viscosity on sand MTC in oil-water-sand flow
5. Explore the suitability and applicability of CFD simulation on the water-sand, high viscosity oil-water and high viscosity oil-water-sand flow characteristics

1.3 Organisation of the Thesis

In Chapter 2, a comprehensive review on heavy oil production methods, and both experimental and CFD studies of multiphase flow were presented. The chapter ends with a review of previous relevant numerical studies on the horizontal flows. In Chapter 3 a horizontal pipe flow loop facility and an experimental procedure for pressure drop measurements are described. The discussions of the data analyses employed are also presented. In Chapter 4, the CFD model developments with the turbulence selection criteria are presented with the preliminary results of single phase flow study. In Chapter 5, the results and discussions of water-sand flow study for both experimental investigations of water-sand flow behaviours in a horizontal pipe are reported, and simulated using Eulerian VOF approach in ANSYS FLUENT. Chapter 6 addressed both the experimental and numerical study of oil-water flow in 1-in ID horizontal pipe. In addition the design of the pipe inlet and turbulence model modification was considered. Chapter 7 presents Oil-water-sand flows in horizontal pipes, where the effect of the flow variable (flow rate) on the flow is investigated. The simulations focused on the adoption of turbulence model modifications used in Chapter 7 to predict the pressure gradient of the oil-water-sand and the flow patterns. Lastly, conclusions, contributions, and recommendations for future research are provided in Chapter 8. Further CFD parametric study of the effect of water density on oil-water flow was considered in the Appendix B with focus on the flow pattern and pressure gradients.

2 LITERATURE REVIEW

In this chapter, a comprehensive review on heavy oil production methods, experimental and theoretical studies on multiphase flow are presented. The production of heavy oil is the major challenge that is facing the oil industry, (and which is the basis of the motivation for this research), hence this literature survey presents the existing production methods, followed by experimental and numerical review of 2-phase water-sand, oil-water and 3-phase oil-water-sand flows in horizontal pipe configuration.

2.1 High Viscosity Oil

Heavy oil, extra heavy oil, and bitumen do not flow readily in most reservoirs, hence it requires specialized technologically intensive activities or methods to produce them, and their productions have been reported to be energy intensive when ‘unassisted’ because of their resistance to flow. This has forced different kinds of innovation to solving this problem in order to enhance increase in productivity at reduced cost. Some of the recovery methods have been reported to be commercially successful while others are for academic interest. Examples of the successful ones are those based on steam injection (Thomas, 2008). The recovery of oil and gas from the reservoir can be classified into primary, secondary and tertiary stages as summarised in Figure 2-1. In the primary recovery stage, the content is recovered by natural flow of the reservoir due to the expansion of the associated gases and water in the reservoir. This pushes the hydrocarbon content to the wellbore and to the surface facility. This is generally possible for gas and conventional oils.

The secondary recovery stage is a means of exploring artificial energy by re-injecting water (known as water flooding), gas or both into the reservoir to build the pressure for the flow to take place. Tertiary recovery, otherwise known as enhanced recovery, is a means of enhancing the mobility of the hydrocarbon content within the reservoir in addition to the secondary recovery stage. This can be achieved by introducing one or more mobility agent(s) like low viscosity oils, chemicals, microbes and heat through steam or combustion by injecting oxygen to enable ignition within the reservoir. Some

of the developed transport technologies are categorised into thermal and non-thermal/cold EOR as presented in Figure 2-2 (Thomas, 2008; Speight, 2009b).

2.2 Production Methods

This section presents description of the existing production being employed for heavy oil. These methods are classified into two major groups namely, thermal and non-thermal enhanced oil recovery.

2.2.1 Thermal EOR

Most of EOR methods are thermal related and have been proven to be effective. These have been in used since 1950's. The mechanisms of this method involve reducing heavy oil viscosity and improving the mobility ratio. Some of them are explained below:

2.2.1.1 Steam flooding

This is a main type of thermal stimulation of heavy oil reservoirs for EOR which has gained a commercial acceptance. In this case, a separate well is used as steam injection well while others are used for oil production. This method employs two different mechanisms; the heat transfer from steam to oil in order to decrease the viscosity to

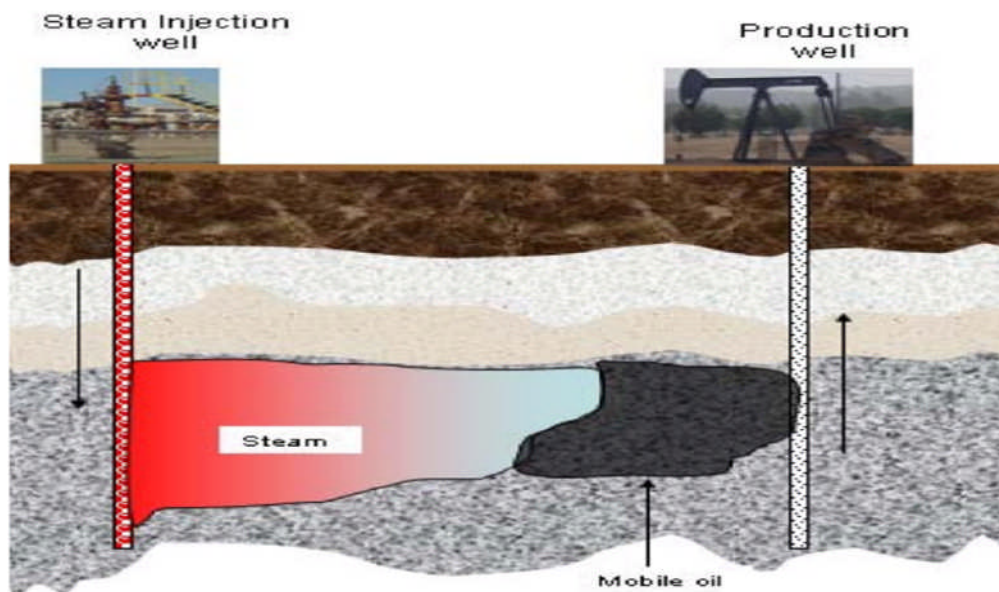


Figure 2-1: Steam flooding (Veil and Quinn, 2009)

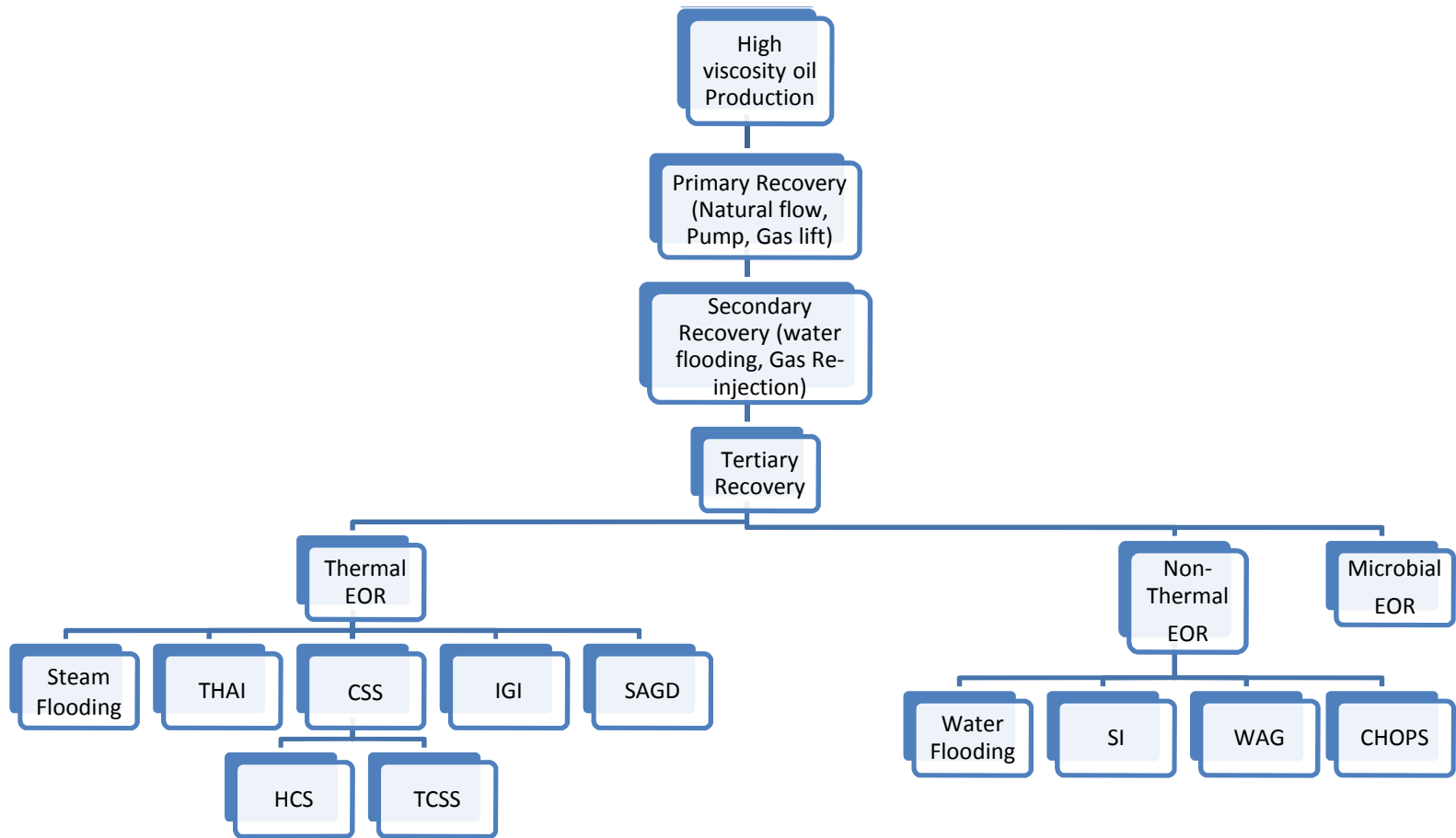


Figure 2-2: Production Technology of High viscosity oil

enable fluidity and the flooding mechanism which generates a push to the production well. A schematic diagram of this phenomenon is shown in Figure 2-1. This method largely depends on energy to raise the steam, the pattern size and geology.

2.2.1.2 Cyclic steam stimulation (CSS)

This method was accidentally discovered by Shell in Venezuela when it was doing a steam flooding. One of its steam injectors blew out and ended up producing oil at much higher rates than a conventional production well in the same environment. This method employs three stages; the injection, soaking and production. The well is injected with steam and left to soak the oil for a certain amount of time to heat the oil in the surrounding reservoirs to a temperature at which it can flow. This increases the reservoir pressure and the artificial lift is used to produce the oil. This method is not a continuous type and production is bound to fall when the temperature falls.

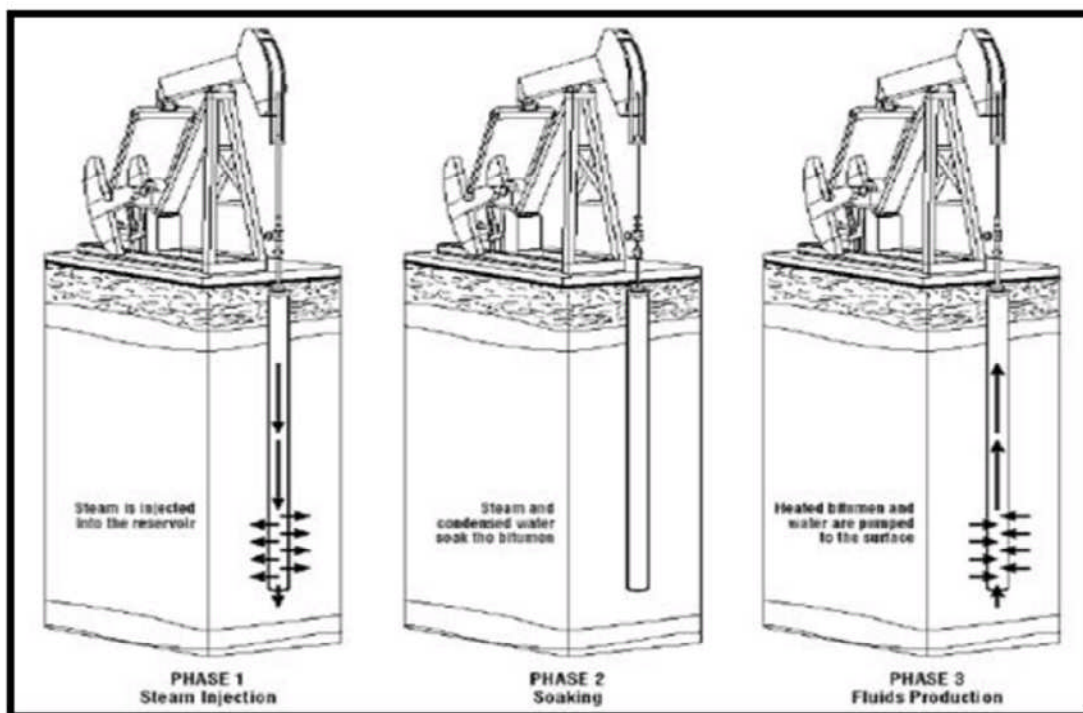


Figure 2-3: Traditional cyclic steam stimulation (Speight, 2009b)

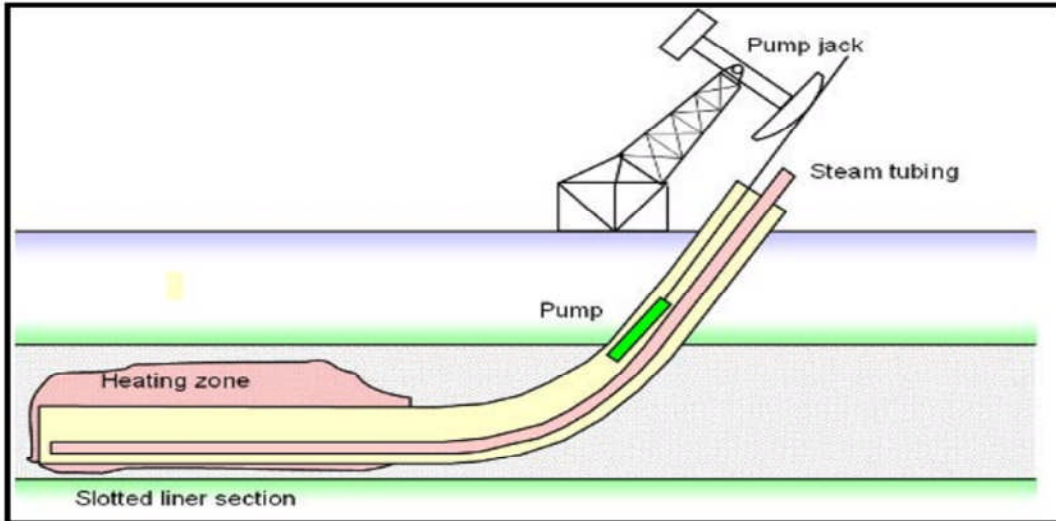


Figure 2-4: Horizontal cyclic steam stimulation (Veil and Quinn, 2009)

2.2.1.3 Steam Assisted Gravity Drainage (SAGD)

This method is a form of a steam flooding but differs by employing two horizontal wells being drilled a few meters above the other. In this case steam is injected through the upper well with the intention of reducing the viscosity of the heavy oil to the point where gravity pulls it down to the production well (lower horizontal well).

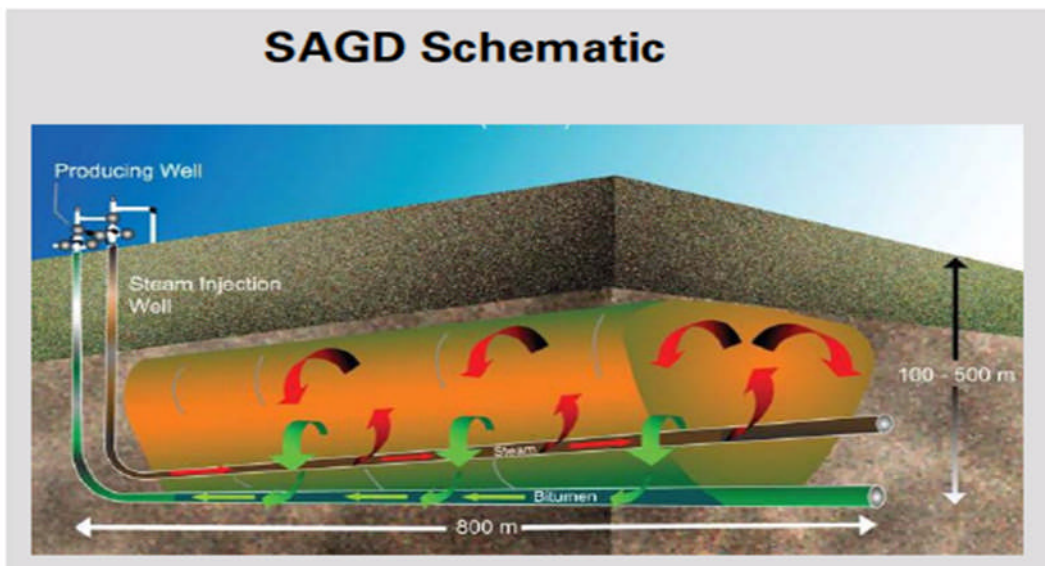


Figure 2-5: Steam assisted gravity drainage (Veil and Quinn, 2009)

2.2.1.4 Inert Gas Injection (IGI)

This method involves injection of gas at the top of the formation in the reservoir to create air-oil interface which forces heavy oil slowly down towards long horizontal production well located near the bottom of the formation.

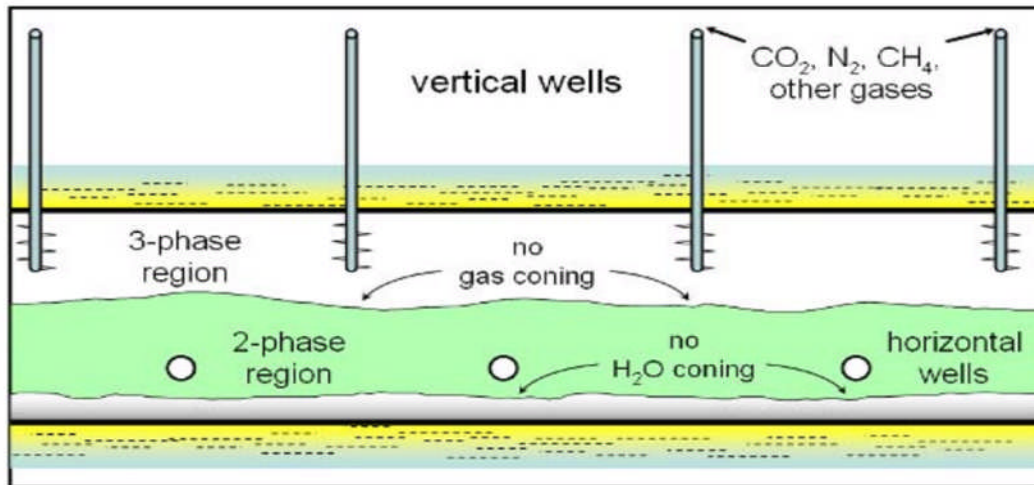


Figure 2-6: Inert gas injection (Veil and Quinn, 2009)

2.2.1.5 Toe-to-Heel Air Injection (THAI™)

This is an in situ combustion method that utilizes a combination of a vertical well and a horizontal well which are placed strategically to suck the mobilized oil. The vertical well is the injector well while the horizontal well is the producing well. The ignition or slow oxidation is initiated by the injected compressed air from the atmosphere to burn a portion of the oil in the reservoir. The ignition of the heavy oil generates high temperature in a range of 450-600°C which reduces the viscosity of the oil and enables it to flow from toe to the heel of the horizontal well (Thomas, 2008).

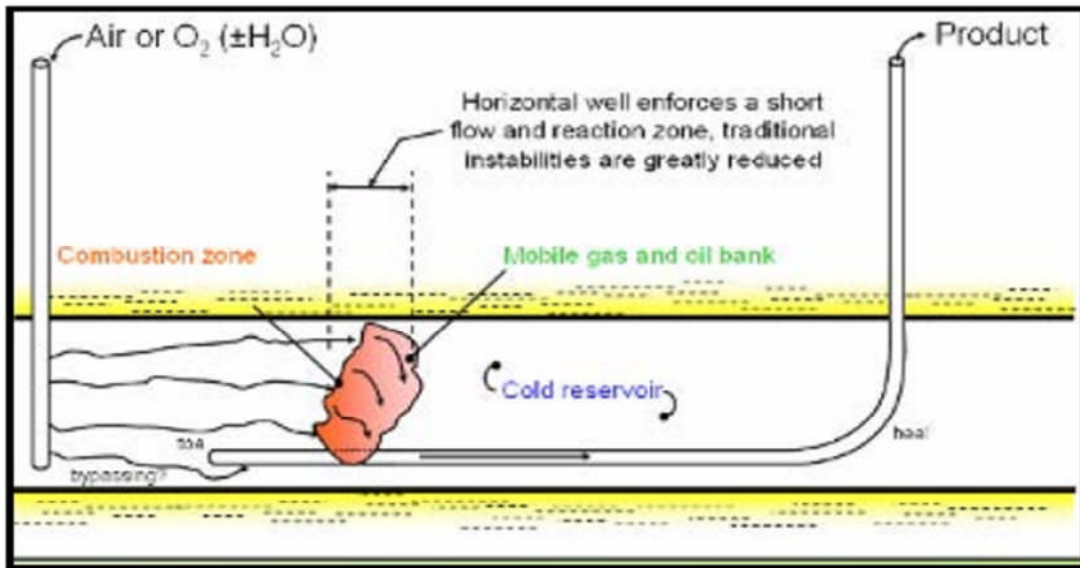


Figure 2-7: Toe-to-Heel Air Injection (Veil and Quinn, 2009)

2.2.1.6 Vapor-Assisted Petroleum Extraction (VAPEX)

VAPEX is a recovery method in which hydrocarbon solvents are injected into the upper well to dilute the bitumen and allow it to flow into the lower well instead of steam in SAGD. It has the advantage of much better energy efficiency than steam injection and it does some partial upgrading of bitumen to oil right in the formation.

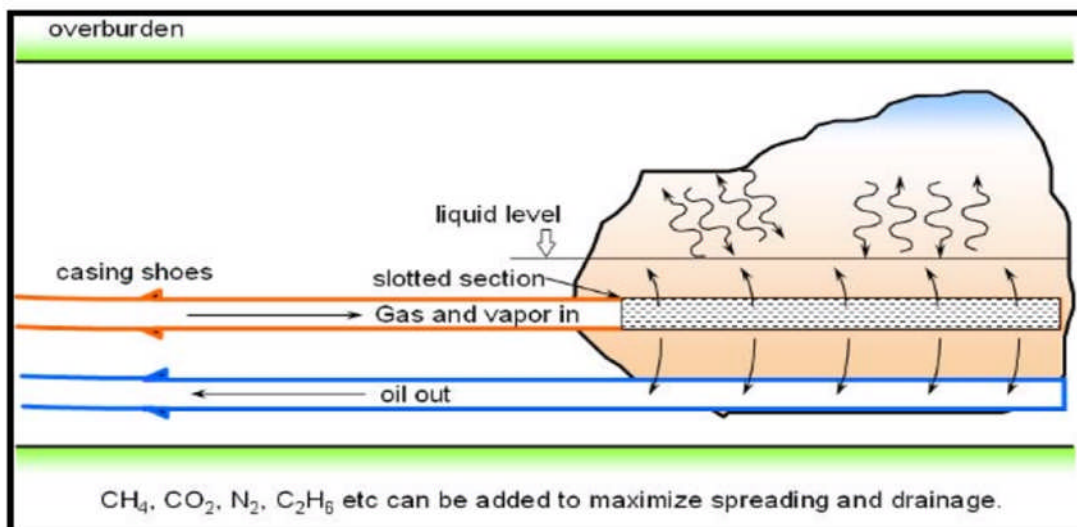


Figure 2-8: Vapour assisted petroleum extraction (Veil and Quinn, 2009)

2.2.2 Non-thermal EOR

This method excludes the use of heat to enhance the production of heavy oil by aiming at lowering the interfacial tension and improving the mobility ratio (Thomas, 2008). This was also reported to be applicable mainly to moderately viscous oils (<2000cP) where thermal methods are not suitable. Most non-thermal methods are still under study for its suitability to recover highly viscous oils. Some of these methods are discussed below:

2.2.2.1 Solvent Injection (SI)

Solvent injection is a type of recovery method in which hydrocarbon or non-hydrocarbon solvents are injected into a heavy oil reservoir to reduce the interfacial tension, to reduce its viscosity through molecular diffusion (Jha, 1986; Das and Butler, 1996) to aid the miscibility and mixing of oil and gas and to enhance the swelling of the oil phase in the reservoir (Yang and Gu, 2006). Munroe (2009) reported that when solvent is being used it gets heavier, thus reduces the quality of the extracted crude, however, carbon-dioxide is employed to erase this problem. In the same vein, solvent extraction is directly tied to the density of the solvents and different solvents are produced with respect to changes in pressure and temperature. This method is also limited by the cost and the recovery of the solvent.

2.2.2.2 Water Alternating Gas (WAG)

This is a method in which two separate mechanisms (i.e. water-flooding and gas injection) are combined to recover heavy oil under miscible and immiscible conditions. It is generally believed that both sweep efficiency and microscopic oil displacement can be improved through this method, however, some factors like wettability of the rock, fluid properties, miscibility conditions and injection techniques contributes to its limitation (Surguchev et al., 1992).

2.2.2.3 CHOPS

CHOPS is known as the most energy efficient as at present, because temperature needs not to be raised to assist heavy oil movement (i.e. only water influences the reduction of pressure losses) compared to other methods of assisting the flow. Pumping out sand with the oil has also been observed to be responsible for more oil to reach the wellbore. It is believed that sand displacement in the reservoir creates open "wormholes" in the reservoir formation which

gives room for associated gases to expand and force the oil to the wellbore. The advantage of this method is better production rates and recovery (around 10%) while the disadvantages are about the issue of disposing the produced sand and the treatment of the water when it gets to the surface in order to be fit for the environment or reuse.

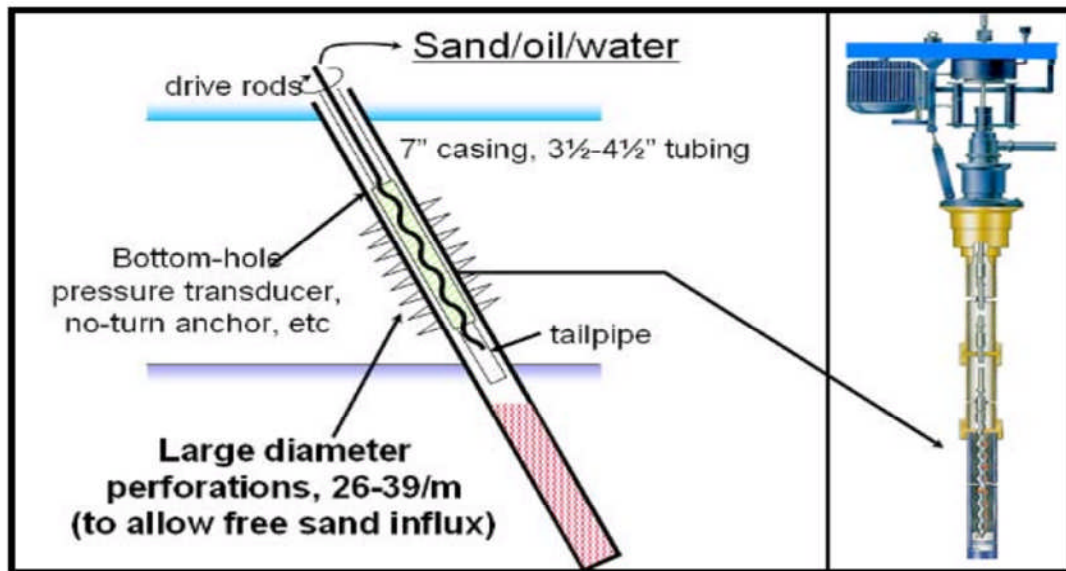


Figure 2-9: Cold Heavy Oil Production with Sand (Veil and Quinn, 2009)

2.3 Multiphase Flow Studies

Multiphase flow is encountered in various industrial processes from the biochemical, chemical, construction, food, mining, Oil & Gas, petrochemical, pharmaceutical, pollution control, and power generation. In Oil & Gas industries, this application includes the transportation of sand, oil water and gas mixtures in horizontal or/and vertical pipes. Multiphase flows are of great interest to a large variety of industries.

2.3.1 Experimental study of multiphase flows

Two-phase solid-liquid, liquid-liquid and three-phase liquid-liquid-solid are part of the branches of multiphase systems that are important to the Oil & Gas industries. The solid-liquid and liquid-liquid-solid are important because solid transport in pipelines could cause a huge loss of production if not properly managed. From experience, Peysson (2004) reported

that understanding of the mechanism of solid transport in multiphase flow lines has direct impact on the design, detailed analysis and estimation of new generation of horizontal oil wells. It has also been observed that most of the published research to-date on multiphase flows in pipeline focused on the dynamics of two-phase liquid-solid or liquid-gas, and three phase liquid-liquid-gas transport, limited research were reported on the simultaneous transport of three-phase flow containing solid particles in liquid-liquid flow in horizontal pipes.

Determination of flow patterns of two-phase flow is a key analysis that has long been employed to monitor the multiphase flow configuration that gives the optimum and beneficial flow condition. This is important because mixtures of fluids are frequently encountered in pipes. The conditions of flow may cause the fluid mixture to arrange itself in different geometric configurations. These configurations are usually referred to as flow patterns or regimes. The role played by gravity, and the density difference between the fluids are believed to be major factors influencing these regimes of multiphase flows in pipes. Many flow patterns/regimes have been named in horizontal, inclined and vertical pipe orientations by different researchers for 2-phase gas/liquid, liquid/liquid and liquid/solid flow in pipes. This is necessary because different flow patterns/regimes arise from different flow conditions. They have their advantages and disadvantages, and are important consideration for the design of facilities for their operations. The survey on the flow regimes of both 2-phase and 3-phase are presented in sections 2.3.2 and 2.3.3.

2.3.2 Two-phase flows

Two phase flow is a kind of multiphase flows in which two phases are simultaneously flowing together, either co-currently or counter-currently.

2.3.2.1 Water-Sand flow

Sand transport has been a long-standing issue in the oil and gas industries which has attracted solutions like pigging and sand exclusion. Production losses and reduction of well life-time production are parts of the disadvantages of these methods of sand control. However, sand management approach, which allows sand to be transported with other fluids from the

reservoir, has proven to increase production performance and reduction of execution cost. It also increases the life-time of wells. On the other hand, this does not hold without its own problems; sand deposition which leads to pipe corrosion occur when the flow rate is low, and even cause pipe blockage, and at the other extreme, when the flow rate is high erosion of the pipe becomes unavoidable. These challenges in slurry pipelines led to the study of the minimum transport condition (MTC) for sand in pipes of different configurations, ranging from horizontal to vertical in order to prevent sand deposit in pipes.

Water-Sand flow regimes

The design of pipelines relies on empirical correlations obtained from the experimental data. These empirical correlations are prone to uncertainty as conditions deviate from the database that supports them. Few experimental data within limited variable conditions are available because of the difficulties in the measurement techniques. Hence there is need for good understanding of the sand behaviour in both single and two-phase flow in the pipeline.

Several researchers reported lack of data on the flow behaviour of solid-liquid (e.g., Lareo et al., 1997(a); Fairhurst, 1998; Fairhurst et al, 2001; Chakrabandhu and Singh, 2005; and Legrand et al, 2007). Lack of sufficient data may be due to the fact that solid-liquid flows are usually complex and their behaviours are governed by a number of factors which gives rise to a range of flow regimes. Amongst such factors are particle size, density, concentration, flow rate, pipe diameter, orientation, and the physical and rheological properties of the carrier fluid. A major factor which influences the flow behaviour of solid-liquid mixtures is the rheological properties of the carrier fluid; this present study acknowledged that the rheological properties of crude oil, (i.e. oil with high viscosity) with the presence of other fluids in the production of heavy oil from the reservoir might make data of pure carrier fluids, like water to be far from the real life flow behaviours. Most of the documented data on solid-liquid flow relate to water-based slurries of fine particles. The common flow regimes that have been identified in the pure carrier fluids, most especially water, are shown and described in Figure 2-10;

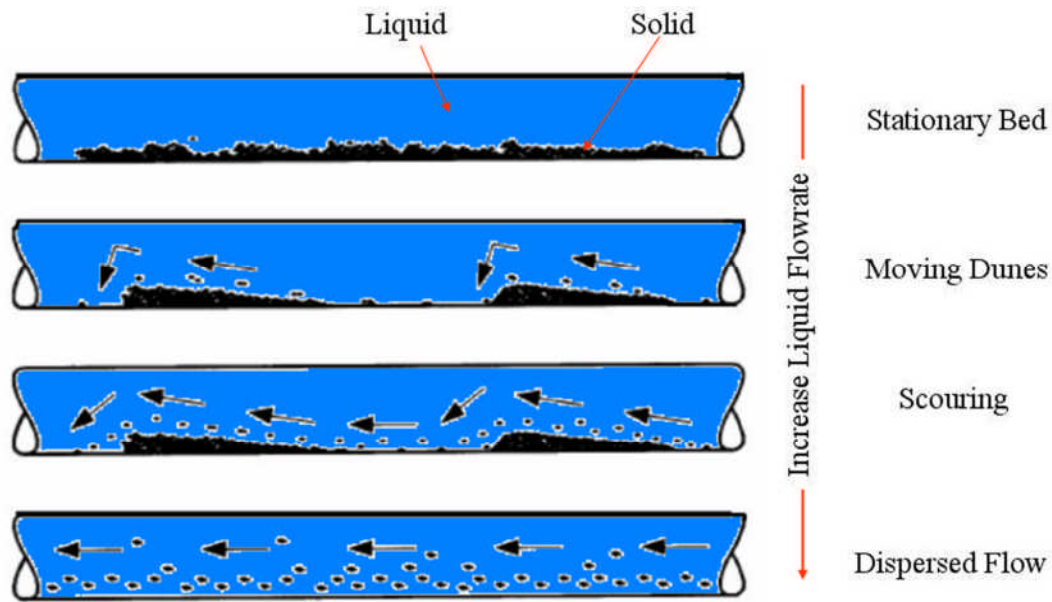


Figure 2-10: Solid-liquid flow regimes in horizontal pipe (Multiphase design handbook, 2005)

i) Stationary bed

A stationary bed is formed with sand particles at the bottom of the pipe with no grains moving when the slurry velocities are very low (Figure 2-10 and Figure 2-11). When the velocity is increased, a stable bed height is reached where the particles at the top are transported further downstream to increase the length of the bed. The upper surface of the sand bed is flat at very low flow rates but becomes wavy as the flow rates increase. The height of the stationary bed decreases at higher liquid flow rates. An equilibrium sand bed is reached when the shear at the upper surface of the bed transports sand downstream at a rate equal to the sand inflow rate.

ii) Moving dunes

The bed breaks up and the particles arrange themselves into moving dunes when the liquid flow rate increases (Figure 2-10). The grains on the upper surface of the dune roll along from back to front (downstream) and those grains then fall into the sheltered region at the front of the dune forming an additional part of the dune. Hence, the dune moves over these particles until they are once again appear at the tail of the dune and also migrate again on the top surface. Smaller dunes have been reported to move faster than larger.

iii) Scouring

As the slurry velocity increased further the grains roll along the top of the dunes with sufficient momentum that they escape from the sheltered region downstream and are swept away as individual scouring grains (Figure 2-10). Dunes can still survive in this environment by replenishment from upstream particles.

iv) Dispersed

The dunes are dispersed at high liquid flow rates (Figure 2-10 and Figure 2-11). The sand particles became evenly distributed in the carrier fluid. This is otherwise known as homogenous flow. However, a good concentration gradient is usually observed.

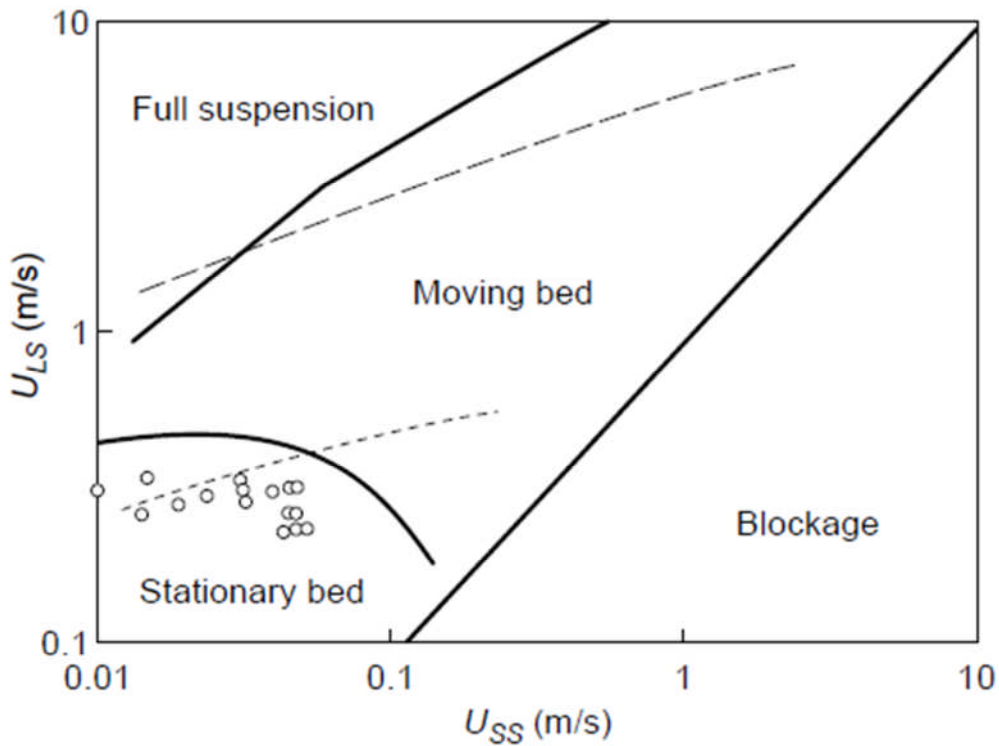


Figure 2-11: Liquid-Solid flow map (Doron and Barnea 1996)

Table 2-1: Survey of experimental study on water-sand flow

Author	Pipe Diameter (mm)	Inclination (°)	Particle Diameter (mm)	Slurry condition (%)	Carrier Viscosity (cP)	Instrumentation	Measurement
Thomas (1979)	9.41 - 105	0	0.095, 0.13, 0.155	12	0.8 - 95	Visualisation	Deposition Velocity
Takahashi (1989)	49.7	0	2.18 – 3.06	3.5 -12.5	1	Visualisation	Pressure, Velocity, Dunes' shape
Gillies (1995)	50	0	0.22		75, 7500	Visualisation	dP, Concentration
King et.al (2001)	152.4	-1.3 - +1.0	263		3, 150, 300	Visualisation	Velocity
Matousek (2005)	150	0 - 90	0.102 – 0.4	>35	1	Conductivity probe, MRI	Concentration
Eesa and Barigou (2008)	45	0, 90	2 - 10	<= 40	Non-Newtonian	PEPT dP transducers	Velocity profile, dP
Krampa (2009)	53.2	90	0.5 2.0	0 – 40 0 – 45	1	Conductivity L-probe, dP transducers	In-situ concentration, Velocity profile, dP
Yan et al. (2009)	50.8, 76.2 101.6	0 0 - 20	0.212	1 -10	1 - 200	Visualisation	Minimum Transport Condition (MTC)

Sand minimum transport condition

One of the key elements that have been considered by various researchers in the study of sand management is known as the sand minimum transport condition (MTC). The study of liquid-solid mixture flows that have been done by some researchers are summarised in Table 2-1 above. They explored the measurement of the minimum transport condition (MTC), in-situ sand concentration and pressure drop. Their studies cover a wide range of particle sizes. These studies have also benefited from the advancement of measuring techniques from intrusive to non-intrusive. However, the study of sand behaviour in multiphase phase flow has been limited to low viscosity carrier fluids, as it exists in conventional oil production.

Over the years, different researchers have given MTC different definitions; in 1952, Durand and Condolios defined MTC as the velocity at which sand particles can be transported without forming stationary bed. In this case, sand bed must have been formed at the bottom of the pipe but may be moving sand bed. Durand and Condolios' definition suggests a means to solve static sand bed problem, hence it is not a full preventive approach, since their proposition may end up as moving sand bed. Newitt (1955) referred to MTC as critical velocity required to move sand bed to suspension. Newitt's (1955) approach is similar to Durand and Condolios' definition except that sand bed may be either moving or stationary. Thomas' (1962) definition is adopted by British Petroleum (BP) for the designing of their pipelines. The definition states that MTC is the average stream velocity required to prevent the accumulation of a layer of sliding particles on the bottom of the horizontal pipe. Zand and Govatos (1967) discussed MTC as the critical transition velocity from saltation to heterogeneous flow. However, in heterogeneous flow, solids are not evenly distributed and concentration gradients exist across the pipe cross-section. When the velocity is reduced, the heavier particles become less uniformly distributed tending to concentrate towards the bottom of the pipe. On this premise, the definition of Zand and Govatos (1967) is not sufficient to prevent the accumulation of sand. Salama (1983) and Davies (1987) reported MTC as the minimum mean flow velocity requires to suspend particles in the carrier fluid in horizontal pipe flow. King (2000) shared the same view with Thomas (1962) and

defined MTC as mean stream velocity required to prevent accumulation of a layer of sliding particles at the bottom of horizontal pipe. Thomas' definition is adopted in this research because it is a transition between the region where sand moves in the mean stream and the region where it is formed as a moving layer at the bottom of the pipe. Although numerous researches exist on sand transport in water flow, lack of literature on the similar studies with the inclusion of high viscosity oil in the water-sand multiphase flows is enough drive to investigate the sand related flow in the oil-water-sand multiphase flow.

Although the research on solid-liquid 2-phase flow has been conducted for decades, it is obvious that they may not suffice for predicting solids in multiphase flows, most especially heavy oil and water. In addition, the measurement technique for monitoring this kind of multiphase flow has not matured. The existing measurement devices have not proven to be reliable to measure these phase behaviours in multiphase flows. For instance, one of the most recent measurement techniques, ECT fails to measure conductive fluid like water which is typically encountered in the Oil & Gas industry (Nooralahiyan et al., 1994; Beck and Williams, 1996). Hence there is need for more investigation on how to detect this multiphase behaviour. Pressure measurement can be employed with other measuring devices to improve monitoring of undesirable conditions which may have adverse effect on the flow system. This research aims at using analysed pressure signals to indicate or capture different behaviours of such flows.

Water-sand pressure gradients

Solid-liquid flows are usually encountered in oil and gas industries. Three of the major factors that are always important in the designing of the hydraulic transport systems are pressure, flow rate and flow regimes/patterns. Amongst these factors in fluid flow in channels, pressure measurement cannot be overlooked because of cost of pumping and safety of operations. The study of slurry behaviour in pipes has largely depended on empirical correlations and this is not surprising because the components of practical slurries vary in physical composition and properties. Some findings were made from the investigations of slurry flow in pipes, for example, Newitt et al. (1955) reported that the

contribution of the solid phase to the frictional loss in the pipe flow is the result of the particles immersed weight being transported to the pipe wall. Charles and Charles (1971) transported fine sand particles in shear thinning clay suspensions and reported head loss which was six times smaller compared to the result gotten when water was used as the carrier fluid. Ghosh and Shook (1990) reported a reduction in pressure gradient when a shear thinning CMC solution was used to transport fine sand particles, but not for larger pea gravel particles; this was attributed to the fact that these larger particles were conveyed in the form of a sliding bed and not as a suspension. All of these findings amongst others formed the basis for the development of the different correlations reviewed in section 2.3.5.5.

2.3.2.1 Oil-water flow

Most times the flows of two immiscible liquids are encountered in a diverse range of processes and equipment. In the petroleum industry, mixtures of oil and water are transported in pipes over long distances and accurate prediction of such multiphase flow characteristics, such as the desired flow pattern, water holdup, pressure gradient and flow stability are important in many engineering applications. Examples of relevant research on this type of flow are shown in Table 2-2. In spite of their importance, these characteristics have not been thoroughly explored to the same extent on heavy oil related flows as they have been explored in light-oil related flows.

Oil-Water flow regimes

A survey of literatures reveals that some studies have been done to identify the flow patterns or interfacial configurations occurring during the flows in pipes. The methods that are usually employed to describe flow pattern are based on the techniques, which have been noted to be effective for gas–liquid systems. Several researchers e.g. Russell and Charles, (1959); Charles et al., (1961), etc. have employed photography and visualization related techniques. These techniques appeared to be very effective under low-phase velocities but fail to identify the distribution at high flow rates of one or both the liquids (Chakrabarti et al., 2007), and also difficult to identify the transitions between the flow patterns. This approach is generally not the best because of its

subjectivity. In order to overcome these limitations, several researches are being embarked upon by researchers (see Table 2-3) on the design and use of measurement devices. Some of these devices are intrusive, and hence have limited applicability. The intruding part of these devices (i.e. conductivity, impedance and isokinetic probes) tends to give instantaneous response however, it becomes wetted/fouled, when it comes in contact with the organic phase, (i.e. oil,) and the results cannot be relied upon any more (Angeli and Hewitt, 1998). Due to this limitation, Chakrabarti et al. (2007) designed a non-intrusive optical probe to investigate the flow regimes of liquid-liquid (i.e. water-kerosene) 2-phase flow in 1-in ID horizontal pipe. Their results, when compared with Angeli and Hewitt (2000) and Lovick and Angeli (2004) showed a good agreement but with some deviations (as shown in the Figure 2-12) which was attributed to the differences in fluid density, viscosity and pipe diameter. However, Chakrabarti did not investigate the effect of oil film on the pipe wall to establish the suitability of optical probe for cases where oil film coats the pipe wall. This may serve as a major limitation to this non-intrusive sensor. The output of whichever instrument used is a collection of different flow patterns. In early experimental research, Russell et al., (1959) and Malinowsky, (1975) observed and reported four flow patterns while Oglesby (1979) observed and proposed that there were 14 different types of flow configurations.

Table 2-2 : Summary of 2-phase oil-water flow experiments in pipes

<i>AUTHORS</i>	<i>PHYSICAL PROPERTIES</i>					<i>VELOCITIES</i>		<i>ID</i>	<i>INCLINATION</i>	<i>FLOW PROPERTIES MEASURED</i>
	<i>Oil</i>		<i>Water</i>		<i>Interfacial tension</i>	<i>Oil</i>	<i>Water</i>			
	$\rho \text{ kg/m}^3$	$\mu \text{ cP}$	$\rho \text{ kg/m}^3$	$\mu \text{ cP}$	$\sigma \text{ mN/m}$	<i>m/s</i>		<i>m</i>	$^\circ$	
Vuong (2009)	884.4	230,440,1070	998	1		0.1 – 1.0		0.0525	0, 90	Pressure drop, water holdup
Grassi et al. (2008)	886	779@ 20°C	1000	1.3	50	0.02 – 0.7 0.1 – 2.5		0.021	-15 to +15	Pressure drop, water holdup Flow regimes
Rodriguez (2006)	830	7.5	1060	0.8	20.4	0.04-5.55		0.0828	0, ±1, ±2, ±5	Pressure drop, water holdup, slip ratio
Lum (2006)	828	5.5	998	0.993	40	0.07-2.78		0.038	-5, 0, 10	Pressure drop, water holdup, slip ratio
Abduvayt (2004)	800	1.88	1000	1		0.025-1.502		0.1064	±3, ±5 0, 5, 90	Pressure drop, water holdup, slip ratio
Elseth (2001)	790	1.6	1000	1.02	43	0.3-1.51	0.1-1.2	0.0563	0	Pressure drop, water holdup, slip ratio, Velocity

Alkaya (2000)	847.7	12.9	994.12	0.72	16.7	0.025-1.75		0.0508	±0.5,±1	Pressure drop, water holdup
									±2, ±5	
Angeli (1999)	801	1.6	1000	1	17	0.3-3.9		0.0243	0	Pressure drop
Nädler (1997)	841	31	998	1		0.014-1.44	0.009-1.48	0.059	0	Pressure drop
Trallero (1995)	884	28.8	1037	0.97	36	0.01-1.59	0.02-1.6	0.0501	0	Pressure drop, water holdup, slip ratio
Scott (1985)	754	1.38	998	0.894				0.0508	15	Pressure drop, water holdup, slip ratio
									30	
Cox (1985)	754	1.38	998	0.894		0.05-0.64		0.0508	-15 -30	Pressure drop, water holdup, slip ratio
Ooms et al. (1983)	970	2300, 3200, 3300	998	1		0.05-0.64		0.051, 0.2	0	Pressure drop, water holdup
Charles et al. (1961)	834	6.29, 16.8, 65	998	1	44, 45 ,30	0.01524 – 0.9144 0.03048 – 1.0688		0.0264	0	Pressure drop, water holdup

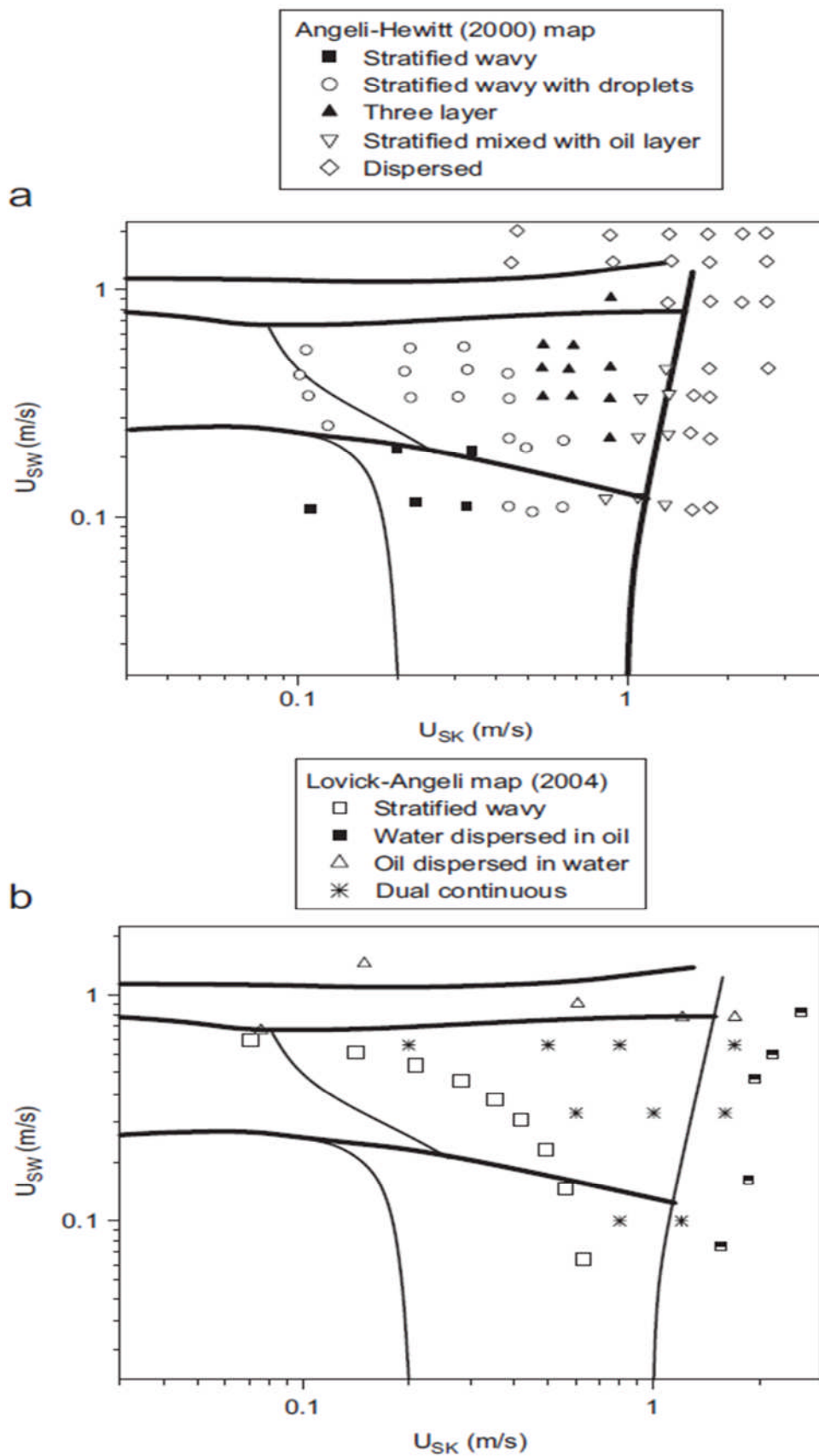


Figure 2-12: Comparison of Chakrabarti's results with existing flow regime data

Table 2-3: Survey of oil-water flow regimes studies

Authors	Measurement device	Diameter	Inclination	Oil viscosity	Flow regime
		(in)	(^o)	(cP)	
Vigneaux et al. (1988)	Impedance probe	7.87	0 – 65	-	Oil droplet in water
Valle and Kvandal (1995)	Conductivity probe	1.48	0	2.3	Stratified wavy
Nadler and Mewes (1997)	Conductivity probe	2.32	0	22 -35	Stratified with mixing at interface
Vedapuri (1997)	Isokinetic probe	3.98	0	2.0	Semi-mixed, Semi-segregated
Angeli and Hewitt (2000)	Impedance probe	0.94	0	1.6	Stratified wavy with drops
Lovick and Angeli (2004)	Impedance, conductivity probe	1.50	0	6.0	Dispersion of o/w, w/o
Jana et al. (2006a)	Conductivity	0.98	90	1.2	Bubbly, Core annular, dispersed

Most of the existing researches on liquid-liquid flow regimes in horizontal pipes have focussed on the low viscosity oil, and a number of flow patterns have been observed and reported. Example of these researches is that of Trallero (1995) which reported different flow patterns like smooth stratified (ST), stratified with mixing at the interface (ST&MI), plug, dispersed, and annular flow type (Figure 2-13).

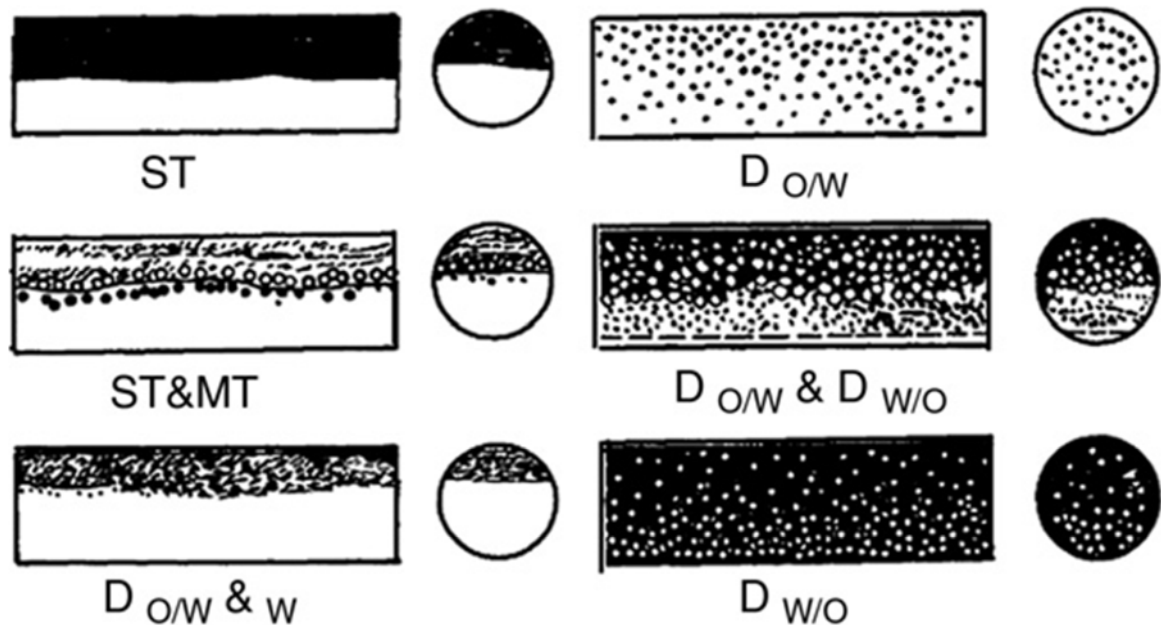


Figure 2-13: Oil-water flow patterns by Trallero (1995)

A typical flow regimes map of high viscosity oil-water distribution in horizontal pipe is illustrated in Figure 2-14 from the research of Sotgia et al. (2008). This map was developed from visualisation and photography. The observed and reported flow regimes are stratified flow (where the gravitational separation is complete); stratified-wavy flow; oil-in-water dispersed flow (where the oil droplets are dispersed in the water continuum); water-in-oil dispersed flow, core annular flow, wavy annular flow and oil slug flow. This latter category includes plug flow, in which there are large oil pocket flowing near the top of the tube.

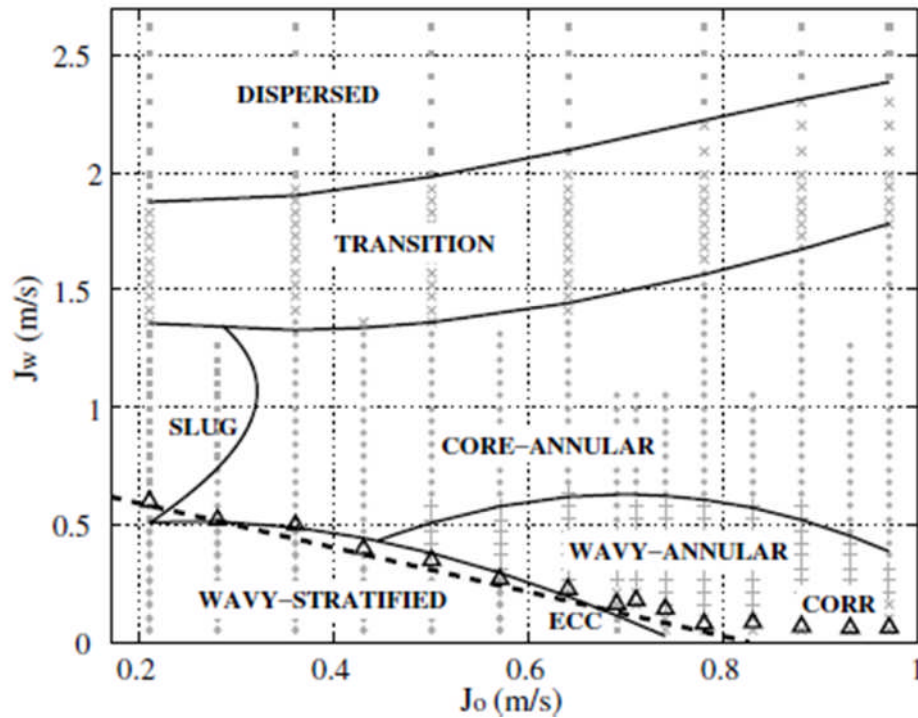


Figure 2-14: Flow pattern map of oil-water for the 26mm horizontal Plexiglas pipe (Sotgia et al., 2008)

i) Core annular flow

Core annular flow is a type of flow in which water is present on the pipe wall, forming an annulus around the oil while oil moves in the core of the pipe. This was defined theoretically by many researchers to be occurring at high velocities (i.e. high water cut) (McKibben et al., 2000a; Bannwart et al., 2004; Rodriguez et al., 2009). Oliemans (1987) carried out a test on core annular flow with 3000mPas fuel oil and water in a 5cm pipe and reported that the waves at the oil-water interface vary with water fraction and oil velocity. In 1990, Bai identified a bamboo wave pattern in upward flow as a result of buoyancy of oil which makes it lighter and therefore stretched while in the downward flow the oil is compressed and formed corkscrew waves; this appeared to be different from the existing patterns in horizontal flows.

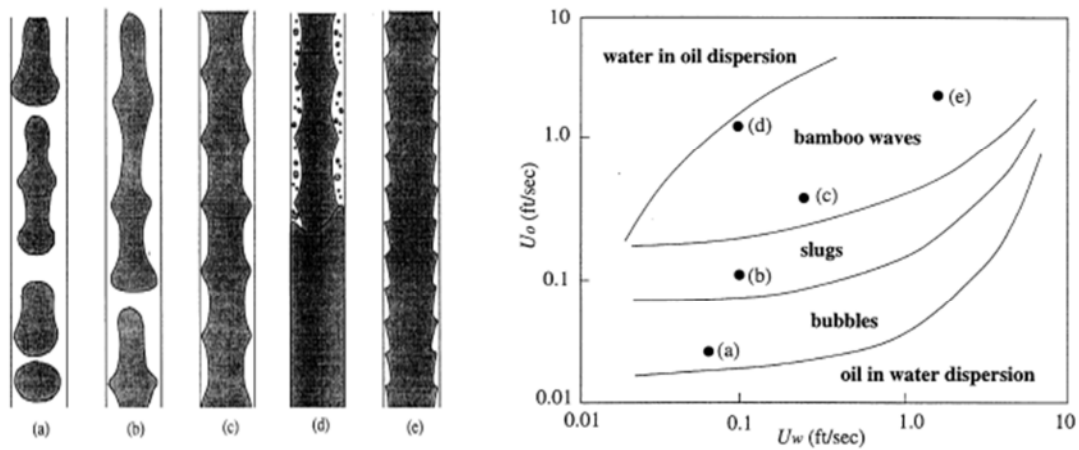


Figure 2-15: Schematic diagram and flow map of up-flows in vertical pipe (Joseph et al., 1997)

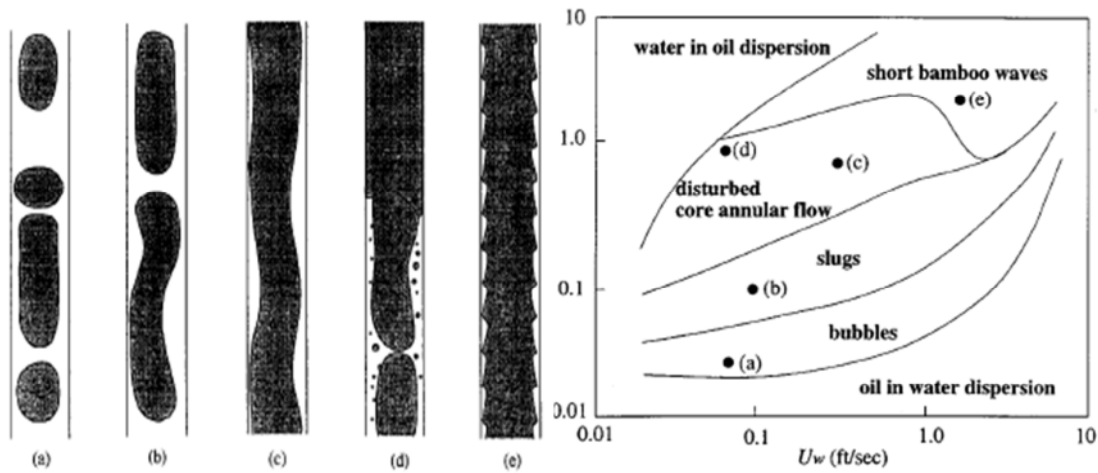


Figure 2-16: Schematic diagram and flow map of down-flows in vertical pipe (Joseph et al., 1997)

Figure 2-15 and Figure 2-16 above show the schematic diagram of upward and downward flows, as well as the flow map as presented by Joseph (1997) and Renardy in 1997. The diagrams and flow map for horizontal flow types are also presented in Figure 2-17 and Figure 2-18. (The flow is from right to left). These patterns are explained by the flow maps.

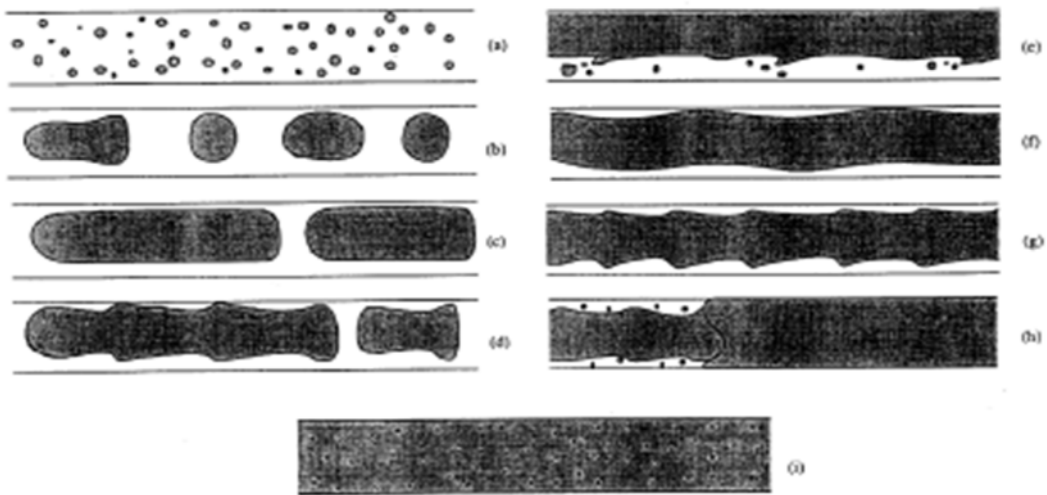


Figure 2-17: Schematic diagram and flow map of flow types in horizontal pipe (Joseph et al., 1997)

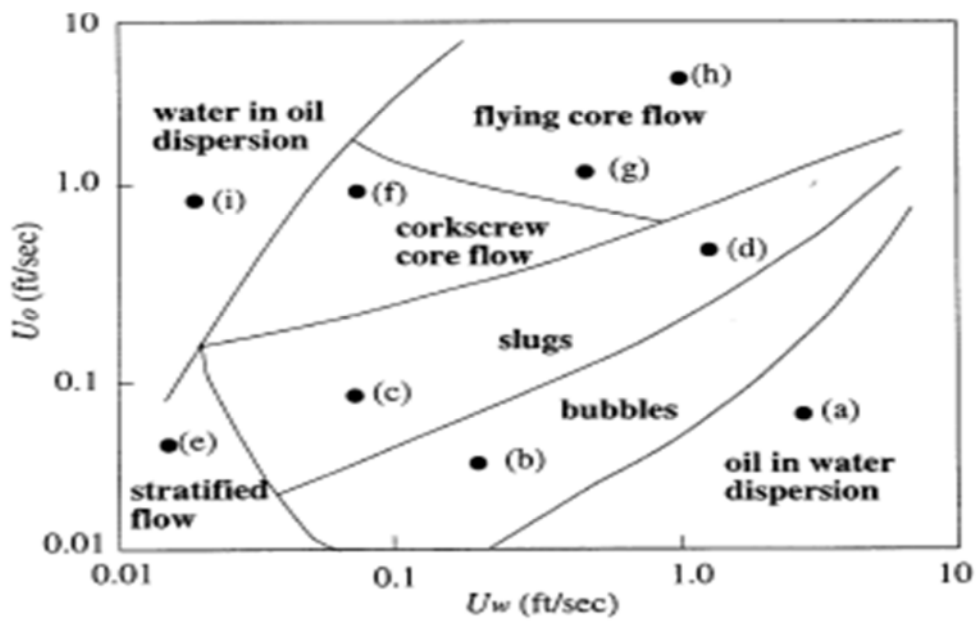


Figure 2-18: Schematic diagram and flow map of flow types in horizontal pipe (Joseph et al., 1997)

Design of pipe inlet condition for flow initiation

In literatures, different inlet designs were adopted by the researchers to study the oil-water annular flow (Sotgia et al., 2008; Prada and Bannwart, 2001b; Bensakhria et al.,

2004a; Balakhrisna et al., 2010a; Strazza et al., 2011). This approach was attempted to impose the core annular flow behaviour.

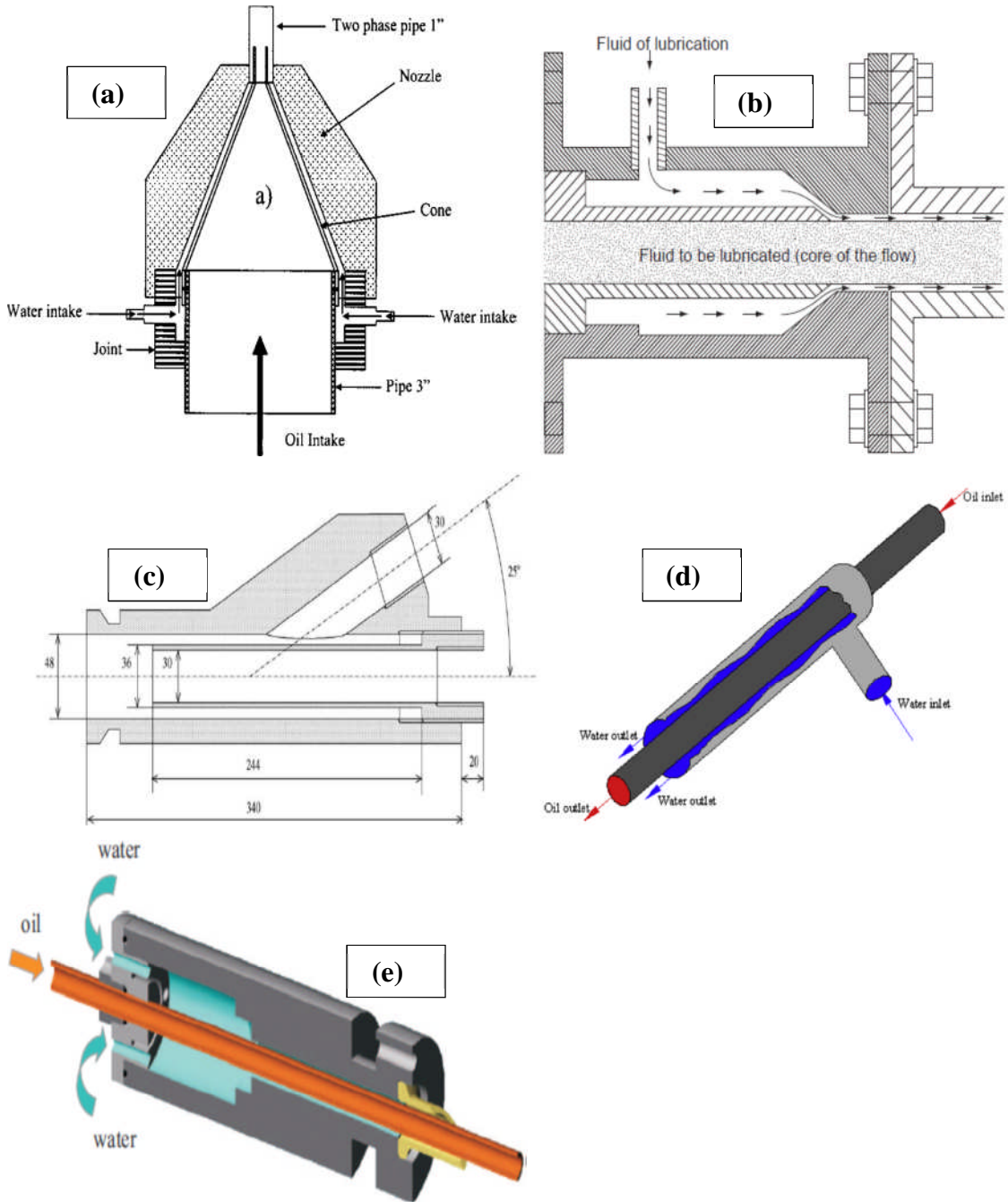


Figure 2-19: Experimental annular flow inlet geometry designs (Sotgia et al., 2008; Bensakhria et al., 2004a; Strazza et al., 2011; Prada and Bannwart, 2001c; Balakhrisna et al., 2010b)

Hasson (1970) designed a nozzle that made the flow path of the wall liquid narrowed gradually. They reported that the symmetrical position of the nozzle was more effective and that their design reduced the inlet disturbances. Prada and Bannwart (2001a) designed a conical injector nozzle to describe lifting of heavy oil from vertical wells. The nozzle injected water laterally to put the oil at the centre of the pipe while the inlet diameter gradually reduced to match the pipe diameter. Bensakhria et al. (2004a) used an injector which introduced water in the annulus while the heavy oil passed through the core region.

Figure 2-19 presents different inlet geometries that have been designed to establish core annular flows. These various designs were used to achieve core annular flow but none gave report on the effective inlet diameter of the oil injector at the entrance.

ii) **Water assist flow**

This is a kind of oil-water flow behaviour that exists at low water-to-oil ratio (velocities). Mckibben et al. (2000b) found out that at low velocity water travels as large slugs in the oil, while oil is present at the pipe wall and yet the frictional pressure gradient was reduced by an order of magnitude. In this case, a significant amount of oil is being transported by the water slug. They discovered that the reduction in pressure drop observed was not due to water movement on the pipe wall, so this phenomenon was termed water assist flow. This phenomenon has not been properly explored nor fully understood.

Phase Inversion in Pipe Flow

One of the important features of two-phase oil-water flow is the phase inversion phenomenon; this is a phenomenon where a small change in the operating condition causes the dispersed phase oil in water (DOW) to change to the continuous phase and vice versa (DWO) (Brauner and Ullmann, 2002). Phase Inversion Point (PIP) was defined by Selker and Sleicher (1965) as an ambivalent range of volume fractions of a phase above which that phase is always continuous and below which that phase is always dispersed. In the ambivalent range, either one of the two phases can be the dispersed phase. PIP is a major factor to be considered in pipeline design because of the rheological characteristics of the dispersion and the associated sudden pressure drop that

is involved (Arirachakaran, 1989). It is a volume fraction at which the dispersed phase will change to become the continuous phase. Many researchers have reported this phenomenon from oil-water experiments carried out in stirred tanks, and several investigations have been conducted on this phenomenon in batch mixers (Quinn and Sigloh, 1963; Norato et al., 1998; Groeneweg et al., 1998), as well as continuous mixers (Tidhar et al., 1986), also including column contractors (Sarkar et al., 1980) and pipe flow (Arirachakaran et al., 1989; Nädler and Mewes, 1997), in order to characterize the effect of the critical volume fraction on the various system parameters like operational conditions, system geometry and materials of construction. However, the knowledge accrued from the studies on the phase inversion in pipe flows is limited to the relatively low viscosities.

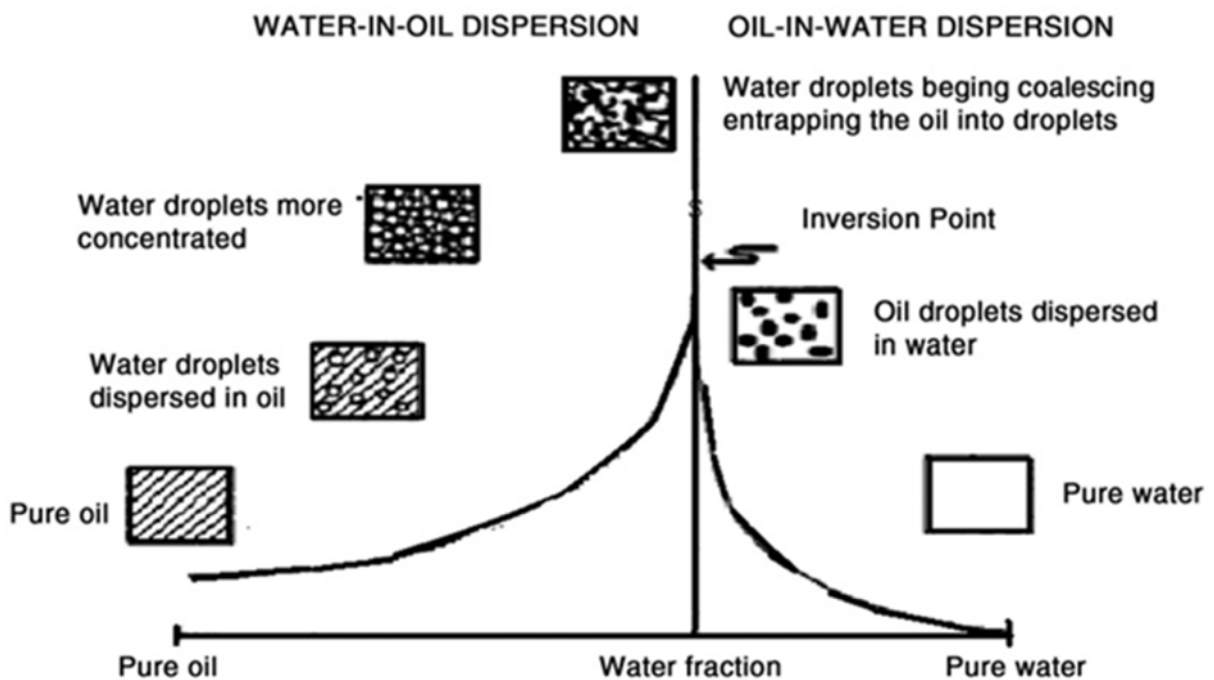


Figure 2-20: Description of phase inversion (Arirachakaran et al., 1989b)

Selker and Sleicher (1965) proposed that the tendency of oil to be dispersed increased by increasing the oil phase viscosity and also the minimal oil volume fraction that can be continuous and its maximal volume fraction that can be dispersed increased. They reported that the widest ambivalent range occurred for liquids of about the same

viscosities. Norato (1998) found that an increase in the viscosity ratio will widen the ambivalent range.

Kumar (1991), Norato (1998) and Yeo (2002) amongst many researchers stated that the ambivalent range is suggested to be influenced by other factors, such as the stirring speed, the wetting properties of the container material, liquids densities and surface tension. All these factors, as well as the initial conditions, were found to have a role in determining the location of the phase inversion. Arirachakaran et al. (1989) observed and reported that the pressure drop changes dramatically at the PIP, and schematically presented how the phase inversion process takes place by using Figure 2-20. Arirachakaran et al. (1989) further reported that as the water droplets became more concentrated and started to coalesce, the water became the continuous phase and the inversion occurred at the maximum apparent viscosity, but after the PIP, the apparent viscosity dropped significantly because water became the continuous phase. It was also reported that as the viscosity ratio increased (i.e. oil-to-water), the water fraction required to cause an inversion decreased. Angeli and Hewitt (1999) found that at high mixture velocities, where dispersed flow patterns prevail, there is a peak in pressure gradient during phase inversion and an apparent drag reduction effect when oil is the continuous phase. They inferred, from their research that the pipe material (wettability) has effect on the PIP.

Xu (2007) stated that the mathematical approach to predict phase inversion point has been universal rather than accurate, since the phenomenon has yet not been clearly and fully understood. Hence, different researchers have come up with different models. Such models were developed by Arirachakaran et al. (1989), Yeh et al. (1964) and Brauner and Ullmann (2002) and are given in Equations 2-1, 2-2 and 2-3 respectively by

$$\varepsilon_w = \frac{1}{1 + (\mu_o/\mu_w)^{0.5}} \quad 2-1$$

$$\varepsilon_w = 0.5 - 0.1108 \log_{10}(\mu_o/\mu_r) \quad 2-2$$

$$\varepsilon_w = \frac{1}{1 + \frac{\rho_o}{\rho_w} \left(\frac{\mu_o}{\mu_w}\right)^{0.4}} \quad 2-3$$

where ε_w , μ_w , μ_o , ρ_w and ρ_o are critical water cut, water viscosity, oil viscosity, water density and oil density respectively, while $\mu_r = 1\text{mPas}$. Xu (2007) commented that this transition phenomenon is usually associated with sudden change in the rate of heat, mass and momentum transfer between the continuous and dispersed phase and also between the dispersion and the system solid boundaries. Wang and Gong (2009) submitted that the main principle that cause phase inversion is the imbalance between breakup and coalescence of droplets in oil and water dispersion and that the breakage and coalescence forces are due to turbulent and viscous shear during two-phase pipe flow. The universality of these experimental studies and phase inversion models, however, are not yet proven for high viscosity based oil-water flow in horizontal pipe. This research intends to verify the efficacy of the popular phase inversion models with respect to heavy oil based oil-water flow.

Oil-water pressure gradients

Since 1950s the effect of water co-flow with oil has been reported to result in the pressure gradient reduction. Arney et al. (1993) measured pressure drop for water lubricated transportation of oil in a 15.9 mm diameter glass pipeline. Angeli and Hewitt (1998) performed measurements on the flow of a low viscosity oil and tap water in two 25.4-mm pipes of acrylic resin and stainless steel and they observed a large difference between pressure gradients measured in the two pipes and attributed the effect to different wettability characteristics of the pipe walls.

Table 2-2 shows the list of experimental research that has been done by various researchers on oil-water flow in pipes which includes the measurement of pressure drop since 1961. The oil viscosity considered in all these research ranges from 1.38 to 3300cP, while the pipe diameter used ranges from 1-in to 8-in ID. Sanders et al. (2004)

reported that measurements of pressure gradient, water holdup, and visual observations revealed that froth containing lower total water content yielded less free water to the lubricating layer. In the froth rheometer, the conditions for which stable, self-lubricated flow could be maintained were comparable to those required to maintain self-lubricated flow in the 25 mm pipe loop.

2.3.3 Three-phase flows

Three-phase flow is another type of multiphase flows in which three different fluid components are being transported together. This type of multiphase system is common in the Oil & Gas industries, either as gas-liquid-solid, gas-liquid-liquid, liquid-liquid-solid and so on. In this section, attention is given to three-phase liquid-liquid-solid (oil-water-sand) flow in pipes.

2.3.3.1 Oil-water-sand

Most of the published research to-date on multiphase flows in pipeline focused on the dynamics of two-phase liquid-solid or liquid-gas and few three phase liquid-liquid-gas transport. Studies by Acikgoz (1992), Taitel (1995), Chen and Guo (1999), Keskin (2007) and Bannwart (2009) provide information on researches on oil-water-gas flow investigations. Very limited researches were reported on the simultaneous transport of three-phase flow containing solid particles in liquid-liquid flow in pipes. The lack of publications on liquid-liquid-solid could be attributed to the complexity of this flow type.

Flow regimes of 3-Phase oil-water-sand flow in pipe

Lack of the published research on the flow regimes of three phase liquid-liquid-solid flow in pipes is enough proof of its complexities. The mechanisms of liquid-liquid-solid flow in pipes are not yet understood.

MTC of 3-Phase oil-water-sand flow in pipe

The tendency for sand accumulation or deposition in horizontal pipe is one of the major concerns of the crude oil production in the oil and gas industries. This has been a serious problem which was observed in the transport of conventional oils (i.e. low viscosity oil) in both the horizontal and dip pipe configurations. Although sand accumulation in pipes is a serious problem, it has been generally reported that co-production of oil with sand improves productivity up to an order of magnitude. There is possibility of sand deposit in pipes, however McKibben (2006) stated that relatively high velocities are needed to ensure that turbulent mixing forces are sufficient to prevent settling out during flow in horizontal pipe. In the light of this, many researchers have laboured to predict such conditions to prevent sand accumulation. Amongst these studies is the concept of sand minimum transport condition (velocity) in single phase water. This is the minimum velocity to keep sand particles moving, provided the sand has not formed scale by other chemicals. This concept has been studied in single phase flow, ranging from water to some viscous oils (Oudemans, 1993; Gillies et al., 1997; King et al., 2001) but the predictions have not been proven to suffice for multiphase flow where the oil is non-conventional (i.e. high viscosity).

Pressure gradient of 3-Phase oil-water-sand flow in pipe

Although it was proposed that the co-flow of water with oil reduces the pressure gradient, the effect of the presence of sand at different concentration in the same oil-water flow has not been verified. A good understanding is inevitable in this kind of multiphase flow since the deposit of sand and the high resistance to flow of heavy oil are combined in the same flow.

Gillies et al. (1995) reported that injection of water into heavy oil containing sand revealed that some were washed out by the water in their study of oil-water-sand flow in horizontal pipeline. They also observed that low pressure gradient resulted from the injection of water at high cut. Since the use of horizontal pipeline configuration is increasing in crude oil production, a good understanding of the flow line pressures is needed so as to alleviate any unexpected and unwanted impact on the entire production. There must be a pressure decrease in the downstream section of the pipe if fluid must

flow in it. Theoretically, if the velocity is very low in the pipe, the pressure gradient is expected to be negligible between the inlet and outlet, but this may not be the case in the production of heavy crude oil, because of the composition of the crude. Homogenous fluid model may not be effective because of the tendencies of depositions of sand and heavy oil in the pipe. Since the research of Gillies et al. (1995) is limited to 66cP oil as against hyper-viscous oil in the heavy oil belongs, adoption of Gillies' report to handle heavy oil production might lead in to chaos in the process design.

McKibben and Gillies (2009) reported a recent research carried out in Saskatchewan Research Council (SRC) on the study of the pressure drop behaviour of oilsand-water flow and the sand transport condition. The tests were conducted in a 0.1m ID pipeline with an average sand diameter of 310 microns. The sand concentrations tested were 6 and 12% v/v. McKibben and Gillies (2009) reported that the pressure gradient changes were not obvious while adding 6% v/v sand into bitumen froth (with total water fraction 33%v/v), unlike 30% increase in pressure gradients expected in slurry flow. In summary, the impact of the addition of sand in the reduction of pressure gradient was not significant. However, the authors proposed that a "scouring process" that occurred during transport is the explanation for the observed reduction of pressure gradient. The sand was believed to be removing some of the bitumen coating on the pipe wall and this increased the pipe cross section area. This "scouring process" needs to be re-observed since no sand transport behaviour studies were conducted. In this case, a similar investigation as in sand MTC in water-sand flows should be conducted and normally it would be expected that there is sand MTC where the pressure gradient starts to increase due to the reduction of cross sectional area of the pipe or blockage.

However, application of this production method to high viscosity oil, known as CHOPS needs to be explored for a better understanding of such characteristic flow. In this research, investigation of pressure behaviour of high viscosity oil-water-sand shall be attempted.

2.3.4 Restart

In this section, a review of studies on an aspect of flow assurance called 'restart' in heavy oil production is presented.

The production systems could be shut down during production for various reasons, most especially for facility maintenance and workover Han (2012) and the restart could be a problem due to resistance to flow that is inherent in high viscosity oils. Hence, the need for more understanding cannot be over emphasised.

Williams et al. (1996) reported that the pressure required to restart flow may exceed the pressure rating of the pump or the pipeline. Hence accurate measurements of the Break Away Yield Stress (BAYS) of many waxy crude oils are needed for the development of informed decisions that can be used during system design. In addition Williams et al. (1996) mentioned pipe material, test temperature, cooling rate, water cut, bubble point and time at test temperature as factors that influence BAYS but viscosity was not considered to be a problem. Chang (1999) stated that there are three possibilities for the start of flow when a constant pressure is applied to the pipeline depending on the wall shear stress; the possible restarts are start-up without delay, start-up with delay and unsuccessful start-up. From his definitions, start-up without delay is a situation where the applied pressure results in the wall shear stress that is higher than the static yield stress of the oil. In this case, the flow starts immediately, but when the wall shear stress lies between the static yield stress and the elastic limit yield stress at the start point, the start-up experiences a delay. In start-up with delay, the flow will start after a delay time since no oil in the pipe yields to the pressure. The last case is the unsuccessful start-up where the wall shear stress is less than the elastic yield stress. Golczynski and Nielsen (2002) stated that transient issues such as restart become increasingly more critical as developments move into deep waters. They also agreed that restoring a shutdown system may become difficult after maintenance, hence how the flow lines and other subsea equipment are treated during a shut down as well as how they are restarted play a major role in production. In short Golczynski and Nielsen (2002) elucidated that restart philosophy has a significant impact on the maximum tieback length, the insulation type

chosen, chemical injection line sizes in the umbilical, and the overall chemical storage topside.

Mehta (2004) listed some of the typical problems the oil & gas industry has face in the past and which have been systematically tackled, as given below:

- Poor performance of well in-flow
- Excessive pumping power requirements
- Low efficiency of electric submersible pumps (ESP's)
- Restart problems often follow the pressure build-up in the flow lines
- Topsides problems associated with water separation due to emulsions and degassing of the oil.

Lin et al (2005) emphasised that one of the challenges facing the engineers in the oil production is the question of how to design pipeline and subsea systems for an economical and safe transport of the multiphase fluids from the well bottom to the processing plant. In addition, Lin et al (2005) concluded that this know-how must be accompanied with the practice of identifying, quantifying and mitigating of all flow risks that are associated with oil production-which is known as flow assurance.

Ekweibe (2008) reviewed the phases of waxy crude evolution during cooling in a shut in subsea pipeline. They reported wax precipitation, deposition gelation and the yielding behaviour of waxy crude gels during pipeline restart. In addition, they studied the effect of system pressure on restart condition. In their research, they examined and found that the formation of a weaker gel with lower yield strength was a product of higher system pressures in subsea pipelines, and that the necessary applied pressure for displacing this gel would be achieved easily and cheaply than might be predicted.

Most researchers including Chang et al. (1999), Davidson et al. (2004), and Vinay et al. (2007) have reported their studies on restart philosophy in oil production but not without wax deposition in pipelines because most of the studies were conducted on low viscosity oils with wax content. It is generally believed in the oil production that wax plays a dominant role in the possibility of restarting a shutdown flow operations. This is

common in waxy crude when either planned or unplanned shut down takes place for the sake of maintenance.

Only few researchers like Mehta (2004), Guevara et al (1997) mentioned the need to verify the impact of high viscosity of oil in the restart problems. Mehta (2004) affirmed that the fact that heavy oils are often characterized by their high viscosity, low API gravity and low reservoir energy, in addition to the tendency to form emulsions, makes the production and transportation of heavy oils a major challenge from a flow assurance perspective. In their studies, Guevara et al (1997) compared different transportation methods for heavy oil and their abilities. They highlighted, as shown in Table 2-4 that restart could be problematic when adopting some methods like heating, annular core flow and emulsion means of producing oil through flow lines.

Bensakhria et al (2004b) conducted steady laminar flow experiments at moderate flow rates to study the transport of high viscous oil in pipe by injecting water to lubricate the pipe. They observed sharp drops of pressure drop and concluded that CAF is possible for heavy oil transport but suggested that restart need to be studied in order to guaranty the complete feasibility of the CAF for an industrial scale. Vinay (2007; 2006) developed both 1-D and 2-D models and used them to study an isothermal start-up process. Vinay claimed that their model was able to explain why pipeline full of compressible fluid may restart earlier than the same pipeline full with less compressible fluid in some circumstances. An isothermal start-up model was developed for pipeline containing gelled waxy crude oils after a period of shut down by Chang (1999). Chang's model was able to predict the oil flow rate as a function of time, and the time required to completely clear the gelled oil off the pipe at a constant applied pressure.

Most researches on the issue of restart have focused on waxy crude oils, which are light oils, and the main approaches employed have been experimental, empirical and mechanistic modelling methods but not has published the study of restart operation on high viscosity oil. Hence, more knowledge is needed on high viscosity oil. The use of CFD to investigate the restart of flow for high viscosity oil flow in the presence of water in the horizontal pipe and at constant temperature (isothermal) after a period of shut

down is being considered. This study is necessary to ascertain the fate of the high viscosity oil production.

Table 2-4: Comparison of different heavy oil transportation methods Guevara et al (1997)

Issues	Heating	Dilution	Annular core flow	Emulsion	Upgrading
Pressure drop	Medium	Maximum	Minimum	Medium	Medium
Flow stability	High	High	High	High	High
Start-up/shut-down operation	Problematic	Flexible	Problematic	Depends on stability of emulsion	Flexible
Required pipe diameter	Normal	Larger	Normal	Larger	Normal
Corrosion problems	None	None	Potential	Potential	None
Additional investment for additional facilities	Normal (heaters)	High (parallel diluent system)	Normal-High (water supply & disposal system)	Normal-High (water + surfactant supply system)	(field refinery)
Prediction models	Conventional non-isothermal	Conventional non-isothermal	Empirical & semi-empirical	Laboratory rheological model required	Conventional non-isothermal

2.3.5 Theoretical Approach

Mathematical models are widely used in petroleum industry to predict multiphase flow behaviours. However, these models have been developed and validated based on data gathered from low-viscosity oil due to the limited experimental data for high viscosity multiphase flow. This section presents a brief review of the model approaches to predicting two-phase flow oil-water behaviour in horizontal pipe. The search for accurate model to predict two-phase flow oil-water behaviour including pressure drop, flow patterns and oil holdups in pipes of different inclination angles which are essential for production system design has led to the following approaches reviewed in section 2.3.5.1.

2.3.5.1 Two-fluid model

Taitel and Dukler (1976a) developed a two-fluid model for gas-liquid flow and since then been adopted for separated flow, especially stratified flow. Hall and Hewitt (1993) employed analytical method to solve this model while Charles and Redberger (1962) attempted the numerical method to solve the model. This model was developed from momentum balance on two separate fluids as shown in Equations 2-4 and 2-5:

$$-A_w \left(\frac{dP}{dZ} \right)_w - \tau_w S_w - \tau_i S_i - \rho_w A_w g \sin \theta = 0 \quad 2-4$$

$$-A_o \left(\frac{dP}{dZ} \right)_o - \tau_o S_o + \tau_i S_i - \rho_o A_o g \sin \theta = 0 \quad 2-5$$

A , (dP/dL) , τ , ρ and g represent area occupied by each phase, pressure gradient, shear stress, density and acceleration due to gravity of oil and water respectively. S_o and S_w represent the perimeter covered by oil and water respectively while S_i is the perimeter of the interface between the oil and water phases.

2.3.5.2 Energy minimisation model

Chakrabarti et al. (2005) developed a mechanistic model for liquid-liquid flow in pipes based on the principle that any system stabilizes to its minimum total energy. The energies considered are potential, kinetic and surface energies. The model was used to predict the pressure drop behaviour of kerosene-water flow through a 1-in diameter pipe. The model could be used for horizontal and near horizontal flows and can predict flow patterns, pressure gradient and volumetric holdup. The authors validated their model with data from Lovick and Angeli (2004). Sharma (2006) used the same approach and validated it using experimental data from the studies of Atmaca (2007), Abduvayt (2006), Alkaya (2000) and Trallero (1995). They reported that the energy minimisation model was developed and used to predict the pressure gradients of smooth stratified, wavy stratified, three-layer and dispersed oil in water and water. Further information about the model could be gotten from Chakrabarti et al. (2005).

2.3.5.3 Hydrodynamic lubrication theory

Ooms et al. (1984) proposed a lubrication mechanism with their focus on levitation mechanism which allows oil to float and surrounded by water film. They developed a model based on hydrodynamic lubrication theory to predict pressure gradient of the oil-water annular flow. The limitation of the model is the requirement for the amplitude, thickness, and wavelength of the oil core for the manipulation of the model. Oliemans et al. (1987) further extended the previously developed theoretical model by Ooms et al. (1984) for steady core annular flow in pipes by incorporating the effect of turbulence in the water film surrounding the oil core. The adapted model was reported to predict the pressure gradient increase with oil velocity correctly provided that actual wave amplitudes and wavelengths observed during these tests are used as input data.

2.3.5.4 Homogeneous model

Homogeneous model is usually applied to predict dispersed flow regime in pipe with the assumption that there is a good mixing which mixing rules for interfacial tension, density and viscosity were developed as closure laws to predict them adequately. These

mixing laws could be found in literatures that report mixture properties. The governing equation adopts Blasius model for single phase flow.

$$(dP/dL)_{TP} = f \frac{\rho_m U_m^2}{2D} \quad 2-6$$

Where $(dP/dL)_{TP}$, f , ρ_m , U_m and D are two-phase pressure gradient, friction factor, density of the mixture, mixture velocity and pipe diameter respectively. In this case, the task is to develop suitable mixing rule for mixture viscosity, density and frictional factor.

2.3.5.5 Empirical model

Many researchers have worked on water-sand flow in pipes and this left the subject with different correlations in literatures but the pioneer and most popular correlation for predicting the pressure gradient in horizontal pipe was developed by Durand and Condolios (1952) and given by Equation 2-7.

$$H_m = H_w \left[1 + KC_v \left[\frac{V^2 \sqrt{C_d}}{gD(s-1)} \right]^{-n} \right] \quad 2-7$$

where K and n were taken by Durand as 84.9 and 1.5 respectively. These constants were adjusted by different authors based on their experimental data that they correlated. Other kind of models developed which are not empirical are the two-layer (Gillies et al., 1991) and three-layer model (Doron and Barnea, 1993).

In the same vein, several models have been developed by different researchers on the transport condition of sand in water-sand flows in pipes. Amongst them is Durand's (1952) model which was developed based on 310 experimental tests on slurry transport in pipes. Durand (1952) identified and defined the boundary between the regions where sand flow and deposit as "limit deposit velocity". The experiment which birthed the model was conducted on pipe diameter ranging from 37.5 to 700mm with particle

diameter and sand concentration ranges from 200 to 25000 micron and 0.02 to 0.23 respectively. The model is given in Equation 2-8.

$$V_c = F_L \left[\sqrt{2gD(\rho_P/\rho_L - 1)} \right] \quad 2-8$$

Where F_L is a function of particle diameter and sand concentration.

$$F_L = (1.3C_v^{0.125})[1 - e^{-6.9d_{50}}] \quad 2-9$$

Due to the poor performance of the model, Wasp (1977) modified Durand (1952) model to reflect the effect of the sand volume concentration and the mean particle size as

$$V_c = F_L' \left[\sqrt{2gD(\rho_P/\rho_L - 1)} \right] \left(\frac{d_p}{D} \right)^{1/6} \quad 2-10$$

Wasp used $F_L' = F_L\sqrt{2}$ as a function of the sand volume concentrations with 1% minimum sand volume concentration. Oroskar and Turian (1980) developed a correlation based on the analysis of balancing the energy required to keep the particles in suspension with that energy derived from dissipation of an appropriate fraction of the turbulent eddies. This correlation was validated by using critical velocity data of the slurry experiments

$$\frac{V_c}{\sqrt{gd_p(\rho_P/\rho_L - 1)}} = 1.85C_v^{0.1536}(1 - C_v)^{0.3564} \left(\frac{d_p}{D} \right)^{-0.378} \quad 2-11$$

$$* \left(\frac{D\rho_L\sqrt{gd_p(\rho_P/\rho_L - 1)}}{\mu_L} \right)^{0.09} x^{0.30}$$

Based on the experimental data x is close to unity (> 0.95).

Wicks (1971) model which was developed based on the balance of forces acting on a particle in order to determine the “critical velocity”. He defined critical velocity as the velocity at which sand start to move when the sum of lift and drag forces which cause rotation of the particle exceed the gravitational force that keeps it in place. Wicks’ used the force balance on a single particle to develop two dimensionless terms S and Ψ to predict the chance of the sand bed formation. These dimensionless term S contains the drag and lift coefficients (f_1 and f_2) with wall shear stress Φ while Ψ depends on the particle diameter d_p , and the particle and liquid physical properties.

$$S = \frac{1}{8}(f_1 + sf_2)\Phi^2 \quad 2-12$$

$$\Psi = \frac{\rho_L^3 d_p V_c^4}{[(\rho_P + \rho_L)g\mu_L^2]} \quad 2-13$$

Nilson and Kvernfold (1998) modified Wicks (1971) model to predict the critical velocity for the formation of sand bed as given in Equation 2-14.

$$V_c = 1.289d_p^{0.179}D^{0.3435}\nu^{-0.015}[2g(\rho_P/\rho_L - 1)]^{0.51} \quad 2-14$$

Davies (1987) also developed a model based on turbulence theory to predict velocity required for particles to be suspended in horizontal pipes. Davies introduced a factor to correct eddy damping by the solids in the flow. He considered that the sedimentation force equals the eddy fluctuation force when the particles are fully suspended in the flow. The model is given as

$$V_c = U_m = 1.08(1 + 3.64C_v)^{1.09} * (1 - C_v)^{0.55n_v - 0.09}d_p^{0.18}[2g \Delta\rho/\rho_L]^{0.54}D^{0.46} \quad 2-15$$

Danielson (2007) developed a correlation based on the experimental data obtained from SINTEF STRONG JIP project. The author employed particle diameter to augment the pipe surface roughness with the assumption of critical slip velocity between sand and liquid which remains relatively constant over a wide range of flow velocities. The model employed the solid and liquid properties with the pipe diameter. The sand used for the experiment had a median diameter of 280 and 550microns with specific gravity of 2.7. The model is given as

$$V_c = 0.23v^{-1/9}d^{1/9}[gD(\rho_P/\rho_L - 1)]^{5/9} \quad 2-16$$

McKibben and Gillies (2009) developed correlations to predict the pressure drop of oilsand froth which is a combination of oil, water and fine sand (i.e. clay and silt). They proposed that the carrier fluid is responsible for the transportation of sand, and hence it has density and viscosity that depend upon water and the concentration of fines in the water. Fine sand and water forms the carrier fluid with a different property from water. The fine sand is assumed to be fully suspended in water without settling. It was also reported that their samples did not have significant sand, therefore their model could be applied to both oil-water and oil-water-sand systems. The governing equation is given as

$$\frac{dP}{dZ} = 4\tau/D \quad 2-17$$

Where $\tau = f\rho V^2/2$ and V is the bulk velocity and f is expressed as

$$f = 11.6 f_{CF}^{1.3} f_{oil}^{0.32} C_{CF}^{-1.5} \quad 2-18$$

Where f_{CF} is the Fanning friction factor when carrier fluid flows by itself at the velocity V , f_{oil} is the Fanning friction factor when the oil flowing by itself at velocity V , and C_{CF} is the volume fraction occupied by the carrier fluid. They employed the correlation of Shook et al. (2002) to estimate the viscosity of the carrier fluid as stated in Equation 2-19.

$$\mu = \mu_w \exp(12.5 C_{fines}) \quad 2-19$$

μ_w is the viscosity of water and C_{fines} is the fines volume fraction in the carrier fluid.

They reported that the water assist flow of crude oils and high viscosity lube oils are different from the bitumen froth flow and it was difficult to establish it at low pipeline operating velocities. This is because they lack significant amount of clay therefore their carrier viscosities are considerably lower than those for bitumen froth mixtures. This reduced capacity at low velocities was captured by using a Froude number

$$\frac{V}{\sqrt{(gD)}} \quad 2-20$$

For mixtures in which the clay concentration in the carrier is low, the following correlation is proposed as

$$f = 15(V/\sqrt{(gD)})^{-0.5} f_{CF}^{1.3} f_{oil}^{0.32} C_{CF}^{-1.2} \quad 2-21$$

In their study, they defined the fines by classifying the particles into three, namely; fine, intermediate and coarse particle. For particles to be classified as fines, its diameter must be less than the viscous sublayer thickness δ in a turbulent flow given by

$$\delta = \frac{5\mu_f}{\rho_f V \sqrt{f/2}} \quad 2-22$$

In order to predict the deposition of fines, Thomas (1979) correlation was adopted and given by

$$V_c = 1.1 \frac{[g\mu_f(\rho_s - \rho_f)/\rho_f^2]^{1/3}}{\sqrt{f_f/2}} \quad 2-23$$

This correlation is limited to solid volume fraction that is less or equal 0.2. The alternative correlation that was also considered is that of Sanders et al. (2004). A particle is referred to as intermediate when its diameter is greater than the viscous sublayer thickness δ and the pipeline Froude number is less than 1.7. The deposition under this condition is defined as a function of infinite dilution, V_∞ .

$$V_\infty = \sqrt{\frac{4gd(\rho_s/\rho_f - 1)}{3C_D}} \quad 2-24$$

Where

$$C_D = \frac{576}{Ar} \quad 2-25$$

for $Ar < 24$; in this case the particle is classified as fine and Stoke's law applies. In McKibben and Gillies (2009) research, the Stoke's law was extended and

$$C_D = \frac{81}{Ar^{0.47}} \quad 2-26$$

was employed for $40 < Ar < 2800$; where

$$Ar = \frac{4gd^3\rho_f(\rho_s - \rho_f)}{3\mu_f^2} \quad 2-27$$

The proposed boundary for particle deposition is given in term of friction velocity V^* as

$$V^* = 9V_\infty \quad 2-28$$

The friction velocity can be expressed as

$$V^* = V_c \sqrt{f/2} \quad 2-29$$

Particles are classified as coarse particles if Froude number is greater than 1.7. Froude number at the onset of deposition is defined as

$$Fr_c = \frac{V_c}{\sqrt{gD(\rho_s/\rho_f - 1)}} \quad 2-30$$

2.3.5.6 CFD of multiphase flow

The usage of Computational fluid dynamics (CFD) for modelling multiphase flows has been gaining ground in the past two decades and the formulations of constitutive models for multiphase flows are attracting attentions of the researchers. This is due to the complex phenomena of fluid-particle, fluid-fluid, particle-particle and particle-wall interactions. In spite of the current capabilities of CFD in investigating multiphase flows, experimental data are still very useful and needed for the verification and validation of any numerical model or simulation.

The two fundamental objectives of the application of computational fluid dynamics (CFD) is firstly, to generate scientific understanding of the mechanisms involved in fluid flows systems, and their behaviours while the second objective is to help in designing the hardware for engineering devices or systems. Hence, the goal of developing CFD technology is to improve its ability to predict the flow behaviours of engineering systems.

Although a number of limitations exist, considerable efforts are being directed at the development of robust CFD models for multiphase systems, and the application of these models in industry is growing steadily. Hence, using of CFD to study multiphase flow is promising but requires experience and further improvement.

However, progress should be made in order to produce a truly predictive computational scheme, and reduce fluid flows (especially complex turbulent flows) to computable phenomena (Abdullah, 2011). Since the use of full governing Navier-Stokes equations is normally computationally impractical for the prediction of turbulent flows, a hierarchy of turbulence models is used to model fluctuations inherent in these equations. In the light of this, closure models are needed and being developed based on certain assumptions and objectives.

2.3.5.7 Two-Phase flows

The success of any of multiphase flows depends on the accurate modelling and appropriate compositions in the governing and closure equations of the various complex effects that occur in multiphase flows. This, however, requires a good understanding of the fundamentals of multiphase flows which can be explored in CFD study. Two categories of two-phase flows are considered in this report; liquid-solid (water-sand) and liquid-liquid (oil-water) flows.

Water-Sand flow

The use of CFD in modelling solid-liquid multiphase flow has been reported to be notably limited. van Wachem and Almstedt (2003) itemise three factors that are responsible for this:

- the complex mathematical treatment of such flows which have not been fully developed
- the inherent complexity of the physical phenomenon of multiphase flow, reflected in the wide range of flow types and regimes encountered in such flows ; and
- the numerics for solving the governing equations and also the closure laws of multiphase flows are extremely complex. Most of the times, multiphase flows show inherent oscillatory behaviour which requires costly transient

solution algorithms. Almost all CFD codes apply extensions of single-phase solving procedures, leading to diffusive or unstable solutions, and require very short time-steps, or CFL numbers.

However, increase of computational power has made it possible to simulate the solid-liquid flow using Eulerian-Eulerian, and Eulerian-Lagrangian approach. These methods are reported to be computationally expensive, while Eulerian-Lagrangian method is valid only for very dilute mixtures, i.e. $< \sim 2\%$ v/v (van Wachem and Almstedt, 2003).

Krampa (2009) developed CFD model using CFX 4.4 software, to predict the flow features of aqueous solid-liquid slurries in turbulent upward pipe flow. Sumner et al.'s (1990) experimental results were used by Krampa (2009) to validate the velocity profile results obtained from the model simulation. The diameters of the particles used are 0.47mm and 1.7mm, with density, 2650kgm^{-3} at concentrations up to 30% v/v. The results of CFD and experiment compared satisfactorily for the smaller particles but deteriorated for the 1.7 mm diameter particles. Krampa (2009) concluded that the code failed to accurately predict important features of the flow using the default settings.

In the present study, the Eulerian VOF CFD model was developed to predict water-sand slurry flow in the horizontal pipe and used to predict the pressure gradients of the flow in question and pictorial profile. The purpose of CFD model is to explore its suitability to give better understanding into the prediction of the sand flow characteristics in 1-in ID pipe.

The review of literatures shows that there is a little progress in the simulation of slurry flow in horizontal pipelines using CFD. For liquid-solid multiphase flows, the complexity of modelling increases and this remains an area for further research and improvement in the models. A general applicable CFD code does not exist for slurry

Table 2-5: Survey of modelling and simulation study on water-sand flow in pipe

Author	Diameter (mm)	Inclination (°)	Particle Diameter (mm)	Slurry condition (%)	Carrier Viscosity (cP)	Model Type	Measurement
Takahashi (1989)	49.7	0	2.18 – 3.06	3.5 -12.5	1	Mechanistic	Pressure,
Frimpong (2004)	30 - 3352	0 – 60	<=50.8		1	Mechanistic	Concentration
Thomas (2007)	69	-1.35, 1,4	0.28 – 0.55	3.5 -12.5	1	Mechanistic	dP, Bed height, Critical Velocity
Eesa (2009)	45	0, 90	2 - 10	<= 40	Non-Newtonian	PEPT	dP, Velocity profile
Ekambara (2009)	50 - 500	0	0.00009 - 0.0005	8 - 45	1	CFD	dP, Velocity profile, Concentration
Bello (2011)	114	0	0.3		1	Mechanistic	dP, Velocity profile

flow, due to the inherent complexity of multiphase flows, from both physical and numerical point of view.

Oil-Water flow

In 1994, the effect of eccentricity on friction factor and holdup for both laminar and turbulent cases of oil-water flow was reported by Huang et al. They used the standard $k-\epsilon$ turbulence model to solve for turbulent annular flow and found the friction factor to increase with eccentricity. Bai (1990) used control volume based methods to simulate core annular flow assuming an axi-symmetric equal density wavy flow. Ko et al. (2002) simulated turbulent wavy core flow and found that the prediction of pressure distribution and wavelength was better when Shear Stress Transport (SST) $k-\omega$ model was used than that of original $k-\omega$ model. Ooms and Poesio (2003) studied core-annular flow through a horizontal pipe and analysed how the buoyancy force on the core is counterbalanced in case of bamboo waves and snake waves.

A number of studies have reported the CFD study of liquid-liquid slug in capillary micro-structured reactor (pipe) (Kashid et al., 2005; 2007; 2008; 2010b; 2010a; 2012b; 2012a). The authors explored the applicability of volume of fluid (VOF) methodology in CFD to investigate the liquid slug generation and its hydrodynamics. Tice's (2004) experimental results were used to validate their simulation results. Ghosh (2010) also studied the core annular flow in a vertical downward direction using CFD to generate the profiles of velocity, pressure, volume fraction and wall shear stress over a wide range of inlet oil and water velocities. Ghosh (2010) found an abrupt change in the radial velocity gradient occurred at the interface and that change became more prominent as flow propagates towards the outlet. The increase in both the frictional pressure gradient and wall shear stress as the superficial velocities of oil and water increased was also reported in addition.

However, none of the research on the models on oil-water flow in pipes has been able to predict the behaviours of high viscosity oil based multiphase flow in horizontal pipes.

2.3.5.8 Three-phase flows

Since three phase flows (e.g. solid particles in gas-liquid or immiscible liquid-liquid flows, and bubbles in liquid-liquid or slurry flows) are close in characteristics to the common flows encountered in engineering industries, like Oil & Gas, the modellers employ the use of CFD to do in-depth investigations to unravel its complexities. Some CFD research could be found on gas-liquid and liquid-solid flow but very few reports are available on three phase flow such as liquid-liquid-solid flow. The CFD study of liquid-liquid-solid is important if a holistic and reliable engineering design must be done for capital intensive projects. Hence this study investigates the behaviour of such multiphase flow where the oil viscosity is above 1000cP.

2.4 Chapter Summary

This chapter addressed the reviews of the problems of heavy oil production, methods of production to alleviate all these problems and the studies on the multiphase flow with focus on oil, water and sand. Some research on low viscous two-phase; (water-sand and oil-water) flow, and three-phase; (oil-water-sand) flows in pipes were also reviewed. Although many methods exist to handle the production of high viscosity oil, all have been reported to be non-cost effective due to the need of energy to arrive at the desired production level except CHOPS. Lack of high viscosity related data for flows in pipes also constitutes to the difficulties that are confronting this production of high viscosity oil. Hence, this research is concerned with the investigation of CHOPS, the cost effective approach of heavy oil related flows of liquid-liquid and liquid- liquid-solid in 1-in ID horizontal pipe with particular interest towards Oil & Gas industry applications.

The experimental studies on multiphase flows, focussing on water-sand, oil-water and oil-water-sand multiphase flows were reviewed in section 2.3.1. The focus was on the determination of flow configurations, the pressure gradients and the transport condition of oil-water including attempts to, experimentally obtain core annular flow (i.e. an hypothetical flow regime in which water is permanently retained on the pipe wall while the oil flows in the core of the pipe), by different pipe inlet designs. The transport of sand, both in water and oil-water flows were reviewed under the same conditions as oil-

water flow. Some works on phase inversion was also reported. This became necessary due to the impacts of these factors on the design of their transfer pipelines. Limited publications were available on oil-water-sand flow due to its complexities.

A review of the theoretical approach to solving the multiphase flow problems in pipes was presented. The CFD investigations on both two (i.e. water-sand and oil-water) and three (oil-water-sand) phase flows were also reviewed in the section 2.3.5.6 above. It was observed that not many researches have been done on them, most especially oil-water and oil-water-sand with high viscosity oil. In addition, none of the existing models have proven reliable in the case of high viscosity oils (where viscosity is higher than 1000cP).

Experimental and numerical modelling approaches are complementary of each other. This is based on the fact that experimental data are indispensable for the development and validation of numerical models whilst numerical models possess the ability to produce more comprehensive data than experiment as at present. A study on the modifications of the existing models is needed to verify the suitability, reliability and capability of CFD in modelling heavy oil related multiphase flows.

3 RESEARCH METHODOLOGY

In this research, multiphase flow experiments were carried out on a horizontal rig in the Process System and Energy Engineering laboratory of the Department of Offshore, Process and Energy Engineering. This chapter presents the experimental arrangements and equipment used to investigate the flow behaviour of high viscosity water-sand, oil-water and oil-water-sand in horizontal pipes. It describes in detail the methodological approach and procedures undertaken to acquire the experimental data. An overview of the experimental facility is given in Section 3.1; Sections 3.2 and 3.3 give further information on important facility components such as data acquisition methods and the properties of the phases respectively, followed by Section 3.4 that describes the experimental procedure. The data analysis approaches were also described in section 3.5.

The investigation of the heavy oil based multiphase flow regime was conducted using a 1-inch pipe test facility in the PASE laboratory at Cranfield University. This rig can be used for two-phase, three-phase and four-phase flows. The rig was designed by the department of Offshore, Process and Energy Engineering in the school of Engineering, Cranfield University. The test loop is made up of three major components; oil-, water-slurry and air- handling facilities, test section, and oil/water separation equipment.

3.1 Oil- Water- and Sand- Handling Facilities

The oil-, water- and sand slurry- handling facilities consist of tanks, Coriolis meter, mass flow meter and progressive cavity pump. The tanks are lagged to keep the temperature variation relatively low.

3.1.1 Oil supply

The oil storage tank is made of plastic fibre material with a capacity of 0.15m³. A variable speed progressive cavity pump (PCP) is connected to the test section through a 1-inch (I.D. = 25mm) pipe line. The flow meter shown in Figure 3-1 is the VARMECA

31T 075. EN60529:IP65. The oil pump has a capacity of $0.72\text{m}^3/\text{hr}$. A Coriolis flow meter in Figure 3 5 is mounted to measure the flow rate of the oil flowing through the 1-inch loop. The range of the flow meter is $0 - 180\text{m}^3/\text{hr}$. The HART output from the meter is 4-20mA which is connected to the data acquisition system.



Figure 3-1: Oil storage tank

3.1.2 Water supply

The water storage tank is made of plastic fibre material with a capacity of 0.15m^3 . A variable speed progressive cavity pump (PCP) is connected to the test section through a 1-inch (I.D. = 25mm) pipe line. The water pump has a maximum discharge pressure of 10 barg. An electromagnetic flow meter is mounted to measure the flow rate of the water flowing through the 1-inch loop. The flow meter shown in Figure 3-2 is the VARMECA 32T 220, Type 1. EN60529:IP65. The water pump has a capacity of $2.18\text{m}^3/\text{hr}$. The range of the flow meter is $0 - 180\text{m}^3/\text{hr}$. The HART output from the meter is 4-20mA which is connected to the data acquisition system.

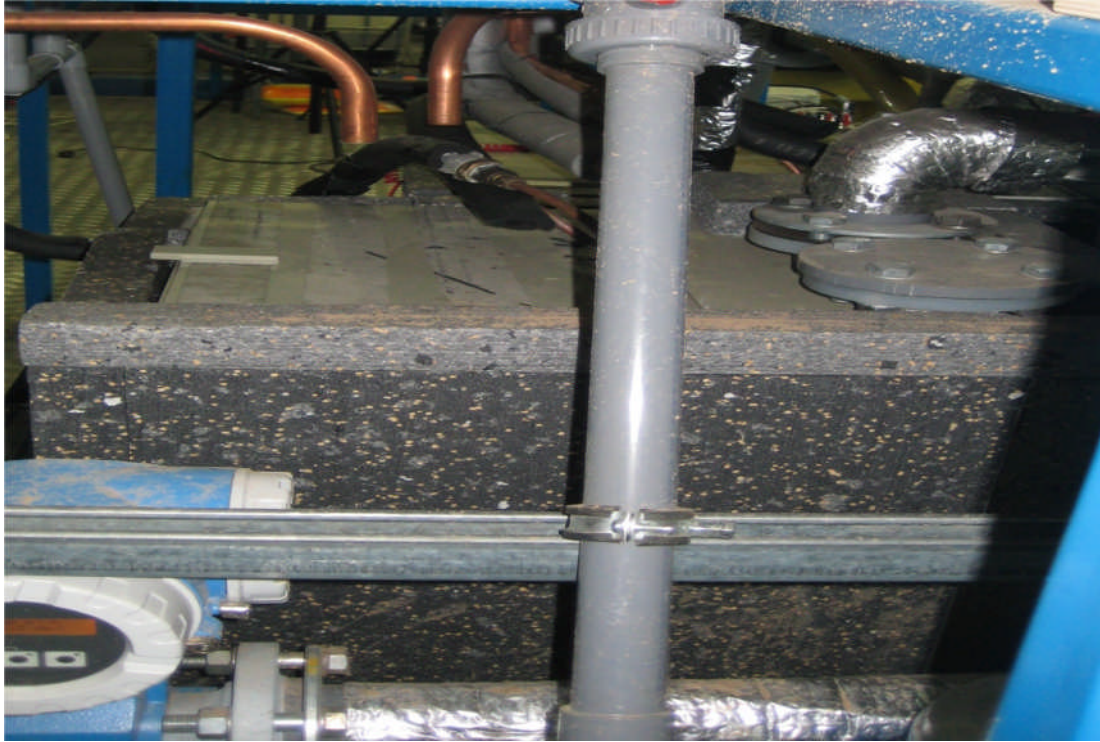


Figure 3-2: Water storage tank

3.1.3 Slurry mixer

Water and sand are mixed in a 0.20 m^3 cylindrical tank capacity (Figure 3-2). The slurry is mixed by a stirrer with a variable speed controller, usually at 50rpm. The slurry is pumped by a progressive cavity pump (PCP) through PVC and flexible pipe. The PCP pump has a maximum capacity of $2.18 \text{ m}^3/\text{hr}$. The safety switch to stop the pump was installed to operate at a maximum discharge pressure of 10 barg. Water flow is measured using an electromagnetic meter, Promag 50P50, DN50, having a range of 0 - $2.18 \text{ m}^3/\text{hr}$. The 4-20 mA HART output is connected to the data acquisition system.



Figure 3-3: Slurry mixer and pumping system

3.1.4 Oil/water/sand separator

A tank was also designed for separation of oil-water/oil-water-sand. The water storage tank is made of plastic fibre material with a capacity of 0.5m^3 . This has two sections, as shown in Figure 3-4 with an internal demarcation having weir for overflow. The mixture goes into the first compartment which has a glass window for viewing the phase interfaces. The dense phase goes to the bottom while the less dense phase at the top moves to the second compartment for further separation. The minimum residence time to separate oil and water is 6-7hours.



Figure 3-4: Multiphase separator



Figure 3-5: Coriolis meter and pressure gauge

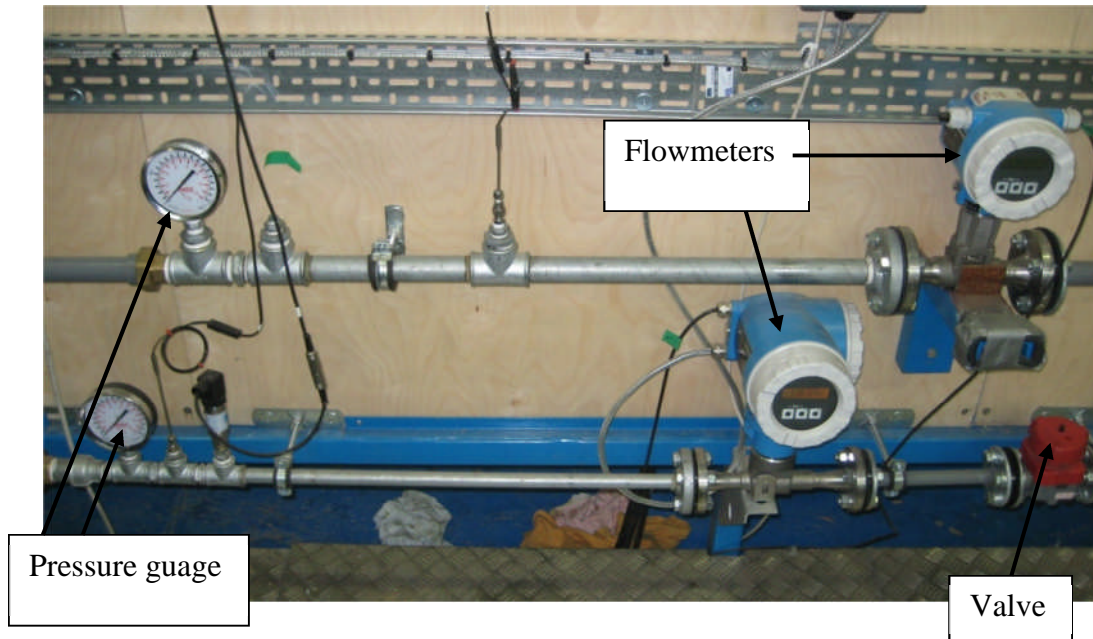


Figure 3-6: Gas flowmeters, valve and pressure guages

3.1.5 Test section

The test section is composed of three T-junction mixing unit segments of water, air and slurry respectively. It is made up of 1-in ID of a 5.5m long transparent acrylic horizontal pipe. The pressure taps are positioned at 2.93m and 5.10m, while differential pressure taps are placed at 2.92m and 5.m. Temperature transducers are also at 0.7m, 1.87m and on the test section. The schematic diagram of the rig is shown in Figure 3-7.

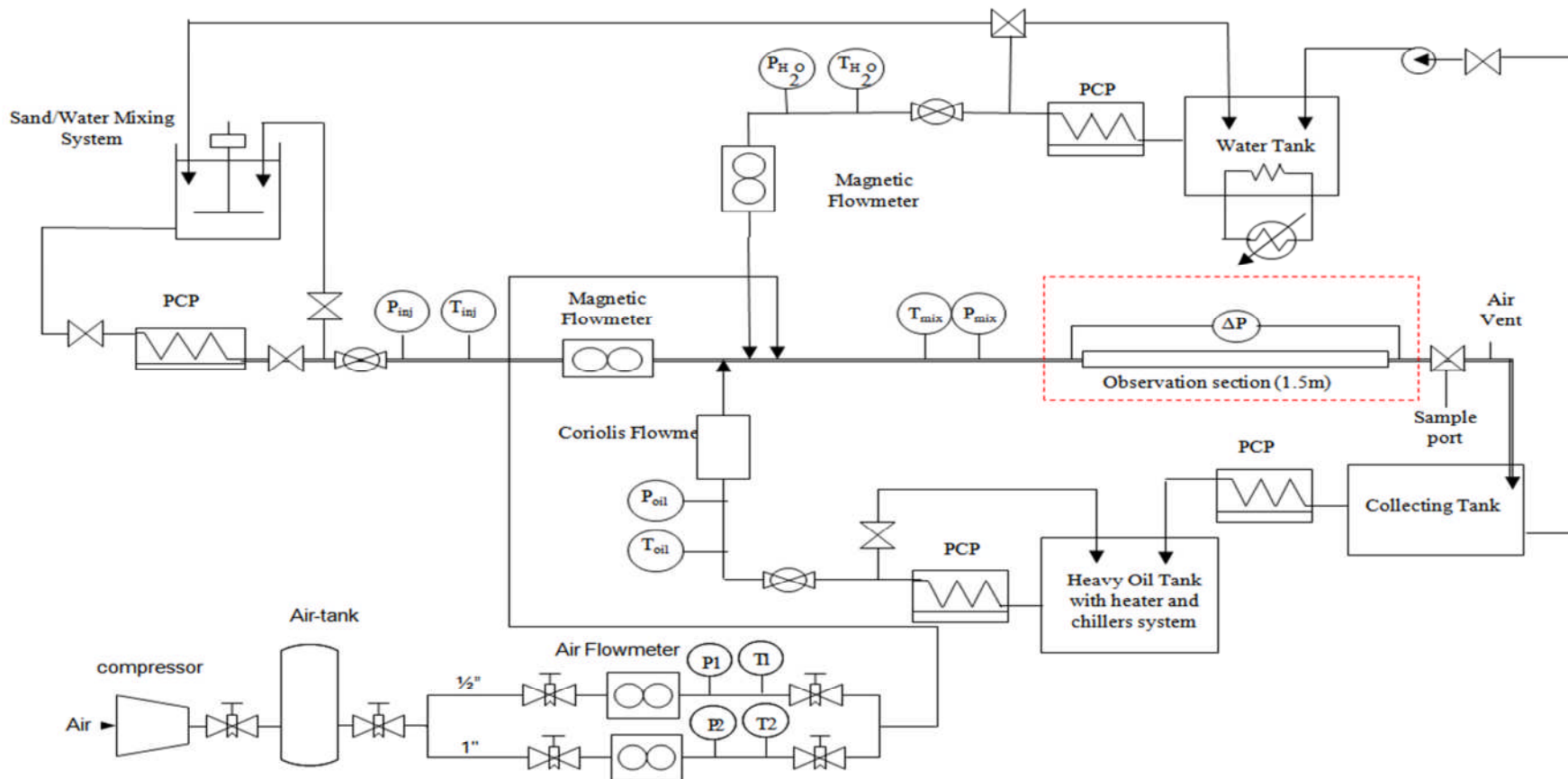


Figure 3-7: Schematic of 1-inch four phase transport facility at Cranfield University PASE laboratory



Figure 3-8: Pictorial view of 1-inch four phase transport facility at Cranfield University PASE laboratory

Table 3-1: Description of components of 1-in rig facility

Full Name	Abbreviations (Symbols)	Description
Coriolis flow meter	CF	Promass 83I50, DN50, Mass flow rate: 0 to 2000kg/h, Density: 0 ~ 1500kg/m ³ , Viscosity: 1000~10000cP (Newtonian fluid), Temperature: 5 ~ 50°C
Diaphragm Valve	DV	2" N.B. PVC, Class C, (minimum 10 barg)
Pressure sensor transducer	P	PMP 4110 Amplified Output Pressure Transducer Pressure Range: -70 to +70 mbar differential Output Voltage: 0 to 2 V (DC) Supply Voltage: 15 to 32 V (DC)
Differential pressure transducer	DP	PMP 1400 Pressure Transducer Output Voltage: 0 to 5 V (DC) Supply Voltage: 9 to 30 V (DC) Pressure range: -200mbar ~ +200mbar, ±0.02%FS
Electromagnetic flow meter for water	MF2	Promag 50P50, DN50, Flow rate : 0 to 2.18 m ³ /h, Temperature: 5 ~ 50 °C
Electromagnetic flow meter for water/sand	MF1	Promag 55S50, DN50, Flow rate: 0 to 2.18 m ³ /h, Temperature: 5 ~ 50°C, Maximum sand volume fraction: 0.15v/v, 4-20mA SIL HART output
Gate valve	GV	2" N.B. Brass body, Class C, (minimum 10 barg)
Heavy oil tank	HOT	0.15m ³

Pressure gauge/transducer	P	4~10 bar, $\pm 0.1\%$ FS
Progress cavity pump for Water (Return)	PCP5	Flow rate: 0 ~ 2.18m ³ /h, Temperature: 5 ~ 50 °C, Discharge Pressure: 10 bara. Equipped with pressure switch.
Progressive cavity pump for heavy oil (Injection)	PCP2	Flow rate: 0 ~ 1.05m ³ /h, Temperature: 5 ~ 50 °C, Discharge Pressure: 10 bara. Equipped with pressure switch.
Progressive cavity pump for heavy oil (Return)	PCP3	Flow rate: 0 ~ 1.05m ³ /h, Temperature: 5 ~ 50 °C, Discharge Pressure: 10 bara. Equipped with pressure switch.
Progressive cavity pump for Water (Injection)	PCP4	Flow rate: 0 ~ 2.18m ³ /h, Temperature: 5 ~ 50 °C, Discharge Pressure: 10 bara. Equipped with pressure switch.
Progressive cavity pump for water/sand (Injection)	PCP1	Flow rate: 0 ~ 2.18m ³ /h, Temperature: 5 ~ 50 °C, Discharge Pressure: 10 bara. Equipped with pressure switch.
Separation tank	ST	0.5m ³
Thermal fisher temperature control system	Chiller/ Heater	Heats or cools down the oil, The range is -45 - +50 °C
Water tank	WT	0.15m ³
Water/sand mixing tank	WST	0.2m ³ , Maximum sand volume fraction: 0.15v/v

3.2 Data collection method

Labview is a program used to automate testing and data gathering. It is basically a graphical programming language in which the user can set up the program to manipulate and store data. Labview has the flexibility of a programming language combined with built-in tools designed specifically for test, measurement, and control. Labview software of National Instruments was used to record voltages through a computer which were converted by calibration to the desired parameters. An application was created and data were taken every 0.004 seconds over 30 seconds for each run.

3.2.1 Numeric data acquisition

The pressure drop is measured between a pair of taps 2.17m apart where the first tap is at a distance of 2.155m from the inlet. A differential pressure transmitter (Honeywell STD120) was used for this purpose. The transducer has a least count of 1.0×10^{-2} Pa and an accuracy of $\pm 0.05\%$ under the experimental conditions. The static water head has been used along with differential pressure drop $(dp)_{diff}$ as obtained from the transmitter to extract the total pressure drop. Figure 3-9 presents the picture of the currently installed differential pressure transducers.

All the pressure sensors were mounted at angle 45° position instead of the bottom position in order to avoid sand blockage. The tubing system of the differential pressure transducer was always purged after each experimental run. The specifications are stated in Table 3-1.



Figure 3-9: Differential pressure transducer



Figure 3-10: Pressure transducer

3.2.2 Image data acquisition

The flow images are recorded at a distance 3.0m away from the inlet. A (DSCH9, SONY) video recorder is used for clip recording of the flow phenomena at different superficial velocities of both the phases.

3.3 Fluid and Solid Properties

The importance of fluid and solid properties is crucial in the study of flow dynamics whether experimentally or numerically. The knowledge of these properties helps to understand the reason for their behaviours. In this section, the properties of both the liquids and solid that were employed in this research are presented.

3.3.1 Fluid

The summary of the viscosities and densities of the heavy oils and water that were considered for this research are shown in Table 3-2. The second and third columns of Table 3-2 present the measurements of fluid densities and viscosities respectively. Density of a fluid is the mass of a fluid per unit volume. The density data provided by the supplier of the oils used in this research were employed for the calculations that involved density. The viscosity of a fluid is the measure of its resistance to gradual deformation by shear stress. It can also be described as the degree of thickness of fluid. The viscosities of fluids in this research were measured with viscometer. The behaviours of CYL 1000, CYL 680 and water were presented at 25°C in Table 3-2 but the detailed viscosity-temperature data of CYL 1000 and CYL 680 are shown in Figure 3-11 and Figure 3-12. Figure 3-11 and Figure 3-12 reveal that the viscosity of both oils decrease with increase in temperature. The last column of Table 3-2 presents the measurements of the interfacial tension between oil (i.e. CYL1000 and CYL680) and water. The interfacial tension is the measurement of the cohesive (excess) energy present at an interface (between two phases) arising from the imbalance of forces between molecules at an interface. When two different phases (e.g. liquid/liquid, gas/liquid, liquid/solid or gas/solid) are in contact with each other the molecules at the interface experience an imbalance of forces. This leads to an accumulation of free energy at the interface. The excess energy is called surface free energy and can be quantified as the energy required to increase the surface area of the interface by a unit amount (i.e. a measurement of energy/area). It is also possible to describe this situation as having a line tension or interfacial tension which is quantified as a measurement of force per length (Harkins and Jordan, 1930; Grain, 1990). The common unit for interfacial tension is dynes/cm or mN/m. Lastly, Table (3-1) equally presents the density of sand considered in this research.

Table 3-2: Phases properties description

Fluid	Density @25°C (kg/m ³)	Viscosity @25°C (Pa.s)	Interfacial Tension @19°C (Nm)
Water	1000	0.001003	0.029
CYL 680 Oil	917	1.830	
Water	1000	0.001003	0.026
CYL 1000 Oil	916.2	3.149	
Sand	2650	-	-

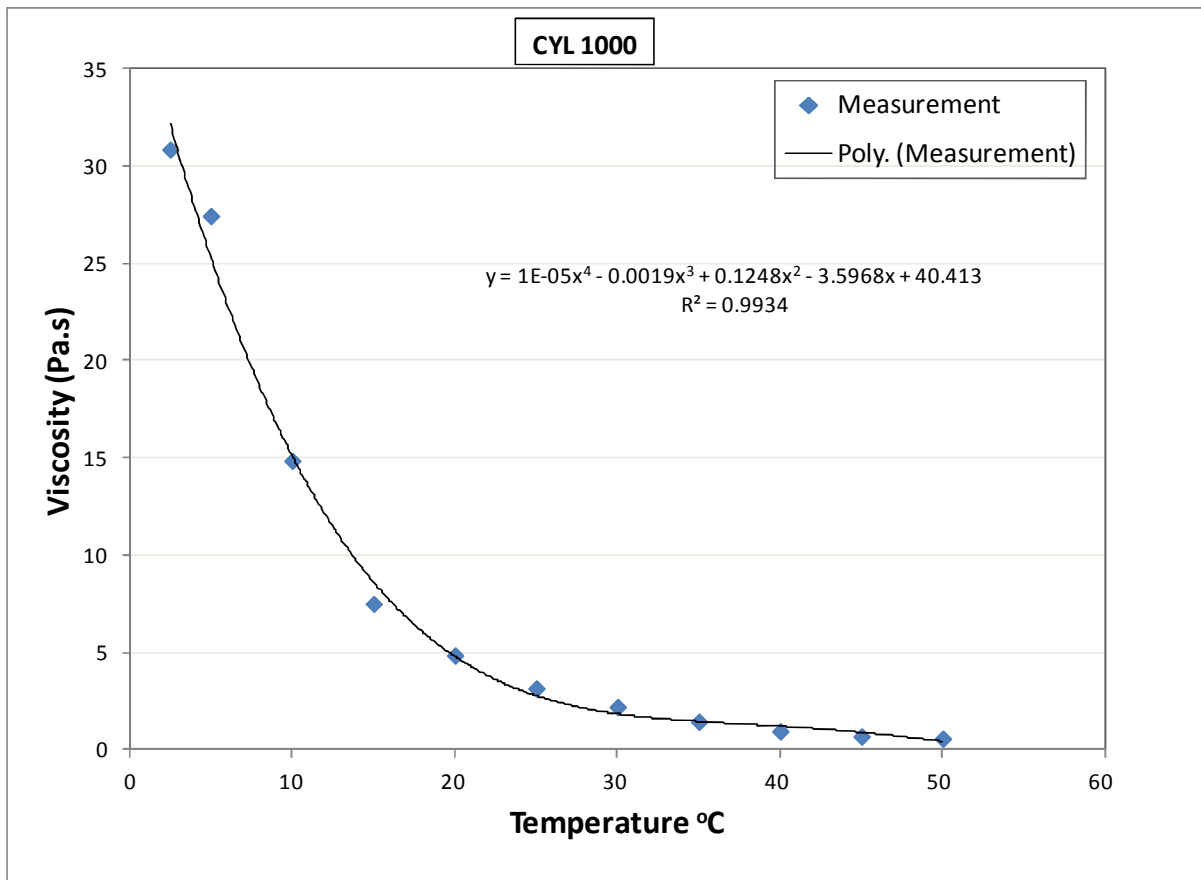


Figure 3-11: Viscosity-Temperature data of CYL1000

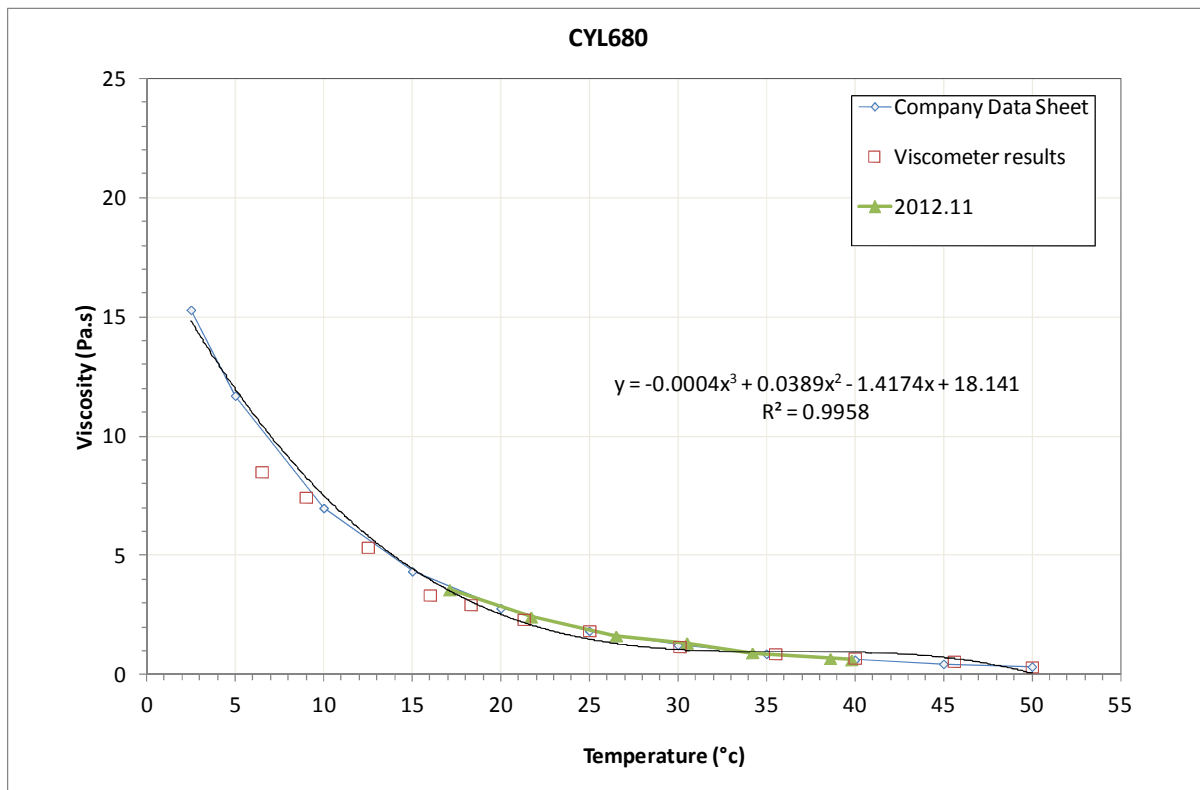


Figure 3-12: Viscosity-Temperature data of CYL680

3.3.2 Particle size distribution

The particle size distribution (PSD) of a solid material is important in understanding its physical and chemical properties. The PSD is usually defined using the method by which it is determined. Sieve analysis is the most easily understood method to determine PSD. In this case the particles are separated on sieves of different sizes. Thus, the PSD is defined in terms of discrete size ranges: for example "percentage (%) of sample between minimum and maximum size" when sieves of those sizes (i.e. minimum and maximum size) are used. The PSD is usually determined over a list of size ranges that covers nearly all the sizes present in the sample. The PSD may be expressed as a range analysis, in which the amount in each size range is listed in order. It may also be presented in cumulative form, in which the total of all sizes retained or passed by a single notional sieve is given for a range of sizes. Range analysis is suitable when a particular ideal mid-range particle size is being sought, while cumulative analysis is used where the amount of under-size or over-size must be controlled.

Sieve analysis is the common measurement method because it is cheap, simple and easy to interpret. This method involves simple shaking of the sample in sieves until the amount retained becomes more or less constant.

The sand used in this experiment is Congleton HST 95 with mean sand particle diameter of 150 microns. The average density of this sample is 2650kg/m^3 . The sand distribution used in these campaigns is shown in the Figure 3-13.

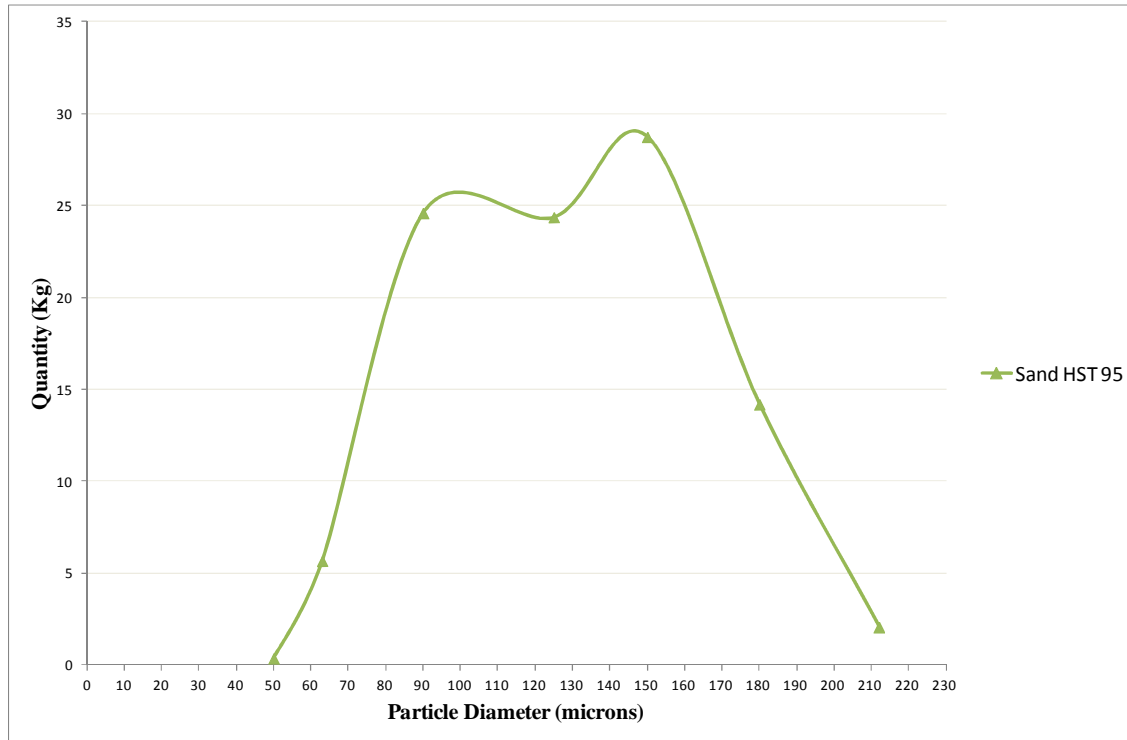


Figure 3-13: Sand distribution of HST 95

3.4 Experimental Procedures

Experiments were run, having checked the valves, oil and water levels to ascertain a good starting condition. Oil valve was set to by-pass and oil pump switched on to check the viscosity reading on Labview while running to acquire the desired viscosity. When the desired oil viscosity is reached, its valve is opened to the test section and its flow rate is set to the desired value, in case of oil-water test, the water valve is opened, the flow regulator set to minimum and the water pump switched on. Water is set to the desired rate as well and the transducer transmitted data are captured using Labview at 250Hz frequency, while the flow images are captured with video camera. The procedural steps for the entire experiments are stated below:

3.4.1 Calibration of pressure transducer

The transducers used for measurements in experiments often need a precise calibration to ensure their performance. This section outlines the procedure employed for calibrating (differential – but could apply to any type of transducer) pressure transducers by establishing a relationship between transducer output and change in voltage readings from the test section. From this relationship the linearity, hysteresis, and repeatability of the (differential) pressure transducer are determined. A pressure *correction* factor which is defined as the slope of a line relating the difference between observed voltage readings and (differential) pressure transducer output to applied lateral pressure is also determined.

Linearity:-This is the variation of transducer output from a straight line. In this procedure, measurements are obtained using a series of applied pressures over the total rated capacity of the (differential) pressure transducer.

Repeatability:- This is the maximum difference between transducer outputs for repeated pressures under identical loading and environmental conditions.

Hysteresis:- This is the maximum difference between transducer output for the same applied pressure; one reading obtained by increasing the pressure from zero to the upper calibration limit, and the other by decreasing the pressure from the upper calibration limit (not to exceed the transducer rated capacity) to zero.

Apparatus

(Differential) Pressure Transducer:- This is a pressure transducer of sufficient range and accuracy for laboratory tests as shown on Figure 3-9 and Figure 3-10.

Pressure Source:-A digital pressure indicator (DPI 602) source (produced by Druck) capable of delivering and maintaining pressure up to the maximum rated pressure of the transducer.

Precautions

Ensure that all electrical wiring is properly connected and powered.

Examine the pressure transducer body for burrs and sharp edges

Store the transducer in a suitable box or case when not in use.

It is recommended that the serial number be used for identification. If the transducer must be marked, use extreme care. Use an indelible marking pencil rather than a scribe to mark on the transducer body.

Procedure

The following procedural steps are employed in the calibration of the pressure transducers that were used in the present research;

1. Zero the pressure on the DPI 602
2. Mount the pressure transducer. A differential transducer should be attached via its +, or “Hi” port
3. Plug the transfer cable from the transducer (which supply power to and transfer voltage V reading from the transducer) to the National Instrument data acquisition box (NI-DAQ) that is linked to Labview on the computer.
4. Gently pump the DPI pressure knob to a value, starting from the minimum to a maximum value closed the transducer upper limit.
5. Take both the pressure P and voltage reading on the DPI 602 and Labview respectively.
6. Repeat step 5 for another pressure value until the allowable maximum value is reached.
7. Then start the process in step 4 to 6 from the maximum to the minimum pressure value by releasing the pressure slowly, using the vent knob.
8. Repeat steps 1 to 7 for repeatability check.
9. Calculate the hysteresis to verify the condition of the transducer whether suitable or not.
10. Plot voltage readings (horizontal axis) versus pressure readings (vertical axis)
11. Read the slope, m , and the intercept c to define pressure correlation in the Labview as

$$P = m(V - V_0)$$

Where $V_0 = -\frac{c}{m}$ known as the offset.

Calculations

Calculations of linearity, hysteresis, and repeatability are as shown on figure 3.

Calculations required to determine the pressure correction factor, V_0 .

3.4.2 Water-sand test procedure

The procedure followed for 2-phase water-sand flow tests in 1-in ID pipe experiments are outlined below:

1. Flush the pipe with water to remove sand remaining from previous experiment in the loop.
2. Prepare water-sand mixture of the required concentration in the hopper (sand mixing tank).
3. Open the slurry pipe valve and its bye-pass valve.
4. Start the slurry pump and adjust the controller until the required slurry velocity is reached.
5. Inject the slurry at a constant flow rate and record the raw data using both Labview and video camera. The data recording takes 30 seconds.
6. Change the slurry velocity and repeat step 5 until the test matrix is finished.

3.4.3 Oil-water test procedure

1. Pre-set the chiller to the temperature that is equivalent to the desired oil viscosity until the viscosity is reached.
2. Check the desired oil viscosity using the Coriolis flow meter readings or Labview while the oil circulates through the bye-pass.
3. Open the oil valves (main and the bye-pass) and power the oil pump. Recirculate oil until the viscosity constant.
4. Inject oil into the loop and set the oil velocity control to the desired point. (Adjust the oil flow rate by controlling the speed of the PCP pump and the bypass valve until the required V_{so} is achieved)
5. Open the water valve and power the water pump.
6. Inject and control the water velocity to the desired point (Open bypass valve to adjust water flow rate).
7. Record the data when the flow stabilises.

3.4.4 Oil-water-sand test procedure

1. Prepare the required concentration of sand in the mixer while the stirrer is power to allow for even distribution of sand in water.
2. Circulate the slurry from the mixer through the bye-pass for at least 5 minutes to ensure homogeneous mixture.
3. Check the desired oil viscosity using the Coriolis flow meter readings or Labview while the oil circulates through the bye-pass.
4. Open the oil valves (main and the bye-pass) and power the oil pump. Recirculate oil until the viscosity constant.
5. Inject oil into the loop and set the oil velocity control to the desired point. (Adjust the oil flow rate by controlling the speed of the PCP pump and the bypass valve until the required V_{so} is achieved).
6. Inject slurry into the flow line from high to low flow rate by opening the slurry pipe valve and set the control to achieve the desire flow rate.
7. Record the data when the flow is stabilise for 30 seconds.

3.5 Data Analysis

The data collected from both the experiment includes pressures at specific locations, and video images at view section along the pipe at a specified frequency.

3.5.1 Flow pattern identification

A survey of literature reveals several studies employed to identify the interfacial configurations of multiphase flows. Different methods are always being employed to identify the flow pattern types in the laboratory depending on the experimental philosophy and limitations. Some of these methods are visual approach, usage of electrical resistance tomography, electrical capacitance tomography conductivity probe etc., but video images and pressure data are analysed in this study.

3.5.1.1 Visual approach

DSCH9, SONY video recorder was used to examine the flow patterns of the flow in question in the transparent Perspex pipe at around 3m away from the inlet. The patterns are determined with the visual observation based on the exiting definitions of the flow configurations.

3.5.1.2 Time dependent variable approach

The usage of pressure fluctuations is explored to identify the flow regimes of oil-water flow. This is reasonable because the flow fluctuations are believed to be closely connected with the flow configuration. This is evident from the research of Hubbard and Dukler (1966), and Matsui (1984, 1986) who suggested the flow pattern identification for vertical flow using the PDF of differential pressure fluctuations. Hence, the pressure signals are considered for PDF analysis in this research to develop an objective flow pattern indicator which identifies different flow regimes.

PDF is an established technique for analysing time series random signals. It gives the time-averaged histogram depicting the distribution of amplitudes of the signal. Some researchers used this technique to identify flow patterns during gas-liquid flows (Jones Jr and Zuber, 1975; Matsui, 1986). Taking a random variable X has a cumulative distribution function $F(x)$ which is differentiable, and its PDF is defined as

$$f(x) = \frac{dF}{dx} \quad 3-1$$

$f(x)dx$ becomes the probability of observing X in the interval $x \leq X < x + dx$ and for several variables $X_1, X_2, X_3 \dots \dots X_n$ the PDF is

$$f(x_1, x_2, x_3, \dots, x_n) = \frac{\partial^n F(x_1, x_2, x_3, \dots, x_n)}{(\partial x_1, \partial x_2, \partial x_3, \dots, \partial x_n)} \quad 3-2$$

In this research, the pressure is normalized by ratio of the difference of the instantaneous and minimum pressure values to the difference between the maximum and minimum pressure values within a certain period of time;

$$\Delta P_n = \frac{P_i - P_{min}}{P_{max} - P_{min}} \quad 3-3$$

where

ΔP_n – Normalised pressure signals at a specific time

P_{max}, P_{min} – Maximum and minimum pressure signals (value) from the overall data

The normalised pressure signals are obtained from the pressure transducer downstream of the pipe. The normalised pressure signals are then fed into the PDF model to give patterns corresponding to the fluctuations. The frequency of the data collection is 250Hz through Labview for a period of 30s. In addition to the PDF, statistical analysis of the random signals is also employed, using standard deviation (Equation 3-4), skewness (Equation 3-5) and kurtosis (Equation 3-6) to quantify the PDF information. Standard deviation explains the measure of distribution about the mean value, the skewness characterises the asymmetry of the PDF while kurtosis describes the flatness of the distribution compared with the Gaussian distribution.

$$\sigma = \left(\frac{1}{N} \sum_{i=1}^N (x_i - \bar{\mu})^2 \right)^{1/2} \quad 3-4$$

$$s = \frac{E(x - \bar{\mu})^3}{\sigma^3} \quad 3-5$$

$$k = \frac{E(x - \bar{\mu})^4}{\sigma^4} \quad 3-6$$

3.5.2 Pressure gradient

Both the differential pressure and static pressure transducer were installed on the test rig to ensure consistent readings of pressure drops of the flow. The upstream and downstream of both devices are 2.17m apart. The ratio of the pressure drops to this distance gives the pressure gradients.

$$\frac{\Delta P}{\Delta Z} = \frac{P_1 - P_2}{Z_1 - Z_2} \quad 3-7$$

3.5.3 Reduction factor

The most interesting characteristic of water assist flow is the pressure drop reduction for heavy oil transportation. In order to quantify the effect of water assistance in the transport of heavy oil through a channel, pressure gradient factor analysis has been employed by many researchers. The adopted approach to evaluate this factor is presented in Equation 3-8 as reduction factor, R_F defined by Sotgia et al. (2008) and Rodriguez et al. (2009) and is given by.

$$R_F = \frac{\left(\frac{dP}{dZ}\right)_{sp}}{\left(\frac{dP}{dZ}\right)_{tp}} \quad 3-8$$

$\left(\frac{dP}{dZ}\right)_{sp}$ = Frictional pressure gradient of single – phase oil flow

$\left(\frac{dP}{dZ}\right)_{tp}$ = Frictional pressure gradient of oil – water flow

The assessment of the pumping power economy relative to single phase flow of oil, known as pressure gradient reduction factor has been employed by some authors like Russell and Charles (1959), Brauner (1991) and Beretta et al. (1997).

3.6 Chapter Summary

In this chapter, the rig equipment and experimental arrangements employed to investigate the flow behaviour of high viscosity water-sand, oil-water and oil-water-sand in horizontal pipes were presented. Table 3-1 presents the summary of the experimental rig components employed in this research. The properties of sand, water and the high viscosity oil were presented. This chapter also described in detail the methodological approach and procedures undertaken to acquire the experimental data for water-sand, oil-water and oil-water-sand. The analytical methods considered to interpret the data were discussed. These analytical methods are the flow visualisation using SONY HD video camera, the trend plot and the PDF of the pressure signals. The statistical analysis employs standard deviation, skewness and kurtosis. The formulae for determining the pressure gradient and the reduction factor were equally stated.

4 COMPUTATIONAL FLUID DYNAMICS APPROACH

A large number of multiphase flows encountered in nature and technology are a mixture of phases and being treated as multiphase systems. The studies of these systems require a lot of details which are difficult to investigate by relying only on experiments and/or one-dimensional (1-D) models. This is because a real life system is a three-dimensional (3-D) entity. The ability of CFD modelling to predict the details of flow field in both 2-D and 3-D encourages its application. In this chapter, the components of the CFD modelling are presented.

4.1 Model Development

There are two main approaches whereby multiphase systems can simulated: the Eulerian-Eulerian approach and the Eulerian-Lagrangian approach. These classifications are explained in sections 4.2 and 4.3.

4.2 Eulerian-Eulerian Model Approach

In the Eulerian-Eulerian approach, the three phases are treated mathematically as interpenetrating continua and the concept of phasic volume fraction is introduced. In Fluent (2009), three types of Eulerian-Eulerian method are presented; they are the Volume of Fluid (VOF), the mixture model (algebraic-slip, drift-flux, local-equilibrium, and the suspension model) and the Eulerian model. The Eulerian model treats particle phase as a continuum and develops its conservation equation on a control volume basis in the same form as fluid.

4.2.1 Volume of fluid model

VOF is designed for surface-tracking of two or more immiscible fluids where position of the interface between the fluids is of interest. It solves a single set of momentum equations shared by the fluids and the volume fraction of each of the fluids is tracked

throughout the domain. VOF is applicable mostly in stratified flow, free-surface flows, motion of large bubbles in a liquid and the like.

4.2.2 Mixture model

Mixture model is designed for two or more phases (fluid or particulates). It solves mixture momentum equation and prescribes relative velocities to describe the dispersed phase. The phases are treated as interpenetrating continua. It can also be used without relative velocities for the dispersed phases to model homogenous flow. It is applicable in particle laden flows with low loading, bubbly flows, sedimentation and cyclone separators.

4.2.3 Eulerian model

This model solves for both continuity and momentum equations for each phase present in a multiphase flow. It couples two or more Eulerian models which are continuous in nature. It is the most complex of the multiphase flow models. It is more accurate than others but not cost effective. It is useful when accuracy is more important than the cost. This model also requires a lot of modelling of interfacial forces compared with VOF model.

4.3 Eulerian-Lagrangian Model Approach

This is an approach that couples the Eulerian model with particle model. Eulerian model is continuous in nature, while Lagrangian model is discrete in nature because it solves particle distribution and motion problems. However, this approach is difficult to use for practical flow analysis because the fluid/particle definition requires millions of droplets/particles. The size of droplets/particles needed for analysis makes their interactions to be more complex. Additionally, all these interactions have to be modelled in order to analyse the fluid motion reasonably, and all these complexities lead to more computational time.

4.4 CFD Models Development

In the present study, VOF model is employed because of its simplicity and reduced computational cost. The governing equations employed in VOF CFD are the mass conservation equation (also known as continuity equation), and Navier-stokes equation (also known as momentum equation).

4.4.1 Model assumptions

Some of the assumptions considered in setting up this model are outlined below.

- 1) The flow is not axisymmetrical.
- 2) The liquid phases are incompressible.
- 3) The pressure in the radial direction is constant.
- 4) The diameter of the pipe is sufficiently small compare with its length; the pipe is long enough for the flow to develop.
- 5) The effect of temperature is negligible

4.4.2 Governing equations

The governing equations employed in computational fluid dynamic are the mass conservation equation (also known as continuity equation), and Navier-stokes equation (also known as momentum equation). In the present research, isothermal motions of an incompressible two-phase flow are considered. The momentum equation is dependent of the volume fractions of all phases. Once the Reynolds averaging approach for turbulence modelling is applied, the Navier- Stoke equations can be written in Cartesian tensor form as shown in Equation 4-1.

4.4.2.1 Continuity equation

The equation for conservation of mass (or continuity equation) and momentum are given (Ansys Inc., 2003; Bird et al., 2006) by;

$$\frac{\partial}{\partial t}(\rho) + \nabla \cdot (\rho \vec{v}) = 0 \quad 4-1$$

4.4.2.2 Momentum equation

A momentum equation is used for the VOF. This depends on the volume fractions of all phases in the flow through density and viscosity parameters as follows

$$\frac{\partial}{\partial t}(\rho \vec{v}) + \nabla \cdot (\rho \vec{v} \vec{v}) = -\nabla p + \nabla \cdot [\mu(\nabla \vec{v} + \nabla \vec{v}^T)] + \rho \vec{g} + \vec{F} \quad 4-2$$

Where \vec{F} is a body force, and μ is the viscosity of the phase. The tracking of the interface(s) between the phases is accomplished by the solution of a continuity equation for the volume fraction (α) of one (or more) of the phases. For the q th phase, this equation has the following form:

$$\frac{\partial \alpha_q}{\partial t} + \nabla \cdot (\alpha_q \vec{v}) = \frac{S \alpha_q}{\rho_q} \quad 4-3$$

Where S is a source. The primary-phase volume fraction will be computed based on the constraint:

$$\sum_{q=1}^n \alpha_q = 1 \quad 4-4$$

The geometric reconstruction scheme was used to calculate the fluxes at control volume faces required by the VOF model.

4.4.2.3 Turbulence models

Turbulence models must be considered in the numerical simulation provided the Reynolds number is in a turbulent region. It is an unfortunate fact that no single turbulence model is universally accepted as being superior for all classes of problems. The choice of turbulence model will depend on considerations such as the physics of the flow, the established practice for a specific class of problem, the level of accuracy required, the available computational resources, and the amount of time available for the simulation (Fluent, 2009).

Two alternative methods are being employed to render the Navier-Stokes equations tractable so that the small-scale turbulent fluctuations do not have to be directly simulated; they are Reynolds-averaging (or ensemble-averaging) and filtering. Fluent (2009) further reported that the above statement is due to the fact that the time-dependent solutions of the Navier-Stokes equations for high Reynolds-number turbulent flows in complex geometries which set out to resolve all the way down to the smallest scales of the motions are unlikely to be attainable for some time to come. The above mentioned methods introduce additional terms in the governing equations that need to be modelled in order to achieve a "closure" for the unknowns.

The Reynolds Averaged Navier-Stokes (RANS)-based modelling approach governs the transport of the averaged flow quantities and greatly reduces the required computational effort and resources. This approach is widely adopted for practical engineering applications. The second method is called Large Eddy Simulation (LES) model which provides an alternative approach in which large eddies are explicitly computed (resolved) in a time-dependent simulation using the "filtered" Navier-Stokes equations. The rationale behind LES is that by modelling less of turbulence (and resolving more), the error introduced by turbulence modelling can be reduced. It is also believed to be easier to find a "universal" model for the small scales, since they tend to be more isotropic and less affected by the macroscopic features like boundary conditions, than the large eddies. For high Reynolds number industrial flows, LES requires a significant amount of computational resources.

However, one of the main problems in turbulence modeling is the accurate prediction of flow separation from a smooth surface. Standard two-equation turbulence models often fail to predict the onset and the amount of flow separation under adverse pressure gradient conditions. In general, turbulence models based on the ε -equation predicts the onset of separation too late and under-predict the amount of separation later on. Therefore, the prediction is not on the conservative side from an engineering standpoint. The models developed to solve this problem have shown a significantly more accurate prediction of separation in a number of test cases and in industrial applications.

Prediction of separation is important in many technical applications both for internal and external flows.

Currently, the most prominent two-equation model in this area is $k - \omega$ based models of Menter (1994). The $k - \omega$ based Shear-Stress-Transport (SST) model was designed to give a highly accurate prediction of the onset and the amount of flow separation under adverse pressure gradients by the inclusion of transport effects into the formulation of the eddy-viscosity. This result in a major improvement in terms of flow separation predictions but its ability to predict the characteristics of high viscosity oil-based multiphase flow has not been proven.

In order to simulate turbulence in the present research, a number of popular RANS turbulent models are compared; Standard k -epsilon, low-Reynolds- k -epsilon, standard k -omega and low-Reynolds- k -omega models. The reason for these models is that they have demonstrated capability to properly simulate many industrial processes including multiphase flow. The models are described by the following equations:

i. Standard k -epsilon model

$$\frac{\partial}{\partial t}(\rho k) + \frac{\partial}{\partial x_j}(\rho k u_j) = \frac{\partial}{\partial x_j} \left[\left(\mu + \frac{\mu_t}{\sigma_k} \right) \frac{\partial k}{\partial x_j} \right] + P_k + P_b + \rho \epsilon - Y_M + S_k \quad 4-5$$

$$\begin{aligned} \frac{\partial}{\partial t}(\rho \epsilon) + \frac{\partial}{\partial x_j}(\rho \epsilon u_j) \\ = \frac{\partial}{\partial x_j} \left[\left(\mu + \frac{\mu_t}{\sigma_\epsilon} \right) \frac{\partial \epsilon}{\partial x_j} \right] - \rho C_{2\epsilon} \frac{\epsilon^2}{k} + C_{1\epsilon} \frac{\epsilon}{k} (P_k + C_{3\epsilon} P_b) + S_\epsilon \end{aligned} \quad 4-6$$

Where

$$\mu_t = \rho C_\mu \frac{k^2}{\epsilon} \quad 4-7$$

$$C_{1\epsilon} = 1.44, \quad C_2 = 1.9, \quad \sigma_k = 1.0, \quad \sigma_\epsilon = 1.2 \quad C_\mu = 0.09 \quad 4-8$$

are the modelling turbulent viscosity, model constant and turbulent intensity respectively, k is the turbulent kinetic energy; ϵ is the dissipation rate of k . The fluid viscosity must be corrected for turbulence in the Navier-Stokes equations employing an effective viscosity

$$\mu_{eff} = \mu_t + \mu \quad 4-9$$

where μ is the dynamic viscosity and μ_t is the turbulent viscosity.

ii. Low Reynolds k-epsilon model

Launder and Sharma (1974) presented an improved model to take care of a viscous dominating wall flow. This model has a general form which is presented in 4-10.

$$\frac{\partial}{\partial t}(\rho k) + \frac{\partial}{\partial x_j} \left[\rho k u_i - \left(\mu + \frac{\mu_t}{\sigma_k} \right) \frac{\partial k}{\partial x_j} \right] = P - \rho \epsilon + \rho D \quad 4-10$$

$$\frac{\partial}{\partial t}(\rho \epsilon) + \frac{\partial}{\partial x_j} \left[\rho \epsilon u_i - \left(\mu + \frac{\mu_t}{\sigma_k} \right) \frac{\partial \epsilon}{\partial x_j} \right] = P - (C_{\epsilon 1} f_1 P - C_{\epsilon 2} f_2 P \rho \epsilon) \frac{\epsilon}{k} + \rho E \quad 4-11$$

$$\mu_t = C_\mu f_\mu \rho \frac{k^2}{\epsilon} \quad 4-12$$

$$P = \tau_{ij}^{turb} \frac{\partial u_i}{\partial x_j}$$

Where $C_{\epsilon 1}$, $C_{\epsilon 2}$, C_μ , σ_k , σ_ϵ are model constants. f_μ , f_1 and f_2 are damping functions while D and E are the source terms which are active close to the walls and makes it possible to solve k and ϵ down to the viscous sublayer.

- **Model constants**

Below are the default model constants that were used in the model selection test.

$$C_{\epsilon 1} = 1.44, C_{\epsilon 2} = 1.92, C_{\mu} = 0.09, \sigma_k = 1.0, \sigma_{\epsilon} = 1.3, \quad 4-13$$

$$f_1 = 1.0, f_2 = 1 - 0.3 \exp - Re_t^2, \quad \epsilon_{wall} = 0$$

$$D = 2\nu \left(\frac{\partial \sqrt{k}}{\partial y} \right)^2, \quad E = 2\nu v_t \left(\frac{\partial^2 u}{\partial y^2} \right)^2, \quad f_{\mu} = \frac{\exp(-3.4)}{\left(1 + R_t/50 \right)^2}$$

iii. Standard k-omega model

The k-omega model is a two-equation model that is an alternative to the k-epsilon model. The transport equations solved are for the turbulent kinetic energy and a quantity called omega, ω which is defined as the specific dissipation rate, that is, the dissipation rate per unit turbulent kinetic energy. The book by D.C. Wilcox (1988) is the most comprehensive reference on the k-omega model, discussing the origin of the model, comparing it to other models, and presenting the latest version of the model. As the originator of the k-omega model, Wilcox touts the superiority of his model over the k-epsilon model, and the superiority of the omega transport equation over other scale equations.

One reported advantage of the k-omega model over the k-epsilon model is its improved performance for boundary layers under adverse pressure gradients. Perhaps the most significant advantage is that it may be applied throughout the boundary layer, including the viscous-dominated region, without further modification. Furthermore, the standard k-omega model can be used in this mode without requiring the computation of wall distance.

The biggest disadvantage of the k-omega model, in its original form, is that boundary layer computations are very sensitive to the values of ω in the free stream. This translates into extreme sensitivity to inlet boundary conditions for internal flows, a problem that does not exist for the k-epsilon models.

The standard k- ω model in ANSYS FLUENT is based on the Wilcox k- ω model (Crowe et al., 1996), which incorporates modifications for low-Reynolds-number effects, compressibility, and shear flow spreading. The Wilcox model predicts free shear flow

spreading rates that are in close agreement with measurements for far wakes, mixing layers, and plane, round, and radial jets, and is thus applicable to wall-bounded flows and free shear flows. The standard k- ω model is an empirical model based on model transport equations for the turbulence kinetic energy k and the specific dissipation rate ω , which can also be thought of as the ratio of ϵ to k. The k- ω model has been modified over the years. Production terms have been added to both the k and ω equations, which have improved the accuracy of the model for predicting free shear flows.

The turbulence kinetic energy k and the specific dissipation rate ω are obtained from the transport equations stated in 4-14.

$$\frac{\partial}{\partial t}(\rho k) + \frac{\partial}{\partial x_i}(\rho k u_i) = \frac{\partial}{\partial x_j} \left(\Gamma_k \frac{\partial k}{\partial x_j} \right) + G_k - Y_k + S_k \quad 4-14$$

And

$$\frac{\partial}{\partial t}(\rho \omega) + \frac{\partial}{\partial x_i}(\rho \omega u_i) = \frac{\partial}{\partial x_j} \left(\Gamma_\omega \frac{\partial \omega}{\partial x_j} \right) + G_\omega - Y_\omega + D_\omega + S_\omega \quad 4-15$$

G_k represents the generation of turbulence kinetic energy due to mean velocity gradients while G_ω represents the generation of omega. Γ_k and Γ_ω represent the effective diffusivity of k and ω , respectively, which are calculated as described below. Y_k and Y_ω represent the dissipation of k and ω due to turbulence. S_k and S_ω are user defined source terms.

- **Modelling effective diffusivity**

The effective diffusivities for the SST k- ω model are given by

$$\Gamma_k = \mu + \frac{\mu_t}{\sigma_k}$$

$$\Gamma_\omega = \mu + \frac{\mu_t}{\sigma_\omega}$$
4-16

Where σ_k and σ_ω are the turbulent Prandtl numbers for k and ω , respectively.

The turbulent viscosity μ_t , is computed as

$$\mu_t = \alpha^* \frac{\rho k}{\omega}$$
4-17

- **Low-Reynolds Number Correction**

The coefficient α^* damps the turbulent viscosity causing a low-Reynolds-number correction and given by

$$\alpha^* = \alpha_\infty^* \left(\frac{\alpha_0^* + Re_t/R_k}{1 + Re_t/R_k} \right)$$
4-18

Where

$$Re_t = \frac{\rho k}{\mu \omega}$$

$$Re_k = 6$$

$$\alpha_0^* = \frac{\beta_i}{3}$$

$$\beta_i = 0.072$$
4-19

In high-Reynolds number form of the k - ω model, $\alpha^* = \alpha_\infty^* = 1.0$

- **Modelling the turbulence production**

- **Production of k**

G_k represents the production of turbulence kinetic energy and defined as

$$G_k = -\frac{\rho \overline{(u'_i u'_j)} (\partial u_j)}{\partial x_i} \quad 4-20$$

In order to evaluate G_k in a manner consistent with the Boussinesq hypothesis

$$G_k = \mu_t S^2 \quad 4-21$$

Where S is the modulus of the mean rate of strain tensor defined as in equation k-epsilon

- **Production of ω**

The production of ω is given by

$$G_\omega = \alpha \frac{\omega}{k} G_k \quad 4-22$$

The coefficient α is given by

$$\alpha = \frac{\alpha_\infty}{\alpha^*} \left(\frac{\alpha_\infty + Re_t / R_\omega}{1 + Re_t / R_\omega} \right) \quad 4-23$$

Where $R_\omega = 2.95$

In the high-Reynolds number form of the k- ω model,

$$\alpha = \alpha_\infty = 1$$

- **Modelling the turbulence dissipation**
 - **Dissipation of k**

The dissipation of k is given as

$$Y_k = \rho \beta^* f_{\beta^*} k \omega \quad 4-24$$

Where

$$f_{\beta^*} = \begin{cases} 1 & \chi_k \leq 0 \\ \frac{1 + 680\chi_k^2}{1 + 400\chi_k^2} & \chi_k > 0 \end{cases} \quad 4-25$$

Where

$$\chi_k \equiv \frac{1}{\omega^3} \frac{\partial k}{\partial x_j} \frac{\partial \omega}{\partial x_j} \quad 4-26$$

And

$$\beta^* = \beta_i^* [1 + \zeta^* F(M_t)] \quad 4-27$$

$$\beta_i^* = \beta_\infty^* \left(\frac{4/15 + \left(Re_t / R_\beta \right)^4}{1 + \left(Re_t / R_\beta \right)^4} \right) \quad 4-28$$

$$\zeta^* = 1.5$$

$$R_\beta = 8.0$$

$$\beta_\infty^* = 0.09$$

○ **Dissipation of ω**

The dissipation of ω is given by

$$Y_\omega = \rho \beta f_\beta \omega^2 \quad 4-29$$

$$f_\beta = \frac{1 + 70\chi_\omega}{1 + 80\chi_\omega}$$

$$\chi_\omega = \left| \frac{\Omega_{ij} \Omega_{jk} S_{ki}}{(\beta_\infty^* \omega)^3} \right|$$

$$\Omega_{ij} = \frac{1}{2} \left(\frac{\partial u_i}{\partial x_j} - \frac{\partial u_j}{\partial x_i} \right)$$

$$\beta = \beta_i \left[1 - \frac{\beta_i^*}{\beta_i} \zeta^* F(M_t) \right]$$

○ **Compressibility correction**

The compressibility correction is given by

$$F(M_t) = \begin{cases} 0 & M_t \leq M_{t0} \\ M_t^2 - M_{t0}^2 & M_t > M_{t0} \end{cases} \quad 4-30$$

Where

$$M_t^2 \equiv \frac{2k}{a^2}$$

$$M_{t0} = 0.25$$

$$a = \sqrt{\gamma RT}$$

In the high Reynolds number form of the k- ω model,

$$\beta_i^* = \beta_\infty^*.$$

In the incompressible form,

$$\beta^* = \beta_i^*.$$

$$\alpha_\infty^* = 1.0, \alpha_\infty = 0.52, \alpha_0 = \frac{1}{9}, \beta_\infty^* = 0.09, \beta_i = 0.072, R_\beta = 8.0$$

$$R_k = 6.0, R_\omega = 2.95, \zeta^* = 1.5, \alpha_k = 2.0, \alpha_\infty = 2.0$$

4-31

iv. Shear Stress Transport k-omega (SST-k-omega)

The SST k-omega model was developed by Menter (1994) to effectively blend the robust and accurate formulation of the k-omega model in the near-wall region with the free-stream independence of the k-epsilon model in the far field. To achieve this, the k-epsilon model is converted into a k-omega formulation. The SST k-omega model is similar to the standard k-omega model, but includes the following refinements:

- The standard k-omega model and the transformed k-epsilon model are both multiplied by a blending function and both models are added together. The

blending function is designed to be one in the near-wall region, which activates the standard k-omega model, and zero away from the surface, which activates the transformed k-epsilon model.

- The definition of the turbulent viscosity is modified to account for the transport of the turbulent shear stress.
- The SST model incorporates a damped cross-diffusion derivative term in the omega equation.
- The modeling constants are different.

These features make the k-omega model more accurate and reliable for a wider class of flows (e.g., adverse pressure gradient flows, airfoils, transonic shock waves) than the standard k-omega model. Other modifications include the addition of a cross-diffusion term in the omega equation and a blending function to ensure that the model equations behave appropriately in both the near-wall and far-field zones.

$$\frac{\partial}{\partial t}(\rho k) + \frac{\partial}{\partial x_i}(\rho k u_i) = \frac{\partial}{\partial x_j} \left(\Gamma_k \frac{\partial k}{\partial x_i} \right) + \tilde{G}_k - Y_k + S_k \quad 4-32$$

and

$$\frac{\partial}{\partial t}(\rho \omega) + \frac{\partial}{\partial x_i}(\rho \omega u_i) = \frac{\partial}{\partial x_j} \left(\Gamma_\omega \frac{\partial \omega}{\partial x_j} \right) + G_\omega - Y_\omega + D_\omega + S_\omega \quad 4-33$$

In these equations, \tilde{G}_k represents the generation of turbulence kinetic energy due to mean velocity gradients, calculated as described in equation 4-32. G_ω represents the generation of omega, calculated as described in equation 4-32. Γ_k and Γ_ω represent the effective diffusivity of k and ω , respectively, which are calculated as described below. Y_k and Y_ω represent the dissipation of k and ω due to turbulence, calculated as described in equation 4-32. D_ω represents the cross-diffusion term, calculated as described below. S_k and S_ω are user-defined source terms. The effective diffusivities for k- ω are the same as in standard k- ω model.

The turbulent viscosity, μ_t is computed as

$$\mu_t = \frac{\rho k}{\omega} \frac{1}{\max\left[\frac{1}{\alpha^*}, \frac{SF_2}{a_1 \omega}\right]} \quad 4-34$$

here S is the strain rate magnitude and

$$\sigma_k = \frac{1}{F_1/\sigma_{k,1} + (1-F_1)/\sigma_{k,2}} \quad 4-35$$

$$\sigma_\omega = \frac{1}{F_1/\sigma_{\omega,1} + (1-F_1)/\sigma_{\omega,2}}$$

α^* is defined in equation 4-18. The blending functions F_1 and F_2 are given by

$$F_1 = \tanh(\Phi_1^4) \quad 4-36$$

$$\Phi_1 = \min\left[\max\left(\frac{\sqrt{k}}{0.09\omega y}, \frac{500\mu}{\rho y^2 \omega}\right), \frac{4\rho k}{\sigma_{\omega,2} D_\omega^+ y^2}\right]$$

$$D_\omega^+ = \max\left[2\rho \frac{1}{\sigma_{\omega,2}} \frac{1}{\omega} \frac{\partial k}{\partial x_j} \frac{\partial \omega}{\partial x_j}, 10^{-10}\right] \quad 4-37$$

$$F_2 = \tanh(\Phi_2^2)$$

$$\Phi_2 = \max\left[2 \frac{\sqrt{k}}{0.09\omega y}, \frac{500\mu}{\rho y^2 \omega}\right]$$

Where y is the distance to the next surface and D_{ω}^+ is the positive portion of the cross-diffusion term.

- **Modelling turbulence production**

- **Production of k**

The term \tilde{G}_k represents the production of turbulence kinetic energy, and is defined as

$$\tilde{G}_k = \min(G_k, 10\rho k\omega) \quad 4-38$$

where G_k is defined in the same manner as in the standard k - ω model.

- **Production of ω**

The term G_{ω} represents the production of ω and is given by

$$G_{\omega} = \frac{\alpha}{\nu_t} \tilde{G}_k \quad 4-39$$

$$\alpha_{\infty} = F_1\alpha_{\infty,1} + (1 - F_1)\alpha_{\infty,2}$$

Where

$$\alpha_{\infty,1} = \frac{\beta_{i,1}}{\beta_{\infty}^*} - \frac{\kappa^2}{\alpha_{\omega,1}\sqrt{\beta_{\infty}^*}} \quad 4-40$$

$$\alpha_{\infty,2} = \frac{\beta_{i,2}}{\beta_{\infty}^*} - \frac{\kappa^2}{\alpha_{\omega,2}\sqrt{\beta_{\infty}^*}}$$

Where $\kappa=0.41$

- **Modelling turbulence dissipation**

- **Dissipation of k**

The term Y_k represents the dissipation of turbulence kinetic energy and is defined as

$$Y_k = \rho \beta^* f_{\beta^*} k \omega \quad 4-41$$

Where $f_{\beta^*} = 1$

- **Dissipation of ω**

The term Y_ω represents the dissipation of ω and is defined as

$$Y_k = \rho \beta f_\beta \omega^2 \quad 4-42$$

Where $f_\beta = 1$

$$\beta_i = F_1 \beta_{i,1} + (1 - F_1) \beta_{i,2} \quad 4-43$$

- **Cross-diffusion modification**

The SST k- ω model is based on both the standard k- ω model and standard k- ϵ model. In order to blend these two models together, the standard k- ϵ model has been transformed into equations based on k and ω , which leads to the introduction of a cross-diffusion term D_ω and define as

$$D_\omega = 2(1 - F_1) \rho \sigma_{\omega,2} \frac{1}{\omega} \frac{\partial k}{\partial x_j} \frac{\partial \omega}{\partial x_j} \quad 4-44$$

- **Model constants**

$$\sigma_{\omega,1} = 2.0, \sigma_{\omega,2} = 1.168, \sigma_{k,1} = 1.176, \sigma_{k,2} = 1.0 \quad 4-45$$

$$a_1 = 0.31, \beta_{i,1} = 0.075, \beta_{i,2} = 0.0828$$

4.4.3 Numerical scheme

Finite Volume Method (FVM) discretisation scheme (in Fluent 12.1) with an algebraic segregated solver and co-located grid arrangement was implemented to solve the system of partial and ordinary differential equations. In this grid arrangement pressure and velocity are both stored at cell centres. (Versteeg and Malalasekera, 2007) explain the details of the FVM discretisation. Since FLUENT uses a segregated solver, the continuity and momentum equations need to be linked. Various techniques are reported in the literature and available in FLUENT. PISO algorithm which stands for Pressure Implicit with Splitting of Operators by (Issa, 1986) was employed because of its good performance to find a fast converged solution. PISO is a pressure-velocity calculation procedure that involves one predictor step and two corrector steps. Fluent (2009) recommends it for unsteady flow problems.

4.4.3.1 Solver controls

All simulations in this research are performed under time dependent (transient) conditions. The main controlling factor is the time step. This is set to give a small number of time steps as possible whilst maintaining a smoothly converging solution. Inside each time interval iterations are carried out to resolve the transport equations for that time step. As long as the time step is small enough to get convergence, the smaller the time step, the fewer iterations, per time step are required. For this iteration process to converge, it may be necessary to control the change of the variables from previous iteration to the present. This is achieved with under relaxation factors. Under relaxation factors of 0.3, 0.5 and 0.9 respectively were applied on pressure, momentum and turbulence kinetic energy parameters.

A measure of how well the solution is converged can be obtained by plotting the residuals errors for each equation at the end of each time step. For a well-converged solution, the maximum residual obtained was set to 10^{-8} .

4.4.4 Mesh

The geometry and mesh that were used in this study were developed with Gambit 2.4 and imported into FLUENT 12.1 for the case simulations. Mesh forms an integral part

of numerical solution, and must satisfy certain criteria to ensure a valid and accurate solution. Gambit 2.4 mesh generation tools has the capability to create grids by dimensions, ranging from geometry in multi-block structured, unstructured hexahedral, tetrahedral, hybrid grids consisting of hexahedral, tetrahedral, pyramidal and prismatic cells and Cartesian grid formats combined with boundary conditions. Within the 3D geometries, different mesh schemes were tested ranging from unstructured tetrahedral to structure hexahedral arrangements.

The geometry for the case study modelled is illustrated in Figure 4-1; it is a 5m long, 1- in internal diameter horizontal pipe similar to the experimental arrangements. The pipe axis is always aligned with the z - axis and several measurements sections were placed along the pipe. The geometry developed for this research is 3-Dimensional.

Table 4-1: Geometry properties

Geometry	Pipe Length (m)	Pipe Diameter (m)	Number of cells
1	5.0	0.0254	480,000

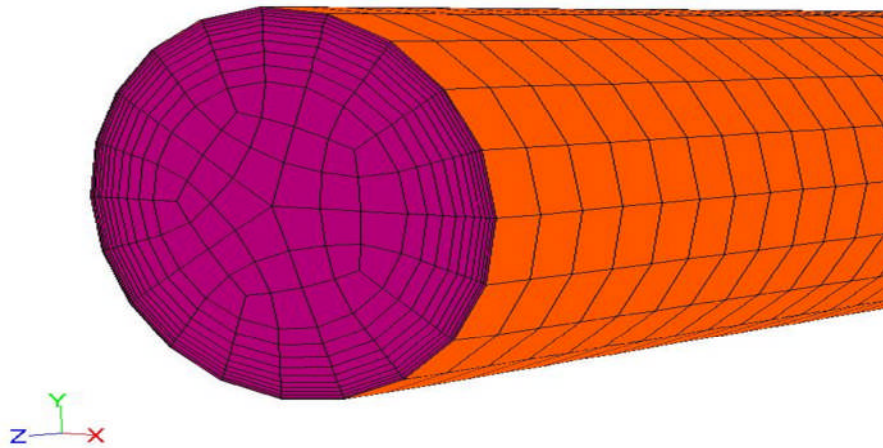


Figure 4-1: Pipe geometry

The region near the wall is meshed finer than the rest of the cross section, as it contains greater amount of gradients. The distance of the first node above the wall is needed,

when using wall functions so that the normalized wall distance, y^+ values may remain within $y_w < 5$ or $y_w > 25$.

$$y^+ = \frac{y_w U_\tau}{\nu} \quad 4-46$$

Where

$$U_\tau = U \sqrt{\frac{f}{2}} \quad 4-47$$

$$f = 0.079 Re^{-0.25} \quad 4-48$$

4.4.4.1 Mesh independent study

One of the most significant factors that influence the computation time is the size of the computational grid. A mesh sensitivity analysis is needed in the construction and analysis of the CFD model to identify the minimum mesh density that ensures that the solution is independent of the mesh size. Since high viscosity oil-water two-phase flow is characterised by pressure gradient along the pipe, hence it was used for this analysis. For the CFD model, in order to determine the pressure gradient along the pipe, the following procedure is adopted: Inside the pipe geometry, some cross sectional area are defined and the Area-Weighted Average value of the static pressure is calculated over the surface. The value of static pressure in this surface is recorded every time step. This area-weighted average of the pressure is computed by dividing the summation of the product of the static pressure and facet area by the total area of the surface as follows:

$$\frac{1}{A} \int P dA = \frac{1}{A} \sum_{i=1}^n P_i |A_i| \quad 4-49$$

These set of static pressure were used to calculate the pressure drops and gradients along the pipe. A suitable grid resolution was found from five different 3D meshes that were examined in the present study for the horizontal pipe geometry illustrated in Figure 4.1. It was observed that when the mesh is too coarse a refinement in the mesh

have a considerable influence on the result, as shown in Figure 4.1 from Mesh-1 to Mesh-5.

Table 4-2: Mesh Dependence Profile

Case	Domain	Structure	Nodes	No of cells
Mesh-1	3D	Hexahedral	75651	70000
Mesh-2	3D	Hexahedral	151151	140000
Mesh-3	3D	Hexahedral	251251	240000
Mesh-4	3D	Hexahedral	502251	480000
Mesh-5	3D	Hexahedral	1002501	960000

It was also observed that when the mesh is too coarse the phase distribution and the numerical results are not stable. It was also found that mesh refinement have a considerable influence on the result, as shown in Figure 4-2 ranging from mesh-1 to mesh-5. The phase distribution in Mesh-3 to mesh-5 appear similar but with a little difference in the pressure gradient. Based on the mesh sensitivity analysis presented in Figure 4-2, mesh-4 is chosen since the pressure gradient is about 6% different from mesh-5; this takes care of the computational cost and time. In addition, the basic idea was to develop a grid that can be suitably used for the simulation of a wide range of inlet flow conditions and which requires a minimum cost and time with reduced numerical restrictions.

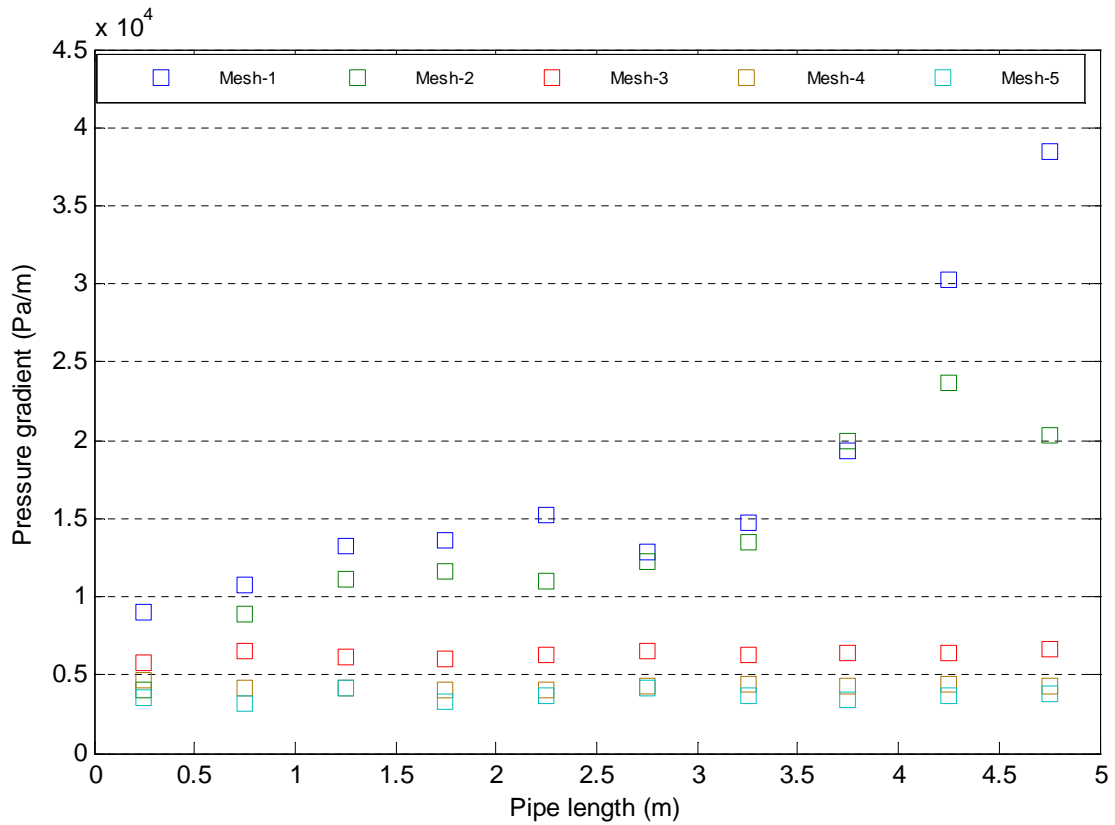


Figure 4-2: Pressure gradients of the mesh profiles

4.4.5 Y+ profile

In the same vein, the resolution of boundary layers requires the grid to be clustered in the direction normal to the surface with the spacing of the first grid point from the wall to be well within the laminar sublayer of the boundary layer. In the case of turbulent flows, the first grid point from the wall should exhibit a y^+ value less than 1.0. This was considered in this research as shown in Figure 4-3 below; the Figure 4-3 shows the average y^+ for different flow velocities for a single-phase water flow.

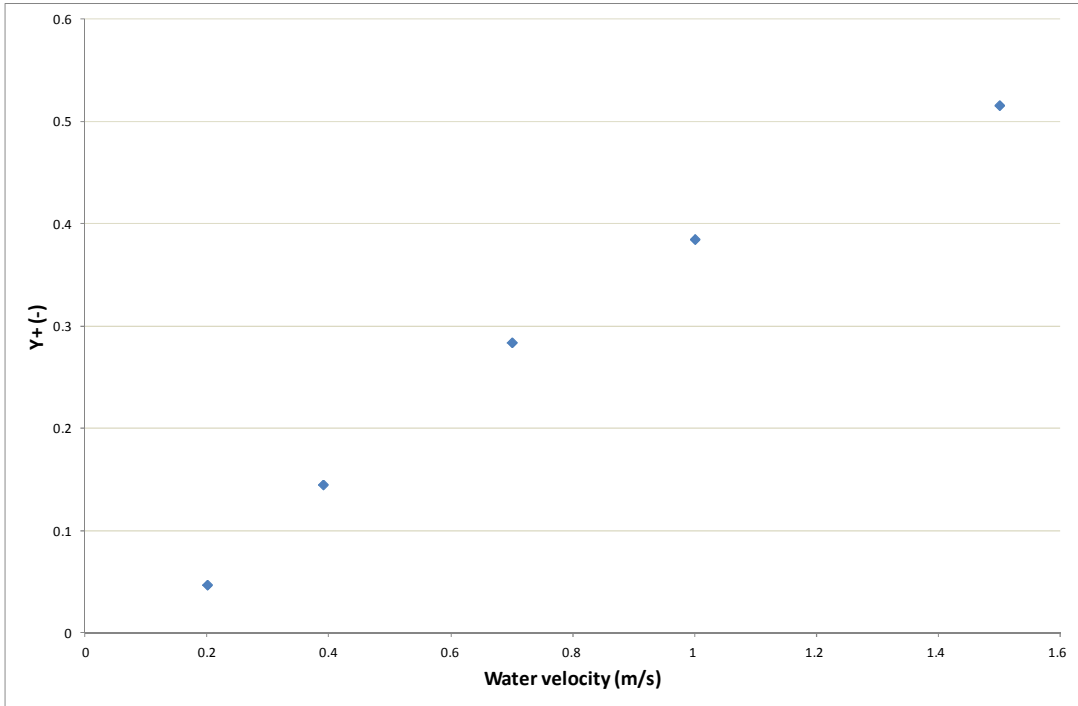


Figure 4-3: Y+ profile for water turbulent flows in 1-in ID pipe

4.4.6 Data analysis

The data collected from CFD includes pressures data downstream of the pipe at specific location (i.e. 3m) along the pipe and at a specified frequency. Volume fraction contours, turbulent kinetic energy, and turbulent dissipation rate were also collected. All these were analysed using the same tools mentioned in section 3.5 (i.e. contours for visual observation, and trend and PDF plot for pressure signals analysis). Pressure gradient calculation was also employed.

4.4.7 Analysis of single phase flow

The CFD model was first validated by using experimental measurements of single phase liquid (water, and oil) flow in horizontal pipe as shown in Figure 4-4 and Figure 4-5. The figures show good matches for water at high flow rate when compared with both theoretical and experimental data, but under predicted the gradients at low flow rate. However, when it was used for high viscous oil, it was an excellent agreement with

the Darcy-Weisbach theoretical model while the experiment relatively reflected some deviations from the model. Generally, the CFD model possessed a good level of confidence for the subsequent simulations. However, CFD performance on the prediction of the pressure gradient of water is poorer than that oil. This could be traced to the fact that the oil flow condition in this study was laminar while water's flow condition was turbulence. This suggests that the turbulence model has an adverse effect on the flow prediction. The CFD model is then used to investigate the effects of sand concentration in water on the pressure gradient in Chapter 5 section 5.5, the effect of water on high viscous oil in Chapter 6 section 6.2 on two-phase flow while Chapter 7 section 7.7 attends to three phase oil-water-sand flows.

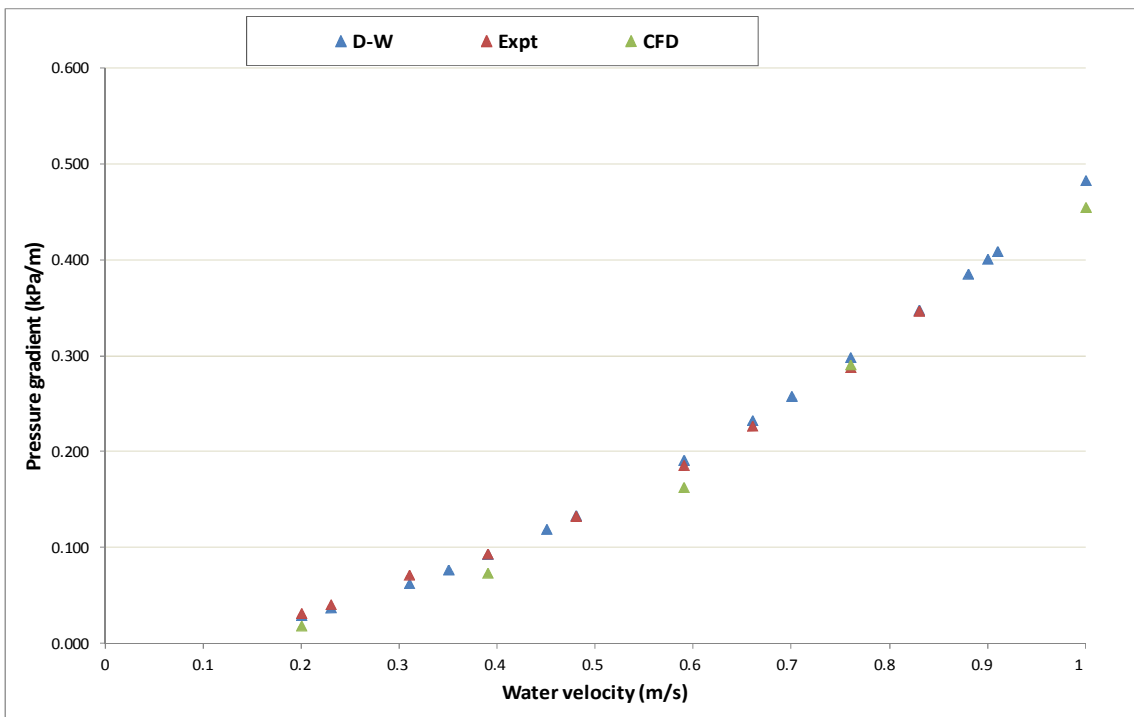


Figure 4-4: Comparison of D-W, Experimental and CFD pressure gradients of a single phase water in 1-in ID 5m long pipe

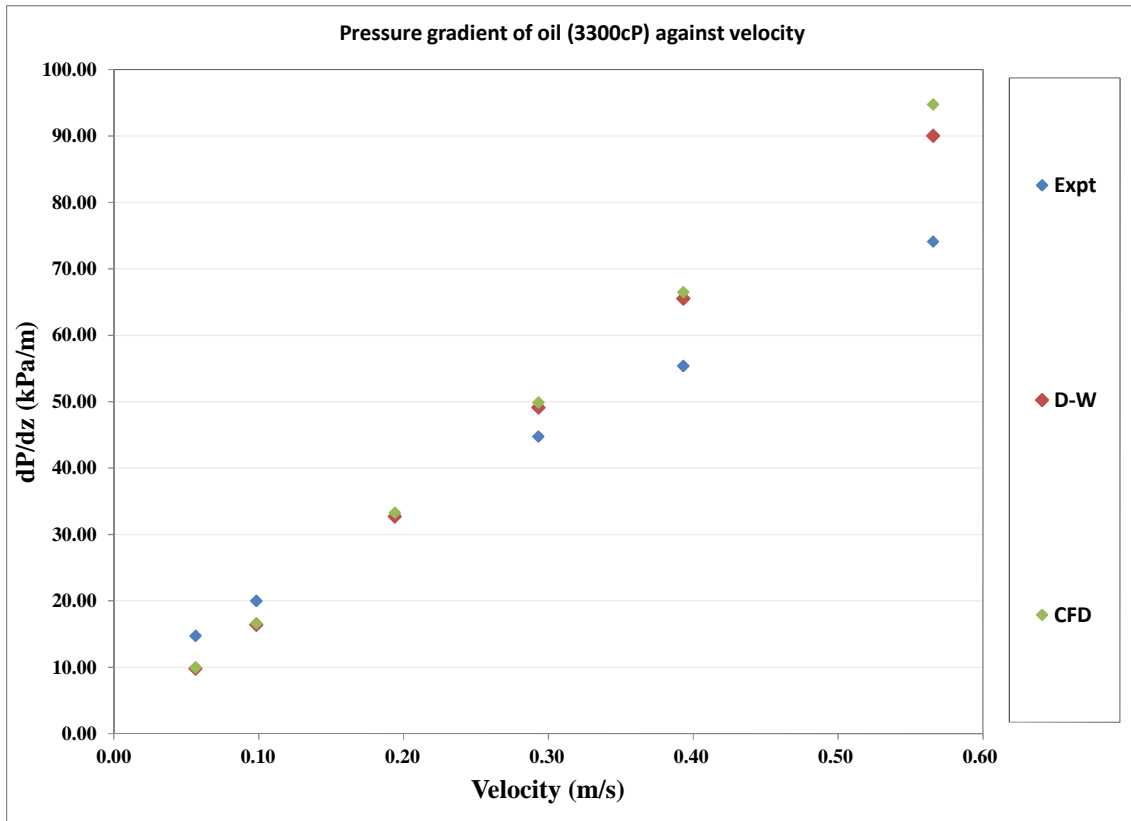


Figure 4-5: Comparison of D-W, Experimental and CFD pressure gradients of a single phase oil in 1-in ID 5m long pipe.

4.5 Chapter Summary

This chapter presented the description of CFD classifications, the model assumptions and the CFD model development adopted in this study; the Navier-Stokes governing equations and the types of turbulence models were discussed. The mesh generation, the mesh independent study on the simulation results and the results of the preliminary study on single phase (water/oil) flow compared with both theoretical and experimental results were presented.

5 WATER-SAND FLOW IN 1” ID HORIZONTAL PIPE

In this chapter, the experimental results of water-sand flow in 1-in ID pipe are presented. This chapter is considered important in order to establish the impact of the presence of sand in the multiphase flow composition. The sand concentrations considered in this study are 2.15e-04%, 5.38e-04%, 8.10e-04%, and 1%, 5% and 10% v/v. In order to characterise the sand behaviour in water, a series of video clips were recorded both from the bottom and side of the viewing section of the horizontal Perspex pipe flow line at different flow conditions.

The output of the simulation in which Eulerian VOF CFD model was employed to study the flow of sand (212microns average particle size) in water at 1% v/v sand concentrations was also presented. The CFD results are validated using experimental measurements of pressure gradient and images obtained from the experiments.

5.1 Test Matrix

In order to observe the behaviours of the water-sand in the horizontal pipe configuration, the experimental campaigns were conducted ranging from high, medium and low flow rates. A total of 99 runs of experiments were carried out on water-sand flow in 1-in rig.

5.2 Flow Regime Identification



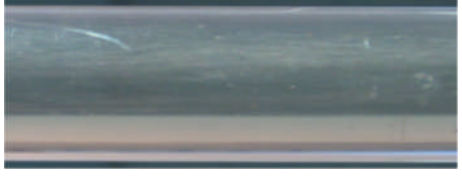
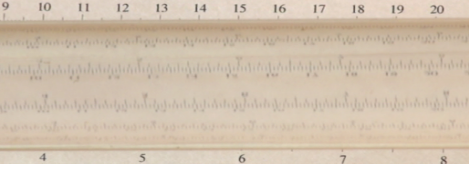

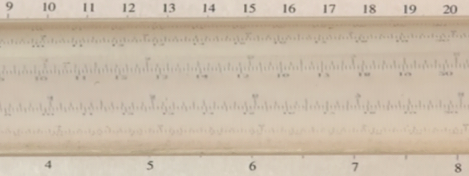
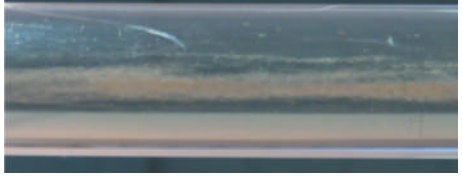
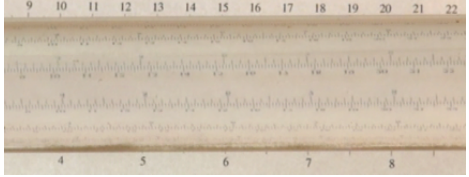


Photographic and pressure data of water-sand flow in 1-in ID horizontal pipe at different sand concentrations were obtained. Samples of photographic data are presented in Table 5-1 and Table 5-2 of sub-section 5.2.1.

5.2.1 Flow regime identification using visual observation

Visual analyses of 8.10e-04% v/v (750lb/1000bbl) and 1% v/v (~90000lb/1000bbl) sand concentration water-sand flow were selected to describe the water-sand behaviour because the image of the regimes of other concentrations are similar. The two

concentrations represent both low and high concentration groups respectively. The sand settling tests were conducted starting from high to low slurry velocities. Table 5-1 and Table 5-2 present both the side view and bottom photographs of the pipe recorded with SONY HD camera.

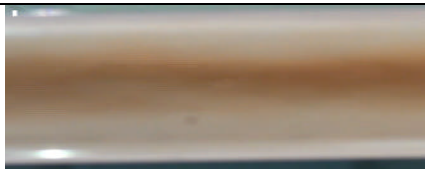
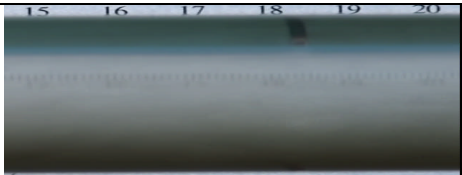
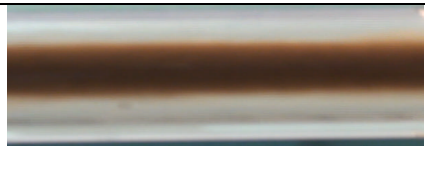
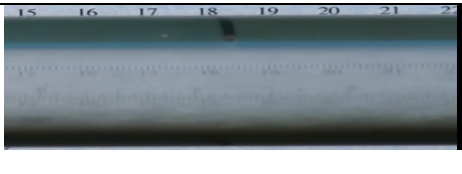


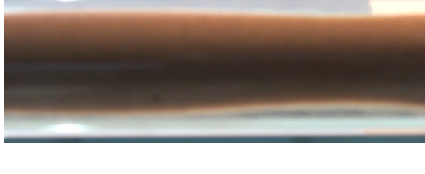

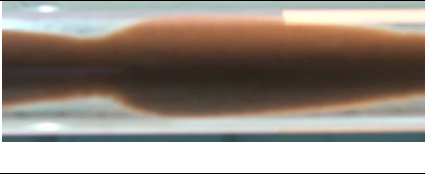

Table 5-1: Visual analysis of 8.10e-04% v/v (750lb/1000bbl) sand concentration water-sand flow

Slurry Velocity, V_{ss} (m/s)	Bottom view	Side view
0.66		
0.60		
0.45		
0.30		
0.25		

In the case of 8.10e-04% v/v concentration, it was observed that sands were fully dispersed in water at higher water-sand velocity until the velocity dropped to 0.60m/s where some sands started separating from the main stream and moving below the

centreline of the pipe and at the bottom of the pipe. At 0.55m/s, thicker sand streaks were observed to be moving at the bottom of the pipe with sand particles saltating along with them. The size of sand streaks was increasing along the centreline of the bottom of the pipe as the velocity decreases. The reluctance to motion kept increasing and the MTC was reached between 0.55 and 0.50 m/s. However, when the condition was below this velocity, the sand streaks broke into parcels and began to crawl as dunes with some sand particles saltating from the tail of the dunes to the front of the dunes. By this saltation, the dunes are changing their position following a straight centreline at the bottom of the pipe.

Table 5-2: Visual analysis of 1% (~90000lb/1000bbl) sand concentration water-sand flow

Slurry Velocity, V_{ss} (m/s)	Bottom view	Side view
0.87		
0.60		
0.50		
0.40		
0.30		

Similar behaviours were observed in 1%v/v slurry concentration presented in Table 5-2 but with a different and higher MTC of 0.75-0.66m/s. The quantity of the sand in water which was high encouraged higher collision of the particles and the effect of the force of gravity, even though the flow is in the turbulence regime and narrow channel. The MTC results of the remaining sand concentrations considered in this research are presented in Table 5-4 and compared with Yan (2009). Comparing the obtained results with Yan (2009) and Al-lababidi et al. (2012), exposed the consistency of the relationship of the MTC with the pipe diameter and the concentrations; one could deduce that the bigger the diameter of the pipe the higher the velocity needed to keep sand in motion above the MTC and also the higher the sand concentration the higher the MTC required for sand transport.

5.3 Sand Minimum Transport Condition

Similar studies have been investigated by several researchers as mentioned in chapter 2 with focus on different particle sizes but fine sand was used in this study because they are easily trapped within the viscous sublayer according to McKibben and Gillies (2009). The results obtained are presented in Table 5-3 which explain the observed MTC gotten by visualisation method from the slurry test conducted at different sand concentrations. It could be observed that the minimum velocity required to prevent sand bed or keep the sand moving is a function of concentration because Table 5-3 shows the corresponding increase in the MTC as the concentration of sand increases. In other words, the higher the sand concentration the higher the velocity required to keep the sand from settling. This could be traced to the fact that at low concentration the collision of particles is less; hence the loss of particle momentum is minimal, while the carrier fluid force dominates the bulk flow in the pipe.

In addition, most of the researchers e.g. Durand and Condolios (1952) and Danielson (2007) who did similar research used higher concentrations than the one used in this research. However, the MTCs trends in this research are similar to the existing research; an example is Yan (2009) whose results are compared with this research's as stated in Table 5-4.

Table 5-3: Observed MTC of sand in 1in-ID pipe flow

Sand concentration (lb/1000bbl)	MTC (m/s)
200 (2.15e-04%)	0.40-0.45
500 (5.38e-04%)	0.45-0.50
750 (8.10e-04%)	0.50-0.55
~90000 (1%)	0.83-0.90
~450000 (5%)	1.00-1.10
~900000 (10%)	1.10-1.20

Yan (2009) studied the effect of very low sand concentration in both 2-in and 4-in pipes while this research was conducted in 1-in diameter pipe with low and high concentrations. A similar scale effect was observed as Yan (2009), with little differences in the MTC which could be traced to the difference in the pipe diameters and particle size.

Table 5-4: Comparison of sand MTC in pipes

Sand Concentration (lb/1000bbl)	V_{MTC}(m/s) 1-inch pipe (Present research)	V_{MTC}(m/s) 2-inch pipe Yan (2009)	V_{MTC}(m/s) 4-inch pipe Yan (2009)
~900000 (10%)	1.10-1.20	-	-
~450000 (5%)	1.00-1.10	-	-
~90000 (1%)	0.83-0.90	-	-
750 (8.10e-04%)	0.50-0.55	-	-
500 (5.38e-04%)	0.45-0.50	0.65-0.75	0.75-0.85
200 (2.15e-04%)	0.40-0.45	0.60-0.70	0.65-0.75
100 (1.075e-04%)	-	0.55-0.65	0.60-0.70
50 (5.375e-05%)	-	0.50-0.55	0.50-0.60
15 (1.613e-05%)	-	0.45-0.50	0.50-0.60
5 (5.375e-06%)	-	0.40-0.45	0.45-0.50

Some MTC correlations were also examined to verify their consistency with this research. Some of them could not predict at different sand concentrations as shown in Table 5-5 because of some factors upon which those correlations were developed. The discrepancies observed in the prediction of MTC by the correlations considered may be due to some assumptions used, like constant concentration parameter. Examples are Durand and Condolios (1952); Thomas (1962) and Danielson (2007); amongst those that were considered in this research. Durand and Condolios' (1952) correlation returns a close transport condition to the experiment due to their perception of MTC as the condition whereby sand can be transported without forming stationary bed, but the deviation comes when scouring sand dunes which develop before sand bed are formed, hence their definition predicts saltation formation and not exactly MTC.

Table 5-5: Comparison of some correlations at sand transport condition with the present research

Sand concentration (%)	2.15e-04	5.38e-04	8.10e-04	1	5	10
Correlation	Predicted MTC (m/sec)					
Durand and Condolios (1952)	0.544	0.562	0.589	0.771	0.997	1.088
Condolios and Chapus (1963)	0.429	0.491	0.522	0.757	0.961	1.065
Wasp et al. (1970)	0.347	0.358	0.375	0.491	0.635	0.693
Oroskar and Turian (1980)	0.344	0.396	0.421	0.618	0.779	0.850
Davies (1987)	0.595	0.595	0.595	0.595	0.595	0.595
Nilson and Kvernfold (1989)	0.525	0.525	0.525	0.525	0.525	0.525
Danielson (2007)	0.245	0.245	0.245	0.245	0.245	0.245
Present research	0.40-0.45	0.45-0.50	0.50-0.55	0.83-0.90	1.0-1.10	1.10-1.20

Condolios and Chapus (1963) appeared relatively suitable in their prediction of the MTC observed in this investigation. The correlation of Condolios and Chapus (1963) performance could be due to the improvement made on Durand (1952) which aimed at preventing the deposit of sand bed. The correlation of Oroskar and Turian (1980) under predicted the MTC in this work because they employed energy balance to determine the condition at which the particles will remain in suspension. In addition, the limitation of Davies' (1987) correlation is similar to Oroskar and Turian (1980) because it is based on turbulent theory applied to the suspension of particles in the flow which may be the outset of heterogeneous flow and this might be too early for the prediction of the MTC.

The disparities observed from these correlations were also observed amongst these correlations by Turian et al. (1987) who reported discrepancies from 33 different correlations when he compared them with the experimental results.

5.4 Pressure Gradient

In this report, pressure gradients are plotted against the water-sand mixture velocities. This is necessary because pressure drop or gradient is one of the most important factors in pipe flow and design. In the same vein, it is a direct measurement and a good parameter to employ in order to determine how much it costs to produce flow-able products (i.e. gas or liquid). The pressure gradient for 2.15e-04%, 5.38e-04%, 1%, 5% and 10% v/v sand concentrations were obtained and analysed at different slurry velocities as shown in Figure 5-1 and Figure 5-2. They are generally observed to be higher than that of water. At higher slurry velocities where the sand is fully suspended the pressure gradient is greater than single phase water. The same behaviour occurs at lower velocities. This corroborated the report of the previous researchers like Doron et al. (1987); and Doron and Barnea (1995).

The trend of the pressure gradients of low sand concentrations is similar to that of single-phase water flow in the same channel. The same behaviour was reported by Gillies (2004) for fine particles of 90micron diameter in 4-in ID pipe. However, the pressure gradients of 1% sand concentration slurry flow are observed to deviate from

single phase water flow both at lower and high flow rates. The deviation at the high flow rates could be referred to as “off-the-wall force” effect according to Wilson et al. (2000). The result obtained also reveals some pressure build up at much lower fluid velocity. This could be due to the fact that there was sedimentation or deposit where the velocity of sand is either near zero or zero and the flow passage became narrower, giving rise to increase in the fluid flow rate that causes increase in dynamic pressure. When compared with water pressure gradient profile, starting from high flow rate to low flow rate, it was observed that the trend started to deviate when the slurry velocity was between 0.76 and 0.66m/s; this of course was observed visually as the condition where the sand was settling out of the suspension. This result also suggests that very low concentration slurry has an advantage of low pressure drop compare to higher concentration.

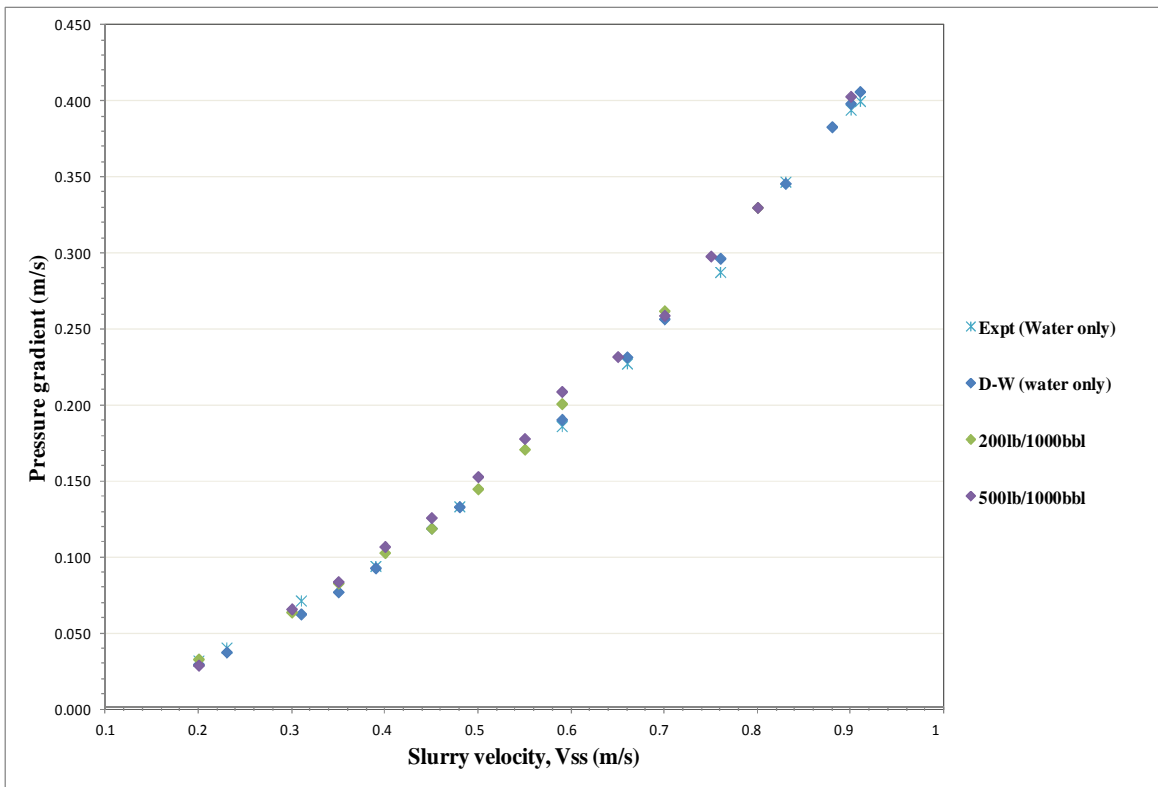


Figure 5-1: Pressure gradients of low concentration slurry flow in 1-in ID horizontal pipe

In Figure 5-2, it was observed that the pressure gradient of 1% and 5% sand concentration slurries are overlapping at high flow rate. Incidentally, the trend of 5%

sand concentration slurry began to deviate when the slurry velocity dropped to 1.02 and 0.9m/s; this range was found to correspond to the sand MTC for 5% sand concentration slurries. Table 5-6 presents the comparison of some pressure gradient correlations with the results of the present research. The correlations that were employed show relatively good agreement with the present results for 2.15e-04% up to 1% sand concentration. All the models over-predicted the gradients at high sand concentration. These discrepancies may be due to the inconsistencies of the MTC correlation that were used to predict the determinant variable which influenced the output of the pressure gradient correlations. This could also be justified by the fact that different correlations evolved from different slurry compositions and other parameters like pipe diameter, pipe material etc.

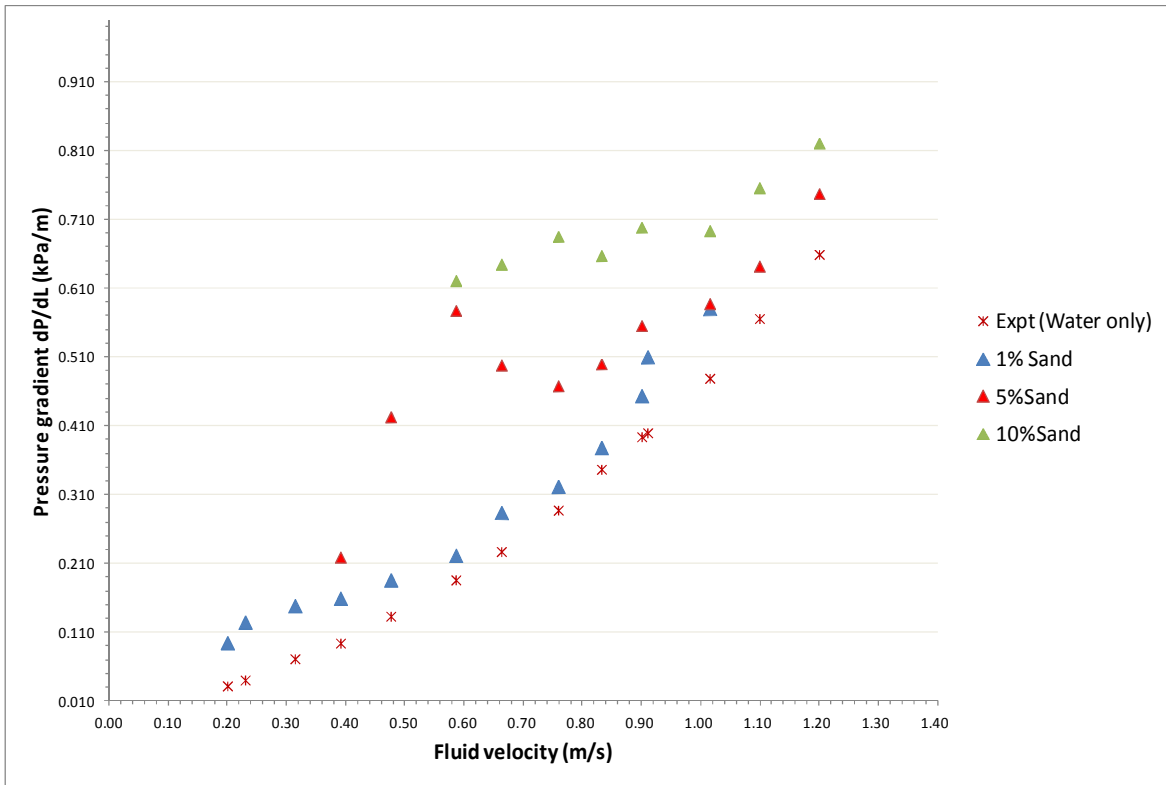


Figure 5-2: Pressure gradients of high concentration slurry flow in 1-in ID horizontal pipe

Table 5-6: Comparison of the pressure gradient and correlations at sand transport condition

Sand concentration (%)	2.15e-04	5.38e-04	8.10e-04	1	5	10
Correlations	kPa/m					
Durand and Condolios (1952)	0.104	0.118	0.134	0.371	1.000	1.621
Condolios and Chapus (1963)	0.090	0.131	0.157	0.564	1.472	2.287
Oroskar and Turian (1980)	0.053	0.078	0.093	0.379	1.167	1.995
Davies (1987)	0.135	0.143	0.150	0.378	1.368	2.604
Nilson and Kvernfold (1998)	0.107	0.116	0.124	0.382	1.506	2.909
Present research	0.103 – 0.119	0.126 – 0.153	0.162 – 0.173	0.378 – 0.454	0.469 – 0.592	0.868 – 0.935

5.5 CFD of Water-Sand Multiphase Flow

In this section, the CFD model formulation of water-sand flow in horizontal pipe and the results of its simulation are presented and analysed. A 3-D CFD model of a 5m long 1-in ID horizontal pipe was developed. The Eulerian VOF model was set up and used to simulate the flow of sand in liquid at 1% v/v particle concentrations. The simulation results are validated using experimentally measured pressure gradient.

5.5.1 Model geometry

The geometry and mesh were created using Gambit 2.4 to model the flow of water-sand in the test section of the 1-inch four phase transport facility described in Chapter 3. Single inlet pipe geometry was designed and hexahedral mesh was employed to discretise the computational domain.

5.5.2 Model formulation

The governing equations are given in equations 4-1 to 4-4. The liquid and solid phases are considered incompressible with constant physical properties. The VOF model was selected to model the water-sand two-phase flow and track the volume fraction of each phase as a fluid. With VOF, the geometrical reconstruction scheme was adopted to represent the interface between the water-sand by applying a piecewise-linear approach. The appropriate turbulence model considered in this research is the LRKE turbulence model because of the flow behaviour which might occur at the wall. The usage of VOF model for water-sand informed viscosity correlation to be adopted for sand as a fluid, hence, the fluid viscosity ratio correlation of Shook et al. (2002) was adopted and given by

$$\mu = \mu_w \exp(12.5C_{fines}) \quad 5-1$$

μ_w is the viscosity of water and C_{fines} is the fines volume fraction in the carrier fluid.

5.5.3 Boundary and initial conditions

In this research constant superficial velocities and atmospheric pressure were specified at the inlet. No-slip condition was imposed at the wall, and pressure outlet condition at the pipe outlet. An isothermal condition was assumed in this simulation. The pressure gradients of slurries with 1% sand concentrations were solved for using FLUENT package and validated with results of experimental runs.

5.5.4 Solution method




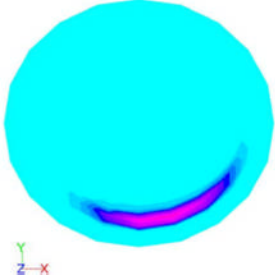



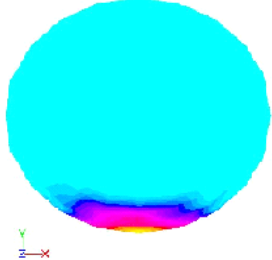
The statistically steady-state of the flow behaviours are made up of several periodic flow patterns hence the unsteady solver was employed to simulate the flow behaviours of this two-phase water-sand flow. The simulation time used for data collection is similar to that of the experiments i.e. 30s. The resulting time step considered is 0.004s, which means 250 data points per second.

In the following sections, samples of contour plots and pressure gradients of 1% sand concentration slurry simulated with CFD are presented.

5.5.5 Flow configuration

Table 5-7 presents the contour plots of sand behaviours at different velocities. The left hand side (LHS) of the table hosts the flow velocity and label for each case, the middle column shows the images of sand on longitudinal plane along the pipe axis while the right hand side (RHS) column shows the cross section of the pipe. Light blue colour represent the perfectly mixed water and sand, while dark blue and red represent sand at different concentration (red is the highest concentration of sand). For case a where the flow velocity is 1.10m/s, the flow contour reveals no accumulation of sand in the entire domain either at the pipe bottom or in the main stream. This suggests that the flow is homogeneous. In case b, when the flow velocity was reduced to 0.83m/s, some sands started separating from the main stream showing that the flow has entered a heterogeneous region but the agglomerating sands are still being conveyed without depositing at the pipe bottom.

Table 5-7: Contours of water-sand (1% v/v sand concentration) flow

Flow condition (m/s)	Side view	Cross section
1.10 (case a)		
0.83 (case b)		
0.75 (case c)		
0.30 (case d)		

The contour of case b on the RHS shows that some sands are being transported closed to the pipe bottom. This is in agreement with the observation made in the experiment, and Qing's (1986) explanation about heterogeneous flow; solids are not evenly distributed and that a pronounced concentration gradient exists across the pipe section.

Further reduction of the flow velocity from 0.83m/s to about 0.75m/s reveals the commencement of the deposit at the pipe bottom (see RHS of case c) as the heavier particles becomes less uniformly distributed. The middle column of case c further exposes the presence of sand in the main stream and also close to the pipe bottom. In case d, the flow velocity was reduced to 0.30m/s, and sand dunes emerged as shown in the middle and RHS column. These plots show the applicability of CFD to predict the behaviour of sand configurations in the horizontal pipe flow, since it is very important to the pipeline engineer to have the prior knowledge of the flow condition before designing the transport system.

5.5.6 Pressure gradient

The knowledge of slurry pressure gradient is an important parameter in slurry transportation, since it helps in the design of functioning transport system. In order to validate the numerical results, water-sand experiments were conducted to generate laboratory scale water-sand pressure gradient data. Table 5-8 compares the water-sand gradients of 1%v/v sand concentration obtained from the experiment with CFD. Generally, it could be observed that the gradients obtained from both the experimental and CFD increases with increase in flow velocity, however, CFD model over predicted the experimental results when the slurry velocity is lower than 0.70m/s and vice versa when it is greater than 0.70m/s. The work of Ling et al. (2003) confirms these discrepancies at low velocity. The over prediction behaviour could be due to the deposition of sand at velocity lower than 0.70m/s which made the mixture to become heterogeneous system and hence complex to be resolved fully. Experimentally, the MTC for 1% sand concentration slurry occurred in the range 0.76–0.66m/s as earlier stated in Table 5-4 above and it is about the same point where the CFD prediction changed from under predicting the pressure gradients to over predict the same. On the other hand, when the slurry velocity is greater than 0.70m/s, the differences in the results is generally less than 10%. These differences decrease as the slurry velocity increases, this could be traced to the fact that the turbulence of the flow increased and promoted the homogeneity of the fluid. The over prediction at velocity lower than 0.70m/s suggests the complexity of the heterogeneous flow.

Table 5-8: Comparison of the experimental pressure gradient of 1% v/v water-sand with CFD

Vss, m/s (1%sand)	Experiment	CFD	%Difference
	Pa/m		
0.30	148.7	190.7	28.245
0.40	159.7	211.9	32.686
0.60	221.8	247.4	11.542
0.75	322.1	303.1	-5.899
0.83	378.6	355.7	-6.049
1.00	510.3	496.2	-2.763
1.10	580.5	581.1	0.103

5.6 Chapter Summary

The experimental and CFD results of water-sand flow in 1-in ID pipe are presented.

The flow patterns and the MTC were identified in horizontal pipe flow through visual observation by HD video camera during the experiments were analysed and discussed.

The MTC of sand in 1-in ID horizontal pipe were compared with Yan (2009) experimental results to establish that the bigger the pipe diameter the higher the velocity needed to keep sand in motion above the MTC. In addition, some MTC correlations were employed to verify how they perform on the present research. A lot of disparities were observed with respect to their definitions of sand MTC and this was in agreement with Turian et al.'s (1987) observation for 33 different correlations that he compared

with the experimental data. It was also discovered that the higher the sand concentration the higher the MTC required for sand in the horizontal pipes to prevent deposition.

The pressure gradients at different flow conditions were also discussed and compared with the literatures. In addition, some pressure gradient correlations were also verified against the experimental results.

The Eulerian VOF CFD model was employed to predict the pressure gradients of 1% v/v slurry at different flow conditions. The results were analysed and related to the MTC. Hence, VOF model was found to be suitable for the study of slurry flow in this research.

6 OIL-WATER FLOW IN 1” ID HORIZONTAL PIPE

In this chapter, the results of the experiments carried out in 1-in pipe are presented. The experimental arrangement was described in Chapter 3. In the experiments performed, the pressure drop was determined by means of two pressure transducers at two points which are 2.17m apart. The following sub-sections provide details on oil-water flow studies; 6.1 Test matrix, 6.2 Flow Regime Identification; 6.2.1 Visualisation of the flow patterns, 6.2.2 Flow regime identification by probability density function, 6.2.3 Flow pattern maps, 6.2.4 PIP flow, 6.3 Pressure gradient, 6.3.1 Reduction factor, and Summary.

6.1 Test matrix

In order to observe the behaviours of the high viscosity oil-water in the horizontal configuration, three experimental campaigns were conducted ranging from low, medium and high flow rates with respect to experimental facility limitations (i.e. oil superficial velocities at 0.06, 0.2 and 0.55m/s). A total of 42 experiments were carried out on oil-water flow on 1-in rig. It is worth mentioning that, in the course of running the experiments, the oil viscosity kept changing due to the changes in the ambient temperature. The water employed for this study was always kept at ambient temperature. The observed change in the oil temperature is between 1 to 2°C. Hence, nominal values between the initial and final viscosities were employed in the discussion of the results in this research.

6.2 Flow Regime Identification

The flow regime identification studies are presented in this section using visualisation (i.e. subjective) and pressure signal trend and PDF analysis (i.e. objective) approaches. Samples of the observed oil-water flow configurations are presented to illustrate the flow patterns obtained in the course of the experiments. The flow pattern images are captured from both side and bottom views of the pipe.

6.2.1 Flow regime identification by visualisation

It is generally believed that flow patterns play very important roles in multiphase flow pipeline design. The simplest approach usually employed to study this flow behaviour is by visualising the flow by direct observation of flow in transparent pipe, and also by means of a high speed video but this is only good for a laboratory scale experiment. In this approach, the description of the flow pattern is based largely on individual interpretation of the visual observation carried out through the view section of the transparent pipe of the rig.

The observed flow patterns are presented as a set of photographs in Table 6-1, Table 6-2 and Table 6-3. Generally, an oil coated wall was observed in all the oil-water flow cases. These coatings appeared wavy on the wall; which suggests that the oil film thickness on the wall was not uniform. It was also observed that this oil coating was affected by the water cut, demonstrated by increased wall transparency as the water cut increased.

At a low oil superficial velocity (V_{so}) of 0.06m/s for 3300cP nominal oil viscosity, plug flow of the oil-phase in water with oil film (OPW/OF) coating the wall was observed when water superficial velocity (V_{sw}) was 0.2m/s. This plug flow continues until V_{sw} reached 0.4m/s. These oil plugs flew along the upper part of the pipe wall as a result of buoyancy/lift force acting on the oil. As the V_{sw} increased from 0.40m/s, this oil plug became streak-like and dispersed in water known as dispersed oil in water (DOW/OF). It was further observed that the higher the V_{sw} the more dispersed the oil in this case (where V_{so} equals 0.06m/s).

However, the flow pattern observed when the V_{so} was increased to 0.20m/s and the V_{sw} was 0.20m/s is called water-assist annular (WA-ANN) flow which is a variant of the core annular flow (CAF) discussed in section 2.3.2.1. In this WA-ANN flow, the oil flows in a continuous manner in the core of the pipe being surrounded by water but with oil film on the pipe wall while CAF does not have oil film on the pipe wall. This WA-ANN flow appeared like bamboo wave when the V_{sw} was 0.20m/s. The annular oil flow in the core began to break when the V_{sw} increased beyond 0.50m/s. In this case

also, it was observed that the core thickness (diameter) was reducing as the water cut increased. From this experiment it was found that CAF pattern is not feasible; this is because it has not been possible to prevent the pipe wall from being fouled by oil. However, the oil in the core of the pipe could still be continuous and increase in diameter with increase in oil flow rate. This is justified by Table 6-3 where V_{so} is 0.55m/s. The WA-ANN continues to exist with increase in V_{sw} , although the core diameter was decreasing with respect to the increase in V_{sw} . From the foregoing, it could be inferred that the increase in V_{so} and/or decrease in V_{sw} (or water cut) promotes WA-ANN flow while the reverse promotes other intermittent flows i.e. OPW/OF and DOW/OF.

Additional flow behaviour observed in this study is the swirl type of oil and water flow as shown in Table 6-4; this behaviour is not continuous throughout the pipe and it is not local to a specific location in the pipe. This was observed to emerge between the oil continuous and water continuous flow. It is difficult to classify this as a stable flow pattern but a transition between oil and water continuous flow condition.

Table 6-1: Oil-water flow pattern at 0.06m/s oil superficial velocity








Flow conditions	Pictures	Flow regime
$V_{so}=0.06\text{m/s}$ $V_{sw}=0.2\text{m/s}$ $w_c = 0.77$ (a)		OPW/OF
$V_{so}=0.06\text{m/s}$ $V_{sw}=0.3\text{m/s}$ $w_c = 0.83$ (b)		OPW/OF
$V_{so}=0.06\text{m/s}$ $V_{sw}=0.4\text{m/s}$ $w_c = 0.87$ (c)		OPW/OF
$V_{so}=0.06\text{m/s}$ $V_{sw}=0.5\text{m/s}$ $w_c = 0.89$ (d)		DOW/OF
$V_{so}=0.06\text{m/s}$ $V_{sw}=0.6\text{m/s}$ $w_c = 0.91$ (e)		DOW/OF
$V_{so}=0.06\text{m/s}$ $V_{sw}=0.8\text{m/s}$ $w_c = 0.93$ (f)		DOW/OF
$V_{so}=0.06\text{m/s}$ $V_{sw}=1.0\text{m/s}$ $w_c = 0.94$ (g)		DOW/OF

Table 6-2: Oil-water flow pattern at 0.2m/s oil superficial velocity





Flow conditions	Pictures	Flow regime
$V_{so}=0.2\text{m/s}$ $V_{sw}=0.2\text{m/s}$ $wc = 0.50$		WA-ANN
$V_{so}=0.2\text{m/s}$ $V_{sw}=0.5\text{m/s}$ $wc = 0.71$		WA-ANN
$V_{so}=0.2\text{m/s}$ $V_{sw}=0.8\text{m/s}$ $wc = 0.80$		DOW/OF
$V_{so}=0.2\text{m/s}$ $V_{sw}=1.0\text{m/s}$ $wc = 0.83$		DOW/OF

Table 6-3: Oil-water flow pattern at 0.55m/s oil superficial velocity








Flow conditions	Pictures	Flow regime
$V_{so}=0.55\text{m/s}$ $V_{sw}=0.2\text{m/s}$ $wc = 0.27$		WAVY WA-ANN
$V_{so}=0.55\text{m/s}$ $V_{sw}=0.3\text{m/s}$ $wc = 0.35$		WA-ANN
$V_{so}=0.55\text{m/s}$ $V_{sw}=0.4\text{m/s}$ $wc = 0.42$		WA-ANN
$V_{so}=0.55\text{m/s}$ $V_{sw}=0.6\text{m/s}$ $wc = 0.52$		WA-ANN
$V_{so}=0.55\text{m/s}$ $V_{sw}=0.8\text{m/s}$ $wc = 0.59$		WA-ANN
$V_{so}=0.55\text{m/s}$ $V_{sw}=1.0\text{m/s}$ $wc = 0.65$		WA-ANN

Table 6-4: Sample of additional oil-water flow pattern

Title	Flow description
SWO	

6.2.2 Flow regime identification by trend and PDF plot of pressure signals

Since it is not practicable to have kilometres of transparent pipes for monitoring the flow patterns in the real life, this section is devoted to an alternative means of determining the flow patterns of high viscosity oil-water multiphase flow in the horizontal pipes.

The experiments carried out covered V_{so} ranging from 0.06 to 0.55m/s, and V_{sw} ranging from 0.01 to 1.0m/s. The V_{sw} was varied from a high to a low value, while keeping the V_{so} constant. Subsequently, the water velocity was reduced to the lowest value, and the experiments were repeated for other V_{so} . The pressure-time series were obtained from the pressure tap downstream of the test section for analysis of the flow pattern in the pipe. In order to compare and classify the PDF output of the pressure signals, and some video graphs were taken concurrently. Table 6-5, Table 6-6 and Table 6-7 presents both the trend and PDF plots of oil-water flows for nominal oil viscosity 3300cP at V_{so} equals 0.06m/s, 0.2m/s and 0.55m/s respectively, using normalised pressure data. Trend plot and PDF are established methods for time series analysis of random signals. Table 6-5, Table 6-6 and Table 6-7 together with Table 6-1, Table 6-2 and Table 6-3 are compared to draw inferences of the flow patterns, in addition to some established researches in the literatures.

The trend plots of the low water flow rates in Table 6-5 (where $V_{so}=0.06$ m/s, and $V_{sw} = 0.05, 0.10$ and 0.11 m/s), Table 6-6 (where $V_{so}=0.2$ m/s, and $V_{sw} = 0.01, 0.03,$ and 0.05 m/s) and Table 6-7 (where $V_{so}=0.55$ m/s, and $V_{sw} = 0.01$ and 0.03 m/s) were

obtained when the flows appeared to be dominated by oil phase and these justify and compare with McKibben's (2000a) explanation as shown in the Figure 6-1. In their investigation of horizontal well heavy oil-water flows in 2-in ID, 12.7m long in which the oil viscosity employed ranged from 325 to 11200cP, similar observation to those in the flow conditions mentioned above were made. This same pattern was referred to as water slug in oil by McKibben et al. (2000a); they proposed this flow pattern from their observation of the behaviour of the anemometer voltage readings during their investigation of similar condition; they explained that the upstream pressure of the probe fell linearly with time as the slug entered the test section and remained very low for about 2 to 3 seconds and then rose as the slug exited the section. The anemometer voltage reading fell as the slug passed, indicating that the oil velocity at this region has become very low, that is, the oil is nearly stationary at this position in the presence of the water slug.

When V_{sw} was increased from 0.11m/s up to 1.0m/s with V_{so} at 0.06m/s, the plots obtained are stable fluctuating signals. The trend plot for these high water flow rates region are similar in all the cases considered. This also corroborated the fluctuating gradient plot from McKibben's research as shown in Figure 6-2 when the V_{sw} increases. In this region, intermittent flows, that is, OPW/OF and DOW/OF were observed when V_{so} equals 0.06m/s, and WA-ANN when V_{so} equals 0.2m/s and 0.55m/s in this research.

Many researchers have adopted both trend and PDF technique to identify the flow patterns of gas-liquid flow (Matsui, 1986; Matsui, 1984) using pressure fluctuations, and liquid-liquid flow (Jana et al., 2006a) using normalised voltage signals of light attenuation of photodiode sensor under different flow conditions and very low oil viscosity (i.e. 1.37cP). The PDF curves are quantified by means of statistical analysis namely, skewness, standard deviation and kurtosis. The skewness characterises the degree of asymmetry of the distribution around its mean. A negative skew value implies that the left tail is longer; the mass of the distribution is concentrated on the right of the figure and it has relatively few low values while positive skew implies the opposite. The kurtosis is a measure of whether the data are peaked or flat relative to a normal distribution. In other words, data sets with high kurtosis tend to have a distinct peak

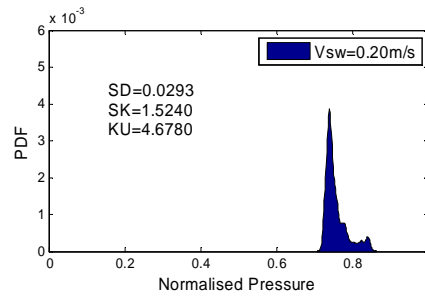
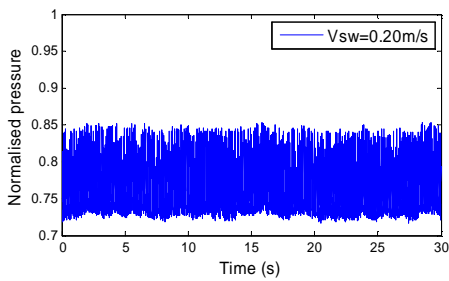
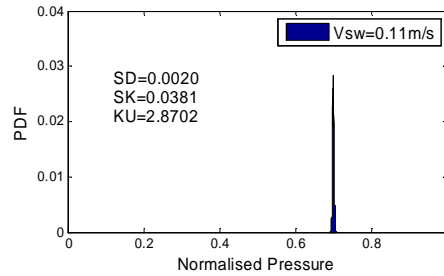
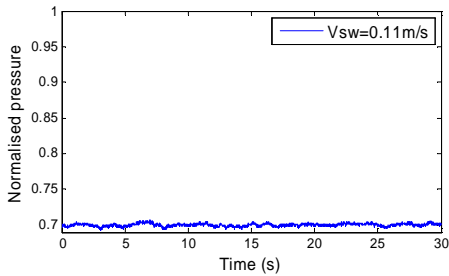
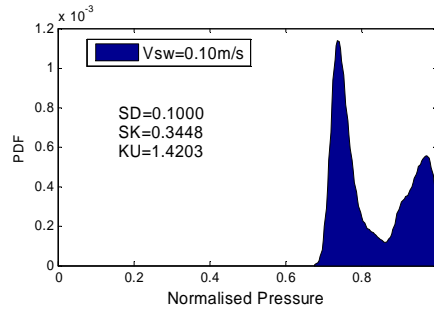
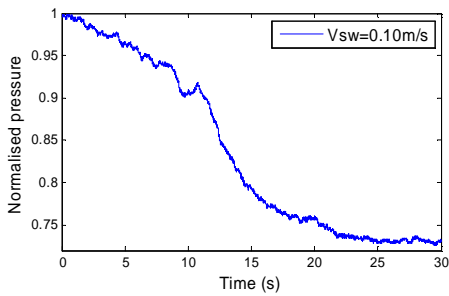
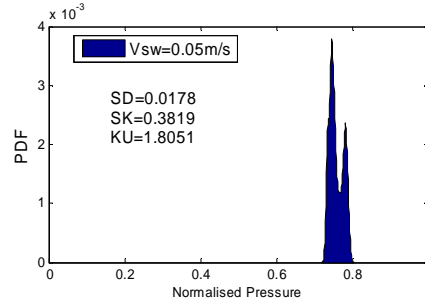
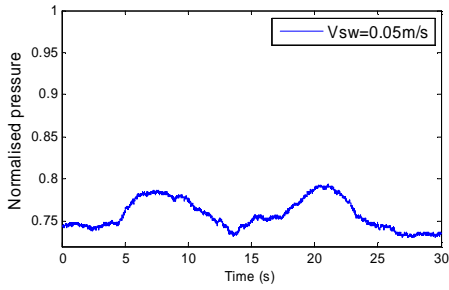
near the mean, decline rather rapidly, and have heavy tails while data sets with low kurtosis tend to have a flat top near the mean rather than a sharp peak.

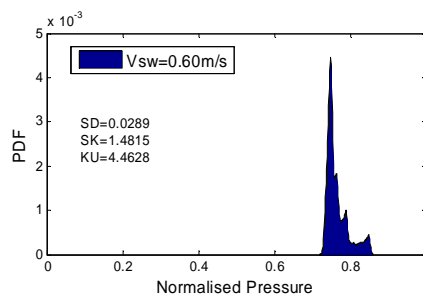
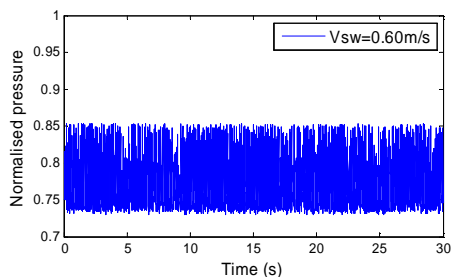
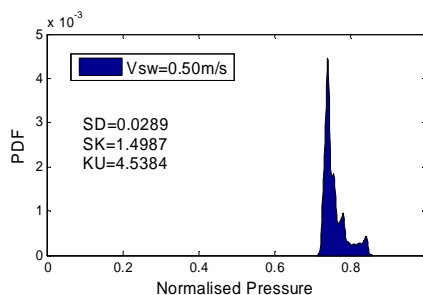
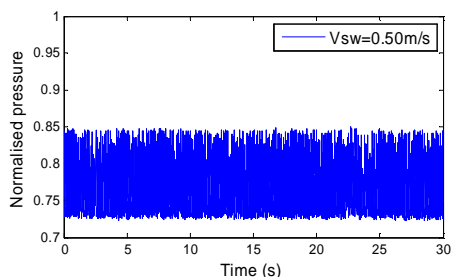
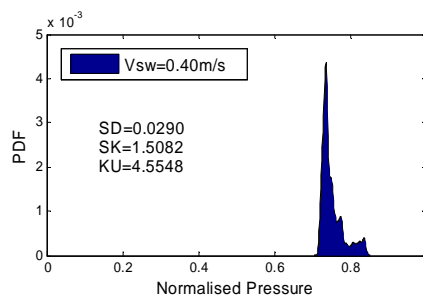
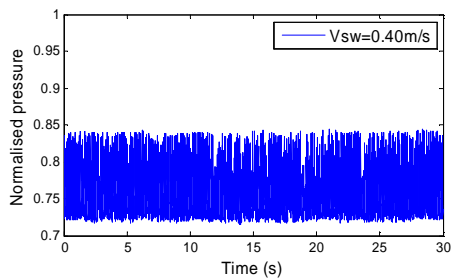
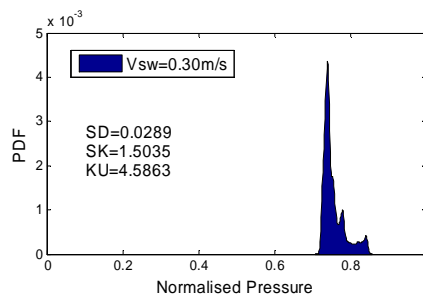
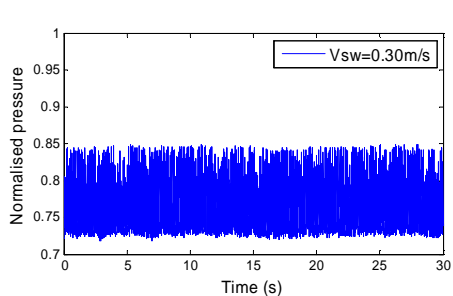
At low oil and water superficial velocities (i.e. $V_{so}=0.06$ and $V_{sw}=0.05\text{m/s}$), the PDF has a peak at a high value of normalised pressure and a positive skewness, and comparing with the observed image during experiment (which appeared like single phase oil because the presence of water could not be seen), it indicates the existence of oil as the continuous phase, and bubbles of water in it as described by McKibben et al. (2000a) in a similar investigation. This could be described as water bubbly/plug flow in oil (WPO). An increase in V_{sw} from 0.05m/s to 0.11m/s at the same V_{so} led to a reduction in the standard deviation, a drift of the skewness towards zero and lower kurtosis were obtained as a result of this thin distribution. Similar distribution was reported in the literature by Jana et al. (2006b), as a condition where no information could be extracted because of the uniform appearance of oil in the flow passage (unfortunately, the video graph or photograph of this pattern is not feasible and available). However, due to the drift in skewness from high to low value and the shift of the peaks, the flow could be described and referred to as the inversion point according to Jana et al. (2006b). In addition, this region where the skewness drifts towards zero could also be referred to as a transition region in which the continuous phase changed from oil to water.

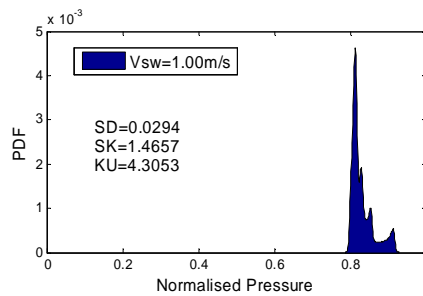
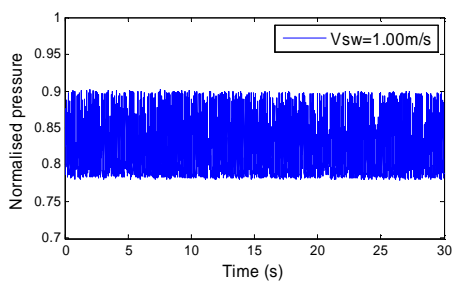
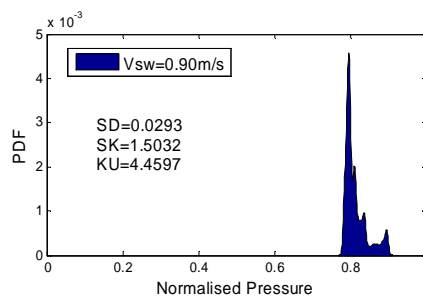
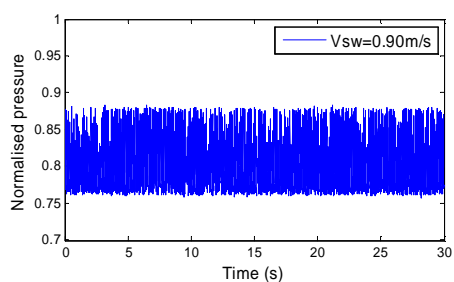
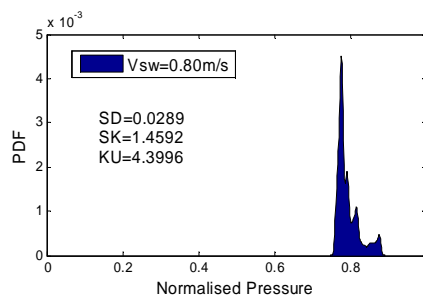
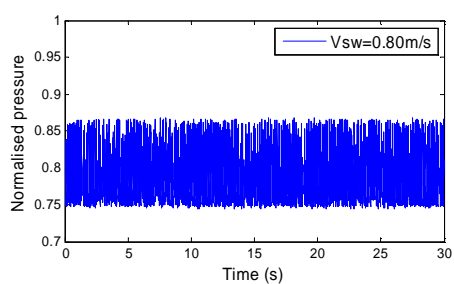
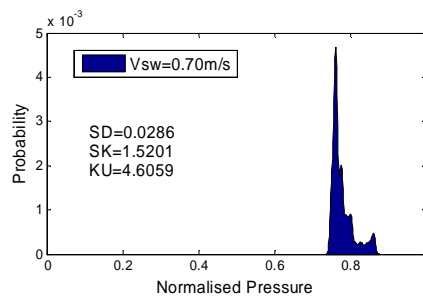
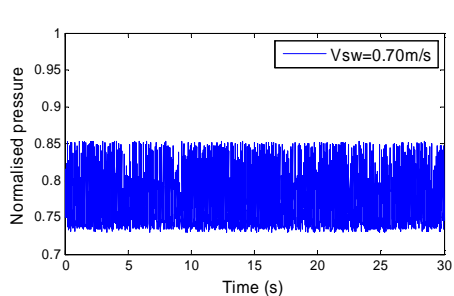
Table 6-5: PDF description of oil-water flow at V_{so} 0.06m/s

Pressure signal trend plot

Pressure signal PDF plot







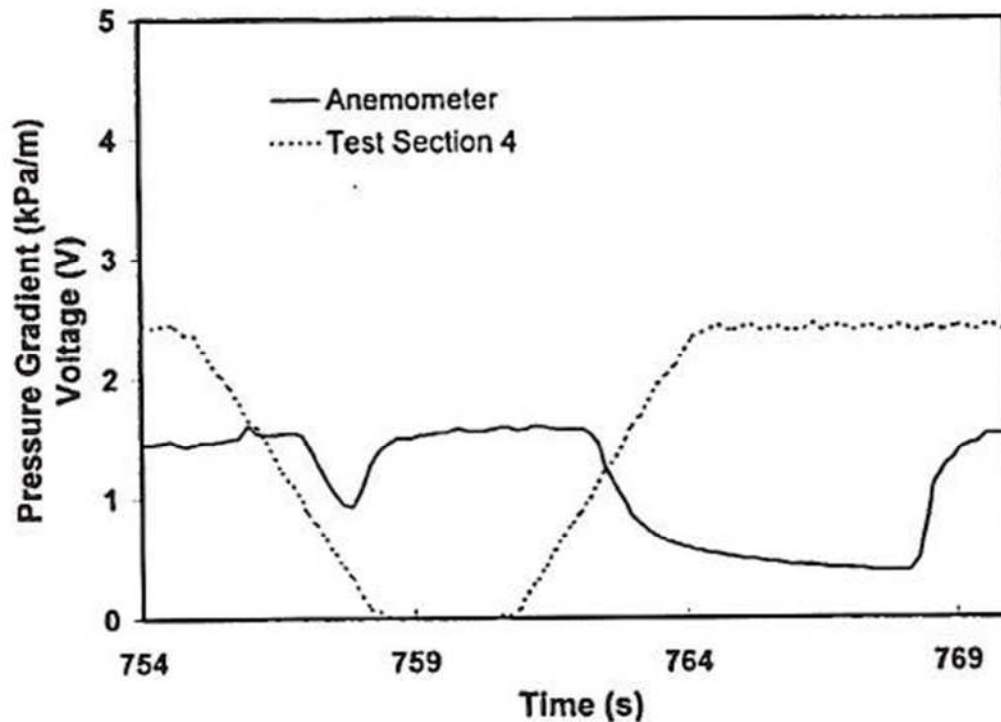


Figure 6-1: Anemometer profile ($r/R = 0.8, \theta = 0$) and pressure gradient result for mixture velocity = 0.038m/s with 10% water cut (McKibben et al., 2000a)

A further increase in the V_{sw} from 0.11m/s upward results in more positive skewness, increase in standard deviation of the data and the kurtosis. As earlier mentioned, for V_{so} equals 0.06m/s and V_{sw} greater than 0.11m/s, OPW/OF and DOW/OF were observed, and WA-ANN when V_{so} equals 0.2m/s and 0.55m/s at V_{sw} greater than 0.10m/s and 0.15m/s respectively. The spread of the base of the PDF curve in this region also suggests the oil film existence on the wall (as commonly refer in the PDF of gas-liquid flow that involves film on the pipe wall). In addition, the PDFs have two small peaks in addition to the main peak. This shows that the flow is intermittent. The spread of the distribution was relatively constant, showing the presence of oil film on the wall at high V_{sw} (i.e. beyond the oil continuous region).

In Table 6-6, the V_{so} was fixed at 0.2m/s with V_{sw} varying from low to high. When the V_{sw} was 0.01m/s, a negative skew value with a standard deviation lower than unity was observed. It has broad distribution, but there is neither video nor photograph to conclude the description because the pipe was dominated by oil. When the water velocity

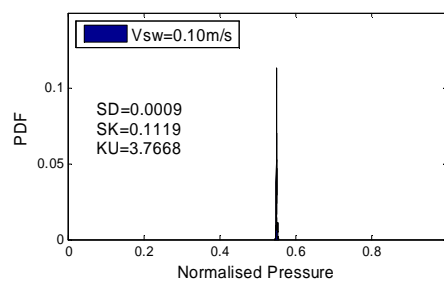
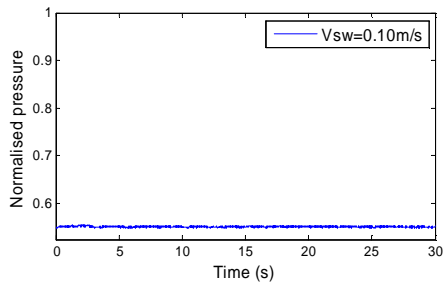
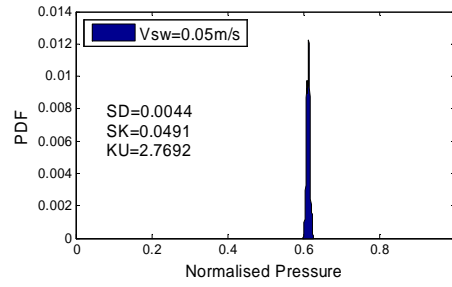
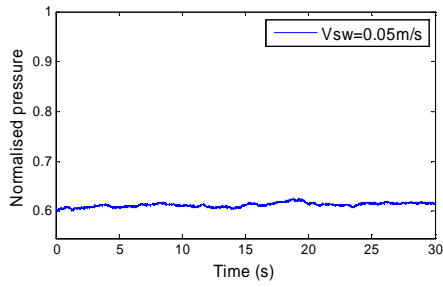
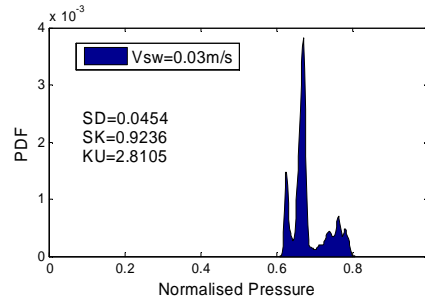
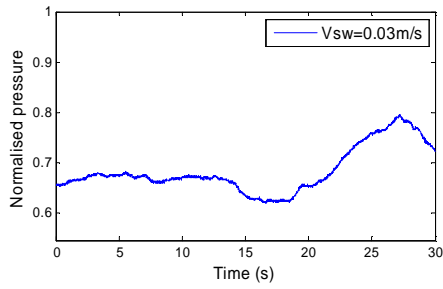
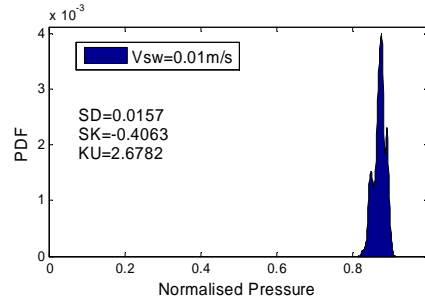
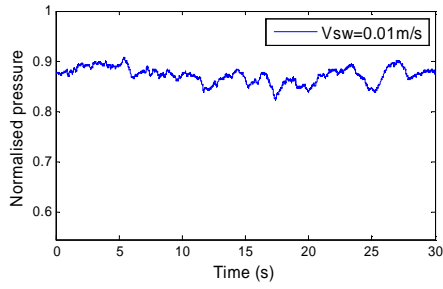
increased to 0.03m/s, there was a shift in skewness to positive accompanied with the broad distribution and some peaks. These peaks suggest that increase in V_{sw} increases the intermittent behaviour, although oil was still the continuous (carrier) phase. When V_{sw} was increased to 0.05 and 0.1m/s the standard deviation reduced drastically with skewness dropping almost to zero. The thin peak PDF curve, as described above, suggests an inversion region. When the V_{sw} was increased above 0.1m/s, the skewness and kurtosis increased as well with PDF having two peaks, which suggests that the flow is intermittent.

The behaviour of the flow when V_{so} equals 0.55m/s at varying V_{sw} was observed to be the same as in V_{so} equals 0.2m/s at varying V_{sw} . It could be deduced that higher V_{so} favours WA-ANN flow.

Table 6-6: PDF description of oil-water flow at V_{so} 0.2m/s

Pressure signal trend plot

Pressure signal PDF plot



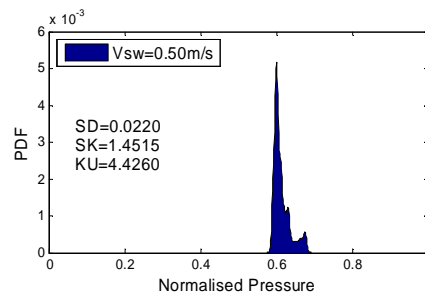
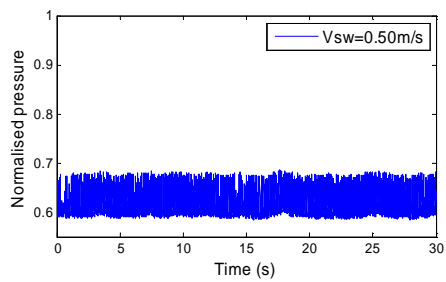
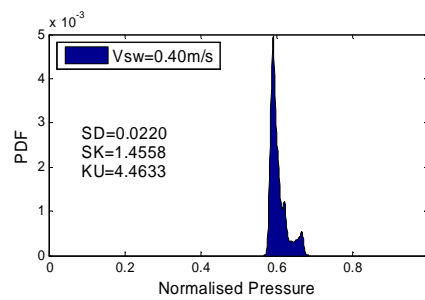
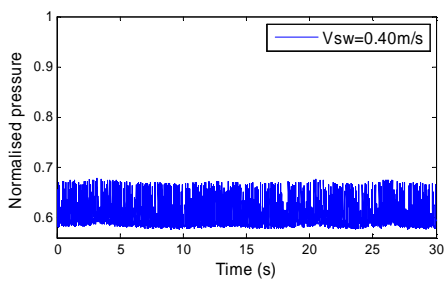
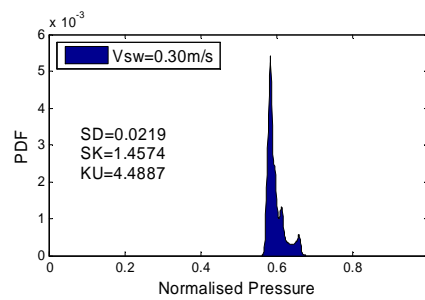
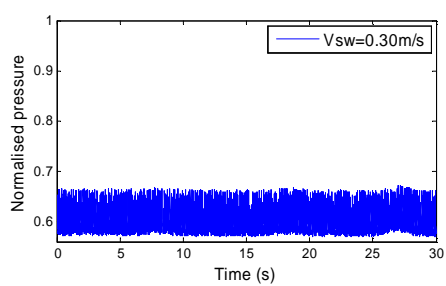
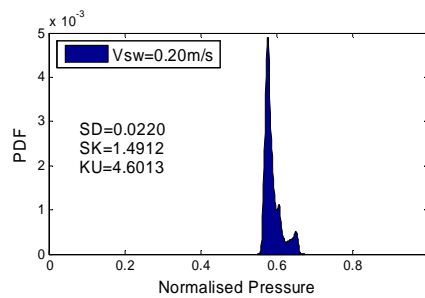
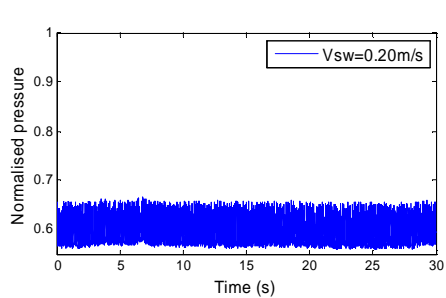
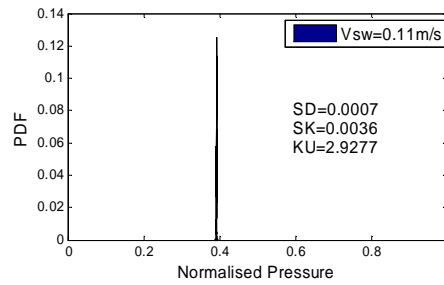
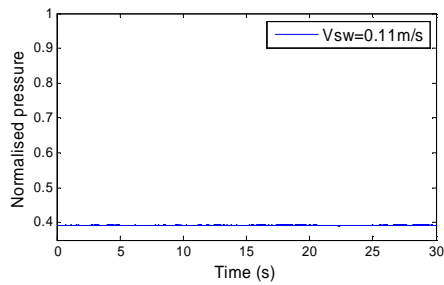
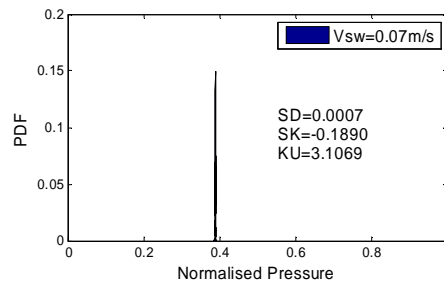
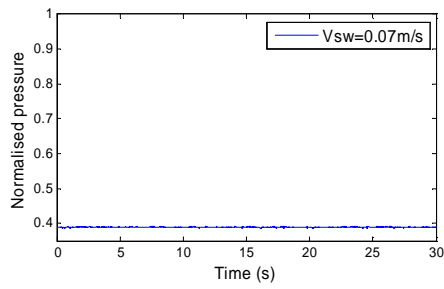
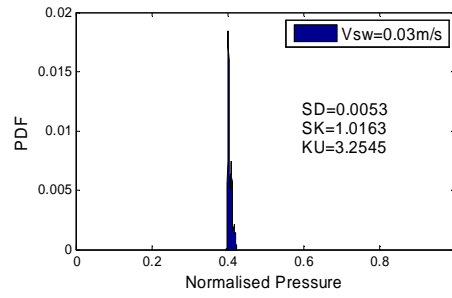
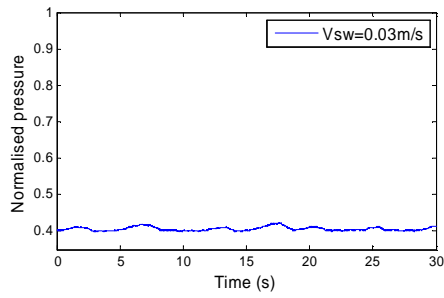
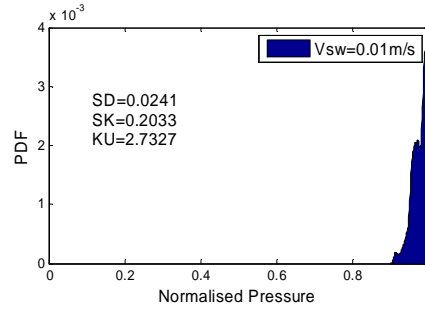
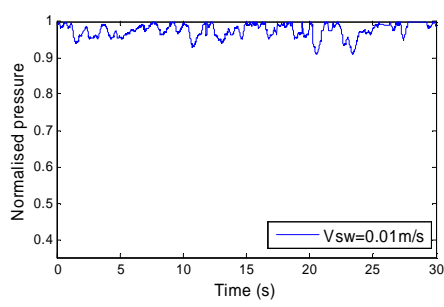
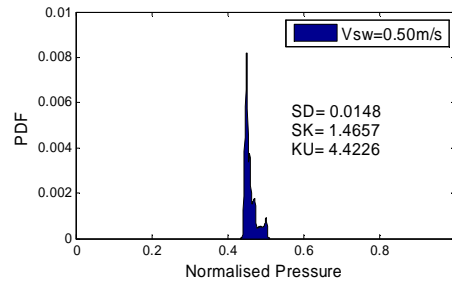
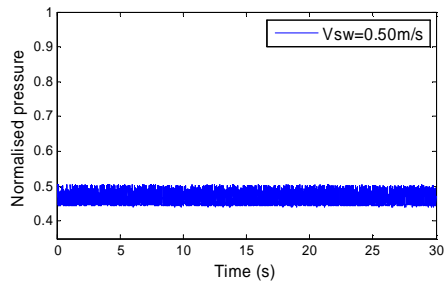
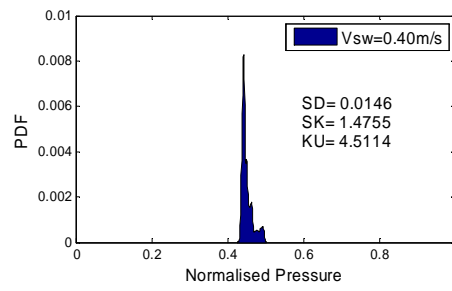
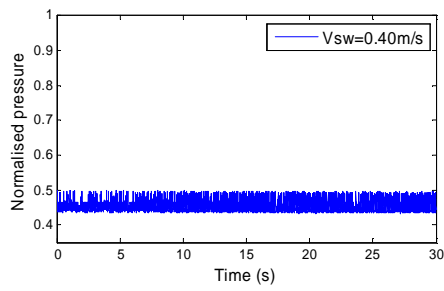
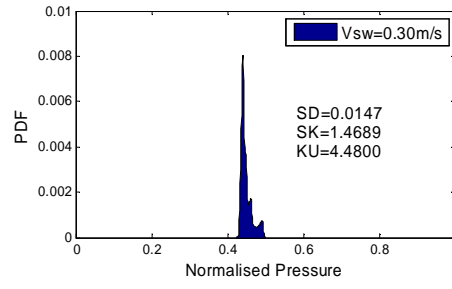
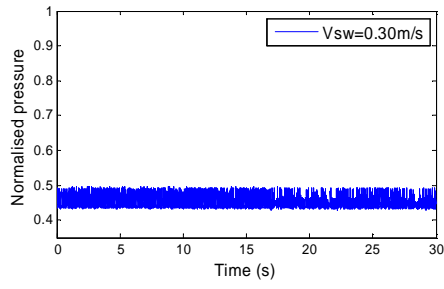
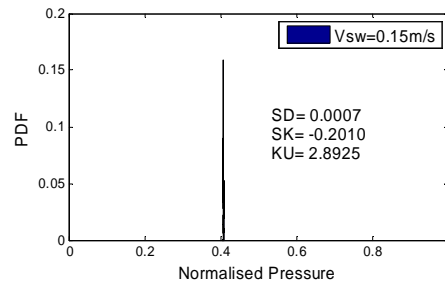
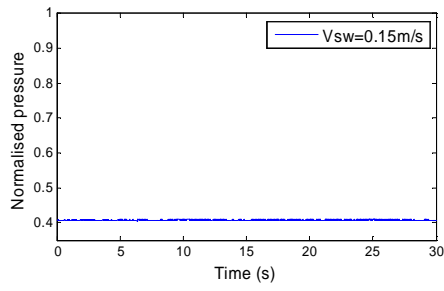


Table 6-7: PDF description of oil-water flow at V_{so} 0.55m/s

Pressure signal trend plot

Pressure signal PDF plot





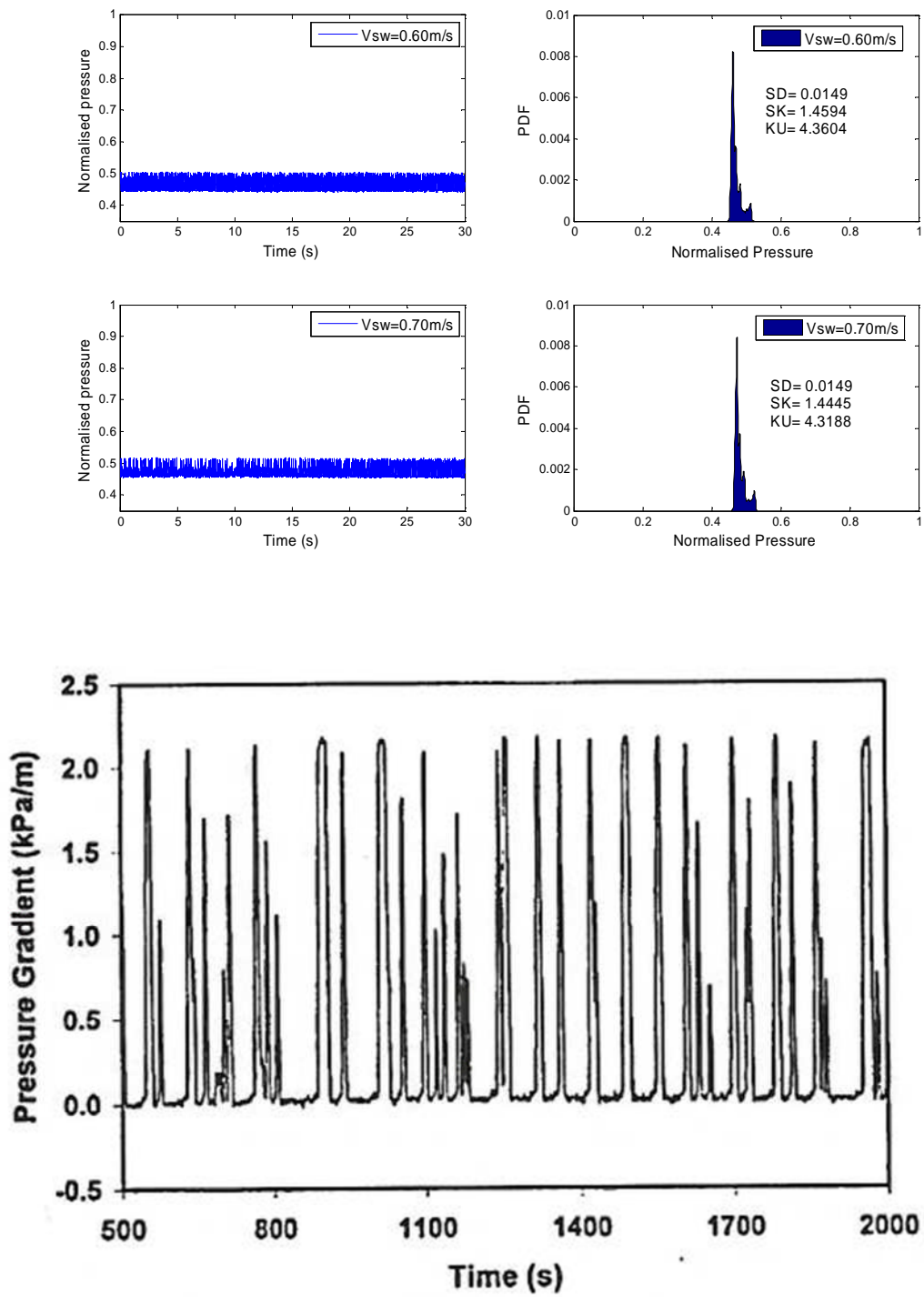


Figure 6-2: Instantaneous pressure gradient data at 67% water cut

6.2.3 Flow pattern map

Figure 6-3, Figure 6-4 and Figure 6-5 represent the flow regime maps gotten from this high viscosity oil-water flow investigation conducted on 1-in ID horizontal pipe for 3300cP, 5000cP and 7500cP respectively. Comparing some of the results obtained from the available visual observation with the trend plots and PDF distributions. The two-phase flow regime starts when the water cut or V_{sw} is greater than zero. The first flow pattern classification (i.e. WPO) was done purely based on the PDF and the pressure gradient because the video graph data did not reveal them as separated flows (this was explained in section 6.2.1). Some behaviour that is classified as swirl water-oil (i.e. SWO) or transition actually has oil on the wall, while water and the core oil formed a spiral kind of movement as shown in Table 6-4 in the core of the main stream. This kind of flow behaviour was observed to be inconsistent because it was not an enduring type throughout the pipe; it occurred randomly at different locations along the pipe unlike other flow patterns that existed continuously from the oil-water mixing point to the exit of the pipe.

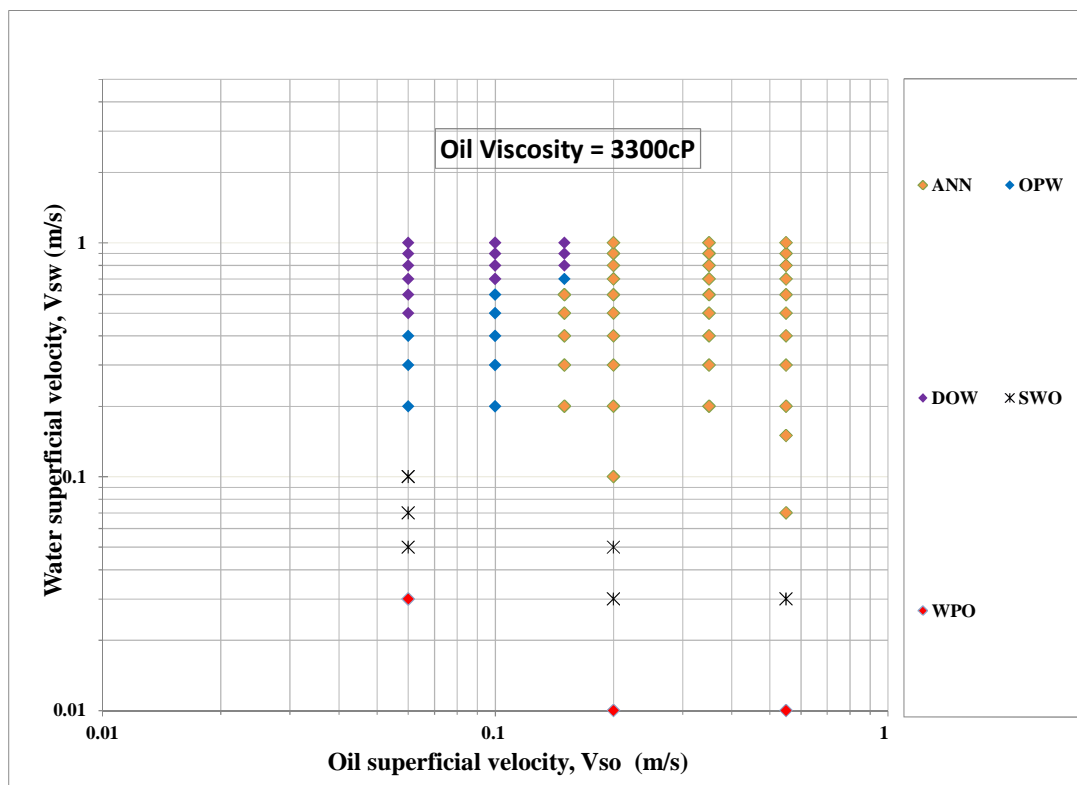


Figure 6-3: Flow regime map for oil-water flow in 1-in horizontal pipe for 3300cP nominal oil viscosity

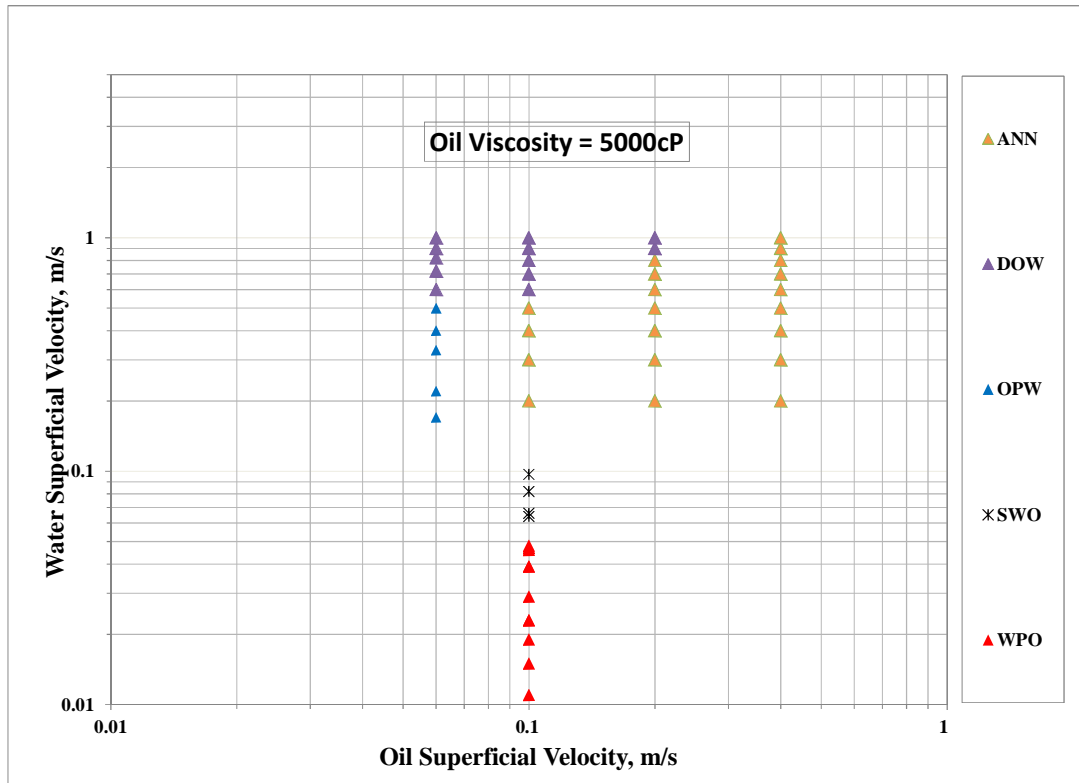


Figure 6-4: Flow regime map for oil-water flow in 1-in horizontal pipe for 5000cP nominal oil viscosity

When the V_{sw} is increased, oil appeared as plug in the water continuous flow known as OPW and further increase of V_{sw} led to the dispersion of oil in the pipe called DOW. However, an increase in V_{so} promoted annular flow types which are identified as WA-ANN as specified in the maps below. All of these flow patterns have oil film on the wall except WPO where oil formed the continuous flow.

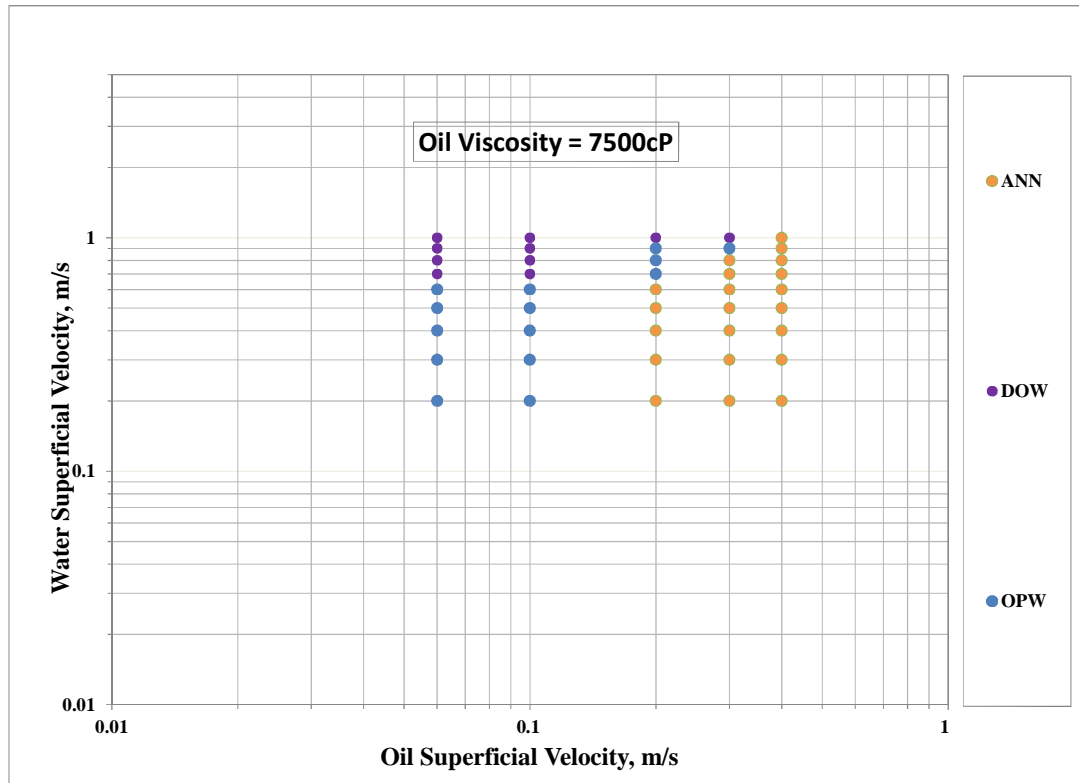


Figure 6-5: Flow regime map for oil-water flow in 1-in horizontal pipe for 7500cP nominal oil viscosity

Figure 6-6, Figure 6-7 and Figure 6-8 present the comparison of the flow pattern maps of the present research with Sotgia et al. (2008). Two maps were generated by Sotgia et al. (2008) based on the pipe materials; plexiglas and pyrex, and diameters; 26mm and 40mm respectively. The results of the present research are compared with the map developed from oil-water flow in 26mm Plexiglas horizontal pipe. Generally, it could be observed from Sotgia's map that good parts of WA-ANN are captured. In the case of slug/ annular flows transition boundary, the boundary exists when the oil flow rate is very low which quite agreed with the present study. However, stratified flows are not obtained in this investigation; perhaps, the variance observed in the map could be traced to the pipe material, or the oil properties used in these studies. Sotgia used mineral oil whose viscosity ratio to water is 900 and density ratio is 0.9 at 20°C, while the present research employs the viscosity ratio of about 3300 and density ratio of 0.924 at 20°C. In addition, their measured oil-water interfacial tension is 0.02, as against 0.026 and 0.029 in this research for CYL680 and CYL1000 respectively.

It could be easily observed in the Figure 6-6, Figure 6-7 and Figure 6-8 that the transition boundaries are functions of the properties of the mineral oils. The figures also show that Sotgia's flow map is not sufficient to predict very high viscosity oil. However, their boundary for slug-annular appear reasonable, although it is not accurate in all these figures.

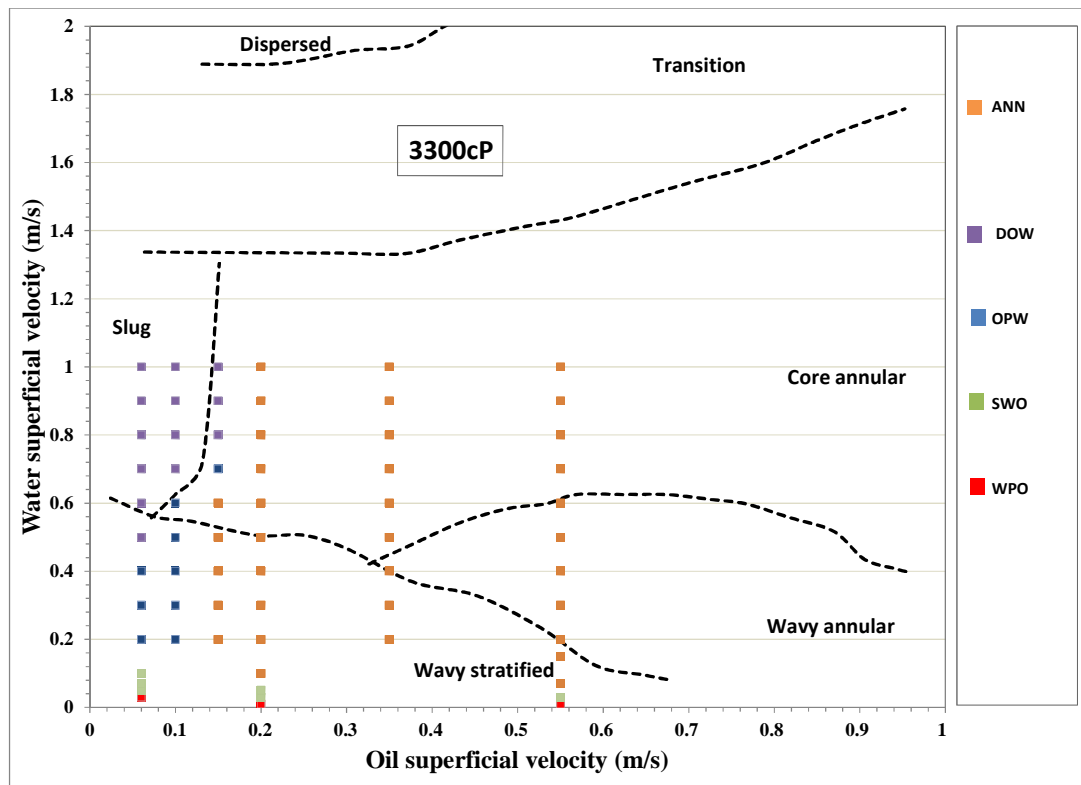


Figure 6-6: Comparing flow pattern of 3300cP oil and water with Sotgia et al (2008) literature data

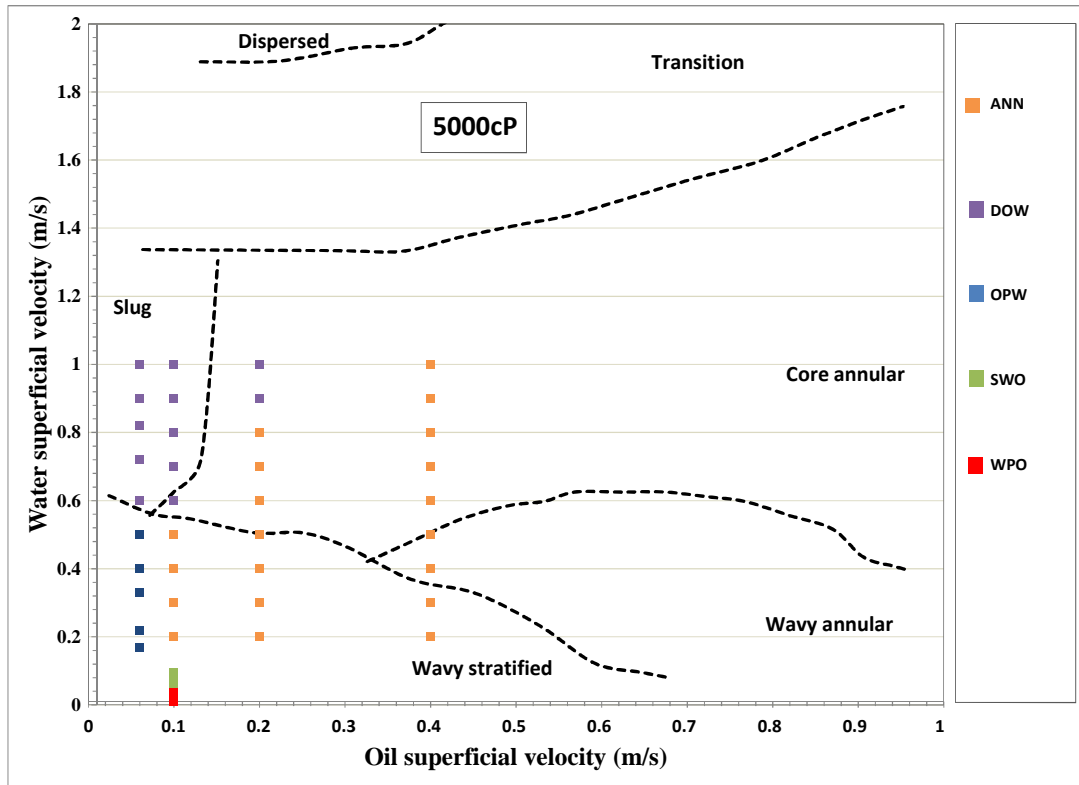


Figure 6-7: Comparing flow pattern of 5000cP oil and water with Sotgia et al. (2008) literature data

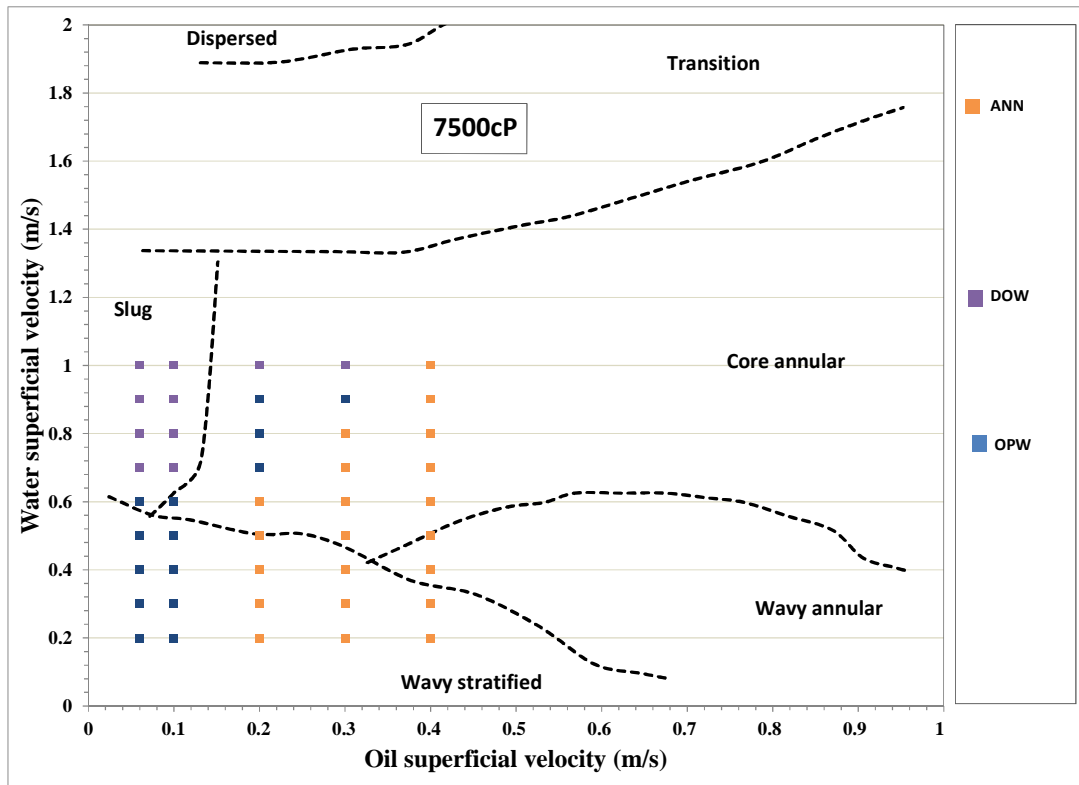


Figure 6-8: Comparing flow pattern of 7500cP oil and water with Sotgia (2008)

6.2.4 PIP flow




Phase inversion is the phenomenon whereby the phases of a liquid-liquid dispersion interchange such that the dispersed phase spontaneously inverts to become the continuous phase and vice versa under conditions determined by the system properties, volume ratio and energy input . In this study, this phenomenon is interpreted as the flow conditions where the phase that is enveloped becomes that which envelops its host by migrating from the core to the annulus, irrespective of which phase is coating the pipe wall.

The approach employed in this research to identify the PIP is the flow visualisation method while pressure gradients shift and the PIP models are employed to verify this PIP identification. Wang and Gong. (2010) suggested that the inversion might not take place at the point where the pressure drop dramatically decreased because of their observation from the sample of the mixture that they collected at low pressure drop which showed that oil was still the continuous phase in that condition. In the light of this, sharp decrease of pressure drop is not sufficient to determine PIP. In the present study, it was also observed that the pressure gradient was quite low compared to single phase oil gradient, in the WPO flow regime, whereas the only visible phase in the pipe is oil. The same phenomenon was also reported by Mckibben and Gillies (2000a). In this case, pressure gradient transition/shift cannot be employed as a condition to determine the PIP.

The author observed that the interpretation of the definition given above took place when a swirl flow of water and oil (SWO) occurred in the course of the flow, shortly after WPO; SWO is a flow condition in which the water phase that was enveloped by oil as WPO breaks out of the envelope and re-enters it intermittently at random location. It is referred to as SWO in this research; it is tricky to refer to this occurrence as a flow regime because it did not occur throughout the pipe continuously and not specific to a location. Sometimes it took place between the pressure taps (or viewing section) and vice versa. After the SWO occurrence, water became the continuous phase; the SWO is

considered in this study as the PIP condition. This definition is shown in Table 6-8 in order of flow pattern evolution;

Table 6-8: PIP identification by visualisation

Title	Flow description
WPO (Oil continuous)	
SWO (PIP)	
OPW/OF (Water continuous)	

The PIPs observed in the present study are obtained from the definition given above and compared with the existing correlations of Yeh et al. (1964), Arirachakaran et al. (1989a), Decarre and Fabre (1997), Ullman and Brauner (2002), and Jing (2006) as stated in section 2.3.2

The phase inversion models mentioned in section 2.3.2 were considered in the Figure 6-9 for oil-water flow where the oil viscosities are 3300 and 5000cP. Arirachakaran et al. (1989) model failed to be consistent in predicting the inversion at low superficial velocity (i.e. 0.06 and 0.2m/s). It is fair when the oil superficial velocity is 0.55m/s. Although Arirachakaran et al. (1989) model was developed based on a wide range of viscosity; it could not be fully relied upon.

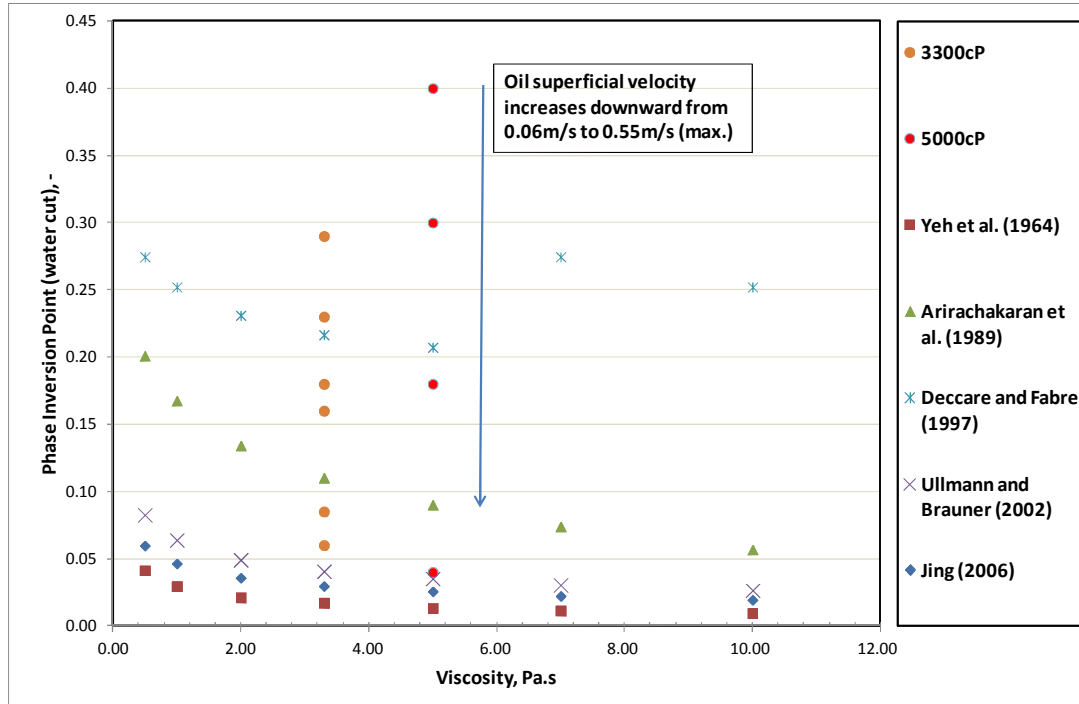


Figure 6-9: Comparison of phase inversion models' prediction at different viscosities with the present research

Other models also are not suitable for any of this flow condition perhaps, because their basis of development was low viscosity oils. In addition, their inadequacy may be traceable to the interfacial tension or the fact that all these models depend mainly on viscosities, densities and water cut assuming that the inversion would be the same irrespective of the flow rates. On the contrary, this research reveals that the oil flow velocities have impact on the accuracy of the phase inversion models.

Figure 6-10 and Figure 6-11 compare the velocities of water and oil obtained from the present study with that which is obtained from the existing models. It is glaring that the models possess linear attributes and predict same but the experimental data are not linear. These figures reveal that the relationship of V_{sw} and V_{so} are not linear, therefore, in agreement with Wang and Gong (2009) it is evident that the inversion model and analysis on PIP for high viscosity oil-water two-phase flow requires more investigations.

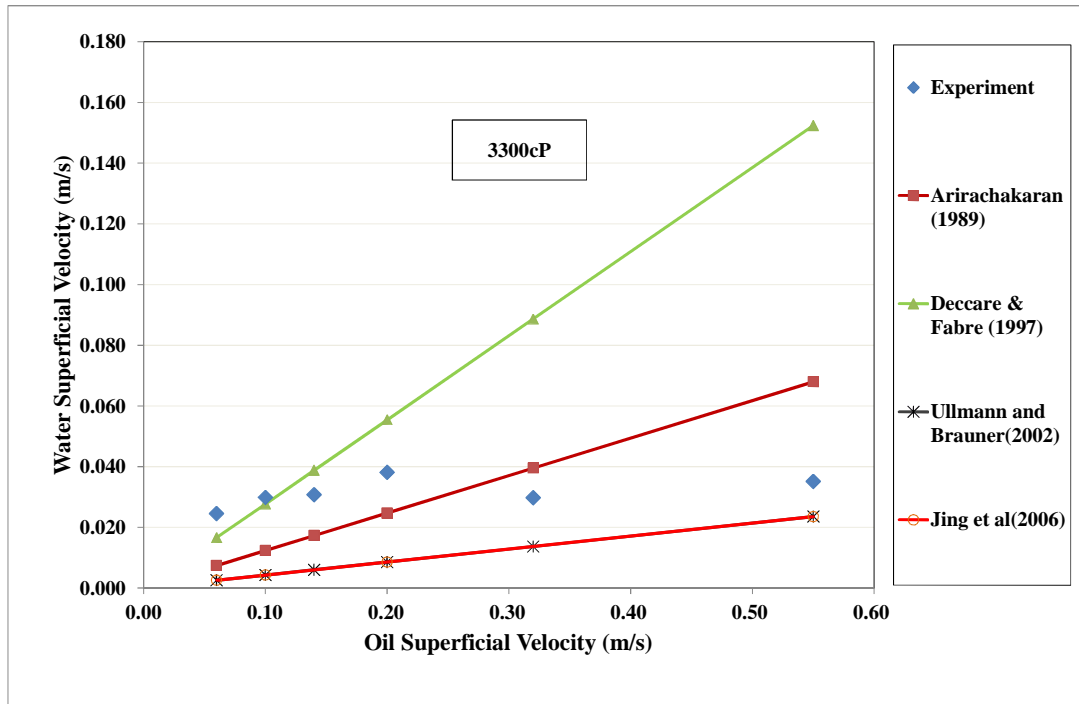


Figure 6-10: Behaviour of water and oil velocity at PIP for 3300cP nominal viscosity

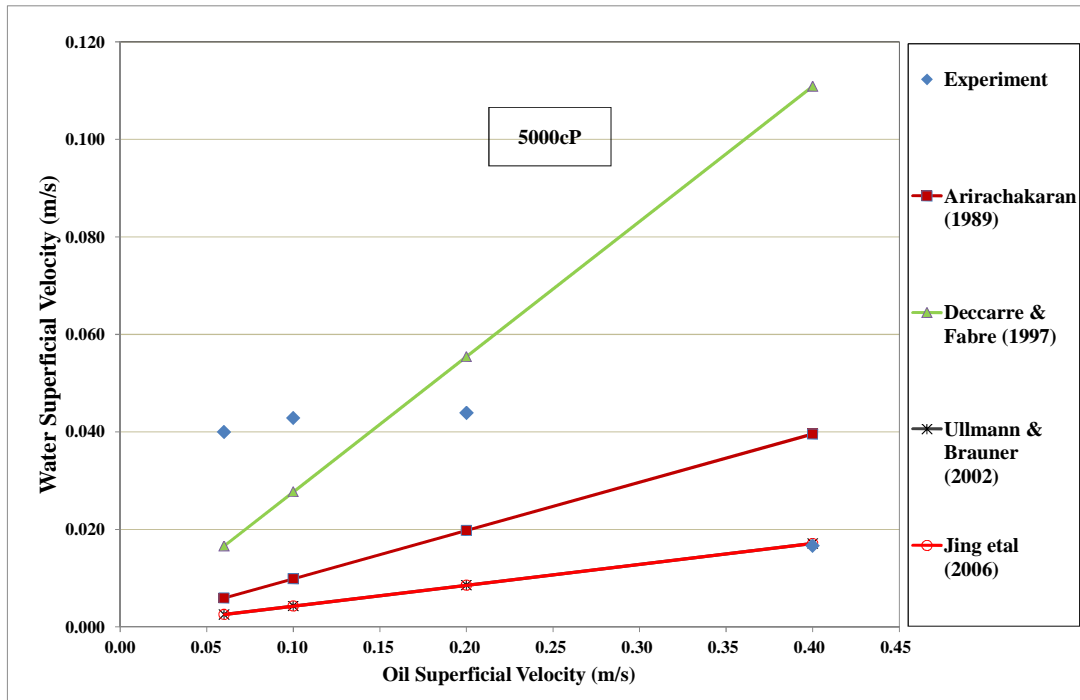


Figure 6-11: Behaviour of water and oil velocity at PIP for 5000cP nominal viscosity

6.3 Pressure gradient

Figure 6-12 to Figure 6-23 show the pressure gradient profile against water cut and V_{sw} for different oil viscosities. Generally, it could be observed that the pressure gradient values are directly proportional to the oil flow rate (i.e. high oil flow rate has a relatively high pressure gradient). Considering each trend in Figure 6-12, Figure 6-14 and Figure 6-16, the pressure gradients were first observed to decrease from the high value corresponding to single phase oil gradients (i.e. at zero water cut where the flow was reduced to single phase oil) to the lowest pressure gradient attainable in each oil flow rate considered in the experiments. After reaching the lowest point, the pressure gradient starts to climb. For example, the lowest pressure gradients attained for 3300cP are 1.54, 1.23 and 2.95kPa/m when the V_{so} were 0.06, 0.2 and 0.55m/s respectively. The increase observed in pressure gradients were also observed to be a function of the increase in the water cut in each of the three scenarios. In summary, the pressure gradient first fell until a minimum was reached and then rose with increase in water cut. It was equally observed that the lowest gradients being discussed here occurred mostly at low water cuts which suggests that the low water cuts are needed to lower the oil-wall friction, while high water cut (after the friction has been reduced to minimum) aids the dispersion of oil and then its transfer back to the pipe wall, which perhaps lead to increase in the wall shear stress. It could also be seen from these figures that the pressure drop reduction of heavy oil is not dependent of viscosity because all the gradients are reduced by at least an order of magnitude.

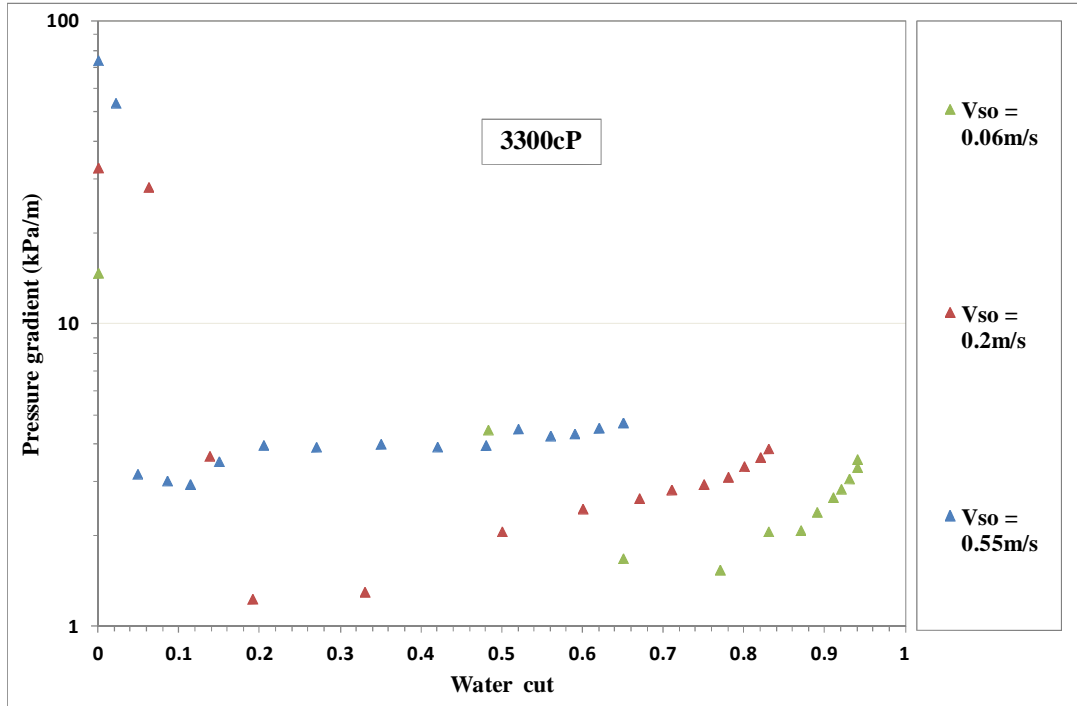


Figure 6-12 Comparison of pressure gradient of oil-water flow for 3300cP nominal oil viscosity at different oil superficial velocities and water cut

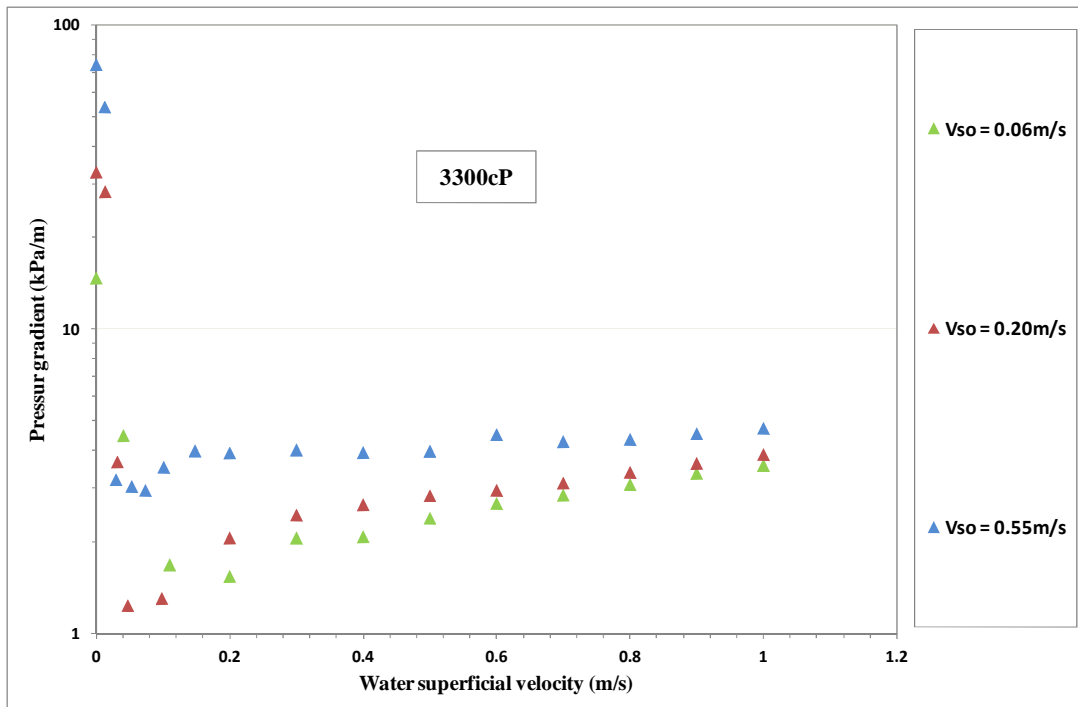


Figure 6-13 Comparison of pressure gradient of oil-water flow for 3300cP nominal oil viscosity at different oil and and water superficial velocities

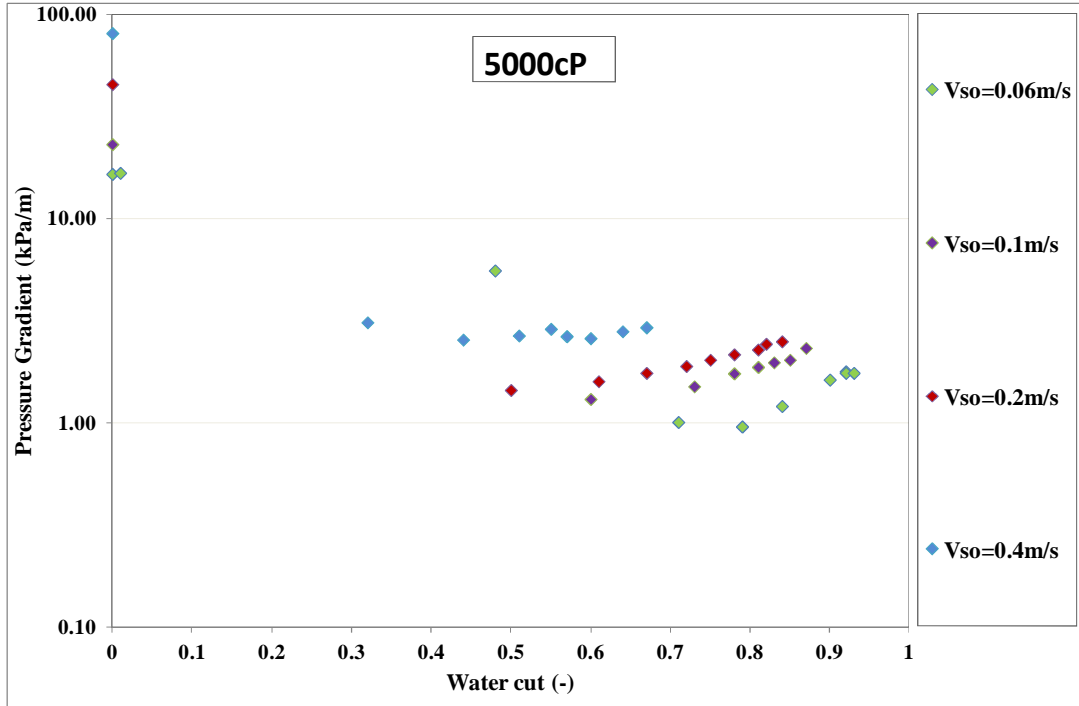


Figure 6-14 Comparison of pressure gradient of oil-water flow for 5000cP nominal oil viscosity at different oil superficial velocities and water cut

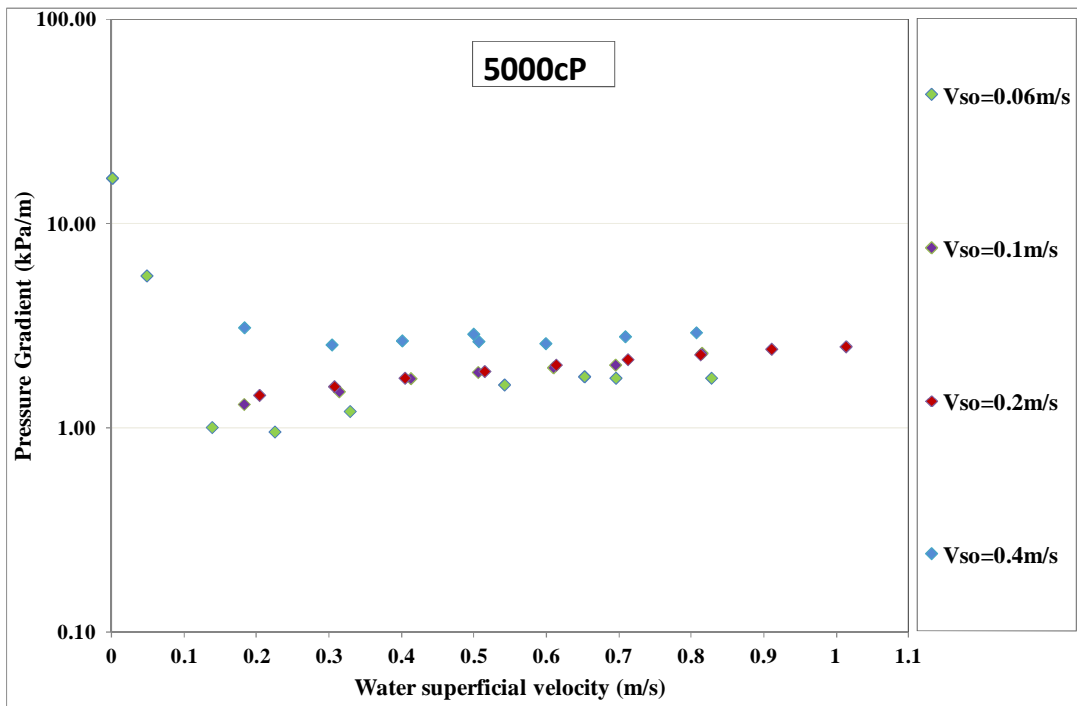


Figure 6-15 Comparison of pressure gradient of oil-water flow for 5000cP nominal oil viscosity at different oil and and water superficial velocities

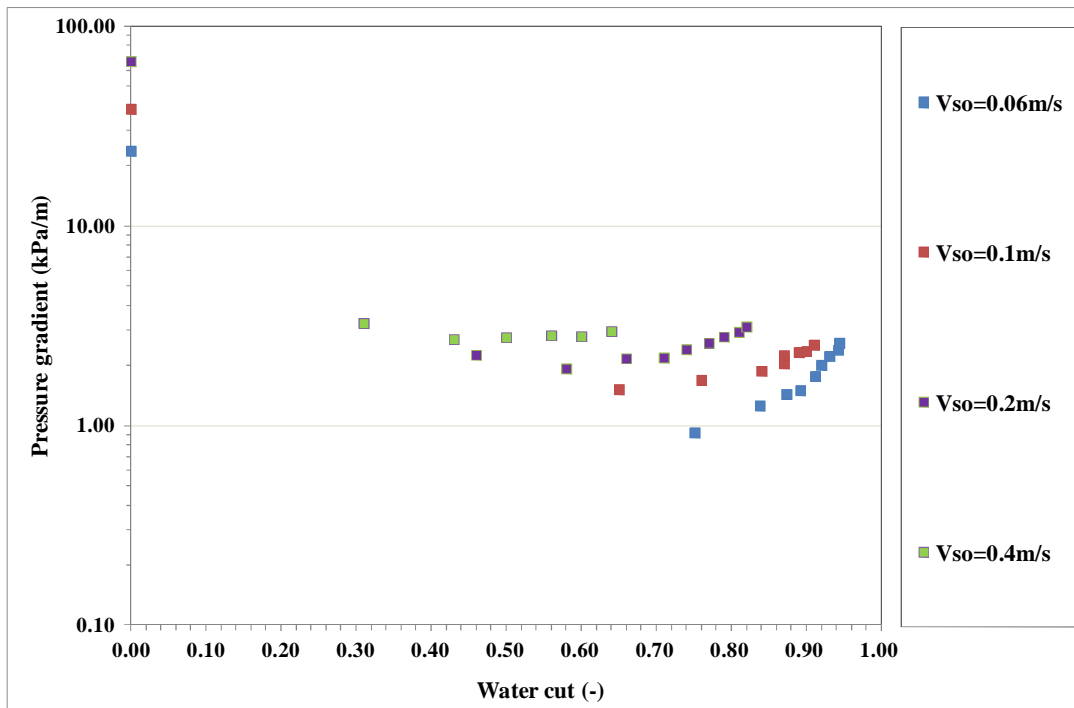


Figure 6-16: Comparison of pressure gradient of oil-water flow for 7500cP nominal oil viscosity at different oil superficial velocities and water cut

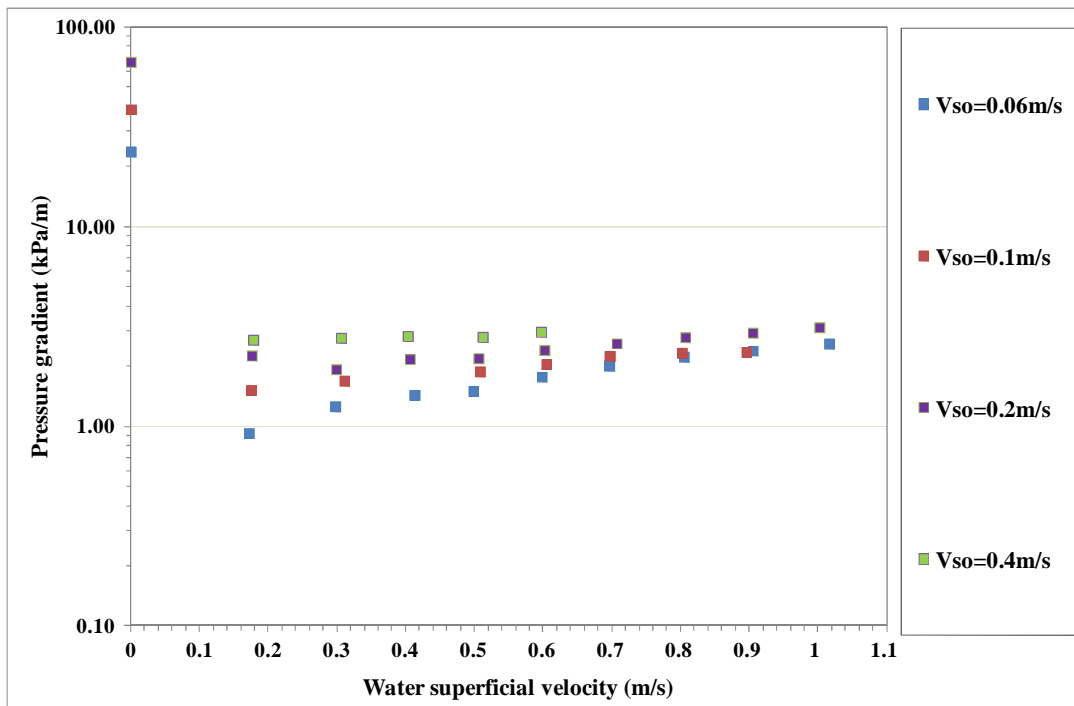


Figure 6-17 Comparison of pressure gradient of oil-water flow for 7500cP nominal oil viscosity at different oil and and water superficial velocities

Figure 6-18, Figure 6-20 and Figure 6-22 present the comparison of the pressure gradients of different oil viscosities to expose the specific behaviour of the oil viscosities considered in this research. Generally, the gradients of 3300cP oil with water appeared higher than both 5000 and 7500cP. In this research, Figure 6-18 and Figure 6-19 reveal that at low oil superficial velocity (i.e. $V_{so}=0.06\text{m/s}$) the differences in the pressure gradients are not quite significant; in fact, the values and the trend of the gradients of 5000cP and 7500cP are quite similar.

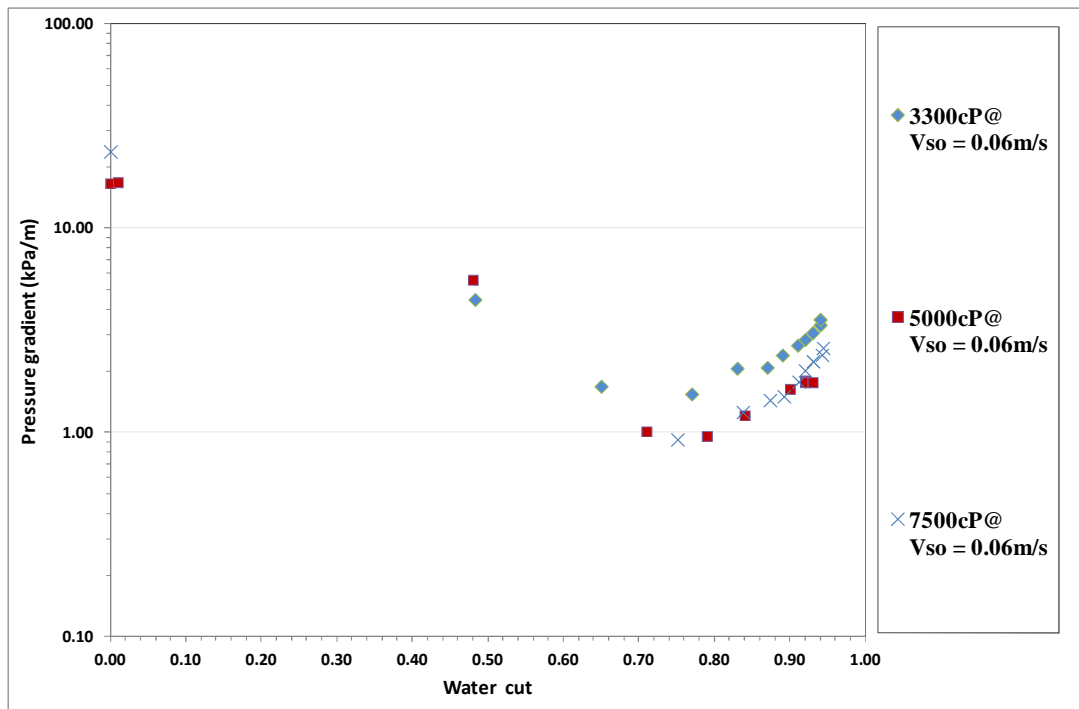


Figure 6-18: Effect of viscosity on pressure gradient @ $v_{so} = 0.06\text{m/s}$ and different water cut

The behaviour of these 2 viscosities (5000cP and 7500cP) differed when the oil superficial velocity was increased from 0.06 to 0.2m/s; at this condition, the gradients of the 3 viscosities are distinctive from one another in Figure 6-20 and Figure 6-21. The gradients of 5000cP oil with water appeared to be lower than both the 3300cP and 7500cP. Further increase of the V_{so} to 0.4m/s (as shown in Figure 6-22 and Figure 6-23) show that 3300cP oil flow with water gives the lowest gradients compare to 5000cP and 7500cP oils. In addition, both the gradients of 5000cP and 7500cP are virtually the same on the high side of the water cut or V_{sw} . This behaviour is quite

unique and has not been reported by any researcher. This behaviour is not understood at the moment; hence, more investigation is needed to verify this behaviour.

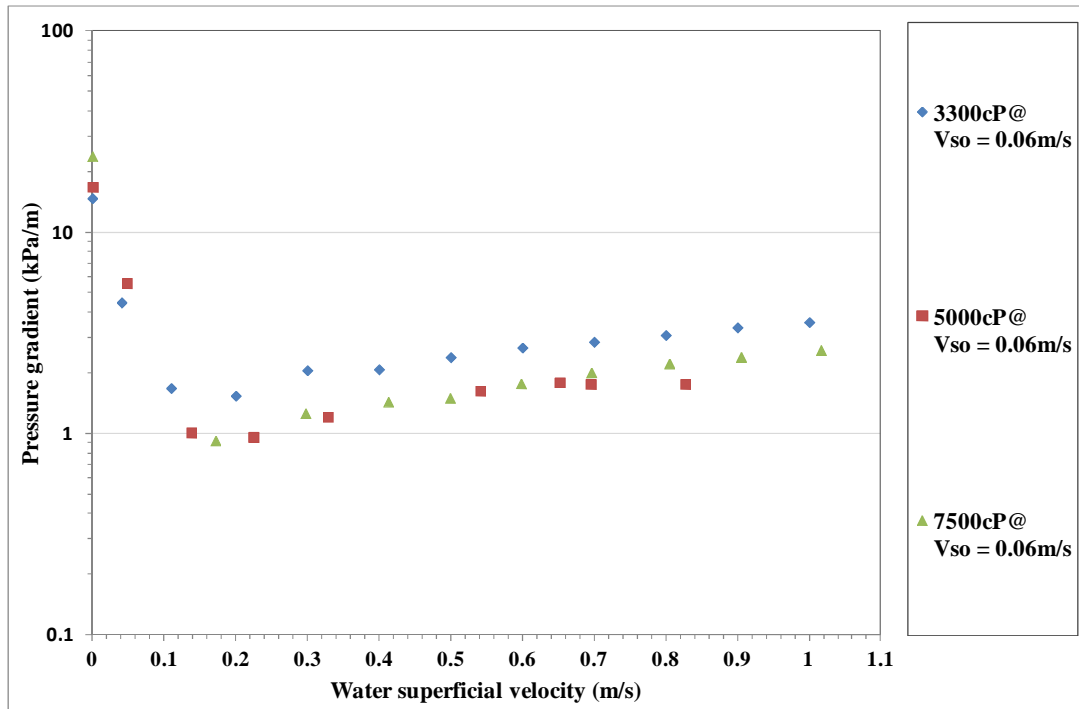


Figure 6-19: Effect of viscosity on pressure gradient @ $v_{so} = 0.06 \text{ m/s}$ and different water superficial velocity

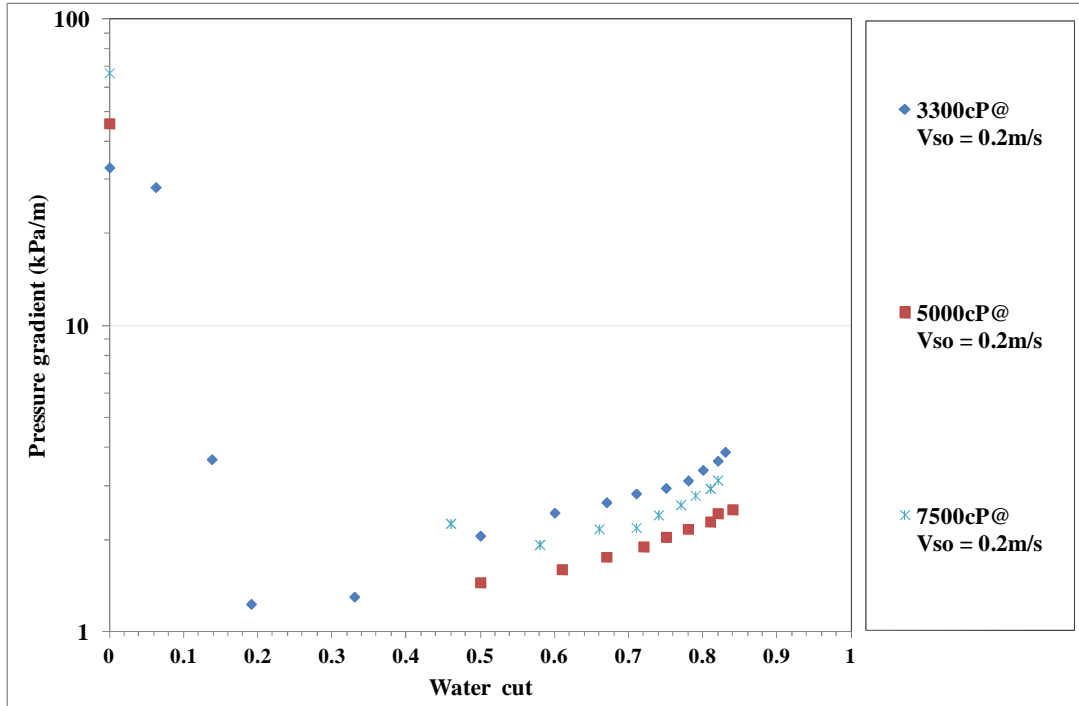


Figure 6-20: Effect of viscosity on pressure gradient @ vso = 0.2m/s and different water cut

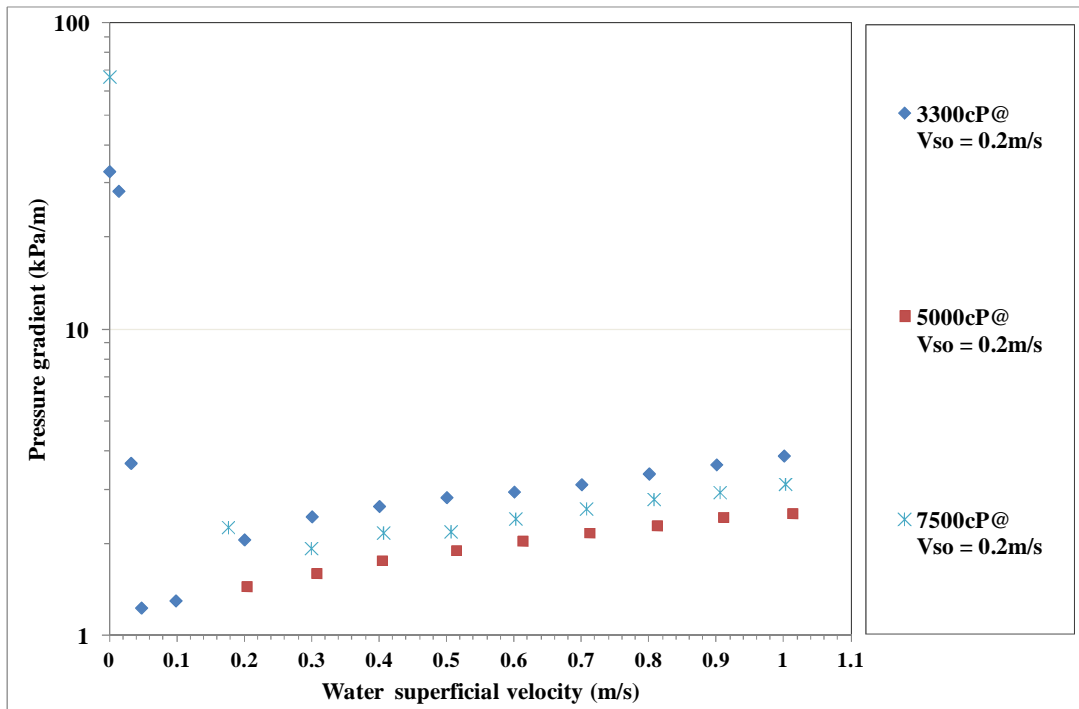


Figure 6-21: Effect of viscosity on pressure gradient @ vso = 0.2m/s and different water superficial velocity

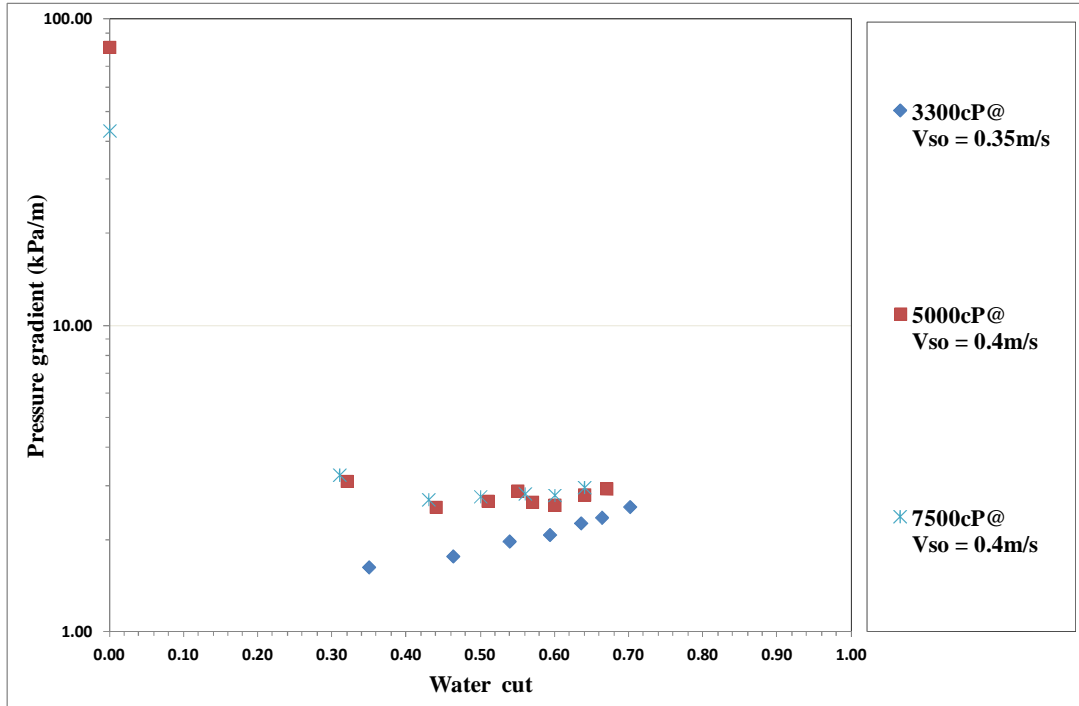


Figure 6-22: Effect of viscosity on pressure gradient @ $v_{so} = 0.4\text{m/s}$ and different water cut

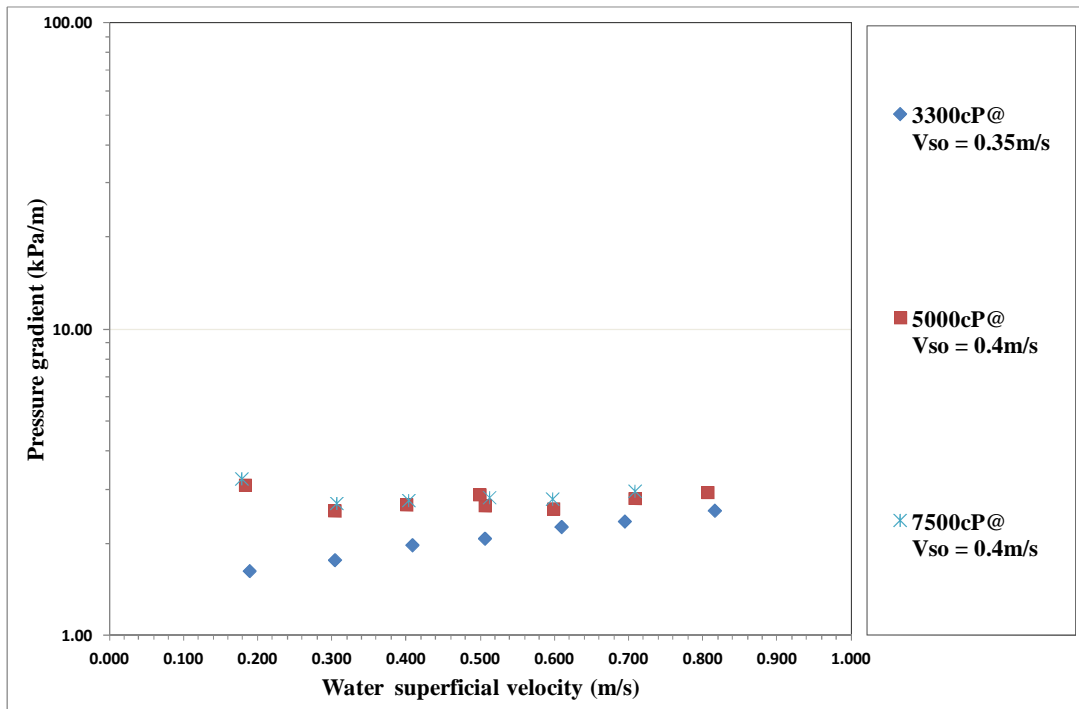


Figure 6-23: Effect of viscosity on pressure gradient @ $v_{so} = 0.4\text{m/s}$ and different water superficial velocity

6.3.1 Reduction Factor

In order to quantify the effect of water assistance in the transport of heavy oil through a channel, the Figure 6-24 was generated from Equation 3-8, which is the ratio of the frictional pressure gradient of single phase oil flow through a channel to the frictional pressure gradient of two-phase oil-water flow through the same channel. It was observed from the Figure 6-24 and Figure 6-25 that the degree of the reduction of the pressure gradient, firstly increases and then decreases with the increase in water cut. In other words, when the water cut becomes too low, the effect of water on the reduction of the pressure gradient is also low. For instance, when the oil superficial velocity was 0.2 and 0.55m/s with the water cut at 0.06 and 0.02 respectively, the reduction factor are about 13 and 27%. The highest pressure gradient reduction factors attained in the three scenario investigated occur at different point that could be referred to as optimum water cut for each respective oil flow rate considered in the test. It is also worthy to note that the reduction factors keep decreasing as water cut continues to increase. This was evident at low V_{so} , i.e. 0.06m/s. These data agree with the behaviour obtained by other researchers' (Sotgia et al., 2008; Bensakhria et al., 2004a; Strazza et al., 2011).

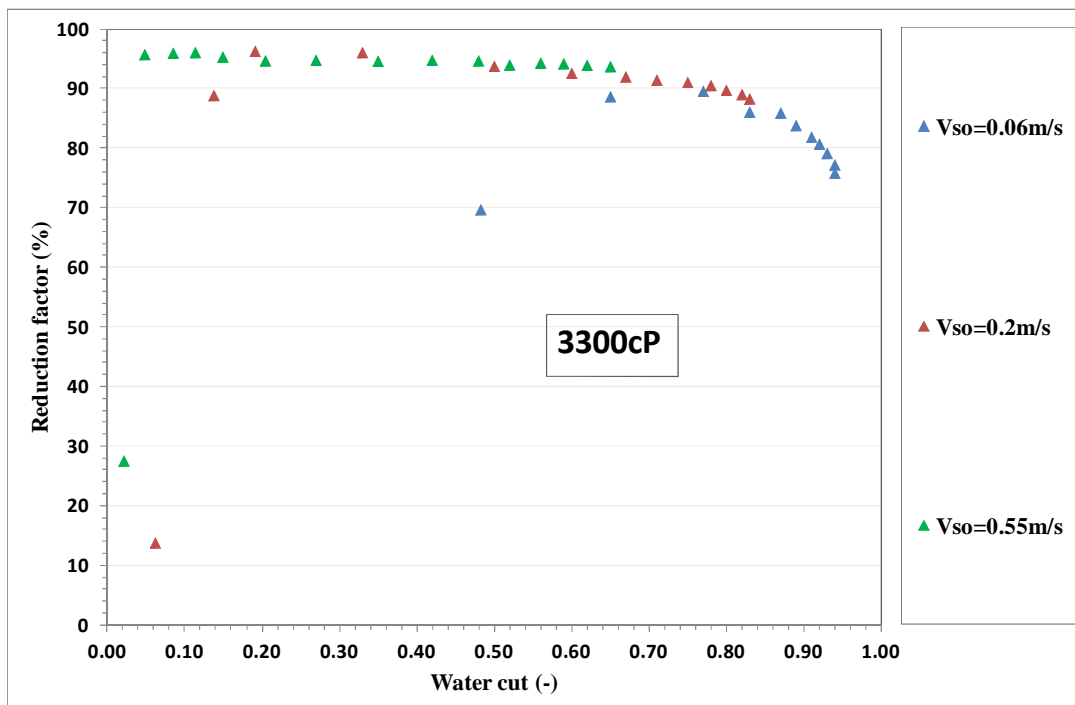


Figure 6-24: Pressure gradient reduction factor against water cut of oil-water flows at 3300cP oil viscosity (nominal)

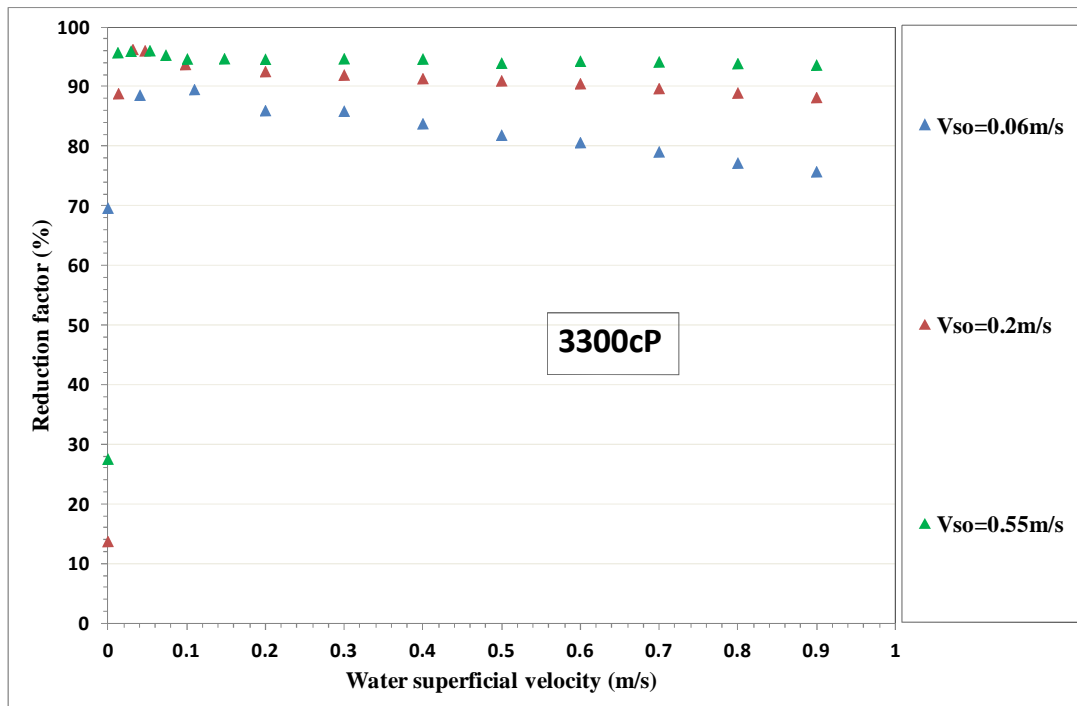


Figure 6-25: Pressure gradient reduction factor against water superficial velocity of oil-water flows at 3300cP oil viscosity

6.3.2 Verification of SRC Model

Figure 6-26, Figure 6-27 and Figure 6-28 present the verifications of the SRC model proposed by McKibben and Gillies (2009) to predict the pressure gradient of both oil-water and oil-water-sand in horizontal pipelines. From general observation, Figure 6-26, Figure 6-27 and Figure 6-28 show that the model effectiveness increases with viscosity. This could be traced to the properties of the oil used to gather the data (Husky crude oil viscosity was 31.4Pas @20°C) for the correlations. The model is found suitable to predict gradients at relatively high V_{sw}. The inability of the SRC model to predict the gradient at very low water cut could be due to the experimental flow condition limit that were investigated. Although the data used to develop the correlations stated in Equations 2-18 and 2-21 were obtained from 2-in, 4-in and 10-in diameters, the ability of the correlation to predict the pressure gradient of the present research reasonably well is commendable. This shows progress made in understanding the mechanisms of high viscosity oils production.

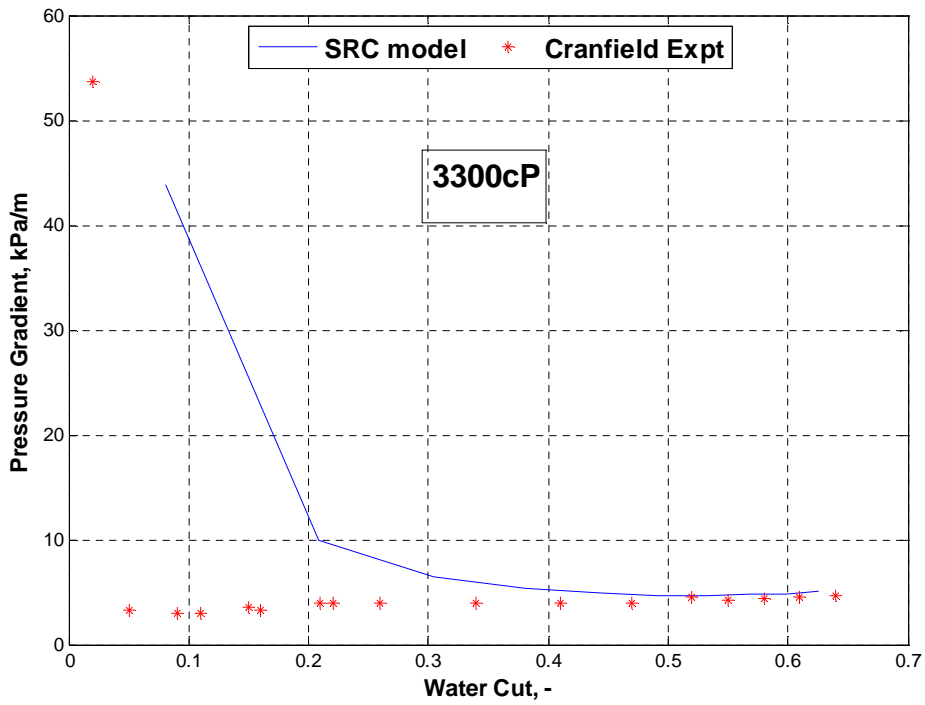


Figure 6-26: Validation of SRC model for 3300cP oil with water at $V_{so}=0.55\text{m/s}$

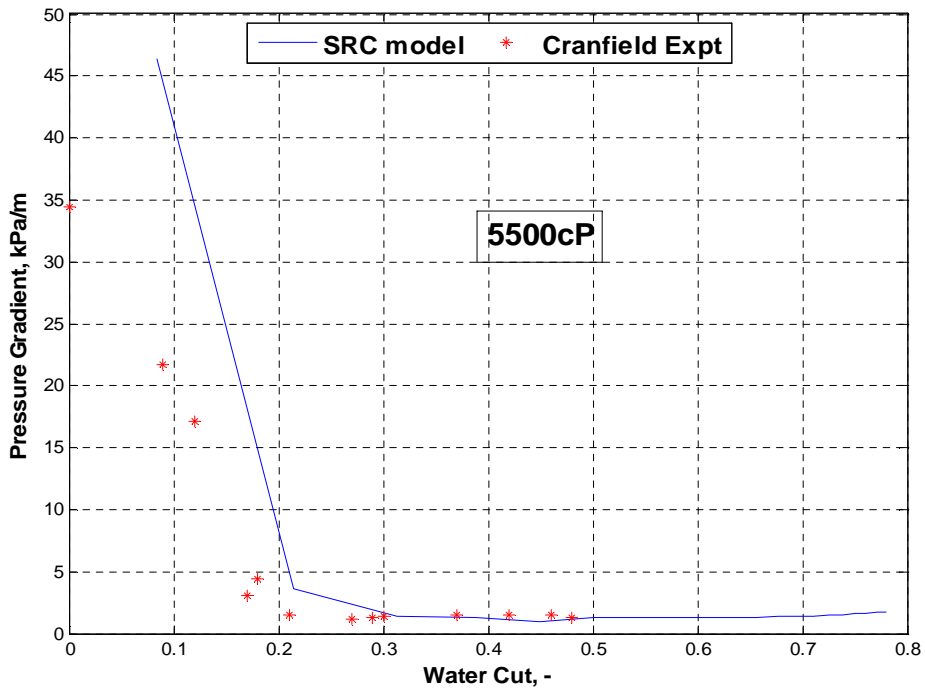


Figure 6-27: Validation of SRC model for 5500cP oil with water at $V_{so}=0.11\text{m/s}$

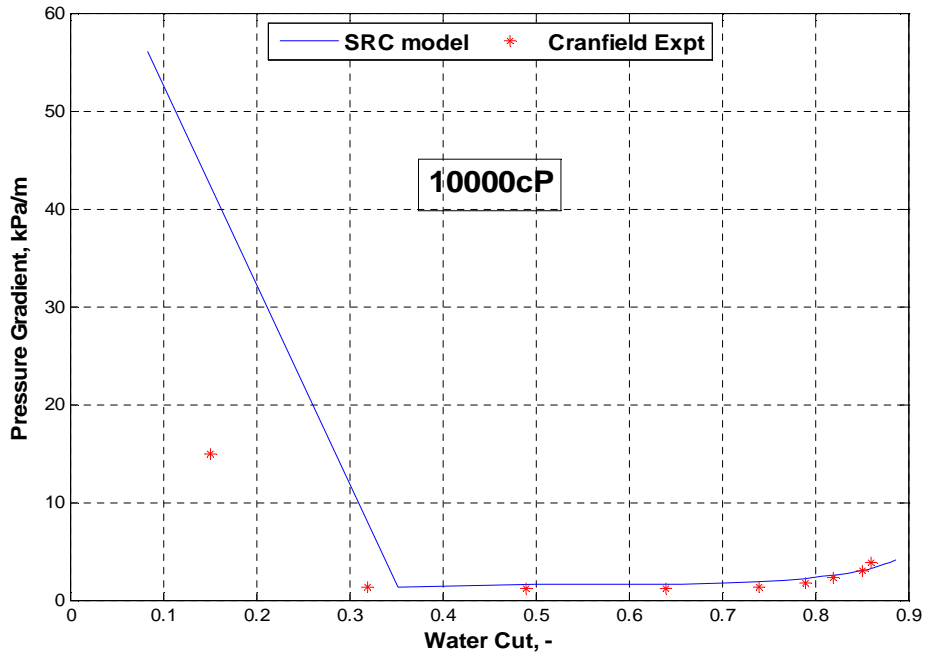


Figure 6-28: Validation of SRC model for 10000cP oil with water at $V_{so}=0.11\text{m/s}$

6.4 CFD of Oil-Water Multiphase Flow

In this section, the results of CFD simulations are presented. This covers the flow pattern identification with volumetric fraction contour and PDF of pressure signals and pressure gradient. The CFD results were obtained from 30seconds simulation time. This is similar to the frequency of data capture in experiment i.e. 250Hz. This section presents 6.4.1 Description of model, 6.4.2 Flow specification, 6.4.3 Pipe inlet geometry design and 6.4.8 Flow pattern identification.

6.4.1 Description of model

The governing equations are given in equations 4-1 to 4-4. The condition of annular flow in a vertical pipe has been simulated with the Volume of Fluid (VOF) model by Ghosh et al. (2010) based on Eulerian-Eulerian approach. Their research also could not show the fouling effect of oil on the wall. In addition, the Eulerian-Eulerian approach is not cost effective in computational modelling because it solves separate set of equations for each phase involve, hence, the Eulerian VOF approach which solves only a set of equations was employed in this research to simulate the oil-water flow in horizontal pipe. VOF is an interface tracking technique that captures the interface between the phases. This powerful tool allows the simulation of complex free surface flows with an arbitrary shape in any situation included folding or break-up (Kvicinsky et al., 1999). As long as the interface resolution and conservation of mass, momentum, and energy is ensured by use of proper numerical techniques, the VOF method is accurate enough to capture essential flow features around the free-surface (Rhee et al., 2004).

The VOF formulation relies on the fact that two or more fluids (or phases) are not interpenetrating. For each additional phase that is added to the model, a variable is introduced: the volume fraction of the phase in the computational cell. The fields for all variables and properties are shared by the phases and represent volume-averaged values, as long as the volume fraction of each of the phases is known at each location. A single momentum equation is resolved throughout the domain, and the continuity equation is

solved to maintain the mass balance in the system. The gravitational force and surface tension are the body forces in the momentum equation.

Generic features of the simulations are stated in this section with the particular features for each boundary condition. Some simulated oil-water flow cases are reported in this section using the commercial CFD code FLUENT 12.1 to solve the governing equations. The simulations were conducted on a Sun Microsystems Inc. server operating on UNIX Release 5.9 operating system. Since the UNIX server was a machine shared by multiple users, the run times were different depending upon the amount of load on the machine at the time a particular run was conducted.

6.4.2 Flow specification

As it was done in the experimental research, the oil and water flows are supplied at the inlet section of the computational flow domain (pipe), then the two-phase mixture flows along the pipe and is finally discharged through the outlet at atmospheric pressure.

6.4.2.1 Fluid properties

The relevant properties of the two fluids (oil and water) used in the simulation are as given in Table 6-9.

Table 6-9: Fluid properties

Fluid	Density @25°C (kg/m³)	Viscosity @25°C (Pa.s)	Surface Tension @19°C (N/m)
Water	998.2	0.001003	0.026
Oil	916.2	3.149	

6.4.2.2 Boundary and initial conditions

The boundary conditions are specifications of flow properties on the computational domain boundaries. They are very important components of the CFD simulations in terms of representing the experimental configuration of the multiphase flow through the

pipe, hence the boundary conditions were chosen based on the experimental setup described in Chapter 3.

At the inlet, a velocity-inlet boundary type is used in which the mixture velocity and the liquid volume fraction are specified. The velocity profile is assumed to be uniform. This approach requires no additional experimental knowledge about the annular in order to setup the numerical simulation. This is also similar to the way experimental research has been carried out. The inlet values for turbulent intensity, I , and viscosity ratio are estimated for fully developed flow with the following equations:

$$I = 0.16Re^{-\frac{1}{8}} \quad 6-1$$

Where Re is the Reynolds number, and I is the turbulence intensity for fully developed pipe flow. The walls of the pipe are assumed to be rigid and impermeable, in which the wall roughness was set as a smooth wall. A no-slip condition is applied to the velocity where there is contact at solid walls at any instant. The pressure and liquid volume fraction at the wall are described by a zero gradient condition since the volume fraction cannot diffuse into the wall. At the outlet, the remaining variables are transported out of the computational domain with zero average static pressure so that the mass balance is satisfied. Operating conditions were specified as being standard atmospheric pressure (101.3 kPa) and temperature 20°C. Gravity effects are accounted for and the acceleration due to gravity taken to be -9.81 m/s². For volume fractions of phases, the specified initial condition depended on the case under study, however, an initial condition of perfectly mixed phases throughout the flow domain was set.

6.4.3 Pipe inlet geometry design

A variant of injection method was considered for inlet type so as to keep the model simple and reduce the computational time. A T-junction approach was used in the experiment. The concentric inlet design was only considered in the CFD simulation to impose the water injection as shown in Figure 6-29; water is injected in the annulus while oil is injected at the centre.

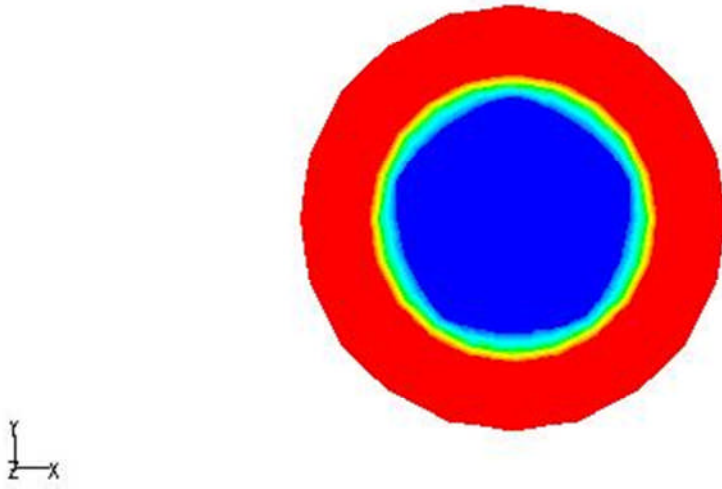


Figure 6-29: CFD annular flow inlet geometry description

The results of the pressure gradient were presented in Figure 6-30 for different core diameters. This is necessary in order to know the effect of the dimension on the flow behaviour. It was observed that the inlet injector diameter has effect on the flow behaviour. When the core diameter is about 60% of the original pipe diameter, the resultant pressure gradient were much lower compared to 50% and 70% of the original pipe diameter. This could be due to dispersion of oil by water in both cases; when the water passage becomes small, the tendency to have increase of water flow rate is unavoidable, and on the other hand when the oil passage at the inlet (i.e. core) becomes narrow, the tendency of increasing the slip on the side of the oil would exist, and this would lead to increase of turbulence at the oil-water interface which might cause dispersion of the oil and migration to the pipe wall which will definitely increase the shear. Hence the optimum diameter (concentric inner-outer) ratio for this inlet design is 0.6 as shown in Figure 6-30.

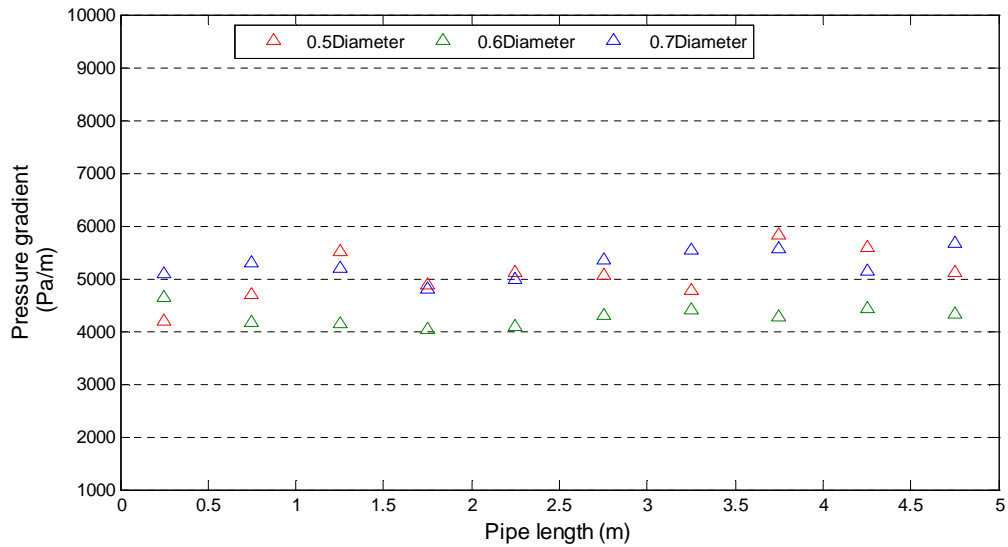


Figure 6-30: Pressure gradients of three different inner-inlet dimensions opening in oil-water transport for oil at 0.55m/s and water at 1.0m/s

6.4.4 Comparison of T-junction with concentric inlet pipe geometry

A T-junction injection type pipe geometry was designed with Gambit 2.4 as presented in Figure 6-31. The geometry is a 3-dimensional, 5.5m long, 1-in ID horizontal pipe similar to the experimental arrangements with the injection point at 0.5m from the oil inlet on the horizontal axis. Water is injected into the flow line from the top inlet of the vertical section of the geometry. The test section of the pipe is aligned with the z - axis and measurements sections were placed along the pipe.

Table 6-10: Geometry properties of T-junction pipe

Geometry	Pipe Length (m)	Pipe Diameter (m)	Number of cells
1	5.5	0.0254	315,666

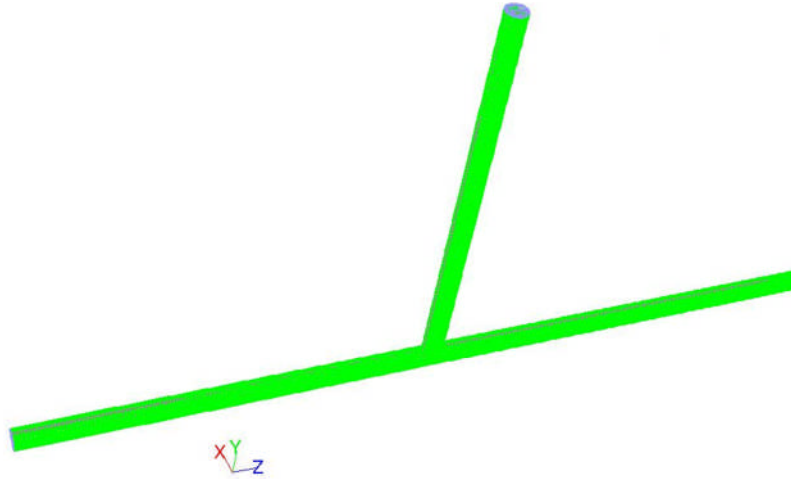


Figure 6-31: T-junction pipe geometry

Simulations were run on both T-junction and concentric type of inlets to verify the need for the modification of the pipe inlet design to enhance the performance of CFD. Table 6-11 presents the comparisons of the experimental results with both inlet designs. Two flow conditions are employed and simulated for 30s each to analyse their performances. The third column from left shows the results obtained from the concentric inlet condition (CIC) while the fourth column shows the results of the T-junction inlet condition (TIC). The viscosity of oil employed for this investigation is 3300cP. The pressure gradients obtained show that there is an impact of inlet design on the simulated results. Comparing the gradients obtained from experiment with CFD when the flow condition is 0.50m/s and 0.20m/s for V_{so} and V_{sw} respectively, one could see that the CIC achieved 0.1 order of magnitude higher than the experimental result while T-junction returned a result that is an order of magnitude higher.


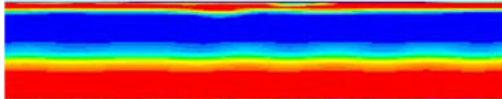
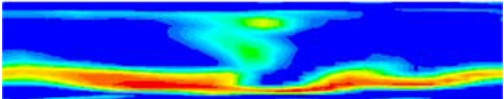
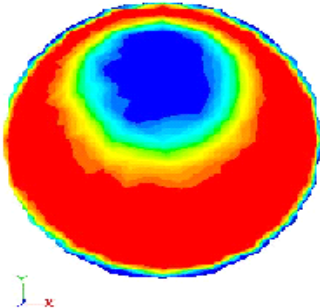
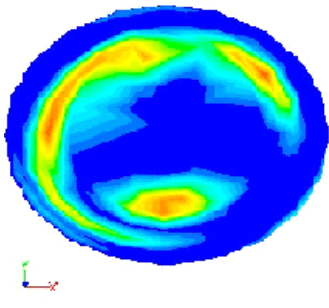
Table 6-11: Inlet condition adaptability check using pressure gradient

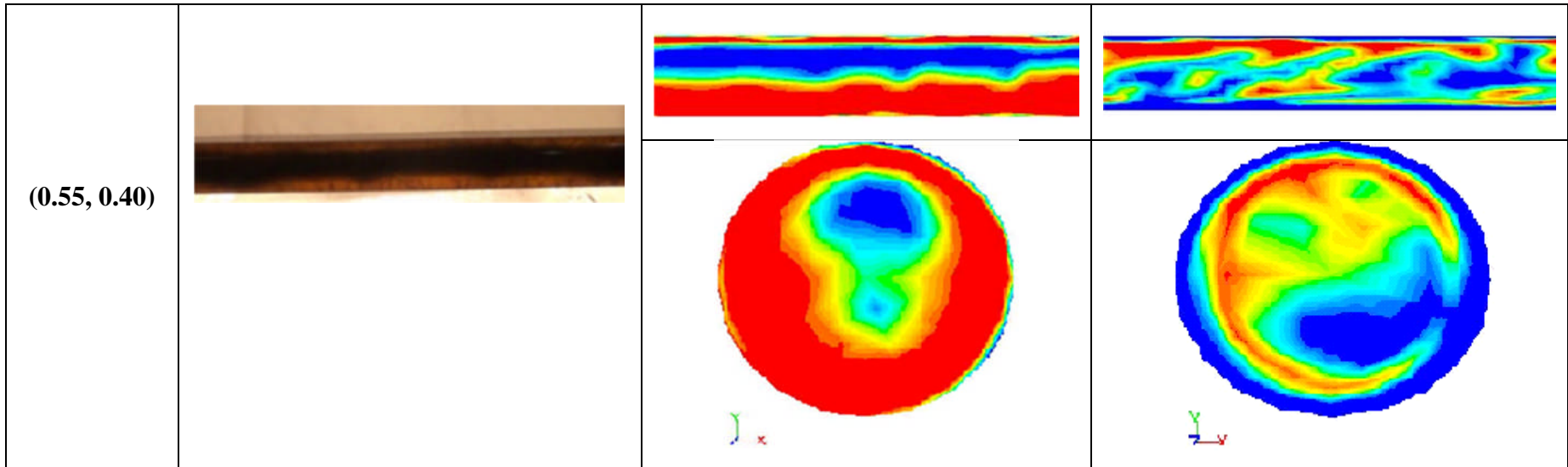
(V_{so}, V_{sw}) m/s	Pressure gradient kPa/m		
	<i>Experiment</i>	<i>CFD</i>	
		<i>Concentric Inlet</i>	<i>T-junction Inlet</i>
(0.55, 0.20)	3.92	4.35	44.34
(0.55, 0.40)	3.93	18.25	29.43

However, when the V_{sw} increased to 0.40m/s, the CIC could no longer sustain the control on the gradient. Both inlet conditions (i.e. CIC and TIC) returned gradients that are an order of magnitude higher than the experiment. The remaining data for CIC which reveal the uprising with increase in V_{sw} are presented in Figure 6-33. The gradient analysis is not sufficient to draw conclusion on the choice of the inlet condition, hence the analysis of the flow configuration.

Table 6-12 reveals the flow configurations of the same cases stated in Table 6-11. Comparing the experimental flow pattern with the flow contours gotten from CIC, one could see good predictions of the flow behaviours which show oil coating on the wall (column 3). The oil coating on the pipe wall is not excessive as it is in TIC (column 4). The excessive oil coating in TIC could be due to the degree of continuous flow disturbance cause by the injection type. The two case studies are annular flows which CIC predicts satisfactorily well but could not be reproduced as expected by TIC. These contour plots suggests that the inlet conditions have impact on the flow development and stability as can be seen from the differences presented by Table 6-11 and Table 6-12. In the light of this, the author decides to employ the CIC for the subsequent simulations in order to save computational time and keep the geometry model simple.

Table 6-12: Inlet condition adaptability check using flow pattern

(V_{so}, V_{sw}) m/s	Flow pattern @30s		
	<i>Experiment</i>	<i>CFD</i>	
		<i>Concentric Inlet</i>	<i>T-junction Inlet</i>
(0.55, 0.20)			
			



6.4.5 Choice of Turbulence Model for 2-Phase Oil-Water Flow

This section compares the performances of four types of turbulence model on oil-water flow in horizontal pipe. This becomes necessary for the selection of the turbulence model that would be employed in this study, since turbulence is crucial to this study. Since some flow conditions of water has been observed to be turbulent as obtained in the experiments. Figure 6-32 shows the trend plot of the pressure drop obtained by employing four different turbulence models to simulate 2-phase oil-water flow; Standard k-epsilon (SKE), low-Reynolds-k-epsilon (LRKE), standard k-omega (SKW) and low-Reynolds-k-omega (LRKW) models. From Figure 6-32, it could be seen that SKE and LRKE models over predicted the trend of the pressure drop, although it appears to be declining with time. The trend reveals that it would take a longer simulation time to attain stability if it will. This may serve as a pointer to the inference made by Bardina (1997) that k-epsilon model always exhibits numerical instability as it is shown in the graph. The performance of SKE also could be traced to the fact that it is mainly valid for fully turbulent flows. Both the SKW and LRKW models are observed to under predict the trend.

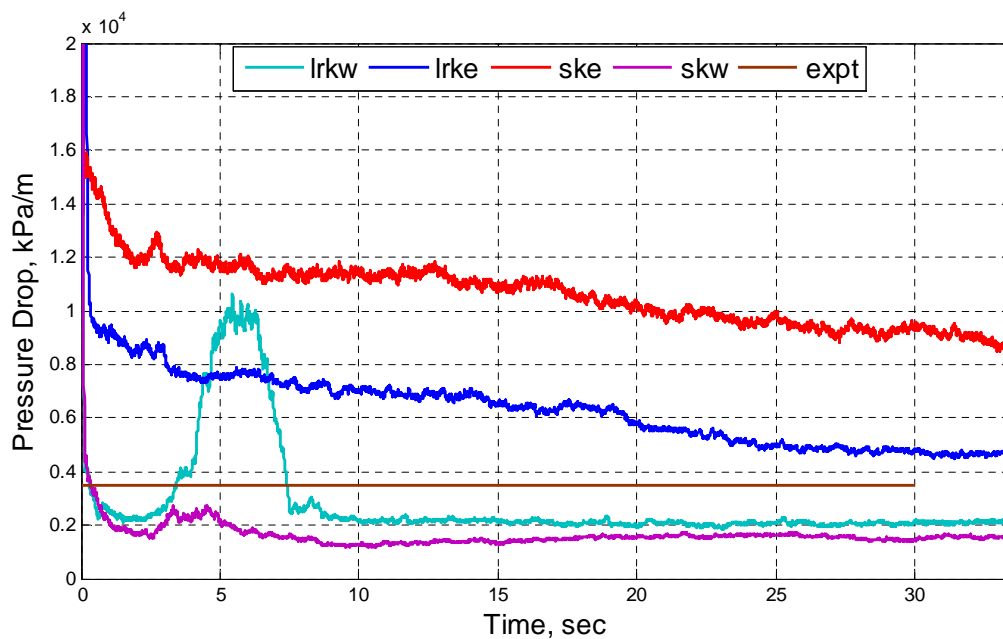


Figure 6-32: Performance analysis of turbulence flow for oil-water flow of $V_{so}=0.55\text{m/s}$ and $V_{sw}=0.2\text{m/s}$

The behaviour of both k-omega models also reveals that these models over-dampened the turbulence near the wall which led to the under prediction of the pressure drop but succeeded to predict the flow separation as early as possible compared to the experiment. However, the k-epsilon models exhibit the opposite behaviour because its flow separation did not start early as observed in the experiment. In this research, the k-epsilon (SKE and LRKE) models would be considered for the simulation because of its wide acceptability and applicability in engineering modelling, by considering the improvement of k and ε models for the study of heavy oil related multiphase flows.

6.4.6 Identification of strategy for improvement of CFD model

CFD performance hinges on the appropriate mesh, fluid physics, initial and boundary condition, appropriate turbulence modelling and the availability of computational facility. In this section, the effectiveness of various low-Reynolds $k - \varepsilon$ turbulent models was evaluated. The performances of low-Reynolds $k - \varepsilon$ turbulence models were examined for the selection of an appropriate turbulent model for the simulation of the multiphase flow in question.

In turbulence modelling, the standard k-epsilon is the most widely used model in engineering calculations, but from the above preliminary tests, it shows that the universal traditional standard k-epsilon model with enhanced wall treatment and LRKE models are preferred because of the effect of the flow separation on the wall for such a complex flow. In addition, the need for model which can be integrated down to the wall is inevitable. Jones and Launder (1973) were the first to propose a LRKE model for near wall turbulence which was followed by quite a large number of similar models. Amongst these numerous LRKE models, five (5) were coded by FLUENT and four (4) were investigated for this present research. This investigation was done to evaluate their ability to model the effect of turbulence on pressure gradient of 2-phase oil-water flow. The main equations remain as Equations 4-10 and 4-11 while the auxiliary models are summarised in Table 6-13;

Table 6-13: Model constants of the low-Re k-epsilon models

S/N	Model	C_μ	$C_{\epsilon 1}$	$C_{\epsilon 2}$	σ_k	σ_ϵ
1	Abe-Kondoh-Nagano (AKN)	0.09	1.50	1.90	1.40	1.40
2	Chang-Hseih-Chen (CHC)	0.09	1.44	1.92	1.00	1.30
3	Launder-Sharma (LS)	0.09	1.44	1.92	1.00	1.30
4	Yang-Shih (YS)	0.09	1.44	1.92	1.00	1.30

Table 6-14: Source terms and boundary conditions

S/N	Model	D	E	Boundary conditions
1	Abe-Kondoh-Nagano (AKN)	0	0	$k = 0;$ $\epsilon = 2v \left(\frac{\partial \sqrt{k}}{\partial y} \right)^2$
2	Chang-Hseih-Chen (CHC)	0	0	$k = 0; \epsilon = v \left(\frac{\partial^2 k}{\partial y^2} \right)$
3	Launder-Sharma (LS)	$2v \left(\frac{\partial \sqrt{k}}{\partial y} \right)$	$2v_t v \left(\frac{\partial^2 u}{\partial y^2} \right)$	$k = 0; \epsilon = 0$
4	Yang-Shih (YS)	0	$v_t v \left(\frac{\partial^2 u}{\partial y^2} \right)$	$k = 0; \epsilon = v \left(\frac{\partial^2 k}{\partial y^2} \right)$

Table 6-15: Damping functions of the low-Re k-epsilon models

S/N	Model	f_μ	$f_{\epsilon 1}$	$f_{\epsilon 2}$
1	Abe-Kondoh-Nagano (AKN)	$\left[1 - \exp\left(-\frac{y^k}{14}\right)\right]^2$ $* \left[1 + \frac{5}{R_T^{3/4}} \exp\left\{-\left(\frac{R_T}{200}\right)^2\right\}\right]$	1	$\left[1 - \exp\left(-\frac{y^k}{3.1}\right)\right]^2$ $* \left[1 + 0.3 \exp\left\{-\left(\frac{R_T}{200}\right)^2\right\}\right]$
2	Chang-Hseih-Chen (CHC)	$\left[1 - \exp(-0.0125R_y)\right]^2$ $* \left(1 + \frac{31.66}{R_T^{5/4}}\right)$	1	$\left[1 - \exp(-0.01R_T^2)\right]$ $* \left[1 - \exp(-0.0631R_y)\right]$
3	Launder-Sharma (LS)	$\exp[-3.4/(1 + R_T/10)^2]$	1	$1 - 0.3\exp(-R_T^2)$
4	Yang-Shih (YS)	$1 - \exp\left(\frac{1.5 \times 10^{-4}R_y -}{5.0 \times 10^{-7}R_y^3 -}\right)$ $1.0 \times 10^{-10}R_y^5$	$\frac{1}{1 + \frac{1}{\sqrt{R_T}}}$	$\frac{1}{1 + \frac{1}{\sqrt{R_T}}}$

Where $R_T = \frac{k^2}{(v\epsilon)}$, $R_y = \frac{yk^{1/2}}{v}$, and $y^k = u_\epsilon y/v$

Figure 6-33 and Table 6-16 represent the typical gradients and flow patterns of the turbulence models examined for the selection of a suitable model for the prediction of oil-water flow in horizontal pipe. Figure 6-33 shows that the existing turbulence models are not capable of simulating oil-water pressure gradient in their present default state except they are improved or modified. It could be observed that the pressure gradient is on the increase with increase in the water superficial velocity; this presupposes that turbulence dictates the flow characteristics. Therefore if any of these turbulence will give a better prediction of pressure gradient, an improvement of such is inevitable.

Table 6-16 shows the comparison of the experimental flow pattern of oil-water flow at 27% water cut with collection of the flow contours gotten from different turbulence models. Most of these models returned stratified pattern except for SKE turbulence models which gave annular flow of oil surrounded by water and also the presence of oil film on the pipe wall.

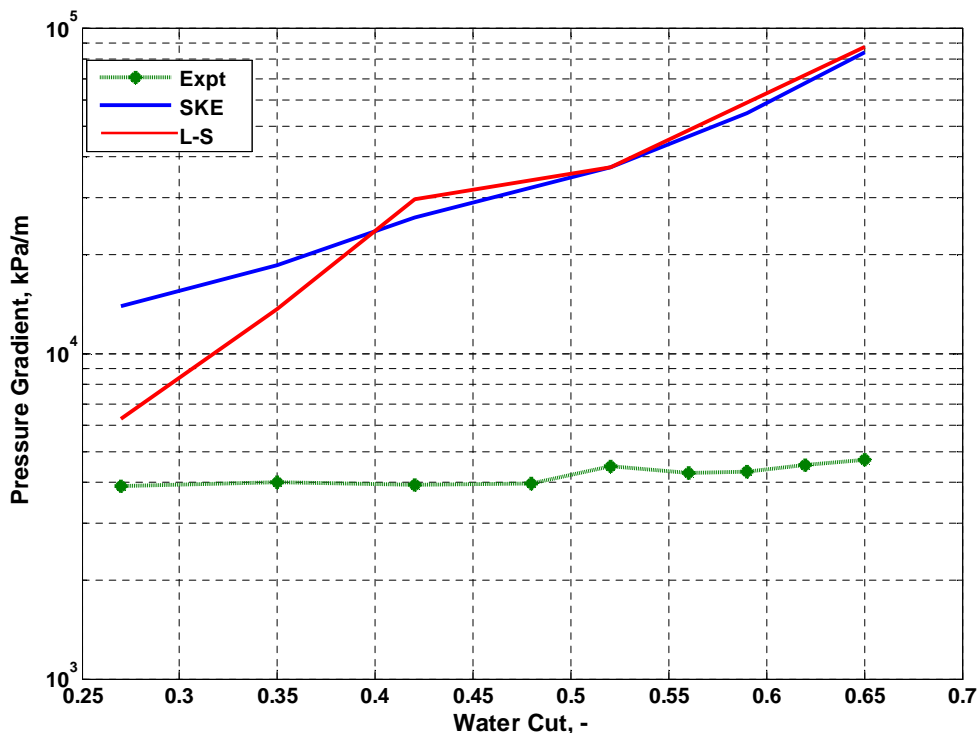
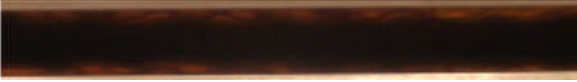
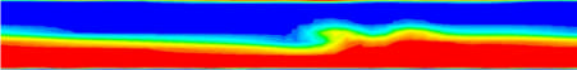
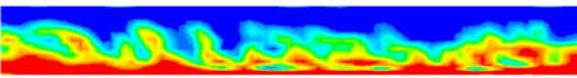
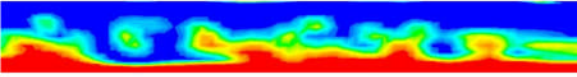
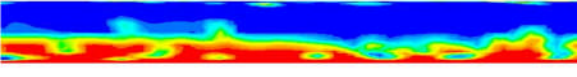
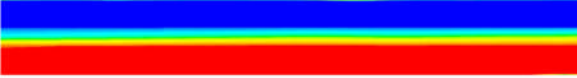


Figure 6-33: Comparison of default turbulence models results with experimental data of oil-water flow at 0.55m/s oil superficial velocity

Although this model presents good contour plot, this is not enough description of the flow behaviour as the pressure drop obtained does not compare well with the experimental result. Hence, there is need for inputs that influence these turbulence models to accommodate the impact of the second phase in this kind of flow. Section 6.4.7 presents the attempts made in the present research to address this problem.

Table 6-16: Comparison of flow pattern of experimental and CFD turbulence models of oil-water flow at 27% water cut

Mode	Pattern
Experiment	
SKE	
AKN	
YS	
CHC	
LS	

6.4.7 Turbulence kinetic energy budget

The SKE model is widely used in industrial turbulent flow and heat transfer computations mainly due to its robustness, computational economy, and reasonable accuracy for a wide variety of turbulent flows. It is somewhat a semi-empirical model, mainly because the modelled transport equation for dissipation used in the model depends on phenomenological considerations and empiricism. The exact transport equation for the kinetic energy of the turbulence and the rate of dissipation of turbulence kinetic energy as obtained from the literature is given by Tennekes and Lumley (1972)

$$U_j \frac{\partial}{\partial x_j} \left(\frac{1}{2} \overline{u_i u_i} \right) = - \frac{\partial}{\partial x_j} \left(\frac{1}{\rho} \overline{u_j p} + \frac{1}{2} \overline{u_i u_i u_j} - 2\nu \overline{u_i s_{ij}} \right) - \overline{u_i u_j} s_{ij} - 2\nu \overline{s_{ij} s_{ij}} \quad 6-2$$

The quantity s_{ij} is the fluctuating rate of strain, defined by

$$s_{ij} \equiv \frac{1}{2} \left(\frac{\partial u_i}{\partial x_j} + \frac{\partial u_j}{\partial x_i} \right) \quad 6-3$$

$$\overline{2\nu \frac{\partial}{\partial x_j} [N(u_i)] \frac{\partial u_i'}{\partial x_j}} = 0 \quad 6-4$$

$$N(u_i) = \rho \frac{\partial u_i}{\partial t} + \rho u_k \frac{\partial u_i}{\partial x_k} + \frac{\partial p}{\partial x_i} - \mu \frac{\partial^2 u_i}{\partial x_k \partial x_k} \quad 6-5$$

The exact transport equation for the dissipation gotten after analysis could be taken as

$$\begin{aligned}
\frac{\partial \varepsilon}{\partial t} + \bar{u}_j \frac{\partial \varepsilon}{\partial x_j} = & -2v \left[\overline{u'_{i,k} u'_{j,k}} + \overline{u'_{k,l} u'_{k,j}} \right] \frac{\partial \bar{u}_i}{\partial x_j} - \frac{2v \overline{u'_k u'_{i,j}} (\partial^2 u_i)}{\partial x_k \partial x_j} \\
& - 2v \overline{u'_{i,k} u'_{i,m} u'_{k,m}} - 2v^2 \overline{u'_{i,km} u'_{i,km}} \\
& + \frac{\partial}{\partial x_j} \left[v \frac{\partial \varepsilon}{\partial x_j} - v \overline{u'_j u'_{i,m} u'_{i,m}} - 2 \frac{v}{\rho} \overline{p'_m u'_{j,m}} \right]
\end{aligned} \tag{6-6}$$

Equation 6-6 is more complex compared to the exact equation for turbulent kinetic energy. Equation 6-6 has total of ten terms. The standard unsteady and convection terms are on LHS while other complex terms are on the RHS which are denoted as the production of dissipation, dissipation of dissipation, turbulent transport and molecular diffusion of dissipation. These terms could be modelled except the unsteady, convection and molecular diffusion. Unfortunately there is no assistance from the experimental data to provide any guideline for modelling these different terms of Equation 6-6. The modelled form of the dissipation equation used in the literature is a major weakness of the $k-\varepsilon$ model as stated by Dewan (2010). This could be traced to the fact that the terms in the exact dissipation equation is modelled by few terms. Tennekes and Lumley (1972) stated that the rate of change of $\frac{1}{2} \overline{u_i u_j}$ is due to transport by turbulent velocity fluctuation, pressure gradient work, transport by viscous stresses and two kinds of deformation works. In other words, the modelling of the k and ε profiles is still the heart of $k - \varepsilon$ model.

This development was based on the observation made on the behaviour of the pressure gradient profile, flow pattern and the fluctuating kinetic energy when the experimental data were compared with the simulation data, as shown in Figure 6-33, Table 6-16 and Figure 6-34. It was observed in Figure 6-33 that irrespective of the damping functions from the existing models, the deviations of the pressure gradient were on the increase with the increase in the velocity of the secondary phase which is not the case in the obtained gradients from the experiments. Hence, the magnitude of the fluctuating energy predicted by the CFD and its dissipation was proposed to be contributing to the divergence of the gradient profile. Table 6-16 shows that quite a number of the flow configurations gotten from the existing models are not the true image of the flow pattern obtained from the experiment. And lastly, Figure 6-34 reveals the uncorrelated feature

of the energy fluctuations and their magnitudes when compared with those of the experiments. All of these observations and analyses led to a proposition to redefine the kinetic energy and its dissipation rate in order to suit this peculiar flow environment. This decision is in accordance to Tennekes and Lumley (1972) assertion that turbulence behaviour and description depends on environment. Hence, the turbulence kinetic energy was assumed and proposed to behave linearly with respect to the velocity while its dissipation is assumed to have a quadratic behaviour as given in equations 6-7 to 6-9 below.

In order to improve the turbulence effect in this unique high viscosity oil –water flow, four assumptions are proposed by the author to drive the development;

- the production of turbulent kinetic energy is not equal to its dissipation and
- the turbulent kinetic energy and its dissipation are dependent of the fractional constituents of the multiphase flow,
- turbulence behaviour is suppressed with increase in the superficial velocities of the phases because oil dispersion increases with increase in the superficial velocities of the phases, hence the mixing fluid becomes more viscous.
- the turbulent kinetic energy is described as a linear function of the superficial velocities of the phases involve while its dissipation rate is defined as a quadratic function.

The correlations were developed by trial and error method using the qualitative analysis of Figure 6-34 whereby the fluctuating kinetic energy obtained from the experiments are compared with CFD's. It could be deduced that the fluctuations of flow in the CFD is about 5 to 8 order of magnitude different from that of the experiments. Figure 6-34 also reveals that the fluctuation in the experiments decreases with increase in water cut and vice versa in the CFD. Hence the turbulent kinetic energy and dissipation rate are randomly modified for three cases and the remaining were obtained by curve fitting as shown in Appendix F.

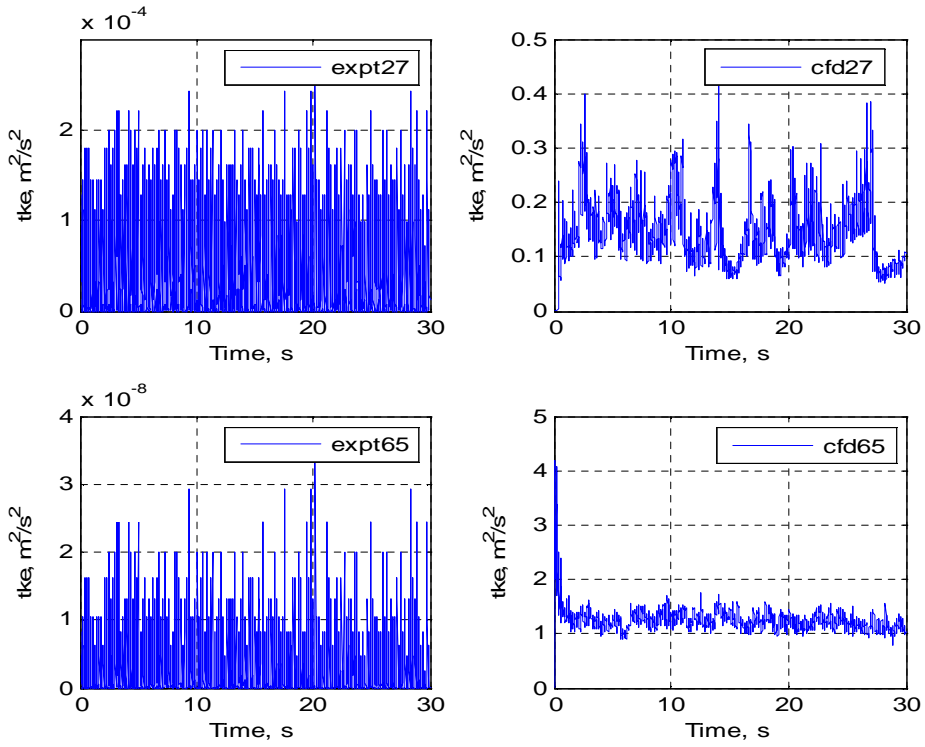


Figure 6-34: Comparison of fluctuation kinetic energy of experiment and CFD at 27% water cut

The correlations gotten as functions of superficial velocities are stated as

$$k = Ax_1 + B \quad 6-7$$

and

$$\varepsilon = Cx_2^2 + Dx_2 + E \quad 6-8$$

Where

$$x_1 = x_2 = \left(\frac{1}{\frac{V_{so}}{V_{sw}} + 1} \right) \quad 6-9$$

Where

$$A = -0.2099 \text{ m}^2/\text{s}^2, B = 0.1976 \text{ m}^2/\text{s}^2$$

$$C = -221.88 \text{ m}^2/\text{s}^3, \quad D = 133.08 \text{ m}^2/\text{s}^3 \text{ and } E = 32.245 \text{ m}^2/\text{s}^3$$

These models are coded and hooked to FLUENT CFD solver as a user defined function (UDF) for two-phase oil-water flow simulations.

- **Boundary Conditions**

Appropriate and commonly encountered boundary conditions at the boundaries for computing the flow in a particular computational domain are employed in this research and stated below:

Inlet: Provide distributions of k and ε along with flow properties, i.e., velocity and temperature, in the corresponding real situation. In some cases, it is difficult to obtain values of k and ε at the inlet and in such cases these can be obtained based on an approximation from the turbulent intensity T_i and a characteristic length L of the flow configuration:

$$k = \frac{3}{2} (u_{ref} T_i)^2, \quad \varepsilon = C_\mu^{3/4} \frac{k^{3/2}}{l}, \quad l = 0.07L \quad 6-10$$

where l denotes a turbulent length scale and L characteristic length.

Outlet: At the outlet usually turbulence k and ε is taken equal to zero, the mean temperature (T_m) equal to the ambient temperature (T_1) and pressure (p) equal to the atmospheric pressure (p_1).

Wall: At the solid wall either the no slip condition using the low-Re version or wall function approach can be applied.

6.4.8 Flow pattern identification

Table 6-17, Table 6-18, Table 6-19 and Table 6-20 present the comparison of CFD contour plots and the photographs of oil-water flow in 1-in ID horizontal pipe. The images were obtained from 3300cP, 7500cP and 10000cP oils as shown in the tables; The CFD contour plots and the photographs were taken from 30seconds run time.

Flow patterns are analysed using the flow PDF of pressure signals, together with the phase contours and/or animations. Two-phase flow, oil-water was tested at V_{so} between 0.1 and 0.55m/s with V_{sw} ranging from 0.2-1.0m/s for 3300, 7500 and 10000cP oil viscosity respectively.

6.4.8.1 PDF of pressure signals and contours of oil-water flow

The PDF analyses of the pressure signals generated from the CFD simulations and compared with the flow contours are summarised in the Table 6-17, Table 6-20, and Table 6-19. Generally, one could observe that all the PDF plots from the CFD have multiple peaks which indicate that all the flows exhibit intermittent behaviours of different kind. The kurtosis and deviations described the degree of intermittent behaviours. The highest standard deviation was observed in the water plug in oil (WPO) and subsequently decreased from one regime to the other; oil plug in water (OPW) was next while dispersed oil in water (DOW) flow type has the lowest signal deviation; this could be due to the fact that dispersed oil mixed with water to form a pseudo-single phase with the remaining oil moving on the wall. Contrary to the standard deviation behaviour, kurtosis and skewness increased from the WPO to the DOW flow pattern.

In Table 6-17 two peaks with broad distribution was obtained, which indicate a slug/plug-like flow; this conclusion was justified by the corresponding contour plot of water plug in the oil and the report of McKibben et al. (2000a) in which the water slug was inferred from the voltage reading of anemometer. Unfortunately, this image of the WPO flow type has not been possible by camera due to the opacity of the oil. It is worth to note that the skewness is negative in this flow type while it is positive in the

remaining flow patterns. This could be due to the fact that oil is continuous and water forms plug in oil, and vice versa when the skewness is positive.

A three peak PDF distribution were observed in the remaining flow patterns, except in the dispersed flow, indicating signals for the continuous phase, the non-dominant phase (i.e. plug, annular) and also the signals of the oil film on the wall.

Considering the flow contours obtained in this research, apart from Table 6-17 where oil is continuous and enveloped pockets of water, all the flow contours have oil film (fouling) on the pipe wall. These are exact prediction of oil fouling observed in all the oil-water experimental campaigns. This was not captured by Kaushik et al. (2012) in their research, perhaps their oil viscosity (0.22Pa.s) was too low or their mesh and/or models were not adequate.

In addition, it is important to mention that the CFD simulation in this research replicated all the flow patterns that were observed in the experiments. Table 6-17 presents a flow configuration labelled Water Plug in Oil (WPO) which was not visible to the camera but compared with the findings of McKibben et al. (2000a). Table 6-18 compared well with the experiment at the same flow condition and labelled Oil Plug in Water (OPW/OF) as mentioned in the experiment. Water Assist Annular (WA-ANN) flow was presented as well in Table 6-19. It also compared favourably with the experiment. The Dispersed Oil in Water (DOW/OF) flow pattern in Table 6-20 was also predicted by the CFD. Although the experiment and CFD methods produced similar results, the oil flow in the CFD appeared closer to the top part of the wall compared to the experiment as in Table 6-19.

Table 6-17: PDF-Contour analysis of oil-water flow of 10000cP at $V_{so}=0.11\text{m/s}$, and $V_{sw}=0.02\text{m/s}$

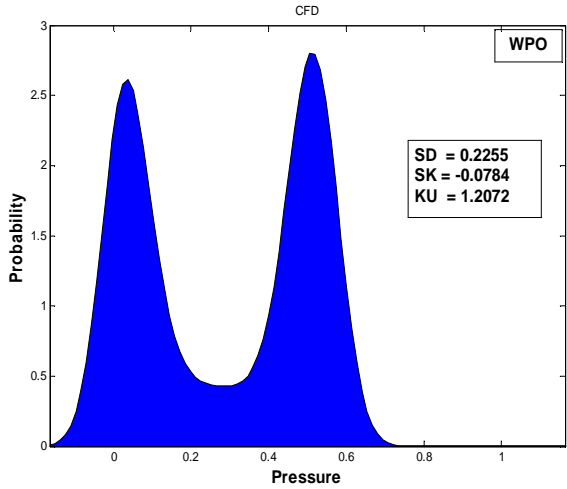
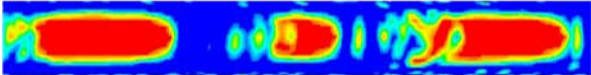
Flow Conditions	PDF (a)	Contour (b)	Video (c)
Water Plug in Oil (WPO)			<p>Not visible because the water plug was covered by oil</p>

Table 6-18: PDF-Contour-Experiment analysis of oil-water flow of 7500cP at $V_{so}=0.1\text{m/s}$ and $V_{sw}=0.8\text{m/s}$

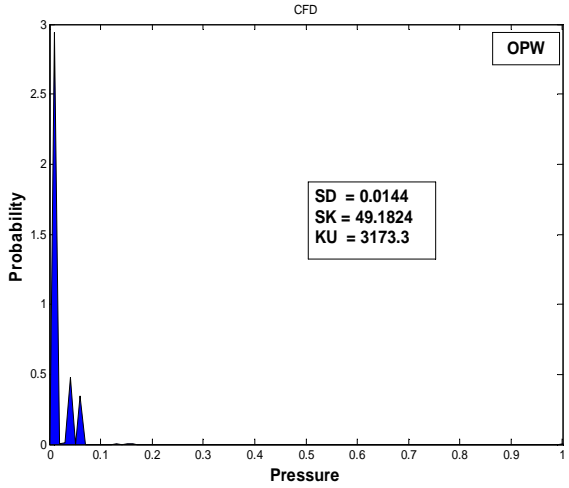
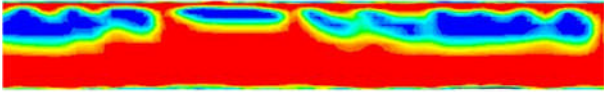

Flow Conditions	PDF (a)	Contour (b)	Video (c)
Oil Plug in Water (OPW/OF)	 <p>CFD</p> <p>OPW</p> <p>SD = 0.0144 SK = 49.1824 KU = 3173.3</p>		

Table 6-19: PDF-Contour-Experiment analysis of oil-water flow of 3300cP at $V_{so}=0.550\text{m/s}$ and $V_{sw}=1.0\text{m/s}$

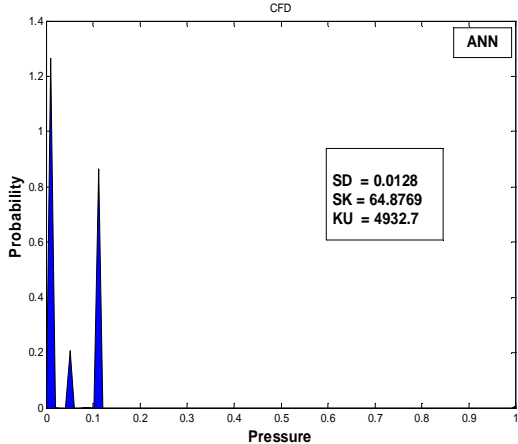
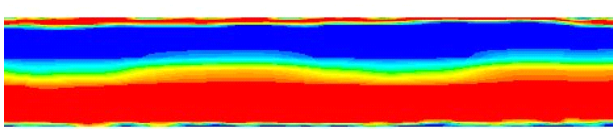

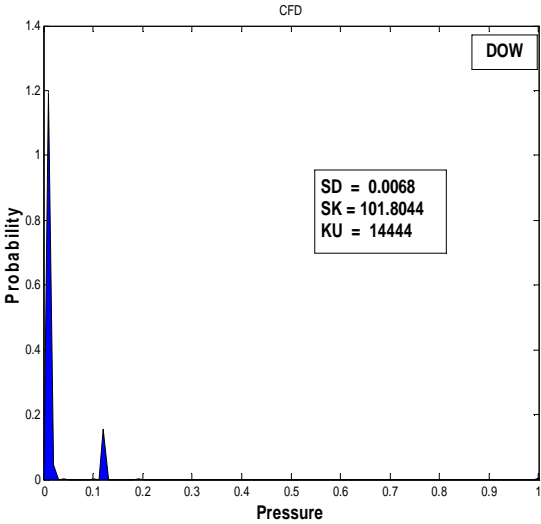


Flow Conditions	PDF (a)	Contour (b)	Video (c)
Water Assist Annular Flow (ANN)			

Table 6-20: PDF-Contour-Experiment analysis of oil-water flow of 7500cP at $V_{so}=0.06\text{m/s}$ and $V_{sw}=0.80\text{m/s}$

Flow Conditions	PDF (a)	Contour (b)	Video (c)
Dispersed Oil in Water (DOW)			

6.4.9 Pressure gradient

The results of both the CFD and experiments are compared in this section in order to make a better evaluation of the performance of the developed model. Figure 6-35 and Figure 6-36 compare the pressure gradients obtained from experiment with the results gotten from modified SKE and L-S respectively for 3300cP oil at 0.55m/s. Figure 6-37 and Figure 6-38 are the comparisons obtained for 5000cP and 7500cP at 0.20m/s and 0.10m/s respectively. All of these plots are drawn from oil-water flow in horizontal pipe for varying water cut ranging from 0.0 – 1.0. Generally, it could be observed that the simulation results fairly compare with the experiments; Figure 6-35 shows that the popular SKE model in engineering field is still very suitable with a little modification, although most of the simulations were run with LRKE model. The choice was based on the fact that LRKE is known with capability to resolve the gradients close to the wall.

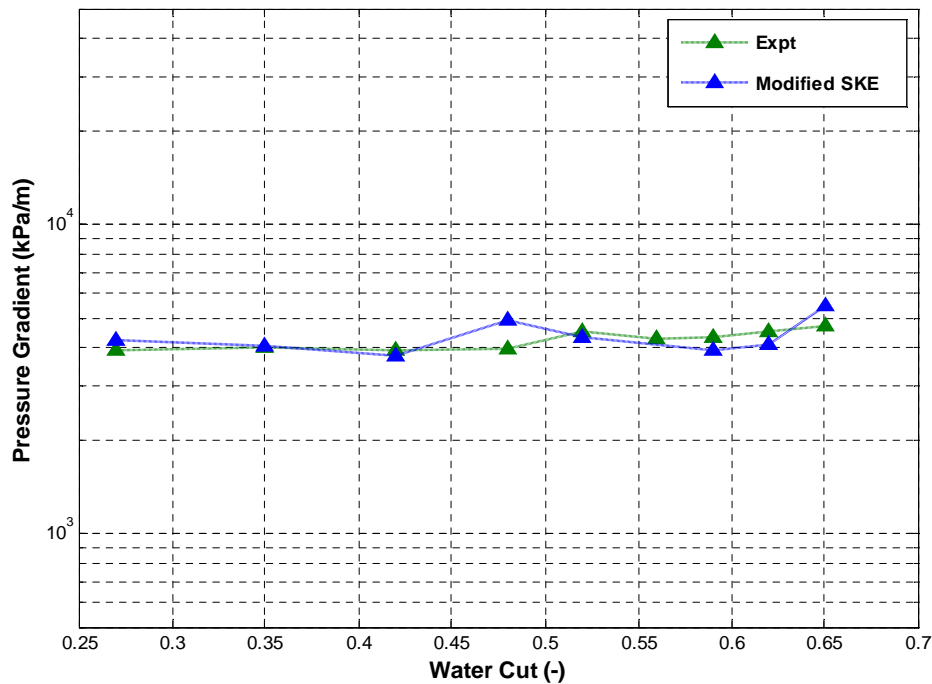


Figure 6-35: Pressure gradient against water cut @ $V_{so} = 0.55\text{m/s}$ for 3300cP oil using modified SKE CFD model

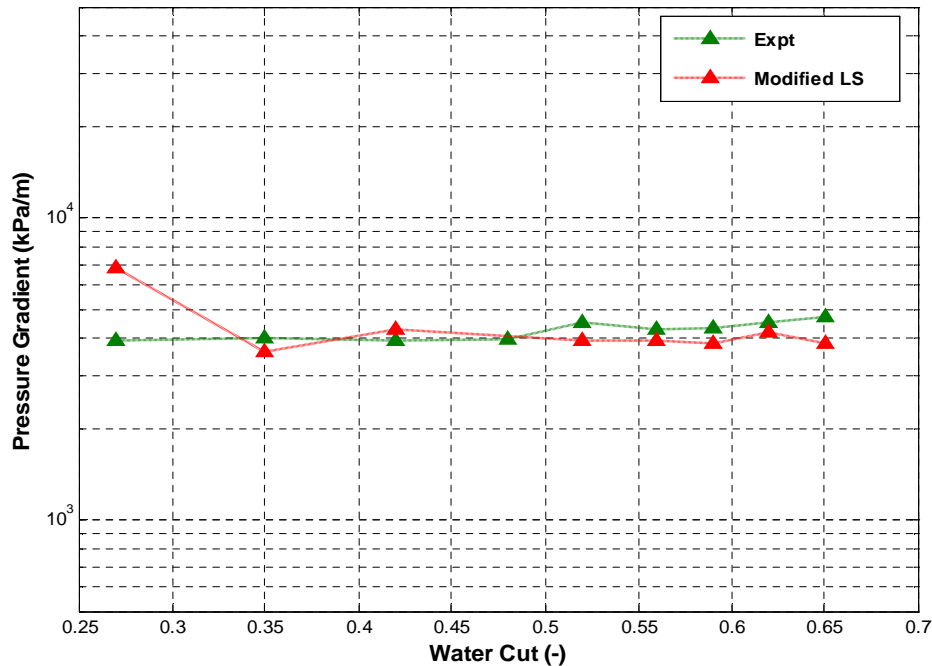


Figure 6-36: Pressure gradient against water cut @ $V_{so} = 0.55\text{m/s}$ for 3300cP oil using modified LRKE (L-S) CFD model

In addition, Figure 6-35 shows a satisfactory comparison with the experiment except at 48 and 65 per cent water cut where CFD returned higher gradients; these could be due to the limitations in CFD or in the experimental data. At 65 per cent, perhaps the water which was the continuous phase due to its attributed turbulence caused an increased dispersion that transported bulk of the oil to the wall and hence increased the gradient. The deviations of the results in Figure 6-36 also could be discussed as the effect of mixing rules for the fluids' properties; at higher water cuts (i.e. greater than 48%), the model under predicted the experimental results while on few occasion at very low water cut, it is vice versa.

In Figure 6-37 and Figure 6-38, when the viscosity of oil was increased to 5000cP and 7500cP respectively, fairly good results were obtained but also with similar deviations of under predictions at very high water cut (say 75%) and vice versa at lower water cut. These deviations might be caused by numerical instability, since they are not present in all the cases simulated.

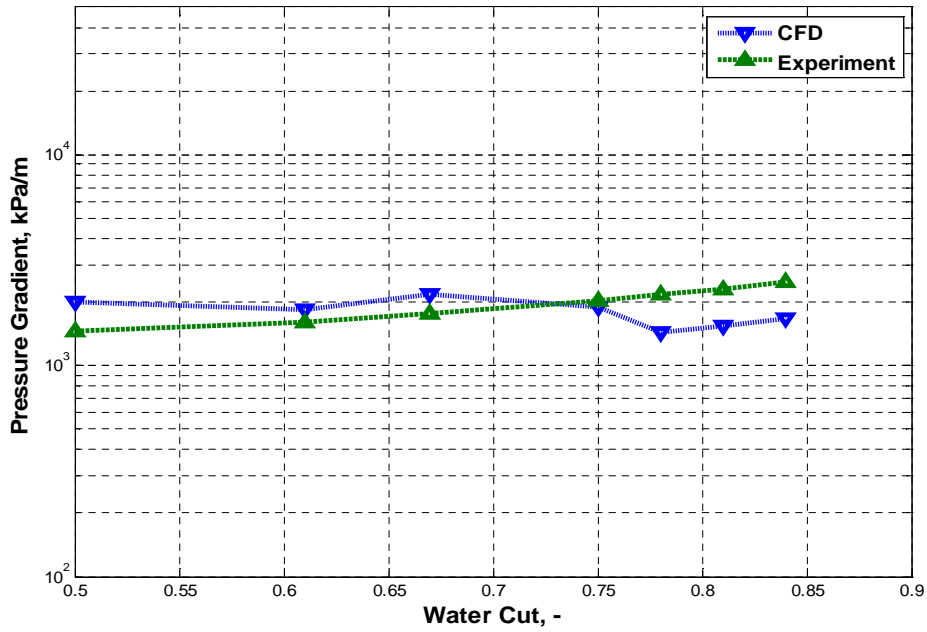


Figure 6-37: Pressure gradient against water cut @ $V_{so} = 0.20\text{m/s}$ for 5000cP oil using modified LRKE (L-S) CFD model

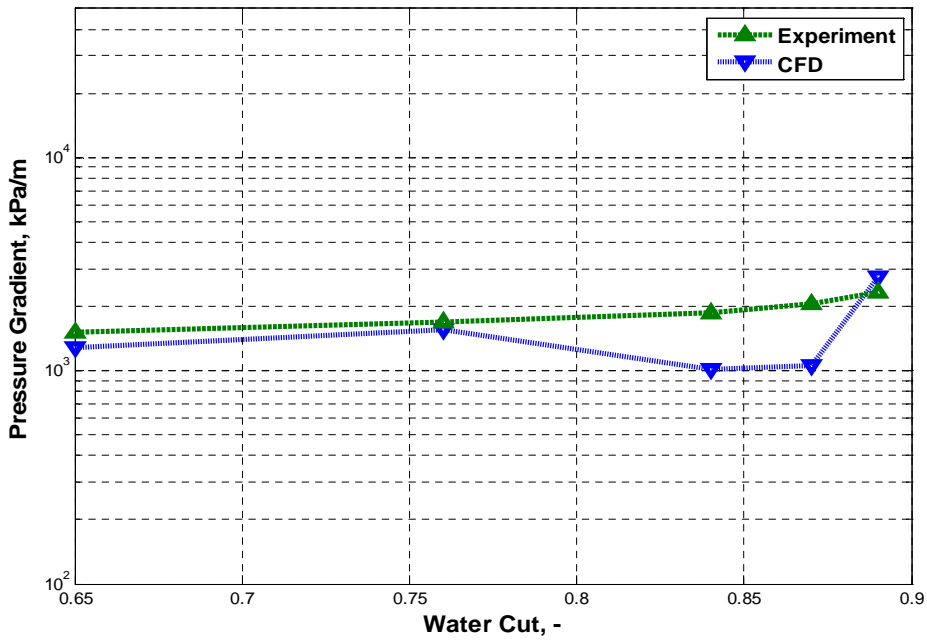


Figure 6-38: Pressure gradient against water cut @ $V_{so} = 0.10\text{m/s}$ for 7500cP oil using modified LRKE (L-S) CFD model

6.5 Restart

The purpose of this section is to present and discuss the CFD simulation results of the minimum pressure required to restart the flow of heavy oil-water in 1-in ID horizontal pipe after a period of shut down. The same geometry, flow conditions samples, and modified TKE and TDR udf were adopted, in addition to a new udf which informs the shut-down and restart process. The L-S LRKE model was used for turbulence simulation. Two different viscosities that were considered for this investigation are 3300cP and 10000cP.

Simulations were performed on a WA-ANN flow regime to investigate the operating philosophy for the pipe flow restart as suggested by Bensakhria et al. (2004b). The choice of the WA-ANN is crucial to this study because it is the regime that is cost effective for the transport of high viscosity oil. The mechanism of restart operation known and studied by several authors is adopted for this investigation, although restart process emerged as a significant process due to the wax deposition which occur during the shut in or shut down when the temperature is low enough for its formation. The restart of flow in which wax has formed and deposited on the pipe wall has been categorised in to three groups; start without delay, start with delay, and unsuccessful start-up as mentioned in section 2.3.4. In a typical restart study, varying pressure is always employed to determine the pressure at which the waxy crude oil gels will yield due to its viscoplastic behaviour, but in the current study, the injection of water for the transportation of heavy oil is the major factor for examining the restart process. The oils used in this study have been de-waxed but possess high viscosity, and hence the behaviour might not be comparable to waxy crude.

The simulation for each flow condition was run from time $t=0s$ until the flow developed and stabilised for about 15s before the flow was shut down for 5s by switching both oil and water velocities to zero. The restart condition kicked off at the end of 5s shut down (i.e. overall 20s) with the former constant oil and water flow superficial velocities and ran for another 10s. Figure 6-39 to Figure 6-41 show the restart trend plots for oil viscosity at 3300cP. All the plots reflect similar behaviour. Prior to restart at 20s, the

plots reveal relatively zero pressure since there was no flow in the pipe. The spike in the pressure trends in Figure 6-39 to Figure 6-41 could be explained as a result of acceleration after a restart which caused additional pressure surge and pressure drop due to the change in the momentum of the fluid. This assertion is in agreement with Tang (2005) who observed similar trend in their study of flow assurance of crude oil with severe emulsion.

The pressure surge and drop occurred gradually as presented in Figure 6-42 and Figure 6-43 showing that there is a delay over a period of time to overcome the spike. These figures further show that the magnitudes of the pressure surge is a function of the flow velocities. For oil viscosity at 3300cP in the presence of water the surge increases with increase in V_{sw} and the highest surge is recorded when the V_{sw} is very high (i.e. high water cut). On the other hand, when the oil viscosity was raised to 10000cP, a reverse of the output of 3300cP was observed when the V_{sw} was increased from 0.21m/s to 0.30m/s; the surge decreases with increase in V_{sw} (or water cut) but increases again when the V_{sw} was further increased. This behaviour is not yet understood.

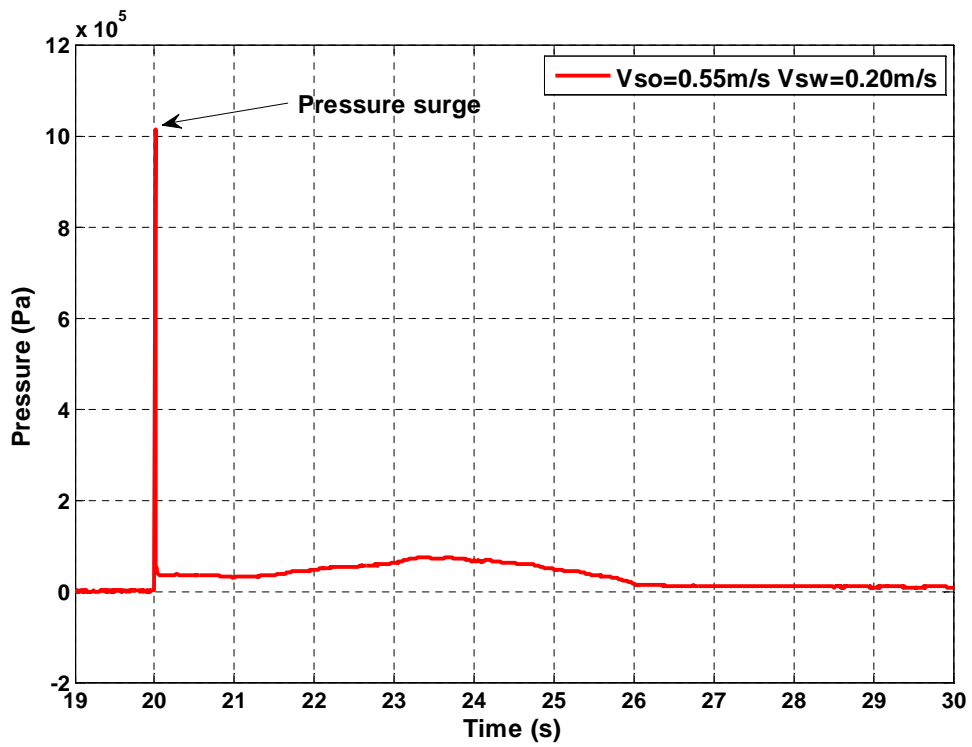


Figure 6-39: Plot of restart process for 3300cP oil at 0.55m/s oil superficial velocity and 0.20m/s water superficial velocity

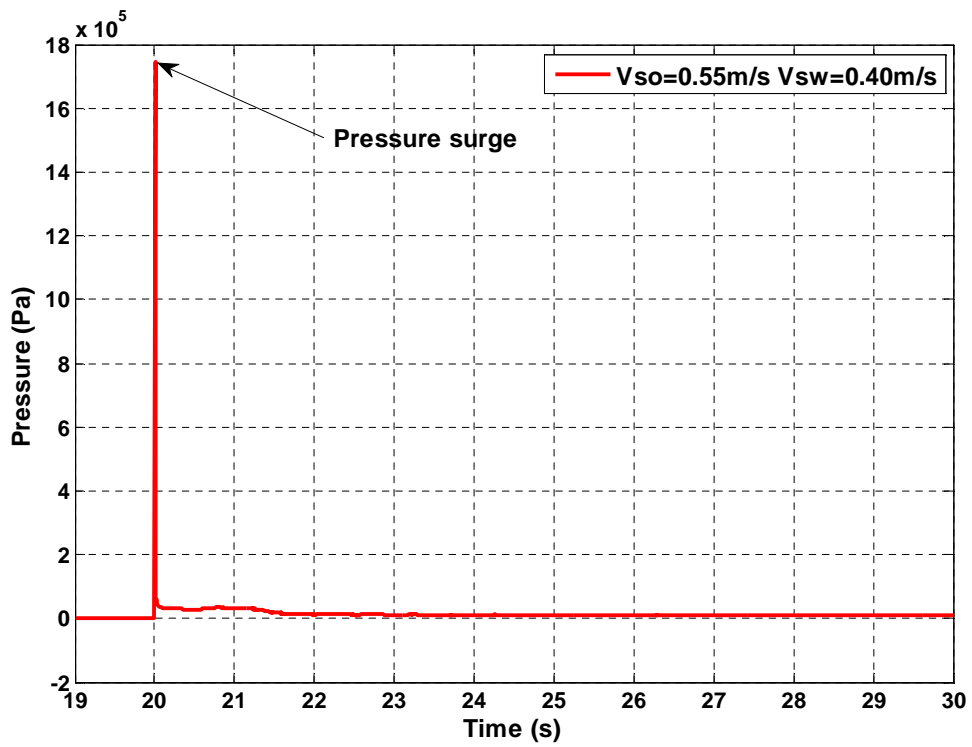


Figure 6-40: Plot of restart process for 3300cP oil at 0.55m/s oil superficial velocity and 0.40m/s water superficial velocity

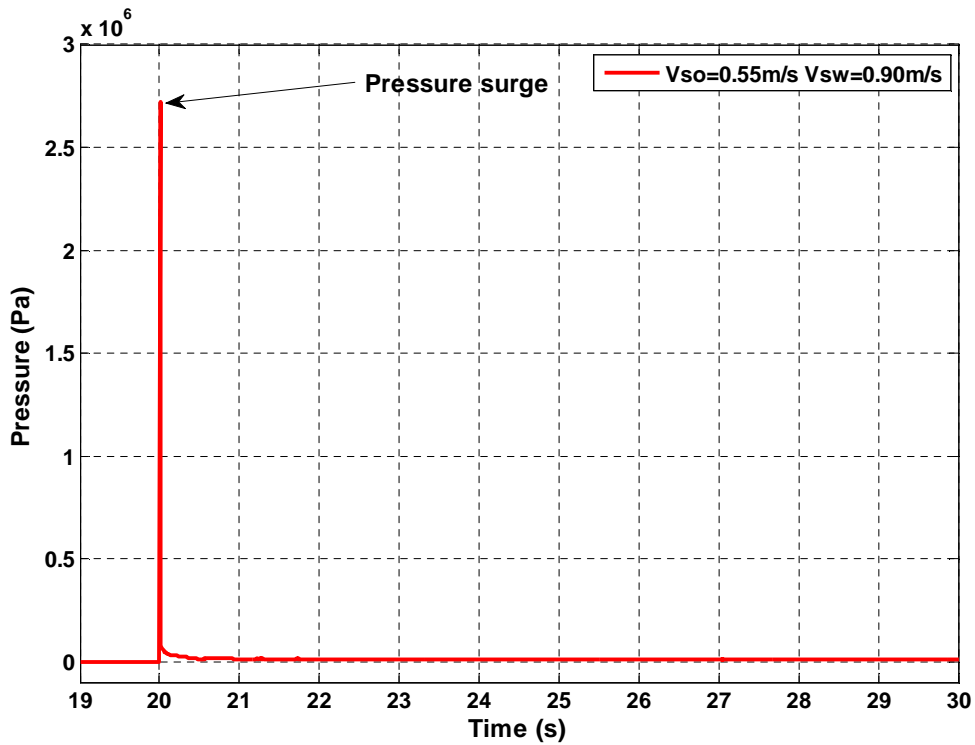


Figure 6-41: Plot of restart process for 3300cP oil at 0.55m/s oil superficial velocity and 0.90m/s water superficial velocity

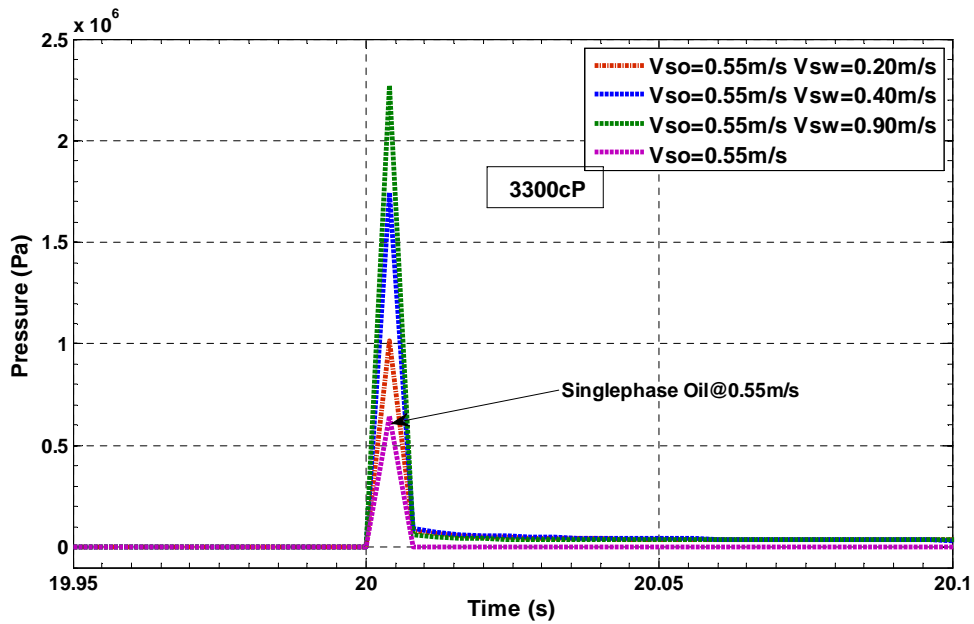


Figure 6-42: Comparison of pressure surges at different flow conditions for 3300cP oil

Table 6-21: Restart pressure of 3300cP at different velocities

V_{so}, V_{sw} (m/s)	Restart Pressure MPa
(0.55, 0.00)	0.647
(0.55, 0.20)	1.014
(0.55, 0.40)	1.744
(0.55, 0.90)	2.723

Comparing the restart output of single phase oil at 3300cP and 10000cP from Figure 6-44, it could be observed that 3300cP oil has higher surge than 10000cP. This could be traced to the viscosity difference which favours 3300cP oil to gain more acceleration than 10000cP. In this case, it could be inferred that the higher the viscosity of a fluid the lower the surge tendency provided it flows alone. In addition, when the restart results of single phase oil are compared with that of two phase oil-water flow as shown in Table 6-21 and Table 6-22, it could be seen that the surges of single phase are an order of magnitude lower than that of two-phase oil-water flows

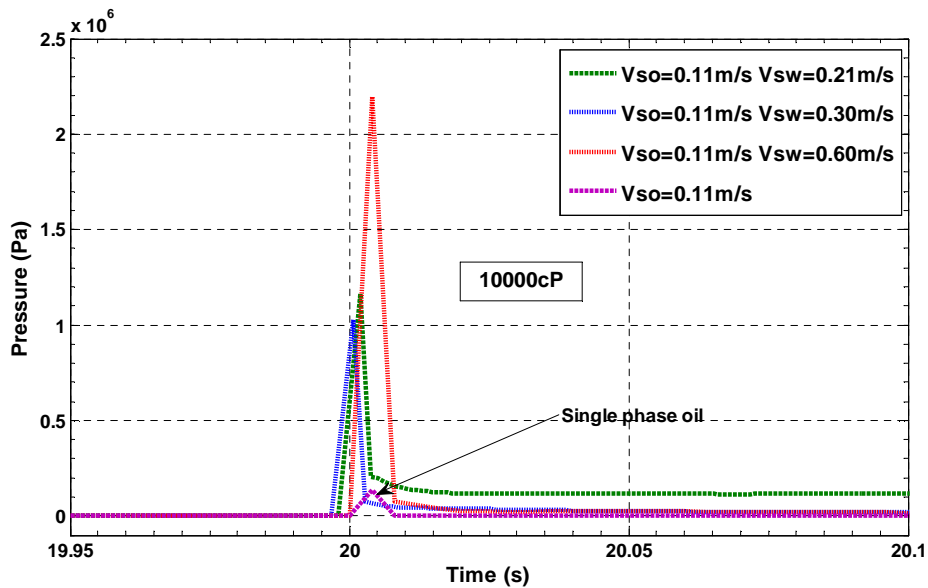


Figure 6-43: Comparison of pressure surges at different flow conditions for 10000cP oil

Table 6-22: Restart pressure of 10000cP at different velocities

V_{so}, V_{sw} (m/s)	Restart Pressure MPa
(0.11, 0.00)	0.136
(0.11, 0.21)	3.214
(0.11, 0.30)	1.025
(0.11, 0.60)	2.194

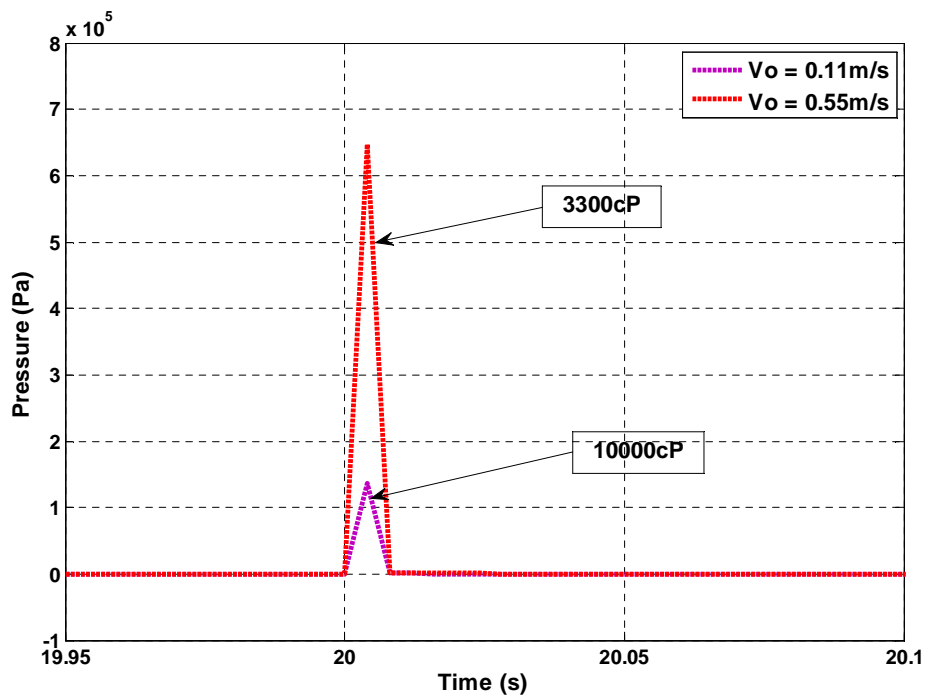


Figure 6-44: Comparison of restart pressure surges at different oil viscosities

6.6 Chapter Summary

In this chapter, the flow pattern types were identified and reported from the visualisation (video) of the flow, description by the trend plot and PDF of the downstream pressure

signals along with the statistical moments. The observed flow patterns are WPO, OPW/OF, WA-ANN, and DOW/OF.

Based on the identified flow pattern through visual observation, the trend and PDF of the downstream pressure signals with statistical moments, the flow regime maps were developed.

Phase inversion, i.e. the flow condition in which the continuous or carrier fluid becomes the 'carried fluid', was also investigated and compared with the existing phase inversion models. It was found that the oil flow rate has influence on the PIP. This research found that the existing models cannot be relied on without modifications.

The pressure gradient of the oil-water flow in the horizontal pipe was analysed at V_{so} ranging from 0.06 to 0.55m/s. The V_{sw} ranges from 0.0 to 1.0m/s. It was observed that the addition of water to oil flow in horizontal pipe reduces the pressure drop effectively. It was also observed from Figure 6-12 to Figure 6-17 that the pressure drop, first of all, decreased to a minimum point as the water cut increased from zero and increased again from that point with increase in water cut.

The pressure gradient reduction factor as shown in Figure 6-24 and Figure 6-25 reveal that the highest reduction of the pressure gradient occurred at high oil velocity. In addition, it was found that the reduction factor decreases with increase in water cut.

TKE budget was developed and coded as UDF to improve the performances of SKE and LRKE in the predictions of the characteristics of the investigated flow.

Both concentric and T-junction inlet geometries were compared. It was found that the concentric inlet with or without modified TKE and TDR has advantage over the T-junction inlet design.

In section 6.4, the results of the CFD study of the oil-water flow in the horizontal pipe were analysed for oil superficial velocity at 0.1 and 0.55m/s. The water cut ranges from

0.2 to 1.0m/s. It was also observed that the addition of water to oil flow in horizontal pipe reduces the pressure drop effectively. The oil-water flow regimes were also investigated in this section. The numerical simulation of oil-water flow focused on the validation of the turbulence models and understanding of the water assist flow phenomenon.

PDF data analysis was also employed on the simulated result data to identify the flow patterns in 1-in ID horizontal pipe. This shows that experimental data analysis can also be replicated by CFD simulation.

In CFD, annular flow pattern was successfully initiated by flow interaction specification of a concentric flow at the inlet boundary condition with the homogenous mixture on the inside of the pipe. Although the concentric design for pipe inlet condition was developed for annular flow studies, it ends up a necessary condition in this study to introduce multiphase fluids in to the pipe for simulation of all other flow configurations. All the flow that were observed in the experiments were successfully predicted by the CFD namely; WPO, OPW/OF, WA-ANN, and DOW/OF.

The CFD simulation results are generally in agreement with the laboratory experimental results. This demonstrates the capabilities of CFD to model water assist flows observed in the experimental study of high viscosity oil-water flow. Major limitations of CFD encountered in this research are the high computational time.

Comparison of both CFD volume fraction contours and experimental flow pattern images of different flow conditions were completed suggesting a relatively good agreement between the two approaches.

In section 6.5, the restart pressure requirement was investigated on the shutdown of some flow regimes using CFD, considering only the isothermal situation in which both the oil and the displacing/carrier fluid (water) are considered as incompressible fluids.

7 OIL-WATER-SAND FLOW IN 1” ID HORIZONTAL PIPE

Sand transport in oil production through horizontal pipeline could lead to flow assurance problem. The present study becomes necessary because of the unavoidable production of sand in oil production which may accumulate and reduce the flow passage or even cause a pipe blockage. Hence the need for investigation on the sand transport behaviour in the production of high viscosity oil with water.

In this chapter, the experimental results of oil-water-sand flow in 1-in ID pipe are presented and the major parameters employed to investigate the flow behaviour of oil-water-sand mixture in horizontal pipe are pressure gradients, the minimum transport condition and the flow patterns. This chapter is presented under the following sections; 7.1 Test Matrix, 7.2 Flow Regime Identification, 7.3 Sand MTC in Oil-Water-Sand Flow, 7.4 Pressure Gradient, 7.5 Comparison of Oil-Water and Oil-Water-Sand Flow Behaviour in Horizontal Pipe Flow, 7.6 CFD of Oil-Water-Sand Multiphase Flow and 7.7 Chapter Summary.

7.1 Test Matrix

In order to observe the behaviours of the oil-water-sand in the horizontal configuration, the experimental campaigns were conducted ranging from high, medium and low flow rates. A total of 30 experiments with 70 runs were carried out on oil-water-sand flow on 1-in rig. The procedure employed for the experiment in this section is stated in section 3.4.4; firstly, the oil is injected into the flow line at a specified superficial velocity followed by the injection of water-sand mixture (slurry) from the high to low superficial velocity. Data are collected through Labview at the period of 30s from the point where the slurry flow velocity is relatively stable. Nominal values were employed for oil viscosities in the discussion of results due to fluctuation of oil viscosity caused by changes in ambient temperature.

Table 7-1: Oil-water-sand flows test matrix

Pipe Diameter (m)	V_{so} (m/s)	V_{ss} (m/s)	Sand loading (%)	Viscosity @25°C(cP)
0.026	0.10 - 0.20	0.1~1.4	1.00, 5.00, 10.00	3.149



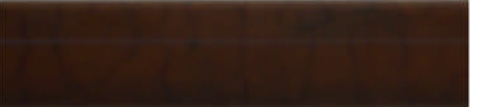



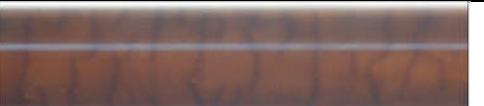







7.2 Flow Regime Identification

Samples of the observed configurations for oil-water-sand flows are presented in this section to illustrate the flow patterns obtained in the course of the experiments. The images of oil-water-sand flow patterns presented are taken from both side and bottom views of the pipe. The two approaches employed for the flow regime identification are discussed below:

7.2.1 Flow regime identification using visual observation

Generally, the flow patterns of oil-water-sand observed at different oil viscosities appeared similar, hence a flow sample of 1% sand concentrations with 3300cP and 10000cP oil viscosity were selected for discussion. It is a bit difficult to compare the present work with Gillies et al. (1995) because their investigation was on water with oilsand (i.e. oil mixed with sand) while the present work is on oil with water-sand (i.e. water mixed with sand). The viscosity of the heavy crude used by Gillies et al (1995) is 8100cP. They observed sand being washed out of oil which is not the case in the present investigation, where sand is already in water phase but some sand are being trapped by oil on the pipe wall. For 3300cP oil, at slurry velocity higher than 0.7m/s the sand was dispersed in the flow with oil moving as dispersed phase, with some sand particles trapped and moved with the wavy oil film on the pipe wall. This type of flow can be referred to as Dispersed Oil in Slurry with sand-oil coating the pipe wall which can otherwise be referred to as Dispersed Oil-Dispersed sand in water as carrier fluid with sand-oil coating (DO-DS/W) as shown in Table 7-2.












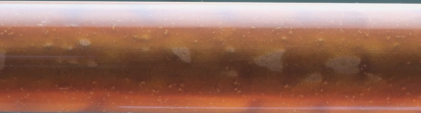


Table 7-2: Oil-water-sand flow pattern for 3300cP nominal oil viscosity at 0.11m/s oil superficial velocity

Flow conditions	Side	Bottom
$V_{so}=0.1\text{m/s}$ $V_{ss}=1.0\text{m/s}$ (a)		
$V_{so}=0.1\text{m/s}$ $V_{ss}=0.8\text{m/s}$ (b)		
$V_{so}=0.1\text{m/s}$ $V_{ss}=0.6\text{m/s}$ (c)		
$V_{so}=0.1\text{m/s}$ $V_{ss}=0.5\text{m/s}$ (d)		
$V_{so}=0.1\text{m/s}$ $V_{ss}=0.4\text{m/s}$ (e)		
$V_{so}=0.1\text{m/s}$ $V_{ss}=0.35\text{m/s}$ (f)		
$V_{so}=0.1\text{m/s}$ $V_{ss}=0.2\text{m/s}$ (g)		

This flow pattern is indeed complex. The water phase in this study was observed not to remain on the pipe wall and this agreed with Gillies et al. (1995) observation as well. The sand particles in the oil film on the wall increased with the decrease in the slurry velocity. The real sand deposit began when the slurry velocity dropped to about 0.5 and 0.4m/s, which is lower than the MTC obtained for water-sand flow (i.e. 0.76-0.66m/s) in the same channel; this presupposed the fact that the viscosity of oil in this case hindered the quick settling of the sand at the bottom of the pipe until the slurry velocity was much lower. In other words, the result suggests that the lift force in the high viscous fluid was higher than that of water. This condition held until the momentum was low enough than it can overcome the gravitational force of sand. At 0.40m/s, the oil plug started appearing close to the upper part of the pipe with moving sand deposit at the bottom of the pipe. This regime could be referred to as Oil Plug with Sand bed in water continuous flow and sand-oil coating (OPS/W). At slurry velocity lesser than 0.40m/s, the sand bed became static. Some part of this sand bed appeared soaked with oil (i.e. oil wetted sand) while others are soaked with water (i.e. water wetted sand). It is worthy to note that saltation and sand dunes were not observed in this oil-water-sand flow in the horizontal pipe (i.e. saltation was only experienced in water-sand flow). The sand movement is purely an axial sliding at the bottom of the pipe along the centreline.

In the case of higher viscosity i.e. 10000cP at 0.1m/s as shown in the Table 7-3, similar behavioural patterns were observed except that the sand MTC was further reduced to 0.30m/s from the range of 0.66-0.76m/s which was obtained in water-sand flow in the same channel. This flow patterns observed are similar at the two different viscosities considered, except for the reduction of the MTC which suggest the effect of viscosity on MTC. The sand bed observed in Table 7-3 increased when the slurry velocity was reduced to 0.20m/s. At 0.20m/s, some water wetted sand were observed at the bottom of the pipe and remained static but was cleared off when the slurry velocity was reduced to 0.1m/s leaving some sand particles on the pipe wall while the flow became dominated by oil.

Table 7-3: Oil-water-sand flow pattern (10000cP at $V_{so}=0.1\text{m/s}$ and 1% sand)

Flow conditions	Side	Bottom
$V_{so}=0.1\text{m/s}$ $V_{ss}=0.7\text{m/s}$ (a)		
$V_{so}=0.1\text{m/s}$ $V_{ss}=0.6\text{m/s}$ (b)		
$V_{so}=0.1\text{m/s}$ $V_{ss}=0.5\text{m/s}$ (c)		
$V_{so}=0.1\text{ m/s}$ $V_{ss}=0.4\text{m/s}$ (d)		
$V_{so}=0.1\text{m/s}$ $V_{ss}=0.3\text{m/s}$ (e)		
$V_{so}=0.1\text{m/s}$ $V_{ss}=0.2\text{m/s}$ (f)		
$V_{so}=0.1\text{m/s}$ $V_{ss}=0.1\text{m/s}$ (g)		

7.2.2 Flow regime identification using PDF of pressure signals

The pressure signals are also considered in this case for trend and PDF analysis to check their suitability and/or consistency for prediction of the oil-water-sand flow behaviours in the horizontal pipe. This is necessary due to the fact that the visualisation method of determining flow patterns, as aforementioned in the previous subsection has been considered subjective and also not practicable in the real life. In this section, the oil-water-sand samples with 3300 and 10000cP nominal oil viscosities flowing at 0.1m/s are used as representative data to draw inferences.

Table 7-4 and Table 7-5 present both the trend and PDF plots. On the left and right column are the trend and PDF plots respectively. Some samples of the flow conditions are compared with the major observations made by visualisation. The region of very high slurry velocities/water cuts (or water superficial velocities) are not the focus of this trend and PDF since the sand particles are dispersed at such region and more importantly, it is desired to operate at low water cuts, hence, the prediction of the flow configurations around the deposition region is crucial and preferred.

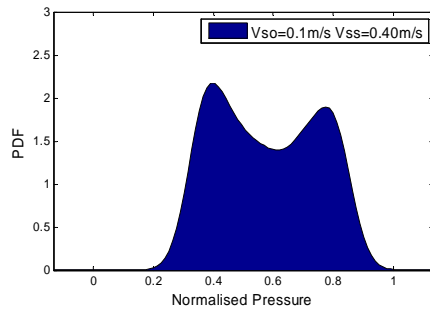
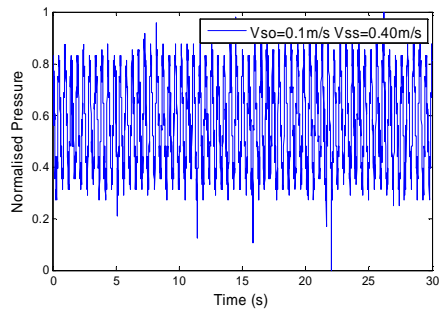
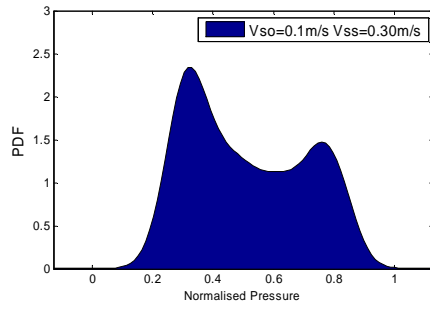
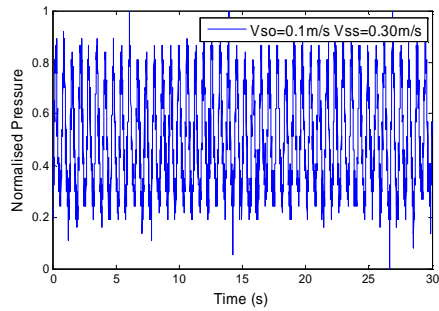
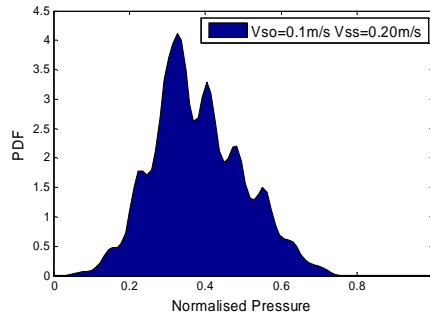
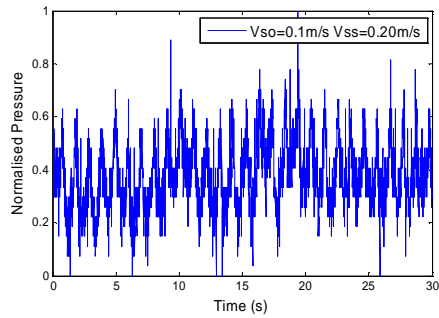
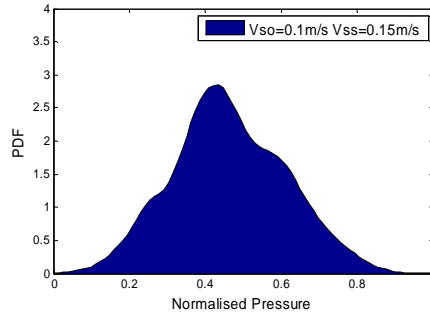
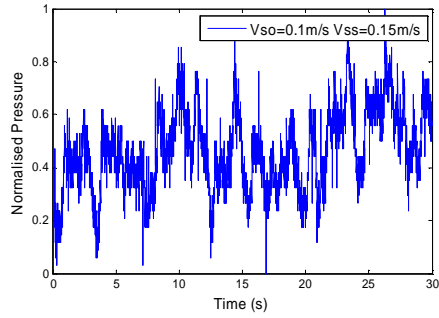
In Table 7-4, at $V_{ss}=0.15\text{m/s}$ and 0.20m/s , the trend plots show fluctuations of signals which indicates that the flow media behaviour is intermittent in nature. Table 7-5 shows similar behaviour at $V_{ss}=0.10\text{m/s}$. The spikes in the normalised trend plots show that there are obstructions which are giving rise to the pressure increase and falling. This presupposes the presence of sand bed which the oil was trying to move. Since oil predominates the flow at very low water cuts, however, the signals need more analysis to expose this characteristic fluctuation. Little or no information could be gleaned from the plots at V_{ss} higher than 0.20m/s . Nevertheless, comparing the trends of both oil viscosities at V_{ss} equals 0.20m/s reflects that there is viscosity effect because the signals are stable at higher viscosity. In summary, similar trends are generally observed from Table 7-4 and Table 7-5.

Considering and comparing the PDF plots from Table 7-4 and Table 7-5 with the visualised images, single peaks are identified at V_{ss} equals 0.15m/s and 0.10m/s for 3300cP and 10000cP respectively.

Table 7-4: Trend and PDF plot of oil-water-sand flow for 3300cP nominal viscosity@ $V_{so}=0.1\text{m/s}$

Pressure signal trend plot

Pressure signal PDF plot

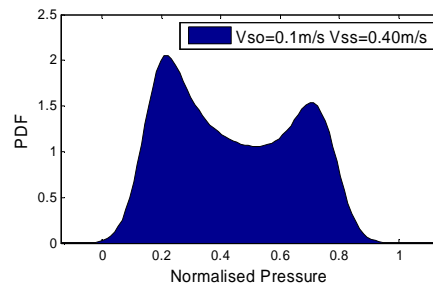
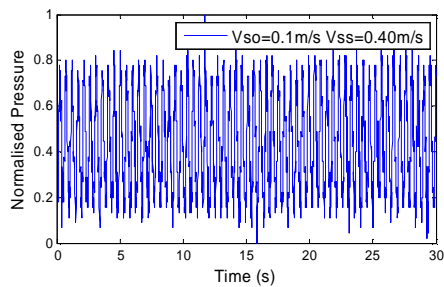
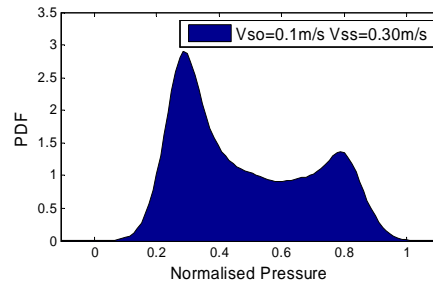
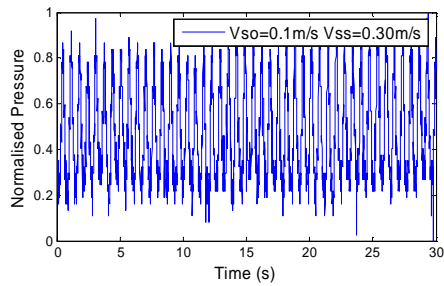
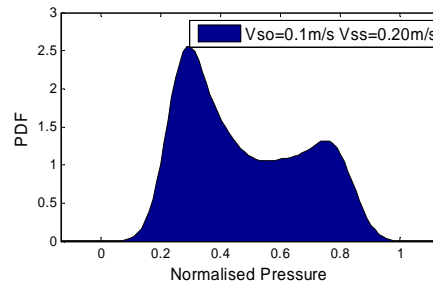
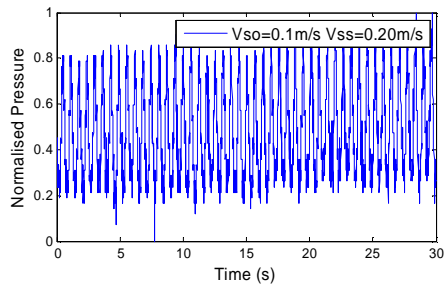
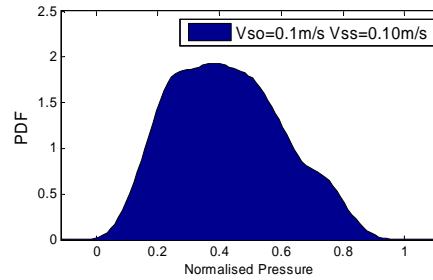
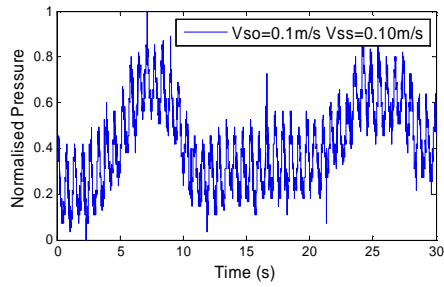


Although the PDF does not show which of the phases predominates the flow. The PDF plot for V_{ss} equals 0.20m/s in Table 7-4 shows multiple peaks and indicates an intense instability or intermittency. Above this velocity, double peaks plot exist until 0.40m/s that was considered the highest (i.e. about 80% water cut) in these campaigns.

Table 7-5: Trend and PDF plot of oil-water-sand flow for 10000cP nominal viscosity @ $V_{so}=0.1\text{m/s}$

Pressure signal trend plot

Pressure signal PDF plot



These double peaks in Table 7-4 and Table 7-5 suggest plug flow as already reported under visualisation method.

7.3 Sand MTC in Oil-Water-Sand Flow

This section presents the results of sand minimum transport condition studies obtained when sand transport was included in the high viscosity oil – water flow in 1-in ID horizontal pipe. Table 7-6 and Table 7-7 summarised the outcomes of different slurry concentrations at different oil superficial velocities. The tables also reveals the effect of the high viscosity oil on the sand MTC by comparing side-by-side the oil-water-sand and water-sand MTCs. Table 7-6 shows that when water flows with 3337cP oil the required sand MTC for 5%v/v sand concentration is higher than that of 1%v/v. It means that more force is required to suspend sand in the flow but on the hand, when these MTCs are compared with the ones required for sand in only water at the same flow conditions, the sand MTC in oil-water-sand are lesser compare to the MTC in water-sand flow. Thus the presence of 3337cP oil has prevented the sand from settling at the bottom of the pipe at lower velocity and saved more energy to keep the sand in the flow.

Table 7-6: Summary of sand MTC in oil-water-sand flow in 1-in ID pipe for 3337cP nominal viscosity at different sand loading

Oil Superficial Velocity (m/s)	MTC Oil-water-sand (m/s)	MTC Water-sand (m/s)	Water cut (-)	Sand Concentration %
0.11	0.31	0.66-0.76	0.73	1
0.11	0.35	1.00-1.10	0.76	5

Table 7-7: Summary of sand MTC in oil-water-sand flow in 1-in ID pipe for 10000cP nominal viscosity at different sand loading

Oil Superficial Velocity (m/s)	MTC Oil-water-sand (m/s)	MTC Water-sand (m/s)	Water cut (-)	Sand Concentration %
0.1	0.41	0.66-0.76	0.80	1
0.1	0.50	1.00-1.10	0.84	5

Table 7-7 which represent 10000cP oil with water and sand shows the same trend as Table 7-6 however, the required MTC appeared to be higher than obtained in Table 7-6. This difference could be traced to either the difference in the oil superficial velocities (superficial velocity of oil in Table 7-6 is 0.11m/s) or viscosities. This behaviour could be further explained using Table 7-8 in the next section; the results of the sand MTC at different oil superficial velocities are presented. The data show that at every particular sand concentration the higher the oil superficial velocity, the lower the sand MTC. This was found to be consistent for the 10000cP oil with water and sand experiments in 1-in diameter horizontal pipe that were conducted in this study.

7.4 Pressure Gradient

Figure 7-1, Figure 7-2 and Figure 7-3 present the comparisons of pressure gradient of 1%v/v, 5%v/v and 10%v/v sand concentration respectively with different oil viscosities. Generally, it could be observed that the effect of slurry on oil irrespective of viscosities is relatively the same as reflected on the pressure gradient; that is the frictional pressure gradients of oil at different viscosities were drastically reduced. This understanding presupposes that the compositions of oil-water-sand flows with sand lower than 1% concentration might follow the same inference. This observation is in agreement with McKibben and Gillies (2009) which says that the addition of sand to oil-water mixture

did not appear to contribute to the increased frictional losses in a horizontal pipeline as would be expected for conventional slurry but rather reduced the losses. In their study, 6 and 12% sand concentrations were employed for the investigation of the effect of sand on friction losses.

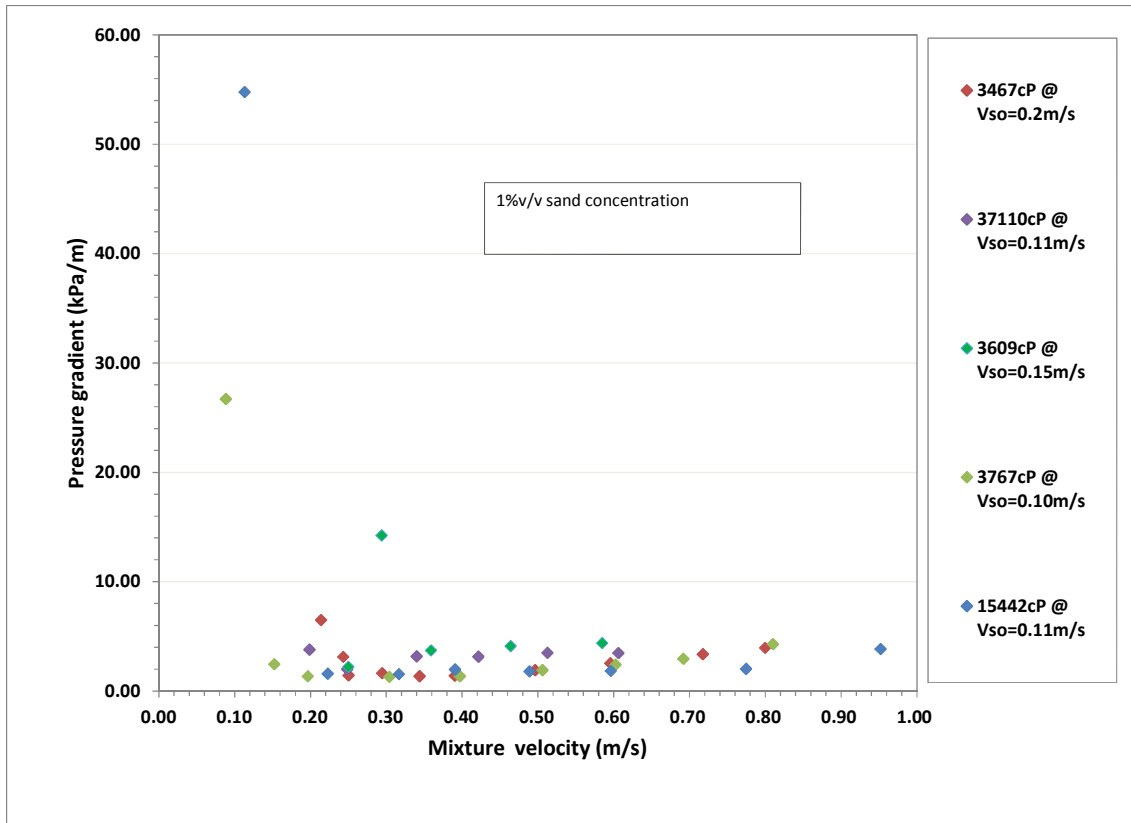


Figure 7-1: Pressure gradient of oil-water-sand flow with 1% v/v sand on different oil viscosities

Although the injection of water in the transport of high viscous oil has been reported in the previous chapter to be responsible for the reduction of pressure losses, and the presence of sand in the conventional slurry (i.e. water-sand) was also reported in chapter 5 to increase the pressure losses, McKibben and Gillies (2009) proposed that the scouring process of the sand removes more oil from the pipe wall than the friction it causes. It could also be observed from the chart that the increase in oil flow rates did not contribute significantly to the pressure losses in the flow. In addition, Figure 7-4 further reveals that at a relatively constant oil viscosity, the difference in the concentration of sand did not have significant effect on the frictional pressure gradient in this study.

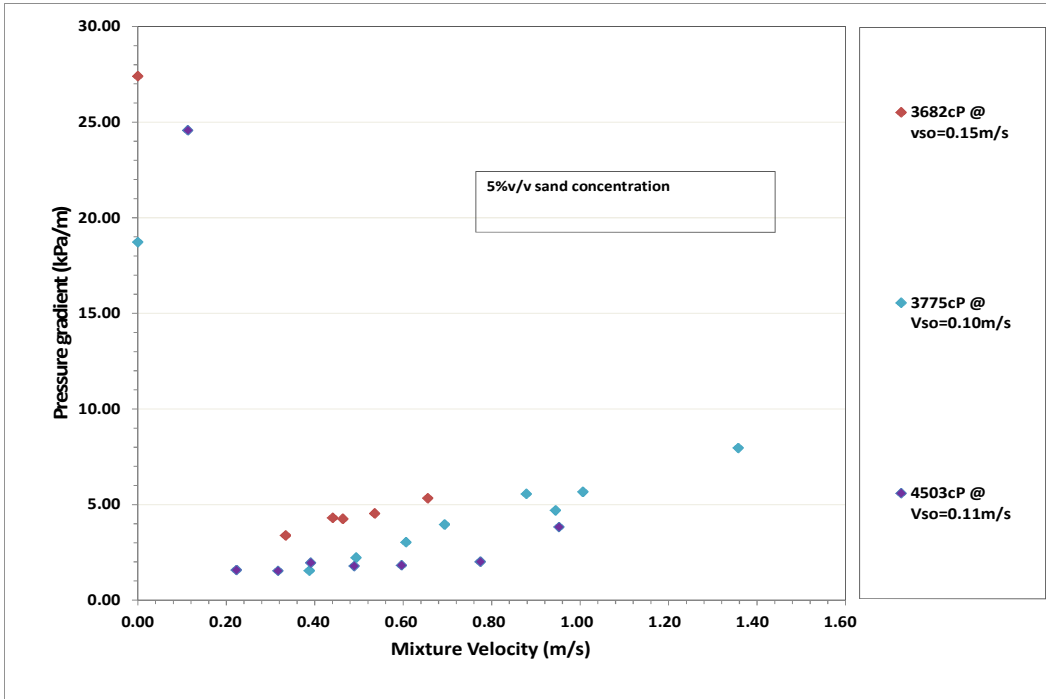


Figure 7-2: Pressure gradient of oil-water-sand flow with 5% v/v sand on different oil viscosities

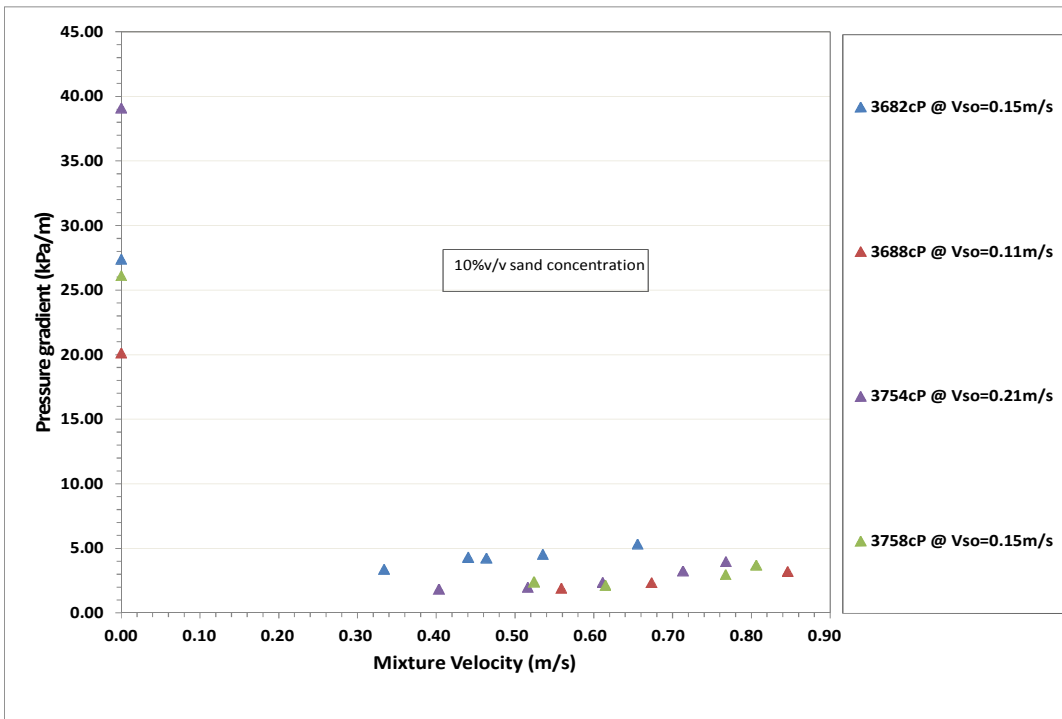


Figure 7-3: Pressure gradient of oil-water-sand flow with 10% v/v sand on different oil viscosities

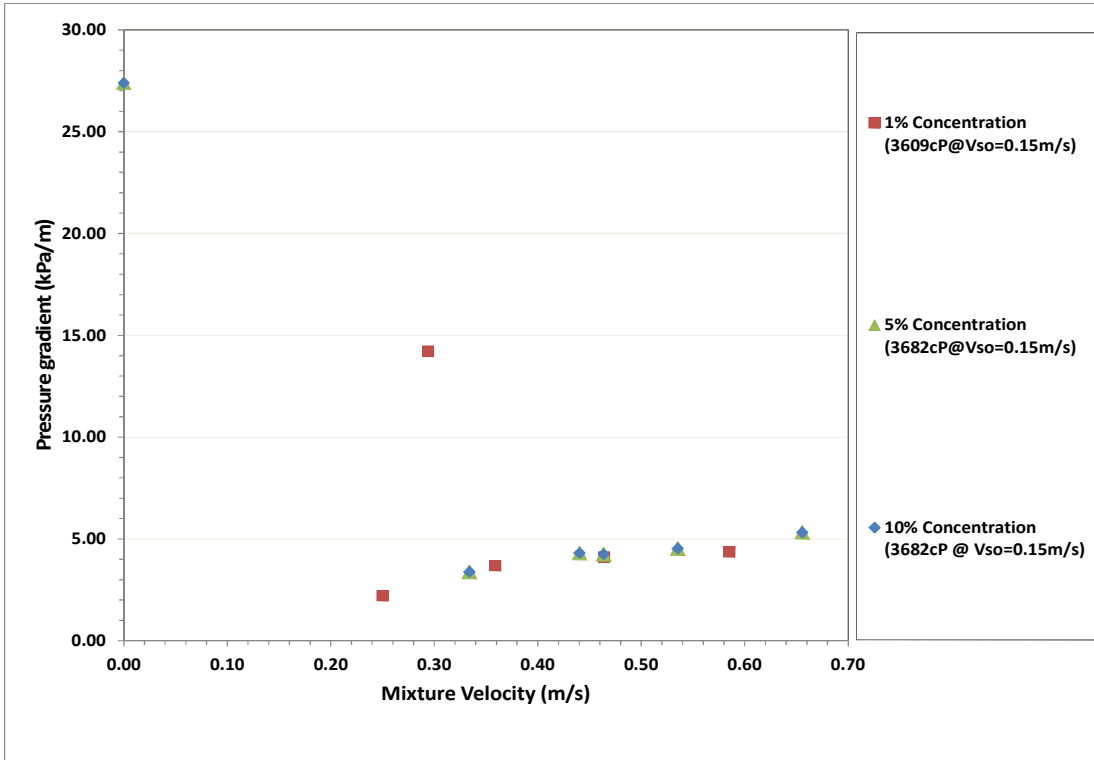


Figure 7-4: Pressure gradients of varying sand concentration for relatively constant oil viscosity

Table 7-8 presents the pressure gradients at different MTC for varying sand concentrations with 10000cP oil and water. It shows that at a specific oil flow rate, the MTC increases with increase in sand concentration (i.e. from 1% to 10%) but the MTC decreases with increase in oil flow rate (i.e. $V_{so}=0.10\text{m/s}$ to 0.20m/s). In addition Table 7-8 also reveals that increase in sand concentration contributes to the increase in the pressure losses but there were occurrences of low pressure gradients observed when the sand concentration was 5%v/v compared to 1 and 10%v/v. The author does not have any explanation for this observation. Further discussions are presented in section 7.5 where the behaviours of oil-water and oil-water-sand flow are compared and analysed.

Table 7-8: Pressure gradient @ MTC in oil-water-sand flow for 10000cP nominal viscosity at different sand loading

Oil Superficial Velocity (m/s)	MTC Oil-water-sand (m/s)	Water cut (-)	Pressure gradient @MTC kPa/m	Sand Concentration %
0.10	0.41	0.80	1.90	1
0.10	0.50	0.83	3.02	5
0.10	0.68	0.87	3.18	10
0.15	0.31	0.67	1.62	1
0.15	0.52	0.78	2.64	5
0.15	0.61	0.92	2.92	10
0.20	0.30	0.60	1.91	1
0.20	0.40	0.67	3.04	5
0.20	0.49	0.71	3.23	10

7.4.1 Verification of SRC model

This section compared the present research results on oil-water-sand with the results obtained from the SRC model reviewed in section 2.3.5.5. SRC model, as earlier mentioned was developed to predict the gradient of bitumen froth and lube oil with water. The correlation proposed that the carrier fluid contained some fine clay sand (referred to as “fines”) which gives it a higher viscosity than pure carrier fluid. The fines concentration was used to describe the carrier’s viscosity which was used in the friction factor correlation that was developed. This correlation performed satisfactorily well with oil-water-sand, as could be seen in Figure 7-5 and Figure 7-6, although more data are needed at very low water cut such are missing in the present study. The good performance could be traced to the data sources for the correlation development; bitumen froth, husky crude and lube oils were employed in both 4-in and 10-in ID pipes for the experiments.

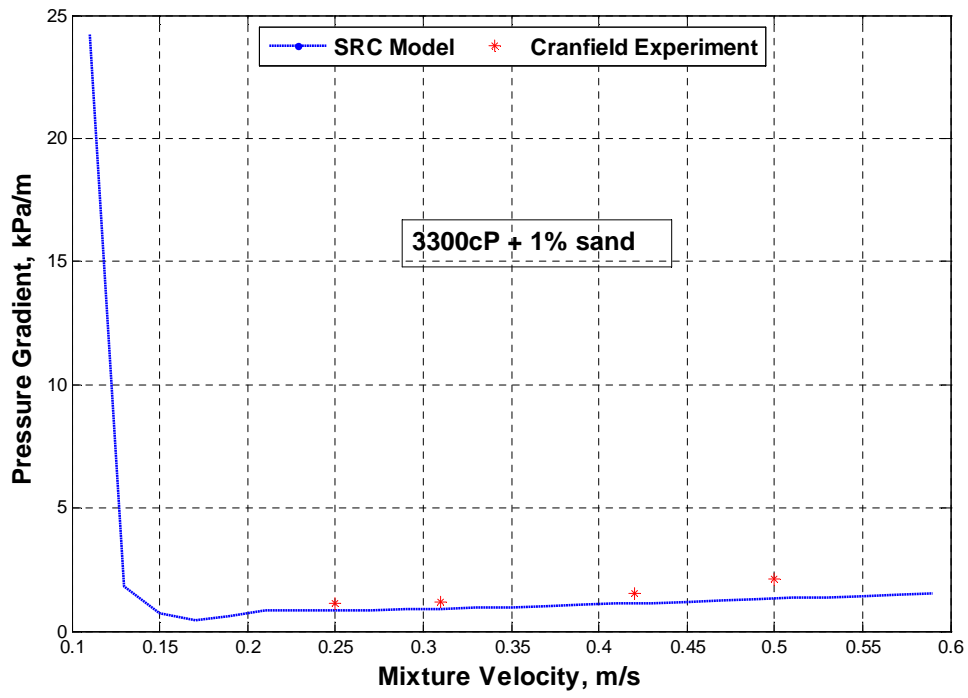


Figure 7-5: Validation of SRC model using 3300cP oil with 1% sand

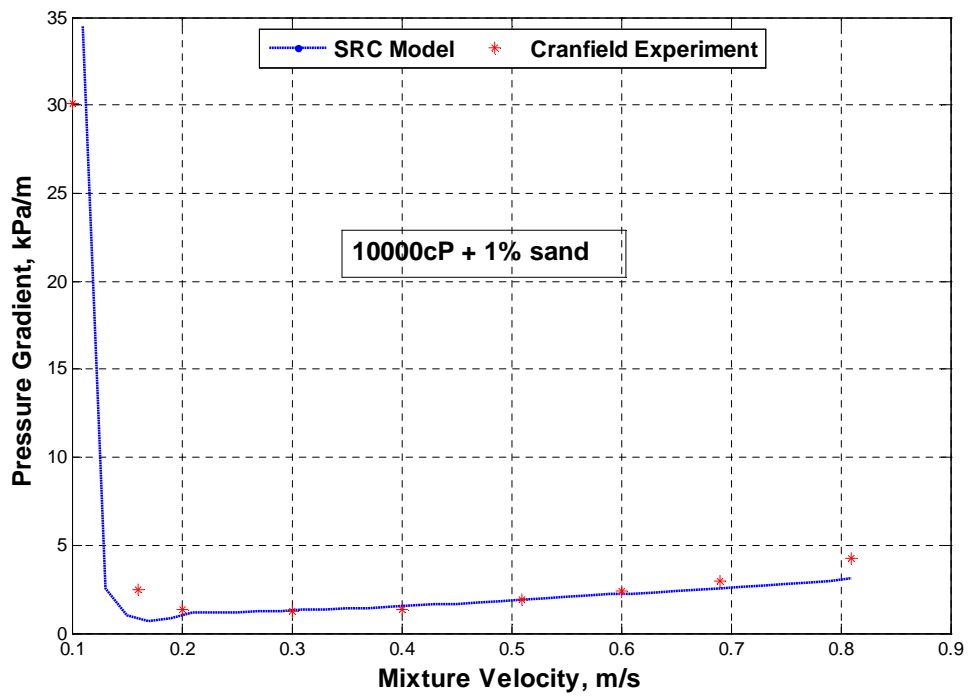


Figure 7-6: Validation of SRC model using 10000cP oil with 1% sand

7.5 Comparison of Oil-Water and Oil-Water-Sand Flow Behaviour in Horizontal Pipe Flow

In this section, the comparison of oil-water and oil-water-sand flow in pipe is presented. Sand management by sand inclusion in the production of oil has been embraced over the years because it reduces the risk of loss of production nevertheless the overall effect must be monitored. This is necessary because the foremost quantity of interest in any multiphase, which is pressure, may result in both safety and profit loss if not properly monitored, hence this analysis. In addition, the viscosities of the oil considered in this research are not common to the oil & gas industries.

The pressure gradient profiles of the oil-water and oil-water-sand are examined in Figure 7-8 through Figure 7-9. Generally, it was observed that the presence of sand had no effect on the pressure gradient profiles. This could be seen from the profiles of different viscosities with 1% v/v sand concentration i.e. the pressure gradients obtained from oil-water-sand experiments are not different from those obtained from oil-water

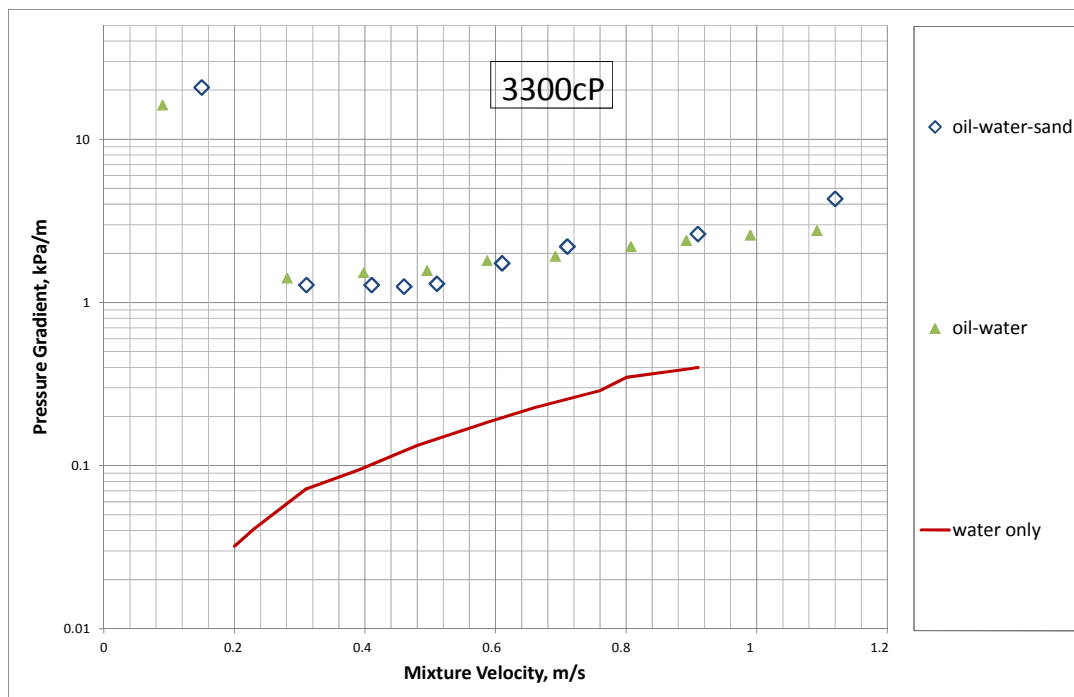


Figure 7-7: Comparison of oil-water and oil-water-sand flow @ $V_{so}=0.1\text{m/s}$ and 1% v/v sand concentration for 3300cP nominal viscosity

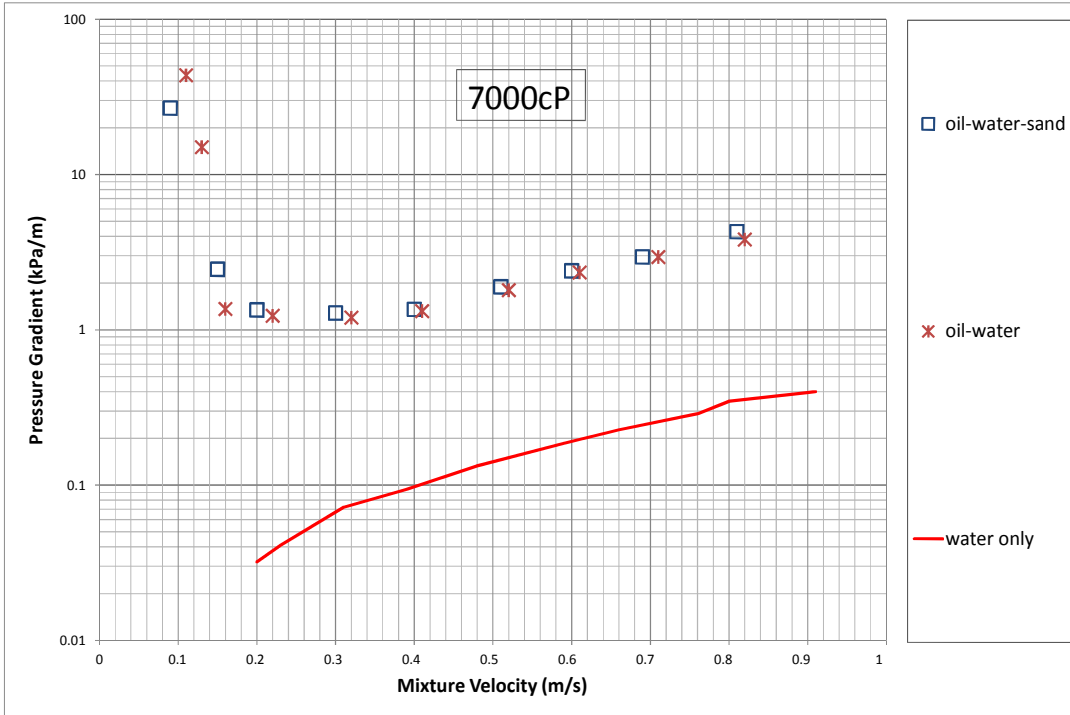


Figure 7-8: Comparison of oil-water and oil-water-sand flow @ $V_{so}=0.1\text{m/s}$ and 1% v/v sand concentration for 7000cP nominal viscosity

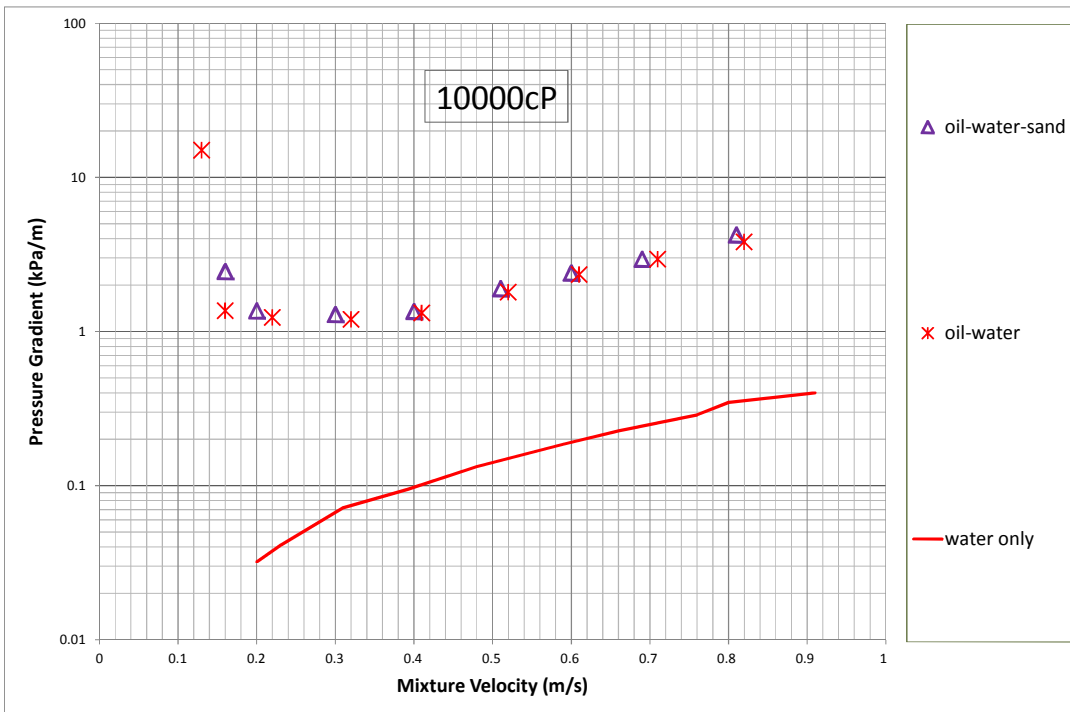


Figure 7-9: Comparison of oil-water and oil-water-sand flow @ $V_{so}=0.1\text{m/s}$ and 1% v/v sand concentration for 1000cP nominal viscosity

flow in the same channel although they are well below single phase oil and a little above that of single phase water. The effect of the addition of the amount of sand under conventional slurry would be to increase the gradient by about 30% (McKibben and Gillies, 2009). However, when the sand concentration increased to 5%v/v, the pressure gradient profile in Figure 7-10 reflects the contribution of sand to the overall flow where the oil nominal viscosity is 3300cP as expected in a slurry flow in pipes when the mixture velocity exceeded 0.25m/s. This profile shows the pressure build up in the pipe but the profiles of the comparison in Figure 7-11 and Figure 7-12 reveal little or no difference of the impact of the 5%v/v sand on 7000cP and 10000cP oil flow with slurry. In other words the gaps observed in Figure 7-10 is closed in Figure 7-11 and Figure 7-12. This suggests that the increase of oil viscosity prevented the sand build up by keeping the sand suspended in the flow and preventing the settlement of sand that can reduce the hydraulic diameter of the pipe. Although the gradient profiles show an increasing pattern with increase in mixture velocity, it does not mean that the sand is responsible for the increase; since the same pattern is already observed in oil-water flow in the same channel.

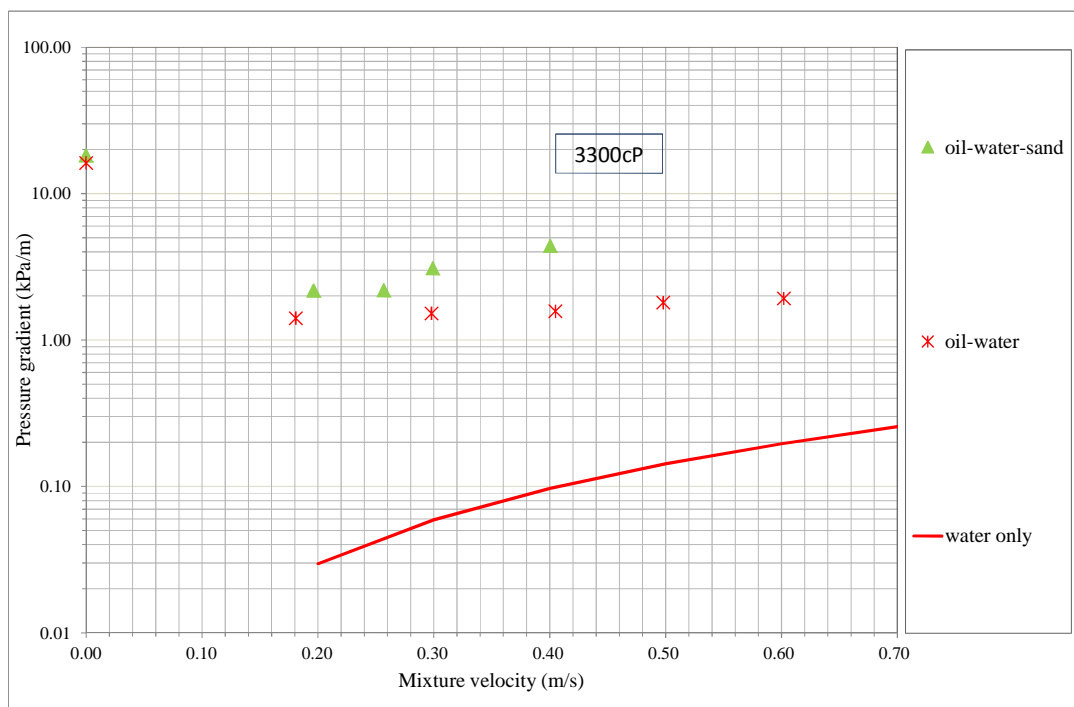


Figure 7-10: Comparison of oil-water and oil-water-sand flow @ $V_{so}=0.11\text{m/s}$ and 5% v/v sand concentration for 3300cP nominal viscosity

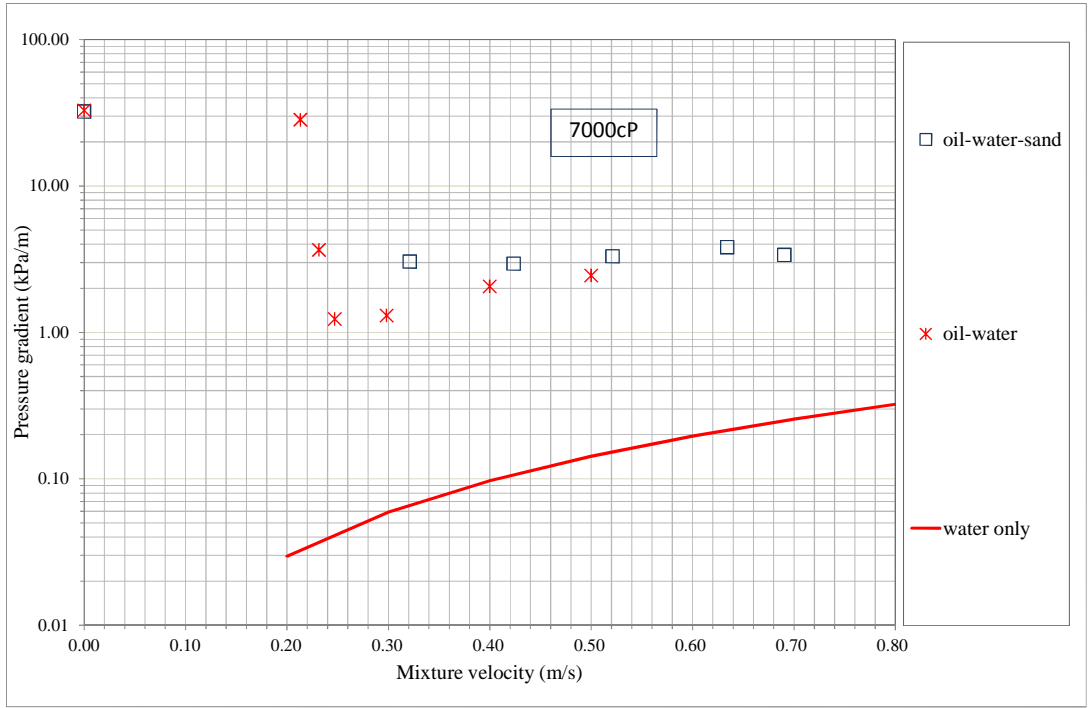


Figure 7-11: Comparison of oil-water and oil-water-sand flow @ $V_{so}=0.1\text{m/s}$ and 5% v/v sand concentration

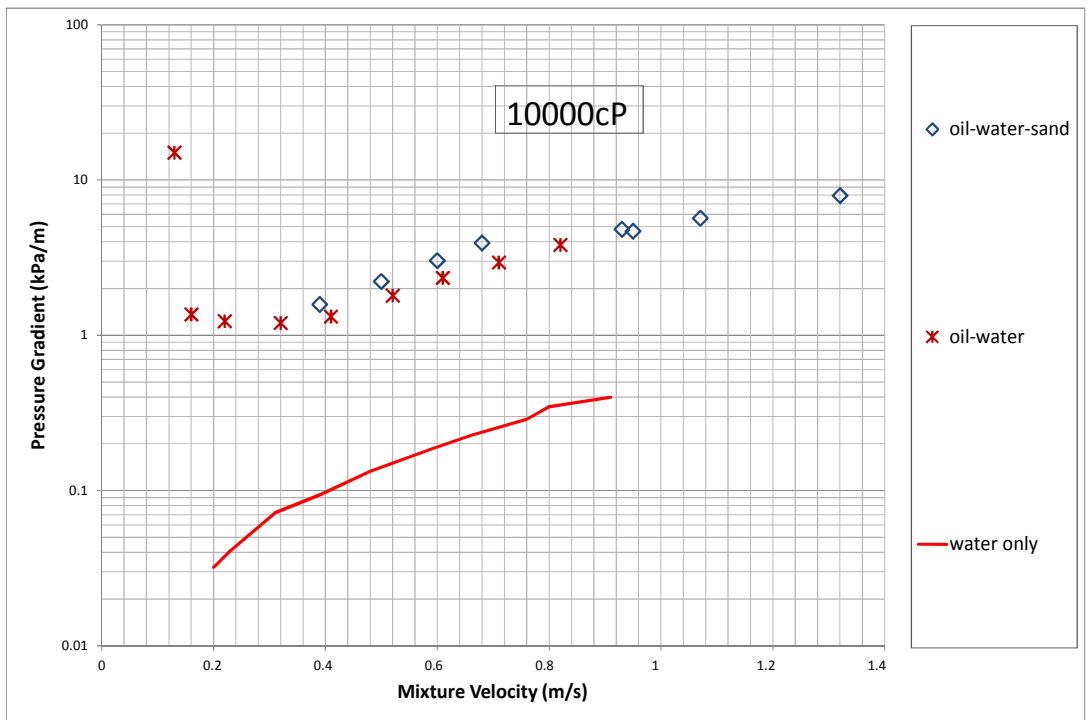


Figure 7-12: Comparison of oil-water and oil-water-sand flow @ $V_{so}=0.1\text{m/s}$ and 5% v/v sand concentration

On a general note, Condolios and Chapus' (1963) discovery and assertion that the presence of fines in a coarse slurry decreases the frictional pressure drop in a horizontal pipe to a much greater extent than might be expected from the relative properties in the solids cannot be extended to the present research because the presence of fines sand does not possess significant advantage over the injection of single phase water in the reduction of the intrinsic pressure drop of single phase high viscosity oil experienced in the horizontal pipe flow.

7.6 CFD of Oil-Water-Sand Multiphase Flow

This section presents the CFD simulation results of oil-water-sand flow in pipe. A 3-D CFD model of a 5m long 1-in ID horizontal pipe was developed. The Eulerian-VOF CFD model which was used to study the flow of water-sand and oil-water was also used in this section to simulate the behaviours of oil-water-sand. The improvement introduced as UDF into the oil-water turbulence (SKE and LRKE) models was also employed in this case to evaluate its applicability and consistency. The CFD results are validated using experimental measurements of pressure gradient profile obtained from the experiments.

7.6.1 Model geometry

The geometry and mesh were created using Gambit 2.4. The test section of the 1-inch four phase transport facility in Chapter 3 was modelled. A simplification to the real test section that was made in section 6.4 to the CFD model was adopted. The water-sand (slurry) mixture was introduced at the annulus inlet section while oil was introduced into the pipe at the core inlet section. This was created to reduce the computational space and time. The mesh size that was used in section 5.5 and section 6.4 was adopted for the simulation. Hexahedral mesh was employed to discretise the computational domain.

7.6.1.1 Boundary and initial conditions

In this research constant superficial velocities and atmospheric pressure were specified at the inlet and pressure outlet at the outlet boundaries of the CFD models in order to keep it simple. Isothermal condition was employed for the simulation; in other words, the effect of temperature was considered negligible. The temperature at both the inlet and outlet was set to be the same.

7.6.1.2 Multiphase and turbulence models

The governing equations are given in equations 4-1 to 4-4. The liquid and solid phases are considered incompressible with constant physical properties. The VOF model was selected to model the oil-water-sand three-phase flow and track the volume fraction of

each phase as a fluid. With VOF, the geometrical reconstruction scheme was adopted to represent the interface between the oil/water-sand, sand/oil-water or water/oil-sand by applying a piecewise-linear approach. The modification employed in k and ε in the turbulence model in the previous chapter was adopted in the turbulence model used in the simulation of oil-water-sand. This was used in the LRKE turbulence model that was considered in this simulation.

7.6.1.3 Solution method

Flow regimes are known to be periodical in nature hence the unsteady solver was employed to simulate the flow behaviours. Since statistically steady-state of the flow behaviours are made up of several periodic flows the time employed to collect data in the experiments was adopted i.e. 30s. The variable time step method was adopted to prevent divergence and also to reduce the computation time of CPU. The time step was adjusted automatically based on the Courant number known as CFL after its authors (Courant-Friedrich-Lewy). The Courant number is a dimensionless number that compares the time step (Δt) in a calculation to the characteristic time of transit for a fluid element across a control volume. The global CFL condition is given by

$$CFL_{global} = \Delta t_{global} * \max \left(\sum \frac{outgoing\ fluxes}{volume} \right) \quad 7-1$$

where Δt_{global} is the global time step. The global Courant number employed in this research was 2 and the resulting time step varied from $1e^{-05}$ to 0.004s.


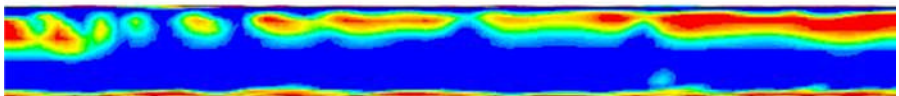
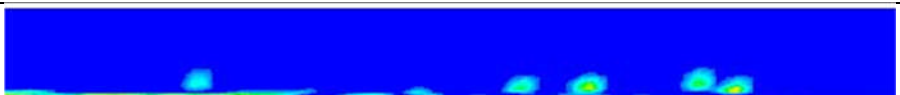
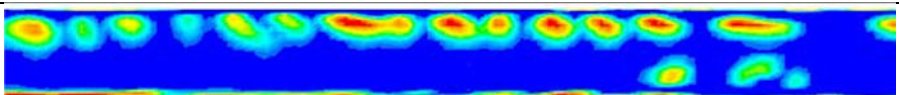
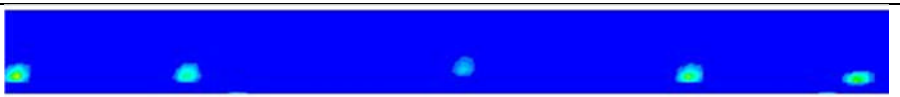
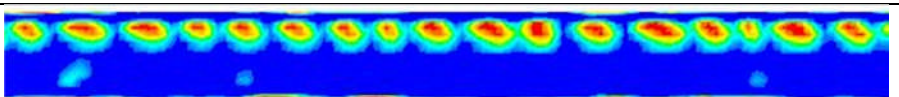

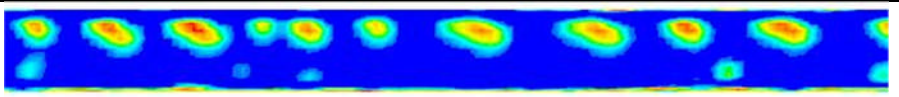
7.6.2 Flow patterns

Table 7-9 summarises the flow configurations obtained from the CFD simulation for the oil-water-sand flow in 1-in ID horizontal pipe for 1% sand concentration in water flowing with 3300cP oil. The colour map of sand from the column under the title sand is ranging from blue to red meaning minimum to maximum (or 0 to 1). The column on the far RHS shows oil using similar colour map. The table column under the title 'sand'

presents sand behavioural patterns at different flow conditions while the RHS column shows the oil patterns as gotten from the simulations. Examining the configurations, one could observe that at high slurry velocities, the presence of sand were not critical (i.e. high) compared with the low slurry velocity. However, the sand minimum transport condition could be estimated. The MTC for the similar case was observed from the video to be about 0.30m/s but not exactly the same value from the CFD but appeared to be lower than 0.30m/s but greater than 0.21m/s, as can be seen from the contour plot. Comparing this contour plot as well with water-sand contour plot in Table 5-7 which shows sand deposit at about 0.75m/s, it reveals in agreement with the experiment that the MTC in oil-water-sand is lower than the MTC in the conventional (water-sand) slurry. It further shows that CFD is capable of predicting the complex behaviour of oil-water-sand.

The RHS column which shows the oil patterns compared with the observation from the experiment as well. It could be seen that the dispersed behaviour of oil in the contour plots occurs at relatively high slurry velocities. From the oil contours, it could also be observed that the oil film thickness at the point where the MTC was observed is high. This could be because the sand was able to trap some oil to form oil-wetted on the wall as equally observed in the experiments. In addition, the contours also reveal that at the lower slurry velocity the oil pattern is plug-like.

Table 7-9: Contour plots of oil-water-sand of 1% v/v sand with 3300cP oil

Flow Condition $V_{so}=0.1$	Contour	
	Sand (a)	Oil (b)
V_{ss} (m/s)		
0.15		
0.21		
0.31		
0.40		

7.6.3 Pressure gradient

Figure 7-13 presents the pressure gradient plot of high viscosity oil with 1%v/v slurry in 1-in ID horizontal pipe with the oil viscosity at 3300cP. The profile is comparable to those obtained from high viscosity oil with water. This is reasonably comparable with

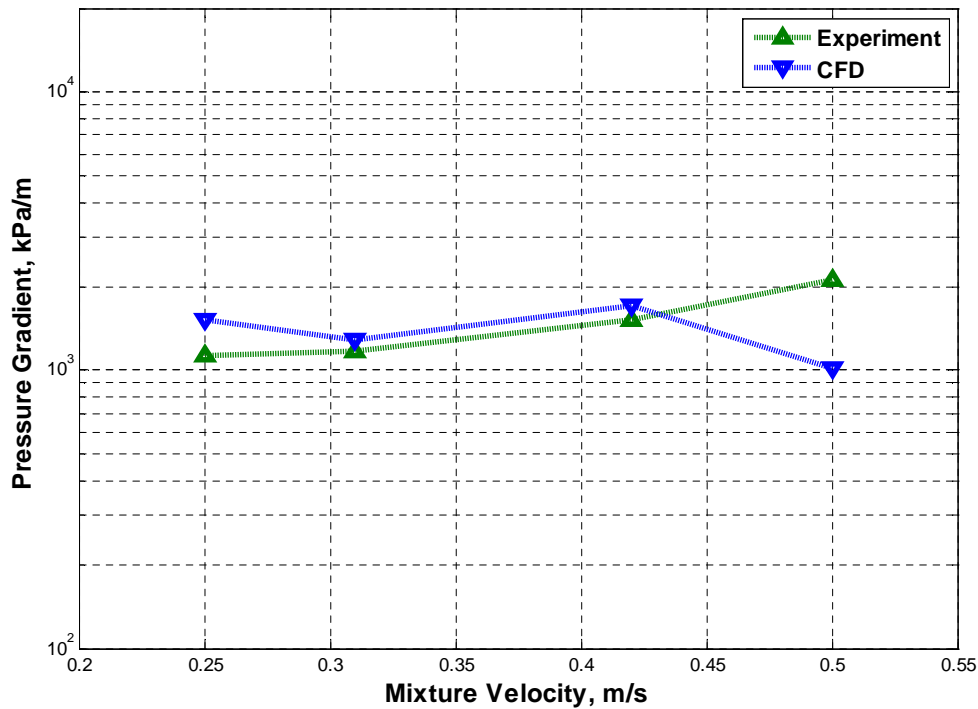


Figure 7-13: Pressure gradient of oil-water-sand @ $V_{so}=0.1\text{m/s}$ with 1%v/v sand concentration (Oil viscosity=3300cP)

the observation made in the experiment for similar case. The inadequacy observed in this profile could be traced to the fact that the turbulent kinetic energy and dissipation correlations did not have any factor for the presence of sand. The CFD under predicted the oil-water-sand in question at a mixture velocity of 0.5m/s and over predicted the gradient at velocities lower than 0.5m/s, unfortunately, the time consumption for this kind of simulation is enormous; this prevents many different runs. Another unfortunate situation is the absence of literature data for similar flow to substantiate the observations made in this study.

7.7 Chapter Summary

In this chapter, the sand minimum transport conditions (MTC) of sand transport in the oil-water flow in the horizontal pipe was analysed at oil superficial velocity ranging from 0.1 to 0.2m/s. The slurry superficial velocity ranges from 0.01 to 1.4m/s.

It was observed that at every particular sand concentration, the higher the oil superficial velocity, the lower the sand MTC. In addition, increase in sand concentration at any given oil viscosity requires increase in the sand MTC.

It was observed that there are no significant differences between the pressure gradients of oil-water-sand with different viscosities at fixed sand concentration (i.e. 1%), however, the pressure losses increased with increase in sand concentration. The SRC model for prediction of pressure gradients was verified suitable for the present research.

The pressure gradient profiles of the oil-water and oil-water-sand were compared and it was found that the pressure gradients obtained from oil-water-sand experiments are not different from that obtained from oil-water test.

The flow pattern types was analysed using the visualisation (video) method of the flow and also described by both the trend plots and probability density function (PDF) of the downstream pressure signals. These methods succeeded in relaying the information about the changes in flow configurations.

In CFD, a limited research was done on the simulations of oil-water-sand due to its complexities and excessive time consumption. The UDF developed for turbulent kinetic energy and dissipation rate in oil-water flow simulation was adopted for the prediction of the pressure gradients and the flow configurations study. The simulation of 1% sand concentration with 3300cP oil and water was attempted, and the simulated result was found to agree with a little over-prediction of the experimental pressure gradient results except at high mixture velocity.

The contour plots of the simulated results reveal the sand and oil positioning at different flow conditions. This compared favourably with the experiments. The sand was found to be settling below 0.31m/s slurry velocity which is the observed MTC in the experiments for the same campaign.

8 CONCLUSIONS AND FURTHER RESEARCH

In this chapter, the summary, conclusions, and contributions are presented. The recommendations for further research are also identified.

The present study involved both the experimental and numerical investigations of water-sand, high viscosity oil-water, and high viscosity oil-water-sand flows in horizontal pipe. The experimental study primarily involved pressure gradient measurements in a 1-in ID horizontal flow facility. Data were collected from both upstream and downstream of the pipe at specific locations (i.e. 2.91 and 5.12m). The liquid phases are water and high viscosity oils (i.e. CYL680 and CYL1000). The density of water used in this research is 1000kg/m^3 . The densities of CYL680 and CYL1000 @ 25°C are 917 and 916.2kg/m^3 while their viscosities are 1.830 and $3.149\text{Pa}\cdot\text{s}$ respectively. The solid-phase concentration ranged from $2.15\text{e-}04$ to 10%v/v with mean diameter of 150micron and with a material density of 2650kg/m^3 .

CFD methodology was developed for the simulations of water-sand, oil-water, and oil-water-sand flow in 1-in ID 5m long horizontal pipe. The simulations were performed both by 12 processors Dell workstation acquired by the Department of Offshore, Process and Energy Engineering, and Cranfield University HPC facility. The numerical study involved the flow of 1%v/v sand concentration in water and also oil-water flow in horizontal pipe. These were simulated with two-fluid VOF model using ANSYS GAMBIT and FLUENT commercial CFD package. Following an extensive review of literature, the inlet condition for imposing annular flow was designed. In addition, various turbulence models were examined to analyse their suitability to simulate these multiphase flows and the model results were compared with the experimental data. The simulations focussed on the prediction of pressure gradients and the flow configurations/patterns.

8.1 Conclusions

The conclusions drawn from the present studies are categorised under experiment and CFD as presented below:

8.1.1 Experiment

The results of the oil-water flow test reveals that the pressure gradient, first of all, decreased from the single phase oil gradient gradually to the minimum as the water cut increases from zero and later increases again with increase in water cut. The pressure gradient reduction factor reveals that the highest reduction of the pressure drop occurred at high oil velocity. In addition, it was found that the reduction factor decreased with increase in water cut. The oil-water flow configurations inferred from both the photographs of the flow and the probability density function (PDF) of pressure signals along with the statistical moments were compared with the existing regime map developed by Sotgia (2008). The existing flow pattern transition models were found inadequate and need to be modified. Similar methods of investigation were employed in the study of oil-water-sand flow in the 1-in ID horizontal pipe. The sand MTC in oil-water flow were studied and obtained for different viscosities and at different sand concentrations. It was found that at a fixed sand concentration, the MTC required decreased with increase in oil superficial velocity, while the MTC increased with increase in sand concentration.

8.1.2 CFD

The numerical simulation of oil-water flow focused on the validation of the turbulence models and understanding of the water assist flow phenomenon. The results of the CFD study of the oil-water flow in the horizontal pipe were analysed for oil superficial velocity at 0.1 and 0.55m/s. The water cut ranges from 0.2 to 1.0m/s. It was also observed that the addition of water to oil flow in horizontal pipe reduces the pressure drop effectively. There were relatively good agreement between the CFD contours and experimental flow pattern of oil-water flow, as well as pressure gradient values for both oil-water and oil-water-sand flow.

In CFD, annular flow pattern was successfully initiated by flow interaction specification of a concentric flow at the inlet boundary condition with the homogenous mixture on the inside of the pipe. Although the concentric design for pipe inlet condition was

developed for annular flow studies, it ended up as a suitable condition in this study to introduce multiphase fluids in to the pipe for simulation of all other flow configurations. PDF data analysis was also explored, using the simulated downstream pressure data to identify the flow patterns in 1-in ID horizontal pipe. This shows that experimental data analysis can also be replicated by CFD simulation. However, further research is needed to increase the confidence in the capability of CFD for modelling of multiphase flows for more accurate predictions of the flow behaviour of complex flow systems. The possibility of restart operation was also simulated. Lastly, the pressure gradient of 1% sand concentration with 3300cP oil and water was simulated and found to compare reasonably well with a little over-prediction excluding the high mixture velocity. The contour plots from the simulation compared well with information about the sand MTC.

8.2 Contributions to Knowledge

This research has succeeded in making contributions to knowledge as summarised below:

8.2.1 Experiment

This research has discovered that the presence of oil film on the pipe wall is not a limitation to the transportation of heavy oil in the core of the pipe as annular flow in the presence of water at low pressure drop.

Analysis of pressure signals using PDF was shown to give good predictions of flow regimes of the transport of heavy oil with water, and this could be used in addition to the dedicated flow measurement devices to inform about the in situ flow regimes in pipe.

The flow pattern maps data were generated for 2-phase high viscosity oil-water flow with the oil viscosity ranging from 3300cP to 10000cP.

At any fixed sand concentration, no significant differences were found between the pressure gradients of oil-water-sand flows for different oil viscosities considered.

It was discovered that the pressure gradients obtained from oil-water-sand experiments are not significantly different from that obtained from oil-water test.

8.2.2 CFD

In CFD, concentric pipe inlet was designed to achieve annular flow but more flow configurations were obtained as in the experiments for oil-water and oil-water-sand flow in the horizontal pipe.

CFD methodology was developed to simulate 2-phase water-sand, oil-water and oil-water-sand flow in 1-in ID 5m long horizontal pipe.

The performance of the existing SKE and LRKE turbulence models were improved by the influence of the developed correlations through the UDF codes.

CFD simulation reveals that turbulence in the water is a major source of drag in high viscosity oil-water liquid-liquid flow.

CFD has been found remarkable for the study of water-sand, oil-water and oil-water-sand but more research are needed to bring it to a reliable level.

It also reveals that stratified flow is promoted as the annulus phase (i.e. water) density increases; although the pressure drops did not noticeable vary from that of the fresh water.

The first study to engage in the comparative evaluation of two-fluid model with the addition of modified k and ε in turbulence model to predict flows with special attention on high viscosity oil based multiphase flows.

The restart studies show that pressure surge is inevitable when water is used to aid heavy oil production and it must be prepared for.

8.3 Limitations of Research

The colour of CYL1000 oil used in this research is brown; therefore some difficulties are encountered in the characterisation of the flow patterns of oil-water flow in 1-in ID horizontal pipe at very low flow rate due to oil opacity.

In this research, collection of holdup data was not addressed because the ECT measurement device available does not work with oil in water. In addition, the issue of oil film covering the probe when it has contact with oil makes it difficult to consider the intrusive type of measurement device.

CFD always requires high computation effort in terms of time, and the FLUENT CFD software package employed in this research allows a minimum interaction with the model equations which makes it difficult to impose an entirely new model.

8.4 Recommendation and Further Research

There is need for heavy oil to be de-colourised with bleaching agents in order to improve the visual judgment of the flow configurations. This should help in the investigation of the flow patterns at very low water flow rate in oil-water flow.

Further investigations is needed on the identification of PIP in oil-water two-phase flow in horizontal pipes of different diameters.

Further research are needed on flow measurement studies of the high viscosity oil in water and oil in slurry flow in the horizontal, inclined and vertical pipes, as well as other diameters because of the failure of Electrical Capacitance Tomography (ECT) to

capture accurate data when water is included in the flow, as reported by Al-Awadi (2011). The use of Particle Image Velocimetry (PIV) and Laser Doppler Technique (LDT) could be employed to investigate these multiphase flows.

Some research on the development of both mechanistic and empirical correlations for these multiphase flows are also recommended for the improvement of the existing commercial software packages. The SRC model has been reported in this research for good prediction of pressure gradient at high water flow rates but failed at low flow rate region. More data points are also needed to establish this model.

Due to the difficulties in the interaction with the turbulence models of the FLUENT CFD software package the use of OPENFOAM software package is recommended.

In the further work, thermal effects and fluid compressibility due to heat transfer between the fluids and the surrounding need to be investigated. With the inclusion of temperature effect in this study, the compressibility of the fluids especially that of the high viscosity oil, might become significant and should be taken into account.

REFERENCES

- Abdullah, A. (2011), "Quantifying guidelines and criteria for using turbulence models in complex flows", .
- Al-lababidi, S., Yan, W. and Yeung, H. (2012), "Sand Transportations and Deposition Characteristics in Multiphase Flows in Pipelines", *Journal of Energy Resources Technology*, vol. 134, pp. 034501.
- Angeli, P. and Hewitt, G. (1999), "Pressure gradient in horizontal liquid-liquid flows", *International Journal of Multiphase Flow*, vol. 24, no. 7, pp. 1183-1203.
- Angeli, P. and Hewitt, G. (2000), "Flow structure in horizontal oil-water flow", *International Journal of Multiphase Flow*, vol. 26, no. 7, pp. 1117-1140.
- Ansys Inc., (2003), "Fluent user's guide", *Ansys Inc.*, vol. 2, pp. 3.
- Arirachakaran, S., Oglesby, K., Malinowsky, M., Shoham, O. and Brill, J. (1989a), "An analysis of oil/water flow phenomena in horizontal pipes", *SPE Production Operations Symposium*, .
- Arirachakaran, S., Oglesby, K., Malinowsky, M., Shoham, O. and Brill, J. (1989b), "An analysis of oil/water flow phenomena in horizontal pipes", *SPE Production Operations Symposium*, .
- Arney, M. S., Ribeiro, G. S., Guevara, E., Bai, R. and Joseph, D. D. (1996), "Cement-lined pipes for water lubricated transport of heavy oil", *International Journal of Multiphase Flow*, vol. 22, no. 2, pp. 207-221.
- Bai, R., Chen, K. and Joseph, D. (1990), "Lubricated pipelining: stability of core-annular flow. Part V: experiments and comparison with theory. Submitted to", *J.Fluid Mech*, .
- Balakhrisna, T., Ghosh, S., Das, G. and Das, P. (2010a), "Oil-water flows through sudden contraction and expansion in a horizontal pipe-Phase distribution and pressure drop", *International Journal of Multiphase Flow*, vol. 36, no. 1, pp. 13-24.
- Balakhrisna, T., Ghosh, S., Das, G. and Das, P. (2010b), "Oil-water flows through sudden contraction and expansion in a horizontal pipe-Phase distribution and pressure drop", *International Journal of Multiphase Flow*, vol. 36, no. 1, pp. 13-24.
- Bannwart, A. C., Rodriguez, O. M. H., De Carvalho, C. H. M., Wang, I. S. and Vara, R. M. O. P. (2004), "Flow Patterns in Heavy Crude Oil-Water Flow", *Journal of*

- Energy Resources Technology (Transactions of the ASME)*, vol. 126, no. 3, pp. 184-189.
- Barnea, D., Shoham, O. and Taitel, Y. (1980), "Flow pattern characterization in two phase flow by electrical conductance probe", *International Journal of Multiphase Flow*, vol. 6, no. 5, pp. 387-397.
- Beck, M. and Williams, R. (1996), "Process tomography: a European innovation and its applications", *Measurement Science and Technology*, vol. 7, no. 3, pp. 215.
- Bensakhria, A., Peysson, Y. and Antonini, G. (2004a), "Experimental study of the pipeline lubrication for heavy oil transport: Pipeline transportation of heavy oils= Ecoulement des bruts lourds dans les conduits", *Oil & gas science and technology*, vol. 59, no. 5, pp. 523-533.
- Bensakhria, A., Peysson, Y. and Antonini, G. (2004b), "Experimental study of the pipeline lubrication for heavy oil transport", *Oil & gas science and technology*, vol. 59, no. 5, pp. 523-533.
- Beretta, A., Ferrari, P., Galbiati, L. and Andreini, P. (1997), "Horizontal oil-water flow in small diameter tubes. Pressure drop", *International Communications in Heat and Mass Transfer*, vol. 24, no. 2, pp. 231-239.
- Besson, C. (2005), *Resources to Reserves: Oil and Gas Technologies for the Energy Markets of the Future*, OECD Publishing.
- Bird, R. B., Stewart, W. E. and Lightfoot, E. N. (2006), *Transport phenomena*, Wiley.
- Brauner, N. (1991), "Two-phase liquid-liquid annular flow", *International Journal of Multiphase Flow*, vol. 17, no. 1, pp. 59-76.
- Brauner, N. and Moalem Maron, D. (1992), "Flow pattern transitions in two-phase liquid-liquid flow in horizontal tubes", *International Journal of Multiphase Flow*, vol. 18, no. 1, pp. 123-140.
- Brauner, N. and Ullmann, A. (2002), "Modelling of phase inversion phenomenon in two-phase pipe flow", *International Journal of Multiphase Flow*, vol. 28, pp. 1177.
- Chang, C., Nguyen, Q. D. and Rønningsen, H. P. (1999), "Isothermal start-up of pipeline transporting waxy crude oil", *Journal of Non-Newtonian Fluid Mechanics*, vol. 87, no. 2, pp. 127-154.
- Condolios, E. and Chapus, E. E. (1963), "Transporting solid materials in pipelines", *Chemical Engineering*, vol. 70, no. 13.

- Danielson, T. (2007), "Sand Transport Modeling in Multiphase Pipelines", *Offshore Technology Conference*, .
- Das, S. K. and Butler, R. M. (1996), "Diffusion coefficients of propane and butane in Peace River bitumen", *The Canadian Journal of Chemical Engineering*, vol. 74, no. 6, pp. 985-992.
- Davidson, M. R., Dzuy Nguyen, Q., Chang, C. and Rønningsen, H. P. (2004), "A model for restart of a pipeline with compressible gelled waxy crude oil", *Journal of Non-Newtonian Fluid Mechanics*, vol. 123, no. 2, pp. 269-280.
- Davies, J. (1987), "Calculation of critical velocities to maintain solids in suspension in horizontal pipes", *Chemical engineering science*, vol. 42, no. 7, pp. 1667-1670.
- Dean, R. (1978), "Reynolds number dependence of skin friction and other bulk flow variables in two-dimensional rectangular duct flow", *J.Fluids Eng*, vol. 100, pp. 215–223.
- Decarre, S. and Fabre, J. (1997), "Phase inversion prediction study", *Journal of L'Institut Francais du Petrole*, , pp. 415-424.
- Dewan, A. (2010), *Tackling Turbulent Flows in Engineering*, Springer.
- Doherty, J., Ngan, P., Monty, J. and Chong, M. (2010), "The development of turbulent pipe flow", *16th Australasian Fluid Mechanics Conference (AFMC)*, 2-7 December, School of Engineering, The University of Queensland, pp. 266.
- Doron, P. and Barnea, D. (1993), "A three-layer model for solid-liquid flow in horizontal pipes", *International Journal of Multiphase Flow*, vol. 19, no. 6, pp. 1029-1043.
- Doron, P., Granica, D. and Barnea, D. (1987), "Slurry flow in horizontal pipes— experimental and modeling", *International Journal of Multiphase Flow*, vol. 13, no. 4, pp. 535-547.
- Doron, P. and Barnea, D. (1995), "Pressure drop and limit deposit velocity for solid-liquid flow in pipes", *Chemical engineering science*, vol. 50, no. 10, pp. 1595-1604.
- Durand, R. and Condolios, E. (1952), "Hydraulic Transportation of Coal and Solid Material in Pipes", *London Colloquium of the National Coal Board*, .
- Durst, F., Ray, S., Ünsal, B. and Bayoumi, O. (2005), "The development lengths of laminar pipe and channel flows", *Journal of Fluids Engineering*, vol. 127, pp. 1154.

- Dusseault, M. (1993), "Cold Production and Enhanced Oil Recovery", *Journal of Canadian Petroleum Technology*, vol. 32, no. 9.
- Dusseault, M., Geilikman, M. and Roggensack, W. (1995), "Practical requirements for sand production implementation in heavy oil applications", *SPE International Heavy Oil Symposium*, .
- Ekweribe, C., Civan, F., Lee, H. S. and Singh, P. (2008), "Effect of system pressure on restart conditions of subsea pipelines", *SPE Annual Technical Conference and Exhibition*, .
- Fluent, A. (2009), "12.0 Theory Guide", *Ansys Inc*, vol. 5.
- Ghosh, S., Das, G. and Das, P. K. (2010), "Simulation of core annular downflow through CFD-A comprehensive study", *Chemical Engineering and Processing: Process Intensification*, .
- Gillies, R., Mckibben, M. and Shook, C. (1995), "Oil, Water And Sand Flow Experiments In a Model Horizontal Well", *Journal of Canadian Petroleum Technology*, vol. 34, no. 9.
- Gillies, R. G., Shook, C. A. and Xu, J. (2004), "Modelling heterogeneous slurry flows at high velocities", *The Canadian Journal of Chemical Engineering*, vol. 82, no. 5, pp. 1060-1065.
- Gillies, R., Shook, C. and Wilson, K. (1991), "An improved two layer model for horizontal slurry pipeline flow", *The Canadian Journal of Chemical Engineering*, vol. 69, no. 1, pp. 173-178.
- Golczynski, T. and Niesen, V. (2002), "Thermal Behavior During Restart of Ultradeepwater Flowlines", *SPE Annual Technical Conference and Exhibition*, .
- Gong, J., Li, Q., Yao, H. and Yu, D. (2006), "Model for predicting phase inversion in oil-water two-phase pipe flow", *Journal of Hydrodynamics, Series B*, vol. 18, no. 3, pp. 310-314.
- Grain, C. (1990), "Interfacial tension with water", *IN: Handbook of Chemical Property Estimation Methods: Environmental Behavior of Organic Compounds*. American Chemical Society, Washington, DC.1990.21.1-21.16.2 fig, 4 tab, 11 ref., .
- Guevara, E., Gonzalez, J. and Ninez, G. (1997), "[8] 4 Highly Viscous Oil Transportation Methods in the Venezuelan Oil Industry", *15th World Petroleum Congress*, .

- Han, G., Ling, K., Khor, S., Zhang, H. and Zhang, H. (2012), "Simulation of Multiphase Fluid-Hammer Effects During Well Shut-In and Opening", *SPE Asia Pacific Oil and Gas Conference and Exhibition*, .
- Harkins, W. D. and Jordan, H. F. (1930), "A method for the determination of surface and interfacial tension from the maximum pull on a ring", *Journal of the American Chemical Society*, vol. 52, no. 5, pp. 1751-1772.
- Hasson, D., Mann, V. and Nir, A. (1970), "Annular flow of two immiscible liquids I. mechanisms", *The Canadian Journal of Chemical Engineering*, vol. 48, no. 5, pp. 514-520.
- Issa, R. (1986), "Solution of the implicitly discretised fluid flow equations by operator-splitting", *Journal of Computational physics*, vol. 62, no. 1, pp. 40-65.
- Jana, A. K., Das, G. and Das, P. K. (2006a), "A novel technique to identify flow patterns during liquid-liquid two-phase upflow through a vertical pipe", *Industrial & Engineering Chemistry Research*, vol. 45, no. 7, pp. 2381-2393.
- Jana, A. K., Das, G. and Das, P. K. (2006b), "Flow regime identification of two-phase liquid-liquid upflow through vertical pipe", *Chemical Engineering Science*, vol. 61, no. 5, pp. 1500-1515.
- Jha, K. (1986), "A laboratory study of heavy oil recovery with carbon dioxide", *Journal of Canadian Petroleum Technology*, , pp. 54-63.
- Jones Jr, O. C. and Zuber, N. (1975), "The interrelation between void fraction fluctuations and flow patterns in two-phase flow", *International Journal of Multiphase Flow*, vol. 2, no. 3, pp. 273-306.
- Jones, W. and Launder, B. (1973), "The calculation of low-Reynolds-number phenomena with a two-equation model of turbulence", *International Journal of Heat and Mass Transfer*, vol. 16, no. 6, pp. 1119-1130.
- Joseph, D., Bai, R., Chen, K. and Renardy, Y. (1997), "Core-annular flows", *Annual Review of Fluid Mechanics*, vol. 29, no. 1, pp. 65-90.
- Kashid, M. N., Gerlach, I., Goetz, S., Franzke, J., Acker, J., Platte, F., Agar, D. and Turek, S. (2005), "Internal circulation within the liquid slugs of a liquid-liquid slug-flow capillary microreactor", *Industrial & Engineering Chemistry Research*, vol. 44, no. 14, pp. 5003-5010.

- Kashid, M. N., Gupta, A., Renken, A. and Kiwi-Minsker, L. (2010a), "Numbering-up and mass transfer studies of liquid–liquid two-phase microstructured reactors", *Chemical Engineering Journal*, vol. 158, no. 2, pp. 233-240.
- Kashid, M. N., Renken, A. and Kiwi-Minsker, L. (2010b), "CFD modelling of liquid–liquid multiphase microstructured reactor: Slug flow generation", *Chemical Engineering Research and Design*, vol. 88, no. 3, pp. 362-368.
- Kashid, M., Agar, D. and Turek, S. (2007), "CFD modelling of mass transfer with and without chemical reaction in the liquid–liquid slug flow microreactor", *Chemical Engineering Science*, vol. 62, no. 18, pp. 5102-5109.
- Kashid, M., Kowaliński, W., Renken, A., Baldyga, J. and Kiwi-Minsker, L. (2012a), "Analytical method to predict two-phase flow pattern in horizontal micro-capillaries", *Chemical Engineering Science*, vol. 74, pp. 219-232.
- Kashid, M., Kowaliński, W., Renken, A., Baldyga, J. and Kiwi-Minsker, L. (2012b), "Analytical method to predict two-phase flow pattern in horizontal micro-capillaries", *Chemical Engineering Science*, vol. 74, pp. 219-232.
- Kashid, M., Rivas, D. F., Agar, D. and Turek, S. (2008), "On the hydrodynamics of liquid–liquid slug flow capillary microreactors", *Asia-Pacific Journal of Chemical Engineering*, vol. 3, no. 2, pp. 151-160.
- Kaushik, V., Ghosh, S., Das, G. and Das, P. K. (2012), "CFD simulation of core annular flow through sudden contraction and expansion", *Journal of Petroleum Science and Engineering*, .
- King, M. J. S., Fairhurst, C. P. and Hill, T. J. (2001), "Solids transport in multiphase flows - application to high-viscosity systems", *Journal of Energy Resources Technology (Transactions of the ASME)*, vol. 123, no. 3, pp. 200-204.
- Ko, T., Choi, H., Bai, R. and Joseph, D. (2002), "Finite element method simulation of turbulent wavy core–annular flows using a $k-\omega$ turbulence model method", *International Journal of Multiphase Flow*, vol. 28, no. 7, pp. 1205-1222.
- Krampa, F. (2009), *Two-Fluid Modelling of Heterogenous Coarse Particle Slurry Flows* (PhD thesis), University of Saskatchewan, Saskatoon, Saskatchewan, Canada.
- Kumar, S., Kumar, R. and Gandhi, K. (1991), "Influence of the wetting characteristics of the impeller on phase inversion", *Chemical engineering science*, vol. 46, no. 9, pp. 2365-2367.

- Kvicinsky, S., Longatte, F., Kueny, J. and Avellan, F. (1999), "Free surface flows: experimental validation of volume of fluid (VOF) method in the plane wall case", *Proceedings of the 3rd ASME/JSME Joint Fluids Engineering Conference*, .
- Lien, K., Monty, J., Chong, M. and Ooi, A. (2004), "The entrance length for fully developed turbulent channel flow", *15th Australasian Fluid Mechanics Conference (Sydney, Australia)*, 13-17 December, .
- Lin, T. R., Guo, B., Song, S., Ghalambor, A. and Chacko, J. (2005), *Offshore pipelines*, Gulf Professional Publishing.
- Ling, J., Skudarnov, P., Lin, C. and Ebadian, M. (2003), "Numerical investigations of liquid–solid slurry flows in a fully developed turbulent flow region", *International Journal of Heat and Fluid Flow*, vol. 24, no. 3, pp. 389-398.
- Martinez, A., Arirachakaran, S., Shoham, O. and Brill, J. (1988), "Prediction of Dispersion Viscosity of Oil/Water Mixture Flow in Horizontal Pipes", *SPE Annual Technical Conference and Exhibition*, .
- Matoušek, V. (2005), "Research developments in pipeline transport of settling slurries", *Powder Technology*, vol. 156, no. 1, pp. 43-51.
- Matsui, G. (1984), "Identification of flow regimes in vertical gas-liquid two-phase flow using differential pressure fluctuations", *International Journal of Multiphase Flow*, vol. 10, no. 6, pp. 711-719.
- Matsui, G. (1986), "Automatic identification of flow regimes in vertical two-phase flow using differential pressure fluctuations", *Nuclear Engineering and Design*, vol. 95, pp. 221-231.
- McKibben, M. J. and Gillies, R. G. (2009), *Water-Assisted Pipeline Transport of Bitumen/Heavy Oils and Co-Produced Sand*, PTRC No. 001-00086-SRC (Year 3), SRC Publication No. 11716-1C09, Saskatchewan, Canada.
- McKibben, M. J., Gillies, R. G. and Shook, C. A. (2000a), "A laboratory investigation of horizontal well heavy oil—water flows", *The Canadian Journal of Chemical Engineering*, vol. 78, no. 4, pp. 743-751.
- McKibben, M. J., Gillies, R. G. and Shook, C. A. (2000b), "Predicting pressure gradients in heavy oil-water pipelines", *The Canadian Journal of Chemical Engineering*, vol. 78, no. 4, pp. 752-756.

- McKibben, M., Gillies, R., Sun, R. and Sanders, S. (2006), *Water-Assisted Pipeline Transport of Bitumen/Heavy Oils and Co-Produced Sand*, PTRC No. 001-00086-SRC (Year 1), SRC Publication No. 11716-1C06, Saskatchewan, Canada.
- Mehrotra, A. K. and Patience, G. S. (1990), "Unified entry length for Newtonian and power-law fluids in laminar pipe flow", *The Canadian Journal of Chemical Engineering*, vol. 68, no. 4, pp. 529-533.
- Mehta, A., Zabaraz, G., Schoppa, W. and Peters, D. (2004), "Unlocking Deepwater Heavy Oil Reserves-A Flow Assurance Perspective", *Offshore Technology Conference*, .
- Monty, J., Stewart, J., Williams, R. and Chong, M. (2007), "Large-scale features in turbulent pipe and channel flows", *Journal of Fluid Mechanics*, vol. 589, pp. 147-156.
- Munroe, N. (2009), *Solvent Based Enhanced Oil Recovery for In-Situ Upgrading of Heavy Oil Sands*, .
- Newitt, D., Richardson, J., Abbott, M. and Turtle, R. (1955), "Hydraulic conveying of solids in horizontal pipes", *Trans.Instn.Chem.Engrs*, vol. 33, no. 1, pp. 93-113.
- Nooralahiyan, A., Hoyle, B. and Bailey, N. (1994), "Neural network for pattern association in electrical capacitance tomography", *Circuits, Devices and Systems, IEE Proceedings-*, Vol. 141, IET, pp. 517.
- Norato, M. A., Tavlarides, L. L. and Tsouris, C. (1998), "Phase inversion studies in liquid-liquid dispersions", *The Canadian Journal of Chemical Engineering*, vol. 76, no. 3, pp. 486-494.
- Oliemans, R., Ooms, G., Wu, H. and Duijvestijn, A. (1987), "Core-annular oil/water flow: the turbulent-lubricating-film model and measurements in a 5 cm pipe loop", *International Journal of Multiphase Flow*, vol. 13, no. 1, pp. 23-31.
- Ooms, G. and Poesio, P. (2003), "Stationary core-annular flow through a horizontal pipe", *Physical Review E*, vol. 68, no. 6, pp. 066301.
- Oroskar, A. R. and Turian, R. M. (1980), "The critical velocity in pipeline flow of slurries", *AIChE Journal*, vol. 26, no. 4, pp. 550-558.
- Owen, N. A., Inderwildi, O. R. and King, D. A. (2010), "The status of conventional world oil reserves—Hype or cause for concern?", *Energy Policy*, vol. 38, no. 8, pp. 4743-4749.

- Perry, A. E. and Abel, C. J. (1978), "Scaling laws for pipe-flow turbulence", *Journal of Fluid Mechanics*, vol. 67, pp. 257-271.
- Poole, R. and Chhabra, R. (2010), "Development Length Requirements for Fully Developed Laminar Pipe Flow of Yield Stress Fluids", *Journal of Fluids Engineering*, vol. 132, pp. 034501.
- Poole, R. and Ridley, B. (2007), "Development-length requirements for fully developed laminar pipe flow of inelastic non-Newtonian liquids", *Journal of Fluids Engineering*, vol. 129, pp. 1281.
- Prada, J. W. V. and Bannwart, A. C. (2001a), "Modeling of vertical core-annular flows and application to heavy oil production", *Journal of energy resources technology*, vol. 123, pp. 194.
- Prada, J. W. V. and Bannwart, A. C. (2001b), "Modeling of vertical core-annular flows and application to heavy oil production", *Journal of energy resources technology*, vol. 123, pp. 194.
- Prada, J. W. V. and Bannwart, A. C. (2001c), "Modeling of vertical core-annular flows and application to heavy oil production", *Journal of energy resources technology*, vol. 123, pp. 194.
- Qing, Y. X. (1986), *The pressure gradient for heterogeneous flow of coal, sand and iron in pipelines*, 86, THDelft, Delft University of Technology.
- Rhee, S., Makarov, B., Krishnan, H. and Ivanov, V. (2004), "Assessment of numerical techniques in volume of fluid method for free-surface wave flows", *Proceedings 9th symposium on practical design of ships and other floating structures, Luebeck-Travemuende*, .
- Rodriguez, O. M. H. and Bannwart, A. C. (2008), "Stability analysis of core-annular flow and neutral stability wave number", *AIChE Journal*, vol. 54, no. 1, pp. 20-31.
- Rodriguez, O., Bannwart, A. and de Carvalho, C. (2009), "Pressure loss in core-annular flow: Modeling, experimental investigation and full-scale experiments", *Journal of Petroleum Science and Engineering*, vol. 65, no. 1-2, pp. 67-75.
- Rodriguez, O. and Oliemans, R. (2006), "Experimental study on oil-water flow in horizontal and slightly inclined pipes", *International Journal of Multiphase Flow*, vol. 32, no. 3, pp. 323-343.
- Russell, T. and Charles, M. (1959), "The effect of the less viscous liquid in the laminar flow of two immiscible liquids", *Can.J.Chem.Eng*, vol. 37, pp. 18-24.

- Sanders, R. S., Ko, T., Bai, R. and Joseph, D. D. (2004), "Factors Governing Friction Losses in Self-lubricated Transport of Bitumen Froth: 1. Water Release", *The Canadian Journal of Chemical Engineering*, vol. 82, no. 4, pp. 735-742.
- Selker, A. and Sleicher, C. (1965), "Factors affecting which phase will disperse when immiscible liquids are stirred together", *The Canadian Journal of Chemical Engineering*, vol. 43, no. 6, pp. 298-301.
- Shook, C. A., Gillies, R. G. and Sanders, R. S. S. (2002), *Pipeline Hydrotransport: With Applications in the Oil Sand Industry*, SRC Pipe Flow Technology Centre.
- Sotgia, G., Tartarini, P. and Stalio, E. (2008), "Experimental analysis of flow regimes and pressure drop reduction in oil-water mixtures", *International Journal of Multiphase Flow*, vol. 34, no. 12, pp. 1161-1174.
- Speight, J. G. (2009a), *Enhanced recovery methods for heavy oil and tar sands*, Gulf Publishing Company.
- Speight, J. (2009b), *Enhanced Recovery Methods for Heavy Oil and Tar Sands*, First Edition ed, Gulf Publishing Company, Houston, Texas.
- Strazza, D., Grassi, B., Demori, M., Ferrari, V. and Poesio, P. (2011), "Core-annular flow in horizontal and slightly inclined pipes: Existence, pressure drops, and holdup", *Chemical Engineering Science*, .
- Sumner, R., McKibben, M. and Shook, C. (1990), "Concentration and velocity distribution in turbulent vertical slurry flow", *Ecoulements Solide Liquide*, vol. 2, no. 2, pp. 33-42.
- Surguchev, L., Korbol, R. and Krakstad, O. (1992), "Optimum Water Alternate Gas Injection Schemes for Stratified Reservoirs", *SPE Annual Technical Conference and Exhibition*, .
- Takahashi, H., Masuyama, T. and Noda, K. (1989), "Unstable flow of a solid-liquid mixture in a horizontal pipe", *International Journal of Multiphase Flow*, vol. 15, no. 5, pp. 831-841.
- Tang, Y. and Wong, S. (2005), "A Flow-Assurance Study for a Satellite Crude-Oil System With Severe Emulsion", *SPE Annual Technical Conference and Exhibition*, .
- Tennekes, H. and Lumley, J. L. (1972), *A first course in turbulence*, MIT press.

- Thomas, A. (1979), "Predicting the deposit velocity for horizontal turbulent pipe flow of slurries", *International Journal of Multiphase Flow*, vol. 5, no. 2, pp. 113-129.
- Thomas, D. G. (1962), "Characteristics of Suspension:Part VI Minimum Transport Velocity of Large Particle Size Suspensions in Round Horizontal Pipes", *A.I.Ch.E Journal*, vol. 8, no. 3, pp. 373-378.
- Thomas, S. (2008), "Enhanced Oil Recovery-An Overview", *Oil & Gas Science and Technology-Revue de l'IFP*, vol. 63, no. 1, pp. 9-19.
- Tice, J. D., Lyon, A. D. and Ismagilov, R. F. (2004), "Effects of viscosity on droplet formation and mixing in microfluidic channels", *Analytica Chimica Acta*, vol. 507, no. 1, pp. 73-77.
- Trallero, J., Sarica, C. and Brill, J. (1997), "A study of oil-water flow patterns in horizontal pipes", *Old Production & Facilities*, vol. 12, no. 3, pp. 165-172.
- Tronvoll, J., Dusseault, M., Sanfilippo, F. and Santarelli, F. (2001), "The tools of sand management", *SPE Annual Technical Conference and Exhibition*, .
- Turian, R., Hsu, F. and Ma, T. (1987), "Estimation of the critical velocity in pipeline flow of slurries", *Powder Technology*, vol. 51, no. 1, pp. 35-47.
- van Wachem, B. and Almstedt, A. (2003), "Methods for multiphase computational fluid dynamics", *Chemical Engineering Journal*, vol. 96, no. 1, pp. 81-98.
- Veil, J. A. and Quinn, J. J. (2009), *Water issues associated with heavy oil production*, ANL/EVS/R-08/4, Argonne National Laboratory (ANL), United States.
- Versteeg, H. K. and Malalasekera, W. (2007), *An introduction to computational fluid dynamics: the finite volume method*, Prentice Hall.
- Vinay, G., Wachs, A. and Frigaard, I. (2007), "Start-up transients and efficient computation of isothermal waxy crude oil flows", *Journal of Non-Newtonian Fluid Mechanics*, vol. 143, no. 2, pp. 141-156.
- Vinay, G., Wachs, A. and Agassant, J. (2006), "Numerical simulation of weakly compressible Bingham flows: The restart of pipeline flows of waxy crude oils", *Journal of Non-Newtonian Fluid Mechanics*, vol. 136, no. 2, pp. 93-105.
- Wang, W. and Gong, J. (2009), "Experiment research of phase inversion in mineral oil-water two-phase flow in horizontal pipe", *Journal of Energy Resources Technology.Transactions of the ASME*, vol. 131, no. 4.

- Wang, W. and Gong, J. (2010), "Flow regimes and flow transition characters of the high viscosity oil-water two phase flow", *CPS/SPE International Oil & Gas Conference and Exhibition*, Vol. SPE 130850, 8-10 June, China, SPE, .
- Wasp, E. J., Kenny, J. P. and Gandhi, R. L. (1977), "Solid-liquid flow: slurry pipeline transportation.[Pumps, valves, mechanical equipment, economics]", *Ser.Bulk Mater.Handl.:(United States)*, vol. 1, no. 4.
- Wicks, M. (1971), "Transport of solids at low concentration in horizontal pipes", *Presented at the ASCE-Pennsylvania University International Symposium," Advances in Solid-Liquid Flow in Pipes and its Applications", Philadelphia, Pennsylvania, March 4-6, 1968.* .
- Williams, T., Hsu, J. and Patterson, H. (1996), "Measurement of break away yield stress of waxy crude oil and pipeline restart system design", *Offshore Technology Conference*, .
- Wilson, K., Sellgren, A. and Addie, G. (2000), "Near-wall fluid lift of particles in slurry pipelines", *Zeszyty Naukowe Akademii Rolniczej we Wroclawiu.Konferencje*, .
- Yan, W., Al-lababidi, S. and Yeung, H. (2009), *Sand Transport in Multiphase Pipelines*, 09/HY/540, Cranfield University.
- Yang, C. and Gu, Y. (2006), "Diffusion coefficients and oil swelling factors of carbon dioxide, methane, ethane, propane, and their mixtures in heavy oil", *Fluid Phase Equilibria*, vol. 243, no. 1-2, pp. 64-73.
- Yeh, G. C., Haynie Jr, F. H. and Moses, R. A. (1964), "Phase-volume relationship at the point of phase inversion in liquid dispersions", *AIChE Journal*, vol. 10, no. 2, pp. 260-265.
- Yeo, L. Y., Matar, O. K., Perez de Ortiz, E Susana and Hewitt, G. F. (2002), "A simple predictive tool for modelling phase inversion in liquid-liquid dispersions", *Chemical engineering science*, vol. 57, no. 6, pp. 1069.
- Zagarola, M. V. and Smits, A. J. (1998), "Mean-flow scaling of turbulent pipe flow", *Journal of Fluid Mechanics*, vol. 373, pp. 33-79.

APPENDICES

Appendix A Test Section

A.1 Pipe Length for Fully Developed Flow

The choice of minimum pipe length for flow simulation in a conduit is an important factor for a meaningful modelling. This choice depends on the flow development (i.e. flow region in which the velocity, pressure profile etc. is not changing or a region where boundary layers meet at the centre of the pipe) which occurs in the region after the entrance length (i.e. the length from the inlet along the direction of flow where the velocity fluctuates). The minimum pipe length for channel flows was determined experimentally by different investigators for both laminar and turbulent flow regimes. Examples of these research are (Lien et al., 2004; Poole and Ridley, 2007; Doherty et al., 2010; Poole and Chhabra, 2010). This is measured by determining the entrance length Le , of the flowing fluid(s) which is the distance between the pipe inlet and the point where the velocity profile is fully developed. The summary of some research is presented in the Table 3-2. In this research, the regime of fluid near wall depends on the composition of the multiphase fluids (oil-water, gas-oil, oil-water-gas, oil-water-sand), hence the choice of pipe length may assume either laminar or turbulent flow at any given condition. Since there is no consensus on which correlation is the best, this research shall employ a sufficiently long pipe (i.e. 200 diameters) for its simulations so as to accommodate all published views.

Table A-1: Pipe length requirement for fully developed flow

Author	Regime	Reynolds ($\times 10^3$)	Minimum Pipe Length
(Perry and Abel, 1978)	Turbulent	80-260	71.9D
(Dean, 1978)	Turbulent	-	23-300D
(Zagarola and Smits, 1998)	Turbulent	300-40000	$\left(\frac{0.5}{f} + \frac{5}{f^{1/2}}\right)D$
(Lien et al., 2004)	Turbulent	40, 105, 185	150D
(Doherty et al., 2010)	Turbulent	100, 200	80D
(Monty et al., 2007)	Turbulent	-	175D
(Mehrotra and Patience, 1990)	Laminar (Newtonian)	>200 ($0.75 < n < 1.5$)	$0.056D(Re)$
(Durst et al., 2005)	Laminar (Newtonian)	$Re \rightarrow 0,$ $Re \rightarrow \infty$	$[0.619 + 0.0567Re]D$
(Poole and Ridley, 2007)	Laminar (Non-Newtonian)	0-1 ($0.4 < n < 1.5$)	$[0.246n^2 - 0.675n + 1.03 + 0.0567Re]D$
(Poole and Chhabra, 2010)	Laminar (Non-Newtonian)	≤ 40	$[0.619 + 0.0567Re]D$

A.2 Flow Development

A fully-developed flow can be defined as a flow condition when the flow parameters do not change with the length of the flow channel. In this section the development of the

flow was studied from a CFD simulation point of view to determine whether the length of pipe used in the experiment and the CFD simulation is sufficient enough for studying the flow behaviour in question. The advantage of the CFD simulation with respect to the physical experiment is the possibility to record the parameters of interest at many measurement sections along the pipe. The comparison of the volume fraction results from the simulation performed with 1, 2.5 and 5m long pipes are presented in the Figure A-1. The holdup in the 5m long pipe appears similar to that of 2.5m long pipe for a good portion time. It shows that the fully developed flow is experienced when the length to diameter ratio, $L/D = 90$.

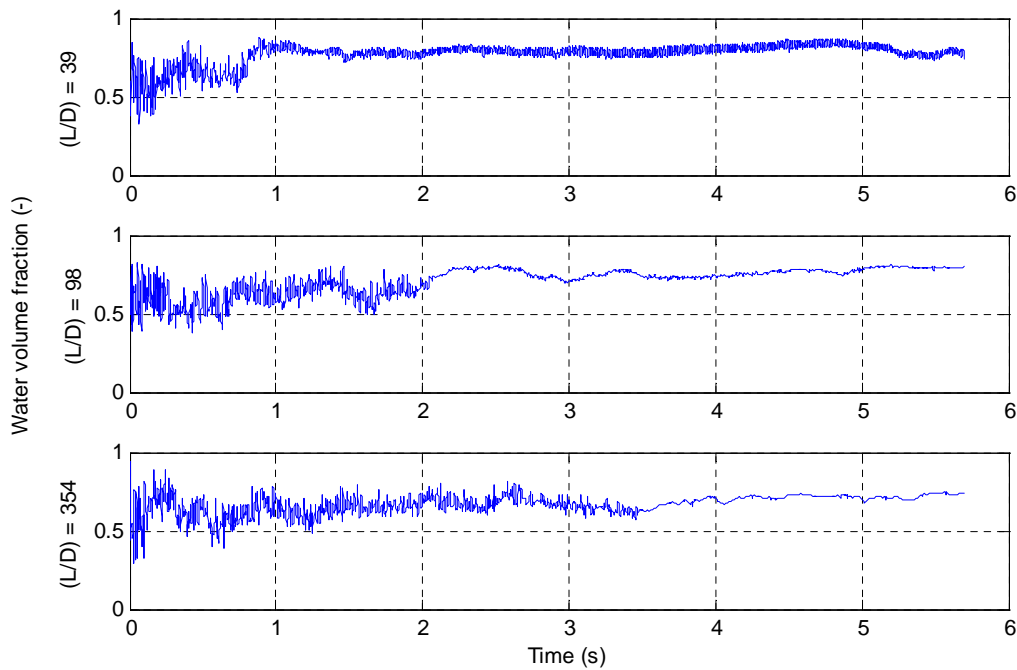


Figure A-1: Water volume fraction time traces

Appendix B Oil-Water Parametric Studies

B.1 Further CFD Parametric Investigations on Oil-Water Flow

This section aimed at exploring the potential of the general purpose CFD code FLUENT for simulating characteristics of oil-water flow in horizontal pipe flow when the carrier fluid has deviated property from that which was used in this research. The assumptions considered in setting up this model in this section remain the same as stated in Chapter 4 above.

In this chapter, a description of the CFD model and the results obtained is presented. The results presented here include the pressure, and phase distribution. The prediction of these behaviours in a flow field is very important for effective and safe pipeline design. In this section, the effects of water density are considered in the transport of two-phase oil-water flow.

B.2 Effect of Water Densities on Oil-Water Flow in Horizontal Pipe

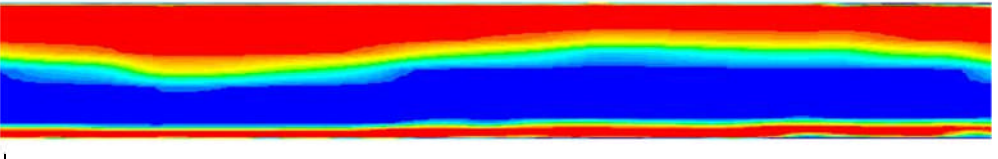
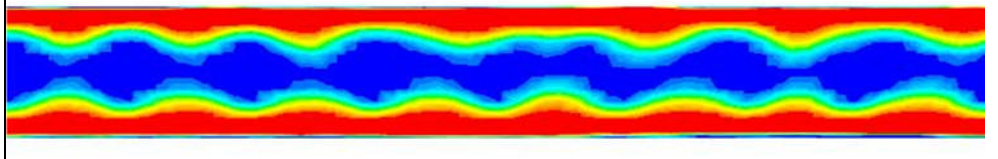
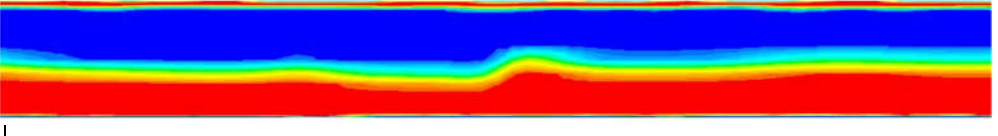
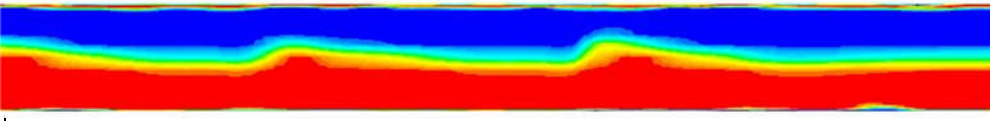
The knowledge of physical properties of the phases in crude oil is necessary if the behaviour and characteristics of their multiphase flows are to be predicted correctly. These properties are essential for the development of multiphase metering devices, equipment and pipeline design. Depending on the flow conditions, flow regime transition could occur and this also could be accompanied by some noticeable anomalies of some physical properties of the phase(s) involved. These may cause a significant increase in the pressure gradient and flow instability in the pipe. In the oilfield, the waters are usually salty having higher densities than the fresh water used mostly in the laboratory. Gillies et al. (1995) reported 1013 kg/m^3 as the density of the produced water used in their oil-water-sand flow experiments in the horizontal wellbore flow tests. Evdokimov et al., (2005) reported some Russia oilfield water to be in the range $1148\text{-}1175 \text{ kg/m}^3$, i.e. salt contents are about 150g/l and Rodriguez and Oliemans (2006) used brine having 1060kg/m^3 for their oil-water tests. This section considers the effects of water density on the pressure gradient and flow regime patterns using CFD simulation.

Table B-1: Pressure gradients of oil-water flow in horizontal pipe at different water densities

Water Cut (-)	Density (kg/m ³)			
	890	924	998	1175
	Pressure Gradients (kPa/m)			
0.27	3.21	2.97	4.16	25.92
0.65	5.27	5.33	5.64	8.09

Table B-1 show that the densities of process water contribute noticeably in the pressure gradient and the flow pattern of the oil-water flow in the horizontal pipe. Table B-1 also reveals that the higher the density of the process waters the higher the pressure gradient. This invariably means that the annular flow might not be sustained when the water density is very high compares to that of the oil. The flow contours in Table B-2 exposes the flow configurations with respect to the water density. It could be seen that the flow stratification is encouraged when the difference between the density of oil and water is significant. Oil flows closed to the bottom of the pipe when its density is higher than that of water and the configuration is vice versa when the order is reversed. This observation is agreement with

Table B-2: Effect of water density on oil-water flow configuration

Water Density (kg/m ³)	Contour
890	
924	
998	
1175	

B.3 Chapter Summary

The CFD parametric study of the effect of process water density was carried out on oil-water flow in this chapter. This is necessary to predict the expected behaviour in such situations. This information will also help in the design of pipeline for heavy oil transport.

The effect of the density of the continuous phase (i.e. water) explored was found to promote flow stratification as water density increases, although the pressure drops did not noticeable vary from that of the fresh water at high flow rates.

Appendix C Single Phase Flow Analysis

The figure below presents the plots and comparison of single phase oil flow at 3300cP employing three different approaches; the experiment, Darcy-Weisbach and CFD. The figure shows that the experimental data had a little deviation from the theoretical while CFD also agrees with the theoretical model.

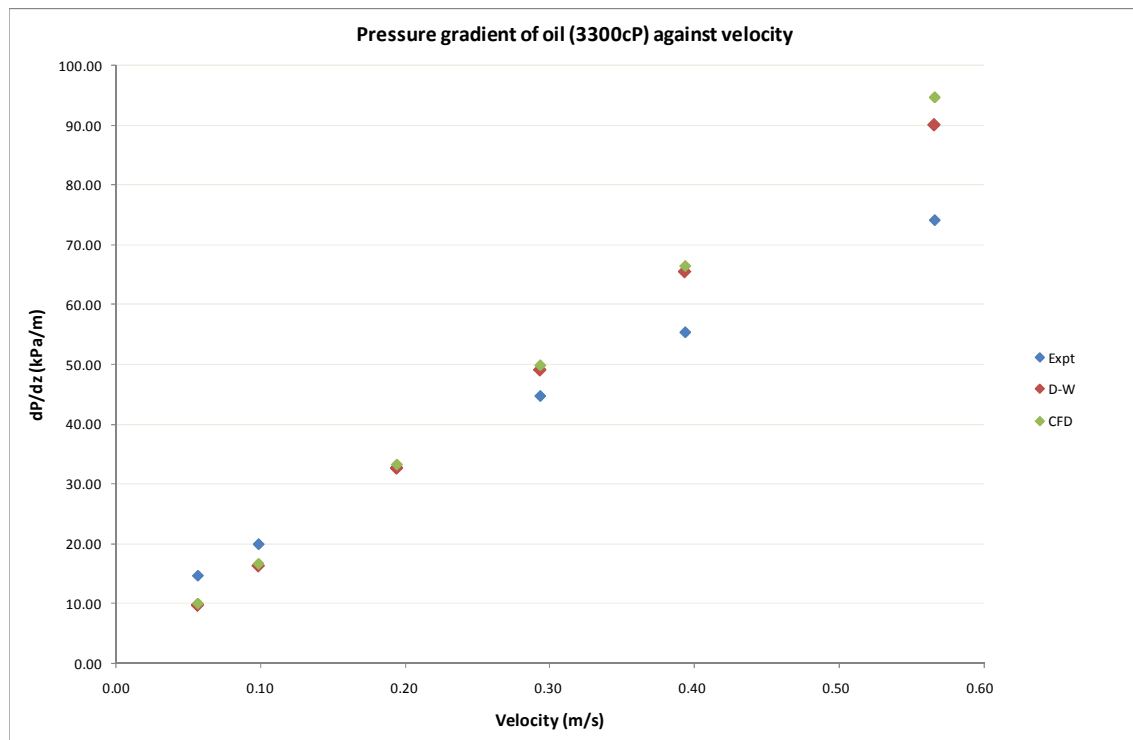


Table C-1: Comparison of CFD, D-W and Experimental pressure gradients of a single phase oil in 1-in ID 5m long pipe

Appendix D Statistical Analysis

The error analysis were carried out using the following approaches; the percentage error is given by

$E_i = \frac{\varphi_{predicted} - \varphi_{measured}}{\varphi_{measured}} \times 100$	D-1
--	-----

While the average percentage error is given by

$\bar{E} = \frac{1}{N} \sum_{i=1}^N E_i$	D-2
--	-----

where N is the total number of test conditions at which values of E_i were obtained and the standard deviation \bar{S} of the percentage error in the predicted values is obtained by

$\bar{S} = \left(\frac{1}{N} \sum_{i=1}^N (E_i - \bar{E})^2 \right)^{1/2}$	D-3
---	-----

the average absolute error in the predicted values is given by

$\bar{E}_{absolute} = \frac{1}{N} \sum_{i=1}^N E_i $	D-4
---	-----

Appendix E Y-PLUS

Y-plus of oil-water flow at different V_{so} and V_{sw} are presented in the Figure E-1. It could be seen that all the points of y-plus are below 1.0 which is the recommended y-plus value for fine mesh that is needed to capture flow gradients close to the wall.

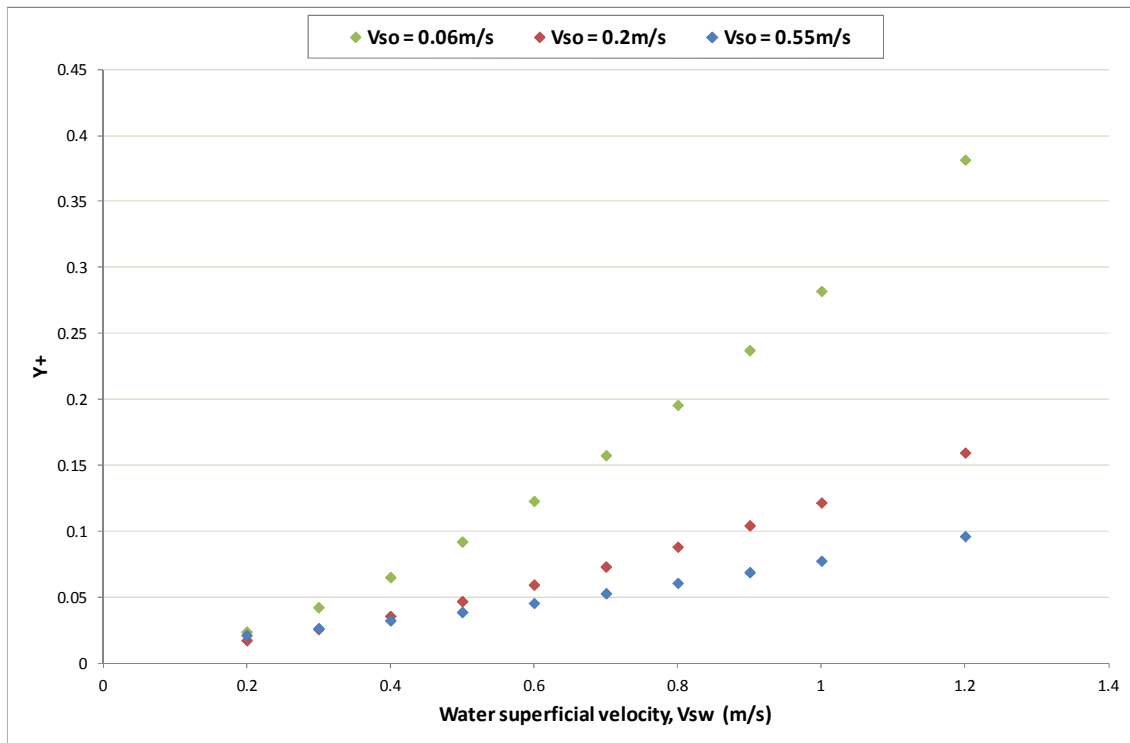


Figure E-1: Plot of $y+$ against superficial velocities of oil-water flow

Appendix F Fluctuating kinetic energy and dissipation rate correlation

The figure below shows the curve fitting plot for the development of the TKE and TDR budget that was employed in this research. The fluctuating (TKE) drops linearly with increase in water cut while the dissipation rate (TDR) drops in a quadratic form with increase in water cut.

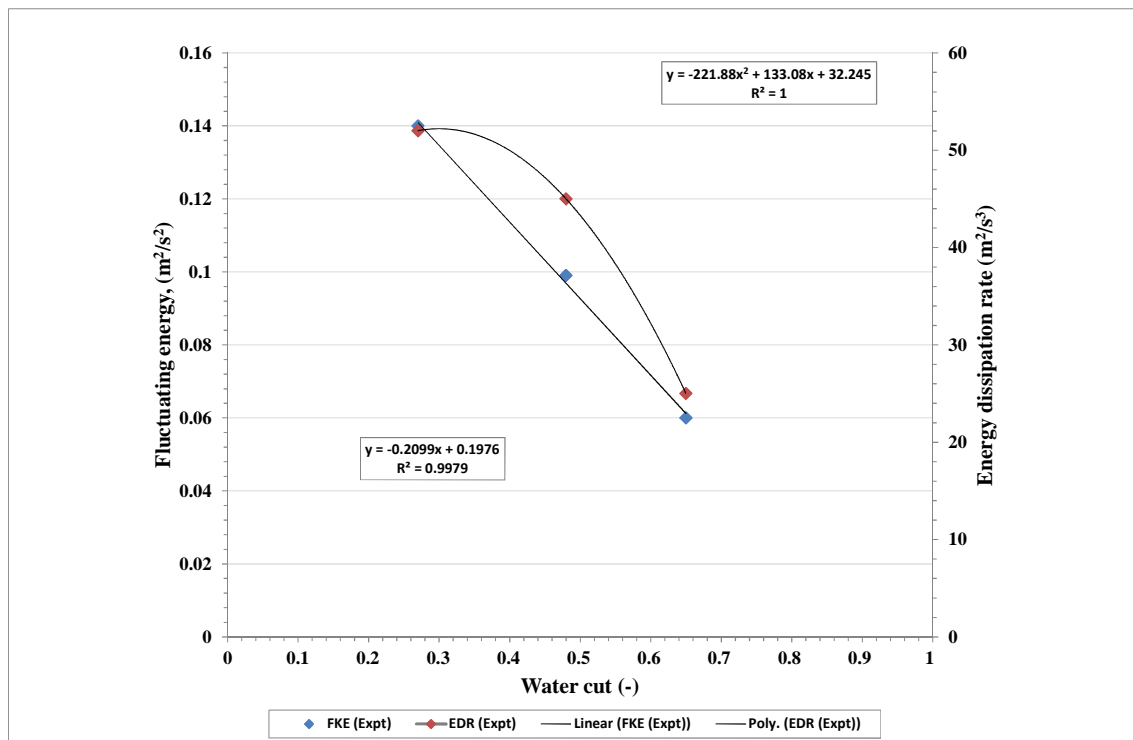


Figure F-1: Correlations of fluctuating energy and energy dissipation rate against water cut.

Appendix G User Defined Function

User Defined Function

```
/*
*****
unsteadytdr.c
UDF for specifying a transient tke/tdr profile boundary
condition
tdr=tdr0+Asin(wt)
*****
*****/
#include "udf.h"
#define wc 0.27 /* water cut */

/* profile for tke */
DEFINE_PROFILE(unsteady_tke, thread, position)
{
    face_t f;
    real t = CURRENT_TIME;
    begin_f_loop(f, thread)
    {
        F_PROFILE(f, thread, position) =ABS((0.1976-
        0.2099*wc)+0.0075*sin(12.5*t));
    }
    end_f_loop(f, thread)
}

/* profile for tdr */
DEFINE_PROFILE(unsteady_tdr, thread, position)
{
    face_t f;
    real t = CURRENT_TIME;
    real tdr;

    begin_f_loop(f, thread)
    {
        tdr = ABS((32.245+133.08*wc-221.88*wc*wc)+0.05*sin(12.5*t));
        if(tdr>15.0)

        F_PROFILE(f, thread, position) =ABS((32.245+133.08*wc-
        221.88*wc*wc)+0.05*sin(12.5*t));

    else

        F_PROFILE(f, thread, position) =16.6798+0.05*sin(12.5*t);

    }
    end_f_loop(f, thread)
}

/*
*****

```

```

UDF for changing velocity for shutin and restart
*****/
#include "udf.h"

#define Initial_Velocity_water 1.46

#define shutin_velocity_water 0.0

#define Restart_velocity_water 1.46

DEFINE_PROFILE(velocity_magnitude_water, t, i)
{
real velocity_mag_water;

real time = CURRENT_TIME;
face_t f;

if ((time>=0.0) && (time<=15.))
{
velocity_mag_water=Initial_Velocity_water;
}
if ((time>15.0) && (time<=20.0))
{
velocity_mag_water= shutin_velocity_water;
}

if ((time>20.0) && (time<30.0))
{
velocity_mag_water= Restart_velocity_water;
}

begin_f_loop(f,t)
{
F_PROFILE(f,t,i) = velocity_mag_water;
}
end_f_loop(f,t)
}

/*****
UDF for changing velocity for shutin and restart
*****/
#include "udf.h"

```

```

#define Initial_Velocity_oil 1.386

#define shutin_velocity_oil 0.0

#define Restart_velocity_oil 1.386

DEFINE_PROFILE(velocity_magnitude_oil, t, i)
{
real velocity_mag_oil;

real time = CURRENT_TIME;
face_t f;

if ((time>=0.0) && (time<=15.))
{
velocity_mag_oil=Initial_Velocity_oil;
}
if ((time>15.0) && (time<=20.0))
{
velocity_mag_oil= shutin_velocity_oil;
}
if ((time>20.0) && (time<30.0))
{
velocity_mag_oil= Restart_velocity_oil;
}

begin_f_loop(f,t)
{
F_PROFILE(f,t,i) = velocity_mag_oil;
}
end_f_loop(f,t)
}

```


Appendix H Experimental Data

Experimental Water-Sand Test Data

Table H-1: Slurry pressure gradients

Concentration	(1%sand)	(5%sand)	(10%sand)
V _{ss} , m/s	Pa/m		
0.20	95.0		
0.23	124.9		
0.30	148.7		
0.40	159.7		
0.60	221.8	421.2	794.6
0.65	-	310.7	820.0
0.75	322.1	313.6	807.4
0.83	378.6	407.8	782.6
0.90	-	423.0	819.2
1.00	510.3	469.7	824.6
1.10	580.5	592.7	868.0
1.20	-	762.7	935.3

Table H-2: Experimental Oil-Water test data

Oil Mass flow Rate	Oil Velocity	Viscosity	Oil Density	Water Velocity	Water Cut	T Oil Injection	T Water Injecton	T Downstream	P Upstream	P Downstream	Pressure Gradient
kg/hr	m/s	cP	kg/m³	m/s		(T7, degC)	(T8, degC)	(T1, degC)	kPa	kPa	kPa/m
157.25	0.09	3707.67	906.18	0.000	0.00	15.48	11.14	14.83	182.78	147.66	16.18
172.45	0.10	3693.97	905.89	0.181	0.64	15.54	10.95	12.64	117.36	114.31	1.41
165.16	0.10	3696.31	905.69	0.298	0.76	15.49	9.69	11.88	116.14	112.83	1.52
161.59	0.09	3696.99	905.86	0.405	0.81	15.49	9.47	10.37	116.07	112.67	1.57
157.85	0.09	3693.04	905.85	0.498	0.85	15.51	9.05	10.17	117.71	113.81	1.80
159.46	0.09	3692.24	905.84	0.602	0.87	15.52	8.43	9.65	119.34	115.16	1.92
168.03	0.10	3690.50	905.86	0.707	0.88	15.52	8.32	9.14	121.85	117.07	2.20
163.58	0.09	3686.44	905.83	0.802	0.89	15.53	8.17	9.09	124.10	118.90	2.40
159.48	0.09	3680.78	905.93	0.900	0.91	15.54	7.74	8.79	126.44	120.82	2.59
161.98	0.09	3678.36	905.89	1.002	0.91	15.57	7.65	8.49	128.98	122.99	2.76

Oil Mass flow Rate	Oil Velocity	Viscosity	Oil Density	Water Velocity	Water Cut	T Oil Injection	T Water Injecton	T Downstream	P Upstream	P Downstream	Pressure Gradient
kg/hr	m/s	cP	kg/m ³	m/s		(T7, degC)	(T8, degC)	(T1, degC)	kPa	kPa	kPa/m
599.37	0.35	3675.25	907.10	0.000	0.00	14.53	15.56	16.02	183.93	134.96	22.56
607.76	0.35	3616.47	906.73	0.188	0.35	14.66	13.87	16.01	115.09	111.56	1.63
609.97	0.35	3587.82	906.49	0.303	0.46	14.80	12.79	15.48	116.54	112.70	1.77
604.65	0.35	3563.83	906.41	0.408	0.54	14.89	12.67	14.32	118.40	114.10	1.98
600.25	0.35	3528.90	906.32	0.506	0.59	15.02	12.96	13.72	119.98	115.47	2.08
605.42	0.35	3504.83	906.28	0.609	0.64	15.09	12.07	13.57	122.65	117.73	2.27
609.86	0.35	3483.24	906.24	0.694	0.66	15.10	11.41	12.77	124.36	119.23	2.37
601.24	0.35	3484.29	906.33	0.816	0.70	15.05	10.83	12.14	127.52	121.95	2.57

Oil Mass flow Rate	Oil Velocity	Viscosity	Oil Density	Water Velocity	Water Cut	T Oil Injection	T Water Injecton	T Downstream	P Upstream	P Downstream	Pressure Gradient
kg/hr	m/s	cP	kg/m ³	m/s		(T7, degC)	(T8, degC)	(T1, degC)	kPa	kPa	kPa/m
114.71	0.07	4913.01	909.66	0.000	0.00	12.25	12.52	14.18	221.65	185.69	16.58
98.79	0.06	4926.84	909.57	0.001	0.01	12.02	11.85	14.00	227.24	190.82	16.78
89.27	0.05	4767.15	909.10	0.048	0.48	12.54	8.47	10.25	113.67	101.57	5.58
100.07	0.06	4717.29	908.74	0.138	0.71	12.64	8.45	10.90	106.38	104.19	1.01
104.34	0.06	4832.57	909.58	0.225	0.79	12.13	11.92	12.96	102.45	100.35	0.96
108.84	0.06	4832.29	909.38	0.329	0.84	12.24	11.82	12.52	103.56	100.95	1.21
101.07	0.06	4831.55	909.31	0.541	0.90	12.26	11.78	12.17	106.91	103.37	1.63
95.62	0.06	4825.73	909.30	0.652	0.92	12.27	11.76	12.13	108.23	104.35	1.79
98.02	0.06	4815.31	909.27	0.695	0.92	12.29	11.64	12.08	108.53	104.71	1.76
111.55	0.06	4440.15	907.79	0.827	0.93	13.23	8.88	9.42	115.43	111.61	1.76

Oil Mass flow Rate	Oil Velocity	Viscosity	Oil Density	Water Velocity	Water Cut	T Oil Injection	T Water Injecton	T Downstream	P Upstream	P Downstream	Pressure Gradient
kg/hr	m/s	cP	kg/m ³	m/s		(T7, degC)	(T8, degC)	(T1, degC)	kPa	kPa	kPa/m
191.71	0.11	4704.42	908.75	0.000	0.00	12.88	12.29	13.43	199.92	149.54	23.22
208.26	0.12	4661.95	908.43	0.182	0.60	12.86	11.72	13.11	112.00	109.16	1.31
203.36	0.12	4653.54	908.42	0.314	0.73	12.92	10.95	11.82	114.48	111.21	1.51
204.72	0.12	4641.62	908.34	0.412	0.78	12.95	10.91	11.34	115.73	111.92	1.75
209.51	0.12	4629.11	908.30	0.505	0.81	12.97	10.89	11.21	115.20	111.11	1.88
213.09	0.12	4613.69	908.20	0.609	0.83	12.99	10.89	11.13	115.19	110.90	1.98
205.06	0.12	4599.08	908.18	0.695	0.85	13.01	10.89	11.12	116.41	111.98	2.04
209.37	0.12	4452.60	908.00	0.814	0.87	13.19	8.91	9.69	119.52	114.48	2.33

Oil Mass flow Rate	Oil Velocity	Viscosity	Oil Density	Water Velocity	Water Cut	T Oil Injection	T Water Injecton	T Downstream	P Upstream	P Downstream	Pressure Gradient
kg/hr	m/s	cP	kg/m ³	m/s		(T7, degC)	(T8, degC)	(T1, degC)	kPa	kPa	kPa/m
346.81	0.20	4835.73	909.17	0.000	0.00	12.24	11.09	12.76	333.56	234.36	45.71
347.61	0.20	4759.99	908.56	0.204	0.50	12.28	10.88	11.98	121.29	118.14	1.45
347.80	0.20	4705.02	908.27	0.307	0.61	12.45	10.07	11.57	119.76	116.28	1.60
349.96	0.20	4672.16	908.13	0.404	0.67	12.49	9.98	10.88	119.81	116.00	1.76
350.65	0.20	4635.67	907.99	0.514	0.72	12.53	10.32	10.60	120.37	116.24	1.90
346.73	0.20	4599.07	907.91	0.613	0.75	12.55	10.02	10.39	121.26	116.83	2.04
346.51	0.20	4576.31	907.84	0.712	0.78	12.58	9.68	10.15	122.51	117.79	2.17
340.12	0.20	4552.07	907.80	0.812	0.81	12.61	9.38	9.85	124.06	119.10	2.29
338.65	0.20	4535.46	907.80	0.910	0.82	12.61	9.27	9.63	126.24	120.94	2.44
342.79	0.20	4518.59	907.80	1.013	0.84	12.59	9.24	9.62	128.33	122.88	2.51

Oil Mass flow Rate	Oil Velocity	Viscosity	Oil Density	Water Velocity	Water Cut	T Oil Injection	T Water Injecton	T Downstream	P Upstream	P Downstream	Pressure Gradient
kg/hr	m/s	cP	kg/m ³	m/s		(T7, degC)	(T8, degC)	(T1, degC)	kPa	kPa	kPa/m
678.62	0.39	4638.22	910.22	0.000	0.00	12.51	11.99	13.16	423.07	246.86	81.20
683.17	0.39	4522.07	908.87	0.183	0.32	12.36	11.44	12.54	128.22	121.47	3.11
675.40	0.39	4494.34	909.30	0.303	0.44	12.28	10.88	12.12	124.39	118.83	2.56
681.73	0.39	4470.50	909.18	0.400	0.51	12.28	10.81	11.64	125.61	119.79	2.68
662.26	0.38	4444.17	909.15	0.506	0.57	12.19	10.92	11.43	126.25	120.47	2.66
701.79	0.40	5096.92	911.94	0.499	0.55	12.01	7.90	8.67	130.41	124.14	2.89
703.69	0.40	5054.88	911.91	0.598	0.60	12.03	7.82	8.42	130.11	124.47	2.60
703.36	0.40	5040.90	911.86	0.708	0.64	12.02	7.18	8.03	132.77	126.67	2.81
704.22	0.40	5033.38	911.78	0.806	0.67	12.00	7.14	7.67	135.36	128.99	2.94

Oil Mass flow Rate	Oil Velocity	Viscosity	Oil Density	Water Velocity	Water Cut	T Oil Injection	T Water Injecton	T Downstream	P Upstream	P Downstream	Pressure Gradient
kg/hr	m/s	cP	kg/m ³	m/s		(T7, degC)	(T8, degC)	(T1, degC)	kPa	kPa	kPa/m
99.72	0.06	7133.06	914.97	0.172	0.75	8.93	6.99	6.55	116.91	114.90	0.92
100.74	0.06	7019.73	914.86	0.297	0.84	8.99	7.07	7.23	119.34	116.60	1.26
104.65	0.06	6960.68	914.85	0.413	0.87	9.01	7.09	7.26	120.34	117.21	1.44
105.76	0.06	6912.27	914.82	0.499	0.89	9.04	7.09	7.28	119.96	116.70	1.50
101.55	0.06	6884.67	914.80	0.598	0.91	9.08	7.60	7.33	121.89	118.05	1.77
106.07	0.06	6859.95	914.81	0.696	0.92	9.10	6.83	7.16	123.99	119.62	2.01
105.19	0.06	6834.89	914.80	0.805	0.93	9.13	6.90	7.11	126.23	121.40	2.23
96.98	0.06	6810.31	914.75	0.905	0.94	9.17	6.90	7.12	128.56	123.36	2.40
105.98	0.06	6793.11	914.64	1.016	0.94	9.21	6.91	7.14	131.08	125.45	2.59

Oil Mass flow Rate	Oil Velocity	Viscosity	Oil Density	Water Velocity	Water Cut	T Oil Injection	T Water Injecton	T Downstream	P Upstream	P Downstream	Pressure Gradient
kg/hr	m/s	cP	kg/m ³	m/s		(T7, degC)	(T8, degC)	(T1, degC)	kPa	kPa	kPa/m
163.36	0.09	7654.11	917.76	0.175	0.65	3.77	10.9	12.73	116.44	113.15	1.52
176.14	0.10	7603.7	917.56	0.311	0.76	3.91	10.72	11.61	117.33	113.67	1.69
171.18	0.10	7459.11	917.03	0.508	0.84	4.5	10.36	10.86	118.36	114.28	1.88
161.52	0.09	7361.04	916.82	0.605	0.87	4.79	9.66	10.21	119.76	115.31	2.05
175.26	0.10	7281.72	916.65	0.697	0.87	5.02	9.6	10.07	121.62	116.74	2.25
170.79	0.10	7153.09	916.4	0.802	0.89	5.38	9.57	10	123.3	118.25	2.33
173.49	0.10	6978.21	916.1	0.896	0.9	5.83	7.97	8.69	124.91	119.79	2.36
171.78	0.10	6871.03	915.93	0.994	0.91	6.11	7.79	8.43	128.31	122.8	2.54

Oil Mass flow Rate	Oil Velocity	Viscosity	Oil Density	Water Velocity	Water Cut	T Oil Injection	T Water Injecton	T Downstream	P Upstream	P Downstream	Pressure Gradient
kg/hr	m/s	cP	kg/m ³	m/s		(T7, degC)	(T8, degC)	(T1, degC)	kPa	kPa	kPa/m
366.01	0.21	6997.1	913.75	0.176	0.46	6	10.23	11.39	124.11	119.22	2.26
371.49	0.21	7144.71	916.01	0.299	0.58	5	9.29	10.61	122.36	118.16	1.93
367.77	0.21	7232.09	916.27	0.406	0.66	5.15	9.22	9.85	123.97	119.25	2.17
367.01	0.21	7218.49	915.97	0.506	0.71	5.37	9.23	9.45	124.45	119.69	2.19
367.92	0.21	7176.59	915.8	0.602	0.74	5.5	8.41	9.12	126.47	121.24	2.41
365.08	0.21	7134.58	915.67	0.707	0.77	5.57	8.36	8.66	128.87	123.22	2.6
375.05	0.21	7090.27	915.5	0.807	0.79	5.66	7.94	8.4	131.3	125.25	2.79
371.61	0.21	7046.6	915.5	0.905	0.81	5.69	7.86	8.28	133.74	127.36	2.94
372.16	0.21	7051.56	915.58	1.002	0.82	5.57	7.69	8.21	136.73	129.94	3.13

Oil Mass flow Rate	Oil Velocity	Viscosity	Oil Density	Water Velocity	Water Cut	T Oil Injection	T Water Injecton	T Downstream	P Upstream	P Downstream	Pressure Gradient
kg/hr	m/s	cP	kg/m ³	m/s		(T7, degC)	(T8, degC)	(T1, degC)	kPa	kPa	kPa/m
701.52	0.4	7162.07	916.21	0.178	0.31	5.76	10.82	10.83	128.59	121.51	3.26
697.37	0.4	7295.29	917.34	0.306	0.43	6.26	9.83	10.23	126.12	120.24	2.71
699.31	0.4	7163.23	917.03	0.403	0.5	6.75	9.71	9.75	126.61	120.61	2.77
701.67	0.4	6980.94	916.83	0.512	0.56	7.19	9.8	9.83	128.04	121.9	2.83
704.82	0.4	6816.44	916.8	0.597	0.6	7.22	9.48	9.74	129.06	122.99	2.8
702.29	0.4	6861.5	917.02	0.708	0.64	6.77	8.76	9.51	131.51	125.07	2.97

Table H-3: Experimental oil-water-sand test data for 1% sand concentration

Oil Velocity	Cor viscosity	Oil Density	slurry Velocity	Vm	T Oil Injection	T Water Injecton	T Upstream	T Downstream	P Upstream	P Downstream	Differential Pressure
m/s	cP	kg/m³	m/s	m/s	(T7, degC)	(T8, degC)	(T4, degC)	(T1, degC)	kPa	kPa	kPa/m
0.11	9077.80	920.20	0.01	0.11	0.21	17.52	20.29	19.65	280.63	161.80	54.76
0.11	7936.88	917.52	0.11	0.22	3.95	14.36	20.03	19.61	99.30	95.89	1.57
0.11	8168.24	917.88	0.20	0.32	3.25	14.29	19.99	19.58	97.23	93.90	1.53
0.11	8380.63	918.24	0.28	0.39	2.67	14.26	20.00	19.59	98.92	94.68	1.95
0.11	8539.69	918.47	0.38	0.49	2.25	14.22	19.99	19.60	98.43	94.56	1.78
0.11	8702.83	918.70	0.49	0.60	1.85	14.17	19.96	19.60	99.03	95.07	1.82
0.11	8864.21	918.88	0.66	0.77	1.46	14.13	19.94	19.62	101.10	96.75	2.01
0.11	8978.04	919.33	0.84	0.95	0.77	14.07	19.97	19.66	107.70	99.40	3.83

Oil Mass flow Rate	Oil Velocity	Viscosity	Oil Density	Slurry Velocity	Vm	T Oil Injection	T Water Injecton	T Upstream	T Downstream	P Upstream	P Downstream	Differential Pressure
kg/hr	m/s	cP	kg/m ³	m/s		(T7, degC)	(T8, degC)	(T4, degC)	(T1, degC)	kPa	kPa	kPa/m
329.53	0.19	7010.42	930.67	0.03	0.21	16.55	14.05	16.72	15.46	121.74	107.67	6.48
348.67	0.20	7181.70	929.59	0.05	0.24	16.22	14.30	1406.39	16.16	105.36	98.58	3.12
336.77	0.19	6981.05	930.26	0.06	0.25	16.61	14.05	16.59	14.90	98.87	95.78	1.42
340.09	0.19	6968.61	930.09	0.10	0.29	16.64	14.04	16.02	14.56	96.16	92.65	1.62
335.56	0.19	6941.89	930.15	0.16	0.34	16.70	14.04	14.54	14.31	95.53	92.58	1.36
336.71	0.19	6930.56	930.21	0.20	0.39	16.73	14.04	13.77	13.92	95.75	92.75	1.38
341.65	0.19	6916.90	930.33	0.30	0.50	16.76	14.05	13.22	13.16	97.68	93.56	1.90
335.67	0.19	6890.76	930.46	0.41	0.60	16.83	14.05	13.05	12.65	100.14	94.65	2.53
333.96	0.19	6882.28	930.74	0.53	0.72	16.85	14.06	12.75	12.28	103.56	96.28	3.36
338.29	0.19	6872.15	930.85	0.61	0.80	16.88	14.07	12.22	12.37	106.24	97.69	3.94

Oil Massflow Rate	Oil Velocity	Cor viscosity	Oil Density	slurry Velocity	Vm	T Oil Injection	T Water Injecton	T Upstream	T Downstream	P Upstream	P Downstream	Differential Pressure
kg/hr	m/s	cP	kg/m³	m/s		(T7, degC)	(T8, degC)	(T4, degC)	(T1, degC)	kPa	kPa	kPa/m
149.87	0.08	7242.91	929.57	0.00	0.09	16.11	14.08	16.16	16.35	174.43	125.54	26.70
169.43	0.10	7259.33	929.45	0.06	0.15	16.08	14.08	15.72	15.82	98.71	93.34	2.45
175.71	0.10	7276.48	929.65	0.10	0.20	16.05	13.95	15.67	15.52	95.83	92.88	1.34
176.54	0.10	7273.14	929.72	0.20	0.30	16.06	13.91	14.84	15.33	94.90	92.16	1.28
169.04	0.10	7294.51	929.79	0.30	0.40	16.02	13.89	14.62	15.02	95.31	92.40	1.35
174.88	0.10	7309.96	929.82	0.41	0.51	16.00	13.88	14.62	14.75	97.31	93.21	1.89
176.25	0.10	7314.24	929.93	0.50	0.60	15.99	13.88	14.71	14.70	99.32	94.13	2.39
173.83	0.10	7320.06	929.99	0.59	0.69	15.98	13.87	14.64	14.60	101.75	95.35	2.94
183.34	0.10	7315.17	930.25	0.71	0.81	15.99	13.85	14.21	14.70	107.70	98.32	4.28

Oil Mass flow Rate	Oil Velocity	Viscosity	Oil Density	Slurry Velocity	Vm	T Oil Injection	T Water Injecton	T Upstream	T Downstream	P Upstream	P Downstream	Differential Pressure
kg/hr	m/s	cP	kg/m ³	m/s		(T7, degC)	(T8, degC)	(T4, degC)	(T1, degC)	kPa	kPa	kPa/m
195.64	0.11	7237.68	930.05	0.09	0.20	16.12	15.55	13.49	13.17	103.22	95.03	3.78
197.21	0.11	7204.01	930.15	0.14	0.25	16.18	15.52	15.51	14.88	96.32	92.00	1.99
187.24	0.11	7210.15	930.08	0.23	0.34	16.17	15.53	14.08	14.32	99.53	92.67	3.16
192.51	0.11	7212.80	930.05	0.31	0.42	16.16	15.54	13.52	13.46	100.32	93.53	3.13
189.66	0.11	7223.08	929.97	0.41	0.51	16.14	15.54	14.69	13.17	101.83	94.26	3.49
192.53	0.11	7234.40	929.98	0.50	0.61	16.12	15.54	13.01	13.06	101.96	94.43	3.47

Oil Mass flow Rate	Oil Velocity	Viscosity	Oil Density	Slurry Velocity	Vm	T Oil Injection	T Water Injecton	T Upstream	T Downstream	P Upstream	P Downstream	Differential Pressure
kg/hr	m/s	cP	kg/m ³	m/s		(T7, degC)	(T8, degC)	(T4, degC)	(T1, degC)	kPa	kPa	kPa/m
256.23	0.14	7067.17	928.31	0.15	0.29	16.43	16.53	17.04	16.15	126.89	96.05	14.21
261.97	0.15	7094.82	928.25	0.21	0.36	16.38	16.60	15.20	15.08	100.81	92.80	3.69
266.49	0.15	7086.09	928.43	0.10	0.25	16.40	16.55	16.72	15.86	95.07	90.27	2.21
262.90	0.15	7115.34	928.24	0.32	0.46	16.34	16.62	15.11	14.76	102.16	93.27	4.10
264.92	0.15	7144.02	928.32	0.44	0.59	16.29	16.62	15.69	14.44	103.24	93.77	4.36

Oil Mass flow Rate	Oil Velocity	Viscosity	Oil Density	Water Velocity	Water Cut	T Oil Injection	T Water Injecton	T Upstream	T Downstream	P Upstream	P Downstream	Differential Pressure
kg/hr	m/s	cP	kg/m ³	m/s		(T7, degC)	(T8, degC)	(T4, degC)	(T1, degC)	kPa	kPa	kPa/m
821.78	0.54	8197.34	848.03	0.08	0.12	15.38	17.29	15.86	16.41	96.73	93.48	1.50
822.64	0.46	6243.59	931.48	0.23	0.34	16.64	17.31	16.72	16.80	109.01	98.49	4.85
813.50	0.46	6280.63	931.10	0.72	0.61	16.74	17.33	15.78	16.33	114.76	101.77	5.99

Table H-4: Experimental oil-water-sand test data for 5% sand concentration

Oil Mass flow Rate	Oil Velocity	viscosity	Oil Density	Slurry Velocity	Vm	T Oil Injection	T Water Injecton	T Upstream	T Downstream	P Upstream	P Downstream	Differential Pressure
kg/hr	m/s	cP Cor viscosity	kg/m³	m/s	m/s	(T7, degC)	(T8, degC)	(T4, degC)	(T1, degC)	kPa	kPa	kPa/m
165.43	0.09	7302.69	929.65	0.29	0.39	16.01	16.43	14.42	13.87	94.38	91.03	1.54
164.46	0.09	7297.94	929.63	0.40	0.49	16.02	16.43	14.73	13.11	96.60	91.78	2.22
174.60	0.10	7300.26	929.63	0.51	0.61	16.01	16.44	14.60	13.00	99.73	93.16	3.03
167.96	0.09	7305.20	929.70	0.60	0.69	16.01	16.45	14.49	13.07	103.72	95.13	3.96
165.48	0.09	7324.19	929.77	0.79	0.88	15.98	16.48	13.71	12.93	109.57	97.52	5.55
173.45	0.10	7286.16	930.17	0.85	0.94	16.04	14.05	14.50	14.23	108.07	97.90	4.69
176.82	0.10	7281.95	930.16	0.91	1.01	16.04	14.08	14.28	14.22	111.48	99.18	5.67
169.73	0.10	7293.78	930.20	1.26	1.36	16.02	14.09	13.57	14.12	120.53	103.27	7.96

Oil Mass flow Rate	Oil Velocity	Viscosity	Oil Density	Slurry Velocity	Vm	T Oil Injection	T Water Injecton	T Upstream	T Downstream	P Upstream	P Downstream	Differential Pressure
kg/hr	m/s	cP Cor viscosity	kg/m ³	m/s	m/s	(T7, degC)	(T8, degC)	(T4, degC)	(T1, degC)	kPa	kPa	kPa/m
188.03	0.11	6190.76	928.55	0.09	0.20	17.02	14.01	16.26	14.40	97.29	92.56	2.18
190.31	0.11	6191.23	928.52	0.15	0.26	16.98	14.02	15.63	13.91	96.71	91.96	2.19
187.00	0.11	6221.23	928.49	0.19	0.30	16.96	14.03	15.70	13.94	98.75	92.04	3.09
184.17	0.10	6250.23	928.55	0.30	0.40	16.90	14.03	15.68	13.62	103.57	94.03	4.39

Oil Massflow Rate	Oil Velocity	viscosity	Oil Density	Slurry Velocity	Vm	T Oil Injection	T Water Injecton	T Upstream	T Downstream	P Upstream	P Downstream	Differential Pressure
kg/hr	m/s	cP Cor viscosity	kg/m ³	m/s	m/s	(T7, degC)	(T8, degC)	(T4, degC)	(T1, degC)	kPa	kPa	kPa/m
365.94	0.21	6174.27	929.52	0.12	0.32	17.31	13.35	18.01	18.44	99.24	92.65	3.04
366.53	0.21	6181.42	929.42	0.22	0.42	17.28	13.36	18.23	18.68	98.86	92.49	2.94
360.53	0.20	6190.24	929.41	0.32	0.52	17.19	13.37	18.36	18.89	99.90	92.73	3.31
367.48	0.21	6188.13	929.38	0.43	0.63	17.13	13.39	18.75	19.06	101.76	93.48	3.82
358.03	0.20	6191.23	929.57	0.49	0.69	16.98	13.41	18.70	19.17	100.36	93.04	3.37

Oil Massflow Rate	Oil Velocity	viscosity	Oil Density	Slurry Velocity	Vm	T Oil Injection	T Water Injecton	T Upstream	T Downstream	P Upstream	P Downstream	Differential Pressure
kg/hr	m/s	cP Cor	kg/m ³	m/s	m/s	(T7, degC)	(T8, degC)	(T4, degC)	(T1, degC)	kPa	kPa	kPa/m
249.50	0.14	7050.88	929.93	0.30	0.44	16.08	14.84	16.05	15.78	98.58	94.43	1.91
245.42	0.14	7068.95	929.95	0.39	0.53	16.08	14.84	16.08	15.42	98.82	94.66	1.92
251.57	0.14	7108.28	929.94	0.52	0.66	16.05	14.85	15.94	15.13	101.40	95.65	2.65

Oil Massflow Rate	Oil Velocity	Viscosity	Oil Density	Slurry Velocity	Vm	T Oil Injection	T Water Injecton	T Upstream	T Downstream	P Upstream	P Downstream	Differential Pressure
kg/hr	m/s	cP Cor viscosity	kg/m ³	m/s	m/s	(T7, degC)	(T8, degC)	(T4, degC)	(T1, degC)	kPa	kPa	kPa/m
269.65	0.15	6755.24	929.65	0.18	0.33	16.28	15.20	15.47	13.69	102.97	95.64	3.38
278.50	0.16	6749.11	929.59	0.28	0.44	16.26	15.22	16.08	13.17	105.67	96.35	4.30
270.29	0.15	6750.07	929.57	0.31	0.46	16.21	15.22	15.86	13.13	105.02	95.80	4.25
270.81	0.15	6746.39	929.60	0.38	0.54	16.17	15.23	15.77	12.92	106.55	96.72	4.53
278.46	0.16	6742.68	929.66	0.50	0.66	16.12	15.24	14.02	12.72	109.52	97.96	5.33

Oil Velocity	Cor viscosity	Oil Density	slurry Velocity	Vm	T Oil Injection	T Water Injecton	T Upstream	T Downstream	P Upstream	P Downstream	Differential Pressure
m/s	cP	kg/m³	m/s	m/s	(T7, degC)	(T8, degC)	(T4, degC)	(T1, degC)	kPa	kPa	kPa/m
0.11	9077.80	920.20	0.01	0.11	0.21	17.52	20.29	19.65	280.63	161.80	54.76
0.11	7936.88	917.52	0.11	0.22	3.95	14.36	20.03	19.61	99.30	95.89	1.57
0.11	8168.24	917.88	0.20	0.32	3.25	14.29	19.99	19.58	97.23	93.90	1.53
0.11	8380.63	918.24	0.28	0.39	2.67	14.26	20.00	19.59	98.92	94.68	1.95
0.11	8539.69	918.47	0.38	0.49	2.25	14.22	19.99	19.60	98.43	94.56	1.78
0.11	8702.83	918.70	0.49	0.60	1.85	14.17	19.96	19.60	99.03	95.07	1.82
0.11	8864.21	918.88	0.66	0.77	1.46	14.13	19.94	19.62	101.10	96.75	2.01
0.11	8978.04	919.33	0.84	0.95	0.77	14.07	19.97	19.66	107.70	99.40	3.83

Table H-5: Experimental oil-water-sand test data for 10% sand concentration

Oil Mass flow Rate	Oil Velocity	Viscosity	Oil Density	Slurry Velocity	Vm	T Oil Injection	T Water Injecton	T Upstream	T Downstream	P Upstream	P Downstream	Differential Pressure
kg/hr	m/s	cP	kg/m³	m/s		(T7, degC)	(T8, degC)	(T1, degC)	kPa	kPa	kPa/m	kg/hr
269.65	0.15	6755.24	929.65	0.18	0.33	16.28	15.20	15.47	13.69	102.97	95.64	3.38
278.50	0.16	6749.11	929.59	0.28	0.44	16.26	15.22	16.08	13.17	105.67	96.35	4.30
270.29	0.15	6750.07	929.57	0.31	0.46	16.21	15.22	15.86	13.13	105.02	95.80	4.25
270.81	0.15	6746.39	929.60	0.38	0.54	16.17	15.23	15.77	12.92	106.55	96.72	4.53
278.46	0.16	6742.68	929.66	0.50	0.66	16.12	15.24	14.02	12.72	109.52	97.96	5.33

Oil Mass flow Rate	Oil Velocity	Viscosity	Oil Density	Slurry Velocity	Vm	T Oil Injection	T Water Injecton	T Upstream	T Downstream	P Upstream	P Downstream	Differential Pressure
kg/hr	m/s	cP	kg/m ³	m/s		(T7, degC)	(T8, degC)	(T1, degC)	kPa	kPa	kPa/m	kg/hr
197.36	0.11	6797.20	929.39	0.45	0.56	16.20	15.98	16.30	15.57	94.85	90.70	1.91
197.42	0.11	6815.86	929.43	0.56	0.67	16.21	15.99	16.08	15.43	96.70	91.66	2.33
200.15	0.11	6838.62	929.42	0.73	0.85	16.19	16.01	15.91	15.67	100.32	93.35	3.21

Oil Mass flow Rate	Oil Velocity	Viscosity	Oil Density	Slurry Velocity	Vm	T Oil Injection	T Water Injecton	T Upstream	T Downstream	P Upstream	P Downstream	Differential Pressure
kg/hr	m/s	cP	kg/m ³	m/s		(T7, degC)	(T8, degC)	(T1, degC)	kPa	kPa	kPa/m	kg/hr
255.06	0.14	6866.19	929.72	0.38	0.52	16.05	16.00	16.57	16.90	97.00	91.81	2.39
253.11	0.14	6881.56	929.67	0.47	0.61	16.06	16.00	16.56	16.81	96.43	91.83	2.12
258.07	0.15	6901.00	929.75	0.62	0.77	16.05	16.00	16.50	16.69	99.48	93.09	2.94
251.50	0.14	6925.74	929.81	0.66	0.81	16.03	16.01	16.45	16.62	102.45	94.39	3.71

Oil Mass flow Rate	Oil Velocity	Viscosity	Oil Density	Slurry Velocity	Vm	T Oil Injection	T Water Injecton	T Upstream	T Downstream	P Upstream	P Downstream	Differential Pressure
kg/hr	m/s	cP	kg/m ³	m/s		(T7, degC)	(T8, degC)	(T1, degC)	kPa	kPa	kPa/m	kg/hr
378.18	0.21	6812.59	930.03	0.19	0.40	16.00	14.90	15.67	15.50	95.47	91.51	1.82
378.54	0.21	6819.16	930.11	0.30	0.52	16.05	14.89	16.05	15.32	95.68	91.36	1.99
375.64	0.21	6832.91	930.12	0.40	0.61	16.08	14.87	16.08	14.78	97.05	91.92	2.36
378.60	0.21	6848.04	930.13	0.50	0.71	16.09	14.86	15.98	14.22	99.93	92.87	3.25
379.47	0.21	6867.37	930.14	0.55	0.77	16.08	14.85	15.94	13.96	102.27	93.66	3.97

Oil Mass flow Rate	Oil Velocity	Viscosity	Oil Density	Slurry Velocity	Vm	T Oil Injection	T Water Injection	T Upstream	T Downstream	P Upstream	P Downstream	Differential Pressure
kg/hr	m/s	cP	kg/m ³	m/s		(T7, degC)	(T8, degC)	(T1, degC)	kPa	kPa	kPa/m	kg/hr
158.41	0.09	6984.56	928.86	0.12	0.21	16.31	13.86	15.87	14.28	106.96	97.53	4.34
167.50	0.09	6963.64	928.88	0.32	0.42	16.30	13.85	15.91	14.71	106.83	96.42	4.80
165.30	0.09	6956.87	928.90	0.35	0.45	16.33	13.83	16.17	15.08	102.95	96.40	3.02
169.99	0.10	6947.03	928.84	0.48	0.58	16.26	13.84	15.54	14.12	107.11	98.19	4.11

Oil Mass flow Rate	Oil Velocity	Viscosity	Oil Density	Slurry Velocity	Vm	T Oil Injection	T Water Injecton	T Upstream	T Downstream	P Upstream	P Downstream	Differential Pressure
kg/hr	m/s	cP	kg/m³	m/s		(T7, degC)	(T8, degC)	(T1, degC)	kPa	kPa	kPa/m	kg/hr
259.89	0.15	5760.68	928.17	0.19	0.34	17.15	18.44	19.18	20.42	95.60	91.11	2.07
256.49	0.14	5752.77	928.13	0.19	0.34	17.23	18.43	18.80	20.18	96.30	91.37	2.27

Appendix I Impact of Model Modifications on T-Junction Pipe Geometry Flow

The table below presents the comparison of the results obtained from concentric and T-junction inlet geometries using modified TKE and TDR models. It is observed that the concentric inlet gave a better prediction of the experimental results although it had an adverse effect on the gradient obtained for Case 1 ($V_{so}=0.55\text{m/s}$ and $V_{sw}=0.2$) but performed reasonable well compare to the T-junction inlet design.

Table I-1: Comparison of inlet designs simulated with modified TKE and TDR

(V_{so}, V_{sw}) m/s		Pressure gradient kPa/m				
		<i>Experiment</i>	<i>CFD</i>			
			<i>Concentric Inlet</i>		<i>T-junction Inlet</i>	
			<i>No TKE modification</i>	<i>TKE modified</i>	<i>No TKE modification</i>	<i>TKE modified</i>
Case 1	(0.55, 0.20)	3.92	4.35	7.03	44.34	41.80
Case 2	(0.55, 0.40)	3.93	18.25	6.62	29.43	22.86

Table I-2: Effect of modified TKE and TDR on the concentric and T-junction inlet designed

(V_{so}, V_{sw}) m/s	Flow pattern @30s		
	<i>Experiment</i>	<i>CFD</i>	
		<i>Concentric Inlet</i>	<i>T-junction Inlet</i>
(0.55, 0.20)	